UNIVERSITY OF CALIFORNIA SAN DIEGO

Therapeutic Restoration of Stathmin-2 RNA Processing in TDP-43 Proteinopathies

A dissertation submitted in partial satisfaction of the
requirements for the degree
Doctor of Philosophy

in

Biomedical Sciences

by

Michael Welton Baughn

Committee in charge:

Professor Don W. Cleveland, Chair
Professor Steven Dowdy
Professor Christopher Glass
Professor Lawrence Goldstein
Professor Karen Oegema

2021

The dissertation of Michael Welton Baughn is approved, and it is acceptable in quality and form for publication on microfilm and electronically.

University of California San Diego

2021

DEDICATION

To my loving wife, Sarah Elizabeth Baughn, for her tireless support.

All of old. Nothing else ever. Ever tried. Ever failed. No matter. Try again. Fail again. Fail better. – Samuel Beckett

TABLE OF CONTENTS

LIST OF FIGURES

ACKNOWLEDGEMENTS

I would like to acknowledge and thank Professor Don W. Cleveland for allowing me to be a member of his amazing team, for his support and patience, his abilities to skillfully inspire and motivate, to command an audience with conviction and inspire the same of his trainees, to distill a simple message from an utterly complex mash of information, and to find positivity where to other eyes there is none.

I would also like to acknowledge and thank Dr. Ze'ev Melamed, Dr. Moira McMahon, and Dr. Haiyang Yu as mentors throughout my doctoral process. They have each pulled me, at various points, from very deep water and given me safe passage back to shore. I would not be the scientist that I am today without their guidance.

I would also like to acknowledge and thank Dr. John M. Ravits and Dr. Clotilde Lagier-Tourenne for their mentorship both leading up to and throughout my graduate education, Dr. Bruce Hamilton for his mentorship in the UCSD Genetics Training Program, my parents Steven and Delinda for their support and encouragement over many years, my in-laws Steve and Anne, and my wonderful wife Sarah and the family we have built together: Apollo, Neil, and Chewie.

Chapters 2, 3, 4, and 5 were supported in part by an institutional award to the UCSD Genetics Training Program from the National Institute for General Medical Sciences, T32 GM008666.

Chapters 3, 4, and 5, in part, are being prepared for publication as "Therapeutic restoration of stathmin-2 expression in TDP-43 proteinopathies." 2021, and also include co-authored unpublished work. Other authors are: Zevik Melamed, Jone Lopez-Erauskin, Mariana Bravo-Hernandez, Haiyang Yu, Melinda Beccari, Melissa Mcalonis, John Ravits, Karen Ling, Paymann Jafar-nejad, Frank Rigo, Aamir Zuberi, Max Presa, Cat Lutz, C. Frank Bennett, Martin Marsala, Clotilde Lagier-Tourenne, Don W. Cleveland. The dissertation author was the primary investigator and author of this material.

VITA

2005-2010 Bachelor of Science, Cell Developmental and Molecular Biology, University of Washington

2014-2021 Doctor of Philosophy, Biomedical Sciences, University of California San Diego

PUBLICATIONS

1. Rabin SJ, Kim JM, **Baughn M**, Libby RT, Kim YJ, Fan Y, Libby RT, La Spada A, Stone B, Ravits J. Sporadic ALS has compartment-specific aberrant exon splicing and perturbation of cell-matrix adhesion biology. ***Human Molecular Genetics***, 2010. PMID: 19864493 PMCID: PMC2796893 DOI: 10.1093/hmg/ddp498

2. Lagier-Tourenne C, Polymenidou M, Hutt KR, Vu AQ, **Baughn M**, Huelga SC, Clutario KM, Ling SC, Liang TY, Mazur C, Wancewicz E, Kim AS, Watt A, Freier S, Hicks GG, Donohue JP, Shiue L, Bennett CF, Ravits J, Cleveland DW, Yeo GW., Divergent roles of ALS-linked proteins FUS/TLS and TDP-43 intersect in processing long pre-mRNAs. ***Nature Neuroscience***, 2012. PMID: 23023293 PMCID: PMC3586380 DOI: 10.1038/nn.3230

3. Harms MB, Cady J, Zaidman C, Cooper P, Bali T, Allred P, Cruchaga C, **Baughn M**, Libby RT, Pestronk A, Goate A, Ravits J, Baloh RH., et. al., Lack of C9ORF72 coding mutations supports a gain of function for repeat expansions in amyotrophic lateral sclerosis. ***Neurobiology of Aging***, 2013. PMID: 23597494 PMCID: PMC3679344 DOI: 10.1016/j.neurobiolaging.2013.03.006

4. Sareen D, O'Rourke JG, Meera P, Muhammad AK, Grant S, Simpkinson M, Bell S, Carmona S, Ornelas L, Sahabian A, Gendron T, Petrucelli L, **Baughn M**, Ravits J, Harms MB, Rigo F, Bennett CF, Otis TS, Svendsen CN, Baloh RH., Targeting RNA Foci in iPSC-Derived Motor Neurons from ALS Patients with a C9ORF72 Repeat Expansion. ***Science Translational Medicine***, 2013. PMID: 24170860 PMCID: PMC3839752 DOI: 10.1073/pnas.1318835110

5. Lagier-Tourenne C*, **Baughn M***, Rigo F, Sun S, Liu P, Li HR, Jiang J, Watt AT, Chun S, Katz M, Qiu J, Sun Y, Ling SC, Zhu Q, Polymenidou M, Drenner K, Artates JW, McAlonis-Downes M, Markmiller S, Hutt KR, Pizzo DP, Cady J, Harms MB, Baloh RH, Vandenberg SR, Yeo GW, Fu XD, Bennett CF, Cleveland DW*, Ravits J.*, Targeted degradation of sense and antisense C9orf72 RNA foci as therapy for ALS and frontotemporal degeneration. ***PNAS***, 2013. PMID: 24170860; PMCID: PMC3839752; DOI: 10.1073/pnas.1318835110

6. William M. Brandler*, Danny Antaki*, Madhusudan Gujral*, Amina Noor, Gabriel Rosanio, Timothy R Chapman, Daniel J Barrera, Guan Ning Lin, Dheeraj Malhotra, Amanda C Watts, Lawrence C Wong, Jasper A Estabillo, Therese E Gadomski, Oanh Hong, Karin V Fuentes

Fajardo, Abhisek Bhandari, Renius Owen, **Michael Baughn**, Jeffrey Yuan, Terry Solomon, Alexandra G Moyzis, Stephan J Sanders, Gail E Reiner, Keith K Vaux, Charles M Strom, Kang Zhang, Alysson R Muotri, Natacha Akshoomoff, Suzanne M Leal, Karen Pierce, Eric Courchesne, Lilia M Iakoucheva, Christina Corsello, and Jonathan Sebat. Frequency and Complexity of De Novo Structural Mutation in Autism. ***Am. J. Hum. Genet.*** 98, 667–679. 2016. PMID: 27018473 PMCID: PMC4833290 DOI: 10.1016/j.ajhg.2016.02.018

7. Jie Jiang, Qiang Zhu, Tania F. Gendron, Shahram Saberi, Melissa McAlonis-Downes, Amanda Seelman, Jennifer E. Stauffer, Paymaan Jafar-nejad, Kevin Drenner, Derek Schulte, Seung Chun, Shuying Sun, Shuo-Chien Ling, Brian Myers, Jeffery Engelhardt, Melanie Katz, **Michael Baughn**, Oleksandr Platoshyn, Martin Marsala, Andy Watt, Charles J. Heyser M. Colin Ard, Louis De Muynck, Lillian M. Daughrity, Deborah A. Swing, Lino Tessarollo, Chris J. Jung, Arnaud Delpoux, Daniel T. Utzschneider, Stephen M. Hedrick, Pieter J. de Jong, Dieter Edbauer, Philip Van Damme, Leonard Petrucelli, Christopher E. Shaw, C. Frank Bennett, Sandrine Da Cruz, John Ravits, Frank Rigo, Don W. Cleveland, Clotilde Lagier-Tourenne. Gain of Toxicity from ALS/FTD-Linked Repeat Expansions in C9ORF72 Is Alleviated by Antisense Oligonucleotides Targeting GGGGCC-Containing RNAs. ***Neuron.*** 90, 535–550. 2016. PMID: 27112497 PMCID: PMC4860075 DOI: 10.1016/j.neuron.2016.04.006

8. Ranjan Batra, Kasey Hutt, Anthony Vu, Stuart J Rabin, **Michael Baughn**, Ryan T Libby, Shawn Hoon, John Ravits, Gene W Yeo. Gene Expression Signatures of Sporadic ALS Motor Neuron Populations. ***bioRxiv.*** 2016. DOI:10.1101/038448

9. Shahram Saberi*, Jennifer E. Stauffer*, Jie Jiang*, Sandra Diaz Garcia, Takuya Ohkubo, Cheyenne L. Schloffman, Marcus Maldonado, Sahana Malik, Hani Basilim, Derek Schulte, **Michael Baughn**, Maria J Rodriguez, Don Pizzo, Don Cleveland, and John Ravits. Sense-encoded poly-GR dipeptide repeat proteins correlate to neurodegeneration and uniquely co-localize with TDP-43 in dendrites of repeat expanded C9orf72 amyotrophic lateral sclerosis. ***Acta Neuropathologica.*** 2018. 135: 459. PMID: 29196813, PMCID: PMC5935138, DOI: 10.1007/s00401-017-1793-8

10. Florian Krach, Ranjan Batra, Emily C. Wheeler, Anthony Q. Vu, Ruth Wang, Kasey Hutt, Stuart J. Rabin, **Michael W. Baughn**, Ryan T. Libby, Sandra Diaz-Garcia, Jennifer Stauffer, Elaine Pirie, Shahram Saberi, Maria Rodriguez, Assael A. Madrigal, Zacharias Kohl, Beate Winner, Gene W. Yeo, John Ravits. Transcriptome – pathology correlation identifies interplay between TDP 43 and the expression of its kinase CK1E in sporadic ALS. ***Acta Neuropathologica.*** 2018. PMID: 29881994, DOI: doi.org/10.1007/s00401-018-1870-7

11. Jone Lopez-Erauskin, Takahiro Tadokoro, **Michael W. Baughn**, Brian Myers, Melissa McAlonis-Downes, Carlos Chillon-Marinas, Joshua N. Asiaban, Jonathan Artates, Anh T. Bui, Anne P. Vetto, Sandra K. Lee, Ai Vy Le, Ying Sun, Melanie Jambeau, Jihane Boubaker, Deborah Swing, Jinsong Qiu, Geoffrey G. Hicks, Zhengyu Ouyang, Xiang-Dong Fu, Lino Tessarollo, Shuo-Chien Ling, Philippe A. Parone, Christopher E. Shaw, Martin Marsala, Clotilde Lagier-Tourenne, Don W. Cleveland* and Sandrine Da Cruz*. ALS/FTD-Linked Mutation in FUS Suppresses Intra-

axonal Protein Synthesis and Drives Disease Without Nuclear Loss-of-Function of FUS. ***Neuron***. 2018. 100(4) 816-830.e7 PMID: 30344044. DOI: https://doi.org/10.1016/j.neuron.2018.09.044

12. Ze'ev Melamed, Jone Lopez-Erauskin, **Michael W. Baughn**, Ouyang Zhang, Kevin Drenner, Ying Sun, Fernande Freyermuth, Moira A. McMahon, Melinda S Beccari, Jon Artates, Takuya Ohkubo, Maria Rodriguez, Nianwei Lin, Dongmei Wu, C. Frank Bennett, Frank Rigo, Sandrine Da Cruz, John Ravits, Clotilde Lagier-Tourenne and Don W. Cleveland. Premature polyadenylation-mediated loss of stathmin-2 is a hallmark of TDP-43-dependent neurodegeneration. ***Nature Neuroscience***. 2019. 22, pages180–190(2019) PMID: 30643298. PMCID: PMC6348009. DOI: https://doi.org/10.1038/s41593-018-0293-z

Anticipated Publications:

13. **Michael W. Baughn***, Ze'ev Melamed*, et. al., Therapeutic restoration of stathmin-2 expression in TDP-43 proteinopathies. *Science*. 2021.

14. Haiyang Yu*, **Michael W. Baughn***, et. al., ShredEx: a modular gene therapy platform to rapidly degrade aggregated cellular protein targets. 2021.

15. Moira McMahon*, **Michael W. Baughn***, Meghdad Rahdar, et. al., Genome-scale CRISPR activation and knockout screens identify genetic modulators of antisense oligonucleotide uptake. 2021.

16. Jone Lopez-Erauskin, Mariana Bravo Hernandez, **Michael W. Baughn**, et. al., Chronic focal suppression of Stathmin2 in the adult mammalian nervous system leads to a loss of motor and sensory synapses and a sensory neuropathy phenotype. 2021.

ABSTRACT OF THE DISSERTATION

Therapeutic Restoration of Stathmin-2 RNA Processing in TDP-43 Proteinopathies

by

Michael Welton Baughn

Doctor of Philosophy in Biomedical Sciences

University of California San Diego, 2021

Professor Don W. Cleveland, Chair

TDP-43 proteinopathies, including amyotrophic lateral sclerosis (ALS), frontotemporal dementia (FTD), and Alzheimer's disease (AD), commonly share features of nuclear clearance and cytoplasmic accumulation of the RNA-binding protein TDP-43 within affected neurons. TDP-43 suppression in an adult nervous system changes expression and splicing of RNAs encoded by hundreds of genes, however, the functional consequences and relevance to

neurodegeneration of these changes have proven elusive. Our team recently discovered that TDP-43 suppression in human cells drives use of cryptic splice and polyadenylation sites in the pre-mRNA encoded by the STMN2 gene (aka SCG10), leading to loss of the stathmin-2 protein it encodes, preventing axonal recovery after injury. This discovery provides a new gene target in TDP-43 proteinopathy and links dysregulated RNA metabolism to impaired microtubule dynamics, two pathways suggested independently without recognized pathophysiologic commonality. I here demonstrate that concomitant loss of full length stathmin-2 mRNA and accumulation of its cryptically spliced and truncated form is a hallmark of TDP-43 proteinopathy. I show that removal of the proposed TDP-43 binding sites within intron 1 of the stathmin-2 pre-mRNA drives constitutive misprocessing. I determine TDP-43's role at this site is to sterically block cryptic site utilization, as synthetically targeting other RNA binding proteins or RNA-targeted CRISPR effectors to this locus restores correct stathmin-2 pre-mRNA maturation. By eliminating either cryptic processing site, I determine that cryptic splicing, not cryptic polyadenylation, is the primary driver of stathmin-2 pre-mRNA misprocessing. Next, a therapeutic strategy for TDP-43 proteinopathies is identified using steric binding antisense oligonucleotides (ASOs) to maintain or restore stathmin-2 pre-mRNA maturation and rescue axonal regeneration in human motor neurons with TDP-43 deficiency. I developed AAV-based experimental approaches to modulate stathmin-2 in an adult mammalian central nervous system, including an AAV delivered RNAi against the stathmin-2 pre-mRNA that is used to determine the consequences of chronic reduction of murine stathmin-2, as well as gene therapy cargos to supplement stathmin-2 expression selectively in neurons with dysfunctional TDP-43. Finally, the STMN2 gene is humanized by knock-in of human exon 2a into the corresponding region of murine STMN2, with or without TDP-43 binding sites. I show humanized mice without the STMN2 TDP-43 binding sites constitutively misprocess stathmin-2 pre-mRNA, enabling therapy development in TDP-43 proteinopathies by identification of stathmin-2-restoring ASOs.

Chapter 1: Introduction:

A brief description of Amyotrophic Lateral Sclerosis

First described by neurologist Jean-Martin Charcot in 1869[1,2], ALS is a fatal neurodegenerative disease characterized by the progressive degeneration and death of 1) upper motor neurons, which project from the motor cortex to the brainstem and spinal cord, and 2) lower motor neurons which project from brainstem and spinal cord to muscles, causing weakness and eventually death. ALS typically affects people in mid-to-late life, at a rate of about 5 cases per 100,000 people in the United States[3], and is believed to have similar rates worldwide. While there is a slightly higher incidence in men than in women before their mid to late 60s, it thereafter has equal incidence. The clinical presentation[4] of ALS suggests a focal onset and three-dimensional spreading within compartments of upper and lower motor system, with the mixture of upper vs lower motor neuron involvement, as well as the location of onset and rate of progression varying between patients, though typically resulting in a relatively constant decline (intermittent remissions an exacerbations are generally rare)[2]. Common signs denoting the degeneration of upper motor neurons of Brodman area 4, their axons traversing the corona radiata, internal capsule, cerebral peduncles, pontine base, medullary pyramids, and lateral corticospinal tracts include: weakness with slowness, hyperreflexia and spasticity. Indeed, the “lateral sclerosis” of ALS is so named because of the gliotic and hardened (or sclerotic) dorsolateral area of the spinal cord which contains these lateral corticospinal tracts. Degeneration of lower motor neurons which project from the brainstem and spinal cord to the muscles results in clinical findings of muscle denervation including weakness, atrophy or “amyotrophy” (“amyotrophic” is Greek for “no muscle nourishment”), and fasciculations[5,6] (spontaneous and intermittent fine and fast contractions of muscle fibers, which some neurologists call verminosis because they look like worms moving below the dermis). Most patients (~80%) present with unilateral limb onset, and will typically (~60%

of the time) next experience involvement of the contralateral limb, then ipsilateral involvement of their other extremity, before onset of contralateral involvement of that body segment[2,7]. About 20% of patients will preset with bulbar onset affecting speech, chewing and swallowing, with weakness and fasciculations in the tongue, and progressing more quickly to fatal respiratory involvement. Bulbar onset patients are also commonly affected by what is called pseudobulbar affect (sometimes colloquially called “emotional incontinence”) with inappropriate laughing, crying or yawning that can be incongruent to emotional trigger or mood. Bulbar onset patients most often progress to unilateral arm involvement before involving the opposite arm and then the muscles involved in respiration (typically resulting in a faster disease course versus limb-onset patients). ALS is sometimes accompanied with cognitive impairment of executive function, with language impairment, and behavioral disfunction and dementia are increasingly recognized as a component of disease in around 15% of patients.

Though ALS is a motor neuron disease and sensory involvement is not an accepted typical feature, mild sensory symptoms (usually tingling) may occur in 20-30% of patients even though clinical sensory examinations are usually normal. Electrophysiologic studies can indicate amplitude reduction on sensory nerves and slowing of dorsal column conduction[8,9] (in one study, 91% of patients who underwent sural nerve biopsy had pathologic evidence of sensory nerve pathology)[10]. In spite of this, patients usually do not complain of general sensation loss. Indeed, to the contrary, pain may be one of the more neglected symptoms of ALS patients even though a majority of patients report some type of pain (not from sensory circuit deterioration but from secondary causes) with the site and type depending on the mechanism, but including painful cramps, nociceptive pain in the shoulders, joint and pressure sores with decreased mobility, and neuropathic pain in the feet and lower limbs. Pain can occur at all stages but can be especially severe toward the end of life where more than half of patients in their last month of life report severe and frequent pain, sometimes requiring sedative analgesic drugs. This is especially true

of the minority of patients who opt to be kept alive by invasive ventilation[11,12]. Autonomic nervous system disturbances are not common in ALS, but have been reported in some patients carrying rare mutations[13,14].

The final result in all cases of ALS is the same, a progressive paralysis and eventually death, typically in 3-5 years, from progressive neuromuscular respiratory failure. Some extremely aggressive mutations confer a disease course of less than one year. A minority of patients (5-10%) opt for permanent ventilation, prolonging their life but leaving them with steadily mounting paralysis, until they can only move their eyes and are eventually "locked in"[15,16].

Three genes and three decades, with the dawn of a fourth: The explosive gene discoveries that have dominated ALS research

SOD1

As of early 2021, at least 43 of genes[17] have been implicated as causes of (or contributors to) Amyotrophic Lateral Sclerosis (ALS) when mutated at the DNA level. However, in diagnostic terms only about 10% of incidences of all ALS are known to be explained by an underlying genetic variant. The first ALS associated gene was discovered by classical genetic mapping of large ALS family pedigrees, revealing in 1993 the Copper Zinc Superoxide Dismutase gene (SOD1)[18,19]. The SOD1 gene explains only as small fraction (about 3-4%) of all ALS[20], although more than 180 different causal genetic lesions in SOD1 have been described in ALS patients. Disease-linked SOD1 mutations are scattered broadly across its 153 amino acid gene product, which is ubiquitously expressed and normally functions as a cytoplasmic homodimer to catalytically convert the free-radical superoxide biproducts of oxidative phosphorylation into water and hydrogen peroxide[21]. Initial proposals that SOD1 might mediated disease might be provoked by oxidative damage stemming from the loss of SOD1 catalytic activity were falsified by further scrutiny of SOD1 G93A mice, that develop progressive motor neuron disease in spite of their

elevated SOD1 enzymatic activity[22], along with additional SOD1 mice (G37R[23] and G85R[24,25]) bearing mutations which show elevated or unchanged enzymatic activity. Independent of animal models of disease, a systematic analysis of human patient mutations in SOD1 found no relationship between enzymatic active site perturbations and ALS onset or disease progression outcomes[26]. Further cementing the divergence from an oxidative stress model of ALS pathology was an SOD1 knockout mouse, which (unlike the mutant transgenic lines) lives to adulthood without signs of overt neurodegenerative disease onset, motor neuron loss, or paralysis[27]. Elevation or knockout of endogenous SOD1 gene expression on a mutant SOD1 transgenic background showed no effect on mutant mediated disease[28], essentially ruling out major roles for normal SOD1 enzymatic function in neurodegeneration in ALS, and demonstrating that the mutant phenotype must be due to a toxic gain of function.

This is not to suggest that knockout of SOD1 has no measurable effect in adult mice, a point that is potentially important for therapeutic considerations surrounding SOD1 mediated disease if mutant-selective reduction proves technically infeasible (which appears to be the case using present technologies). Indeed, the mouse SOD1 knockout model does have some non-causal neuromuscular indications that suggest loss of normal SOD1 could play a role as a disease modifier, including: motor neuron death-rate differences developed after an induced axonal injury,[27] reduced peripheral nerve myelin thickness and conduction velocity[29,30], some denervation at neuromuscular junctions[31], reduced mitochondrial density in neurons[32], and abnormalities in gait and tremor[33], along with various secondary skeletal muscle pathologies. Many of these phenotype observations from the SOD1 knockout mice mimic pathologies found in human patients with homozygous SOD1 truncating null mutations[34,35], who, perhaps most critically, do not develop ALS but instead develop progressive motor deficits starting in childhood. In spite of the mouse and human motor phenotypes described in the case of homozygous loss of SOD1, it is important to note that heterozygous carriers of these SOD1-null mutations are apparently

unaffected by the motor syndromes seen in homozygous individuals, demonstrating that chronic 2-fold reduction in SOD1 levels is apparently well tolerated in the human context, setting a rough threshold guideline for therapeutic reduction of SOD1 level in ALS patients.

Since the weight of the evidence overwhelmingly favors a gain of toxic function in SOD1 as primary to the onset of SOD1 ALS, any on-target therapy for mutations in this gene must work to reduce the synthesis of the toxic gene product. The tolerability of non-specific reduction of total SOD1 levels in this context, while a point of concern, will largely depend mutation-targeting-specificity as well as overall reductions achieved in specific cell types (see "current and future treatments" subchapter).

C9ORF72 hexanucleotide repeat expansion: the most common genetic cause of ALS and FTD

Though a flurry of additional ALS-linked genes were implicated in the years following the first drafts of the human genome, for about 15 years after the initial discover of SOD1 in ALS, most of the effort to understand ALS pathogenesis focused on that single gene[36]. As the falling cost of DNA sequencing technology enabled larger and larger exome- and genome-wide analysis, one significant recurring association to the small-arm of chromosome 9 persistently managed to evade capture (to the frustration of geneticists). Indeed, in 2010 at the "7th Annual International Conference on Frontaltemporal Dementias", I had the pleasure of listening to a poster presentation by a young geneticist by the name of Dr. Rosa Rademakers, regarding the elusive Chromosome 9 genetic association that, by next-generation-sequencing analysis of the linked haplotype block, somehow resulted in no obvious genetic abnormality. Dr. Rademakers and her then graduate student, Mariely DeJesus-Hernandez, would go on just weeks later to discover the causal chromosome 9 linked mutation was actually a hexanucleotide repeat expansion (GGGGCC) located in the first intron of a computationally predicted gene, C9ORF72[37,38]

(chromosome 9, open reading frame 72) positioned between two alternative transcription start sites for that gene. The next-generation sequencing technology used to interrogate the sequence space of the linked haplotype block had been throwing away the disease-causing repeat expansion in the first step of analysis because the sequence fragments from the very long repeat expansion (commonly numbering in the thousands) did not align to the reference genome. The discovery of the C9ORF72 expansion as the most common genetic cause of ALS and frontotemporal dementia (FTD)[37-39] (sometimes called frontotemporal lobar degeneration FTLD, characterized by behavior and personality changes and eventual language skill impairment) was not only a landmark discovery because of the sheer number of patient cases it explains (about 11.5% of all ALS in the United States[20] which includes about 34% of familial ALS cases, and about 12% of FTD[37] overall, including about a quarter of familial FTD cases), it is also perfectly illustrative at of an increasingly recognized overlap[40] between the two diseases and their genetic drivers. In the case of C9ORF72, the same genetic lesion can cause either neurodegenerative disorder (or in some very unlucky patients, a combination of both conditions). ALS is now recognized to have a cogitative component in at least some patients, and some FTD patients meet ALS motor diagnostic criteria, with both categories of overlap occurring at an approximately equal frequency around 15%[41]. Though prior pathological evidence already suggested this relationship, the recognition of this clinical and genetic overlap, and mixed involvement in individual patients, was broadly accepted after the c9ALS/FTD discovery.

The hexanucleotide repeat expansion mutation in c9ALS/FTD additionally places both conditions squarely among the ranks of at least 22 other inherited neurological repeat expansion disorders[42], including myotonic dystrophies 1 and 2, FMR1/2, fragile X ataxia tremor associated syndrome (FXTAS), Huntington's disease, Spinal bulbar muscular atrophy (SBMA) and a subset of the spinocerebellar ataxias (SCA1,2,3,6-8,10,12, and 17). As is true in other repeat expansion diseases, the C9ORF72 hexanucleotide sequences are tolerated in a normal unaffected nervous

system at shorter tandem repeat lengths from 2-25 GGGGCC units. Via some as-yet unknown expansion mechanism, that presumably involves errors in DNA replication and/or DNA repair processes, the repeat sequence expands in ALS and FTD patients to lengths of hundreds or even thousands of these tandem repeats[37-39,43], with heterogeneity between cell types and compartments of the brain suggesting somatic expansion, and with overall repeat length relating to disease severity[44].

The function of the C9ORF72 gene product, normally expressed in both the central nervous system and periphery, is not understood. Although, it has been proposed by in-silico analysis to be a guanine nucleotide exchange factor (GEF) that regulates Rab GTPases[45]. Heterozygous repeat expansion effectively lowers RNA synthesis of total C9orf72 in patients by approximately half[37], leading some to hypothesize that haploinsufficiency could be a contributor to c9ALS/FTD[40]. This initial hypothesis was very much muddled by a set of experiments in a C9ORF72 knockout mouse from the lab of Kevin Eggan, which initially claimed progressive deficits and death (though this was walked-back in the final manuscript after scrutiny by other laboratories). Eggan and colleagues also claimed that neuronal populations vulnerable in ALS/FTD were highest to express C9ORF72[46] (a claim our group later falsified[47]). Follow-up experiments by our group and others demonstrated that C9ORF72 is normally expressed broadly in the nervous system, and that its partial loss (to 50%) is well tolerated with no neurodegenerative signs, while full loss of the gene leads to a peripheral leukemia-like syndrome that includes lymph node swelling and splenomegaly, though, again with no behavioral or neuropathologic abnormalities in the central nervous system were detected in these mice. Loss of mouse C9ORF72 was able to worsen repeat expansion derived phenotypes when the two factors were combined in the same animal. This indicates that, while C9ORF72 expression is important in the periphery, its loss in the central nervous system is quite tolerable[47].

Additionally, I[48] (and others[49]), discovered that like other repeat expansion disorders, this intronic repeat is bi-directionally transcribed to produce both a sense- and antisense-strand repeat RNA transcripts both of which accumulate into RNA foci within nuclei. Both transcribed RNA strands, sense and antisense, are abundantly detected in the cultured fibroblast cells of patients carrying the repeat expansion, with the antisense foci accumulating (perhaps unexpectedly) at nearly twice the number as the sense-strand foci (Figures 1.1 and 1.2). For both strands, most cells accumulate small numbers of foci, with occasional cells bearing foci loads in abundance greater than 10 per cell. The antisense strand RNA foci are apparent in greater numbers-per-cell than the sense strand derived repeat RNA. I additionally demonstrated these nuclear RNA foci can be found in the lumbar spinal cord, primarily within neurons, including 25-30% of lumbar motor neurons (including those affected by nuclear clearance and cytoplasmic phosphorylation of TDP-43), as well as lumbar interneurons, but only rarely in GFAP positive astrocytic cells or IBA1 positive microglia (~1% of cells in both cases). Within the brain, I identified that 30-50% of hippocampal neurons of the CA1 region accumulate foci, as do hippocampal dentate neurons (similar rates), and cerebellar Purkinje cells (~1/3 of cells) although the foci are rare in the far more numerous granular cell type of the cerebellum (found in less than 1% of this cell type) (Figure 1.1).

Figure 1.1 Sense and Antisense Strand RNA Foci Are a Hallmark of C9ORF72 Expansion

(A) Fluorescent in-situ hybridization reveals nuclear sense-strand RNA foci in 25-30% of lumbar motor neurons in affected patients. (B) Motor neuron from an unaffected control patient contains no RNA foci. (C) RNA foci in patient lumbar motor neuron nuclei containing phosphorylated aggregated TDP-43 (green). (D) Patient lumbar interneuron containing sense-strand nuclear RNA foci. (E) Cortical neuron from Layer 3 of the motor cortex showing nuclear sense-strand RNA foci common to about half of all cells examined of this type. (F) Cortical neuron from layer 5 of the motor cortex (Betz cell) showing nuclear sense strand RNA foci, common to about half of all cells examined of this type. (G) Hippocampal neuron from Cornu Ammonis region 1 of the hippocampus of an affected patient showing nuclear sense-strand RNA foci common to 30-50% of cells of this type and region. (H) Sense-strand RNA foci in a patient granule neuron of the hippocampal dentate gyrus, common to 30-50% of cells of this type. (I) Patient cerebellar Purkinje cell with nuclear RNA foci, common to 30-50% of these cells. (J) Patient cerebellar granular cell showing multiple sense-strand RNA foci, this is a rare event in granular cells which appear mostly unaffected. (K) Patient GFAP-positive astrocyte with sense-strand RNA foci, this is a rare event in astrocytes which are mostly unaffected. (L) Patient Iba1-positive microglia cell with nuclear sense-strand RNA foci, this is a rare event in microglia, which are mostly unaffected. (M) Patient spinal motor neuron containing nuclear antisense strand RNA foci. (N) Patient spinal interneuron containing nuclear antisense strand RNA foci. (O) Non-neuronal cells of a patient spinal cord containing nuclear antisense-strand RNA foci. (Sense or antisense strand targeting in-situ hybridization probes shown in red, DAPI staining shown in blue, immunofluorescence staining for indicated targets shown in green)

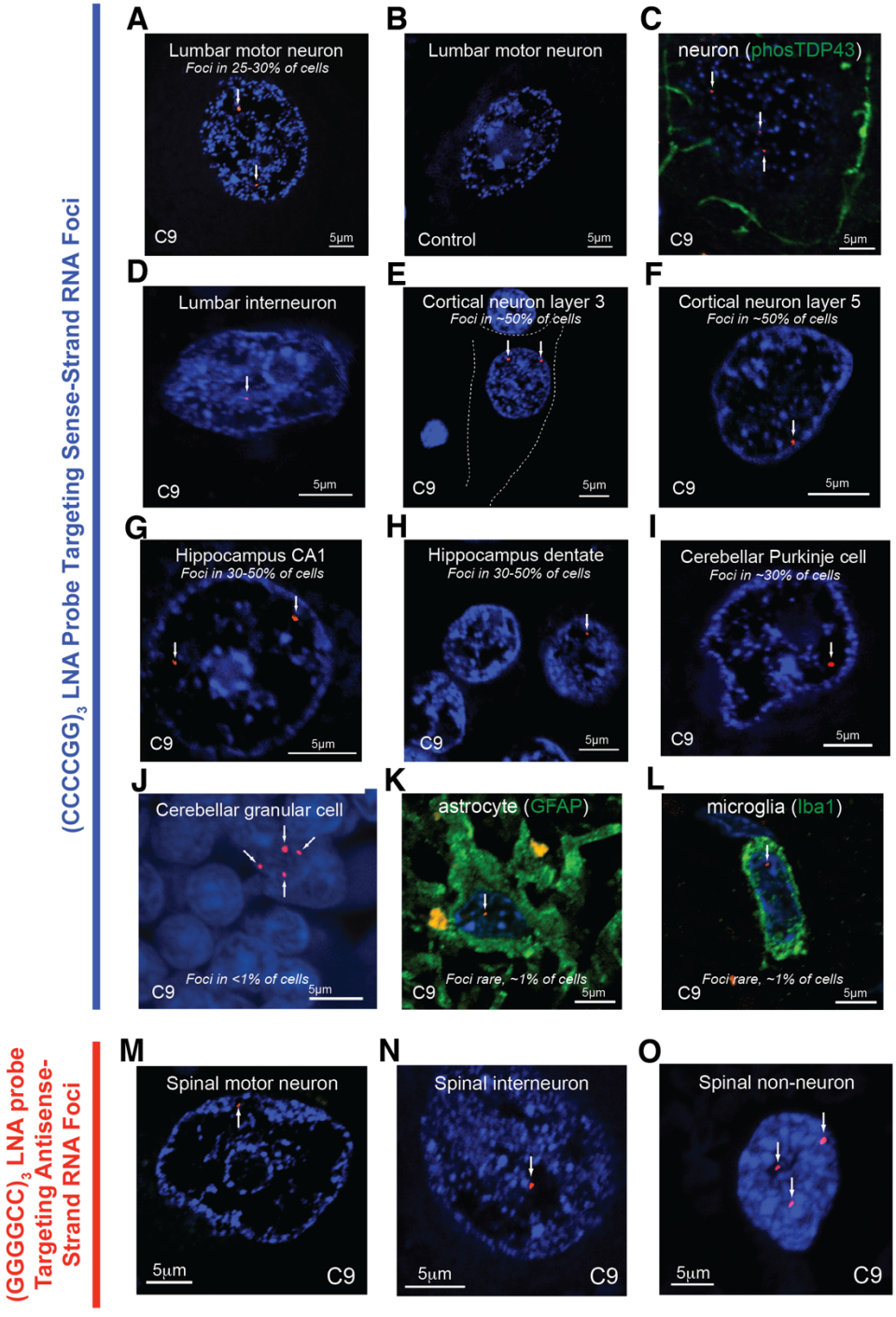
(CCCCGG)3 LNA Probe Targeting Sense-Strand RNA Foci
A
Lumbar motor neuron
Foci in 25-30% of cells
C9
5µm
B
Lumbar motor neuron
Control
5µm
C
neuron (phosTDP43)
C9
5µm
D
Lumbar interneuron
C9
5µm
E
Cortical neuron layer 3
Foci in ~50% of cells
C9
5µm
F
Cortical neuron layer 5
Foci in ~50% of cells
C9
5µm
G
Hippocampus CA1
Foci in 30-50% of cells
C9
5µm
H
Hippocampus dentate
Foci in 30-50% of cells
C9
5µm
I
Cerebellar Purkinje cell
Foci in ~30% of cells
C9
5µm
J
Cerebellar granular cell
Foci in <1% of cells
C9
5µm
K
astrocyte (GFAP)
Foci rare, ~1% of cells
C9
5µm
L
microglia (Iba1)
Foci rare, ~1% of cells
C9
5µm
(GGGGCC)3 LNA probe Targeting Antisense-Strand RNA Foci
M
Spinal motor neuron
5µm
C9
N
Spinal interneuron
5µm
C9
O
Spinal non-neuron
5µm
C9

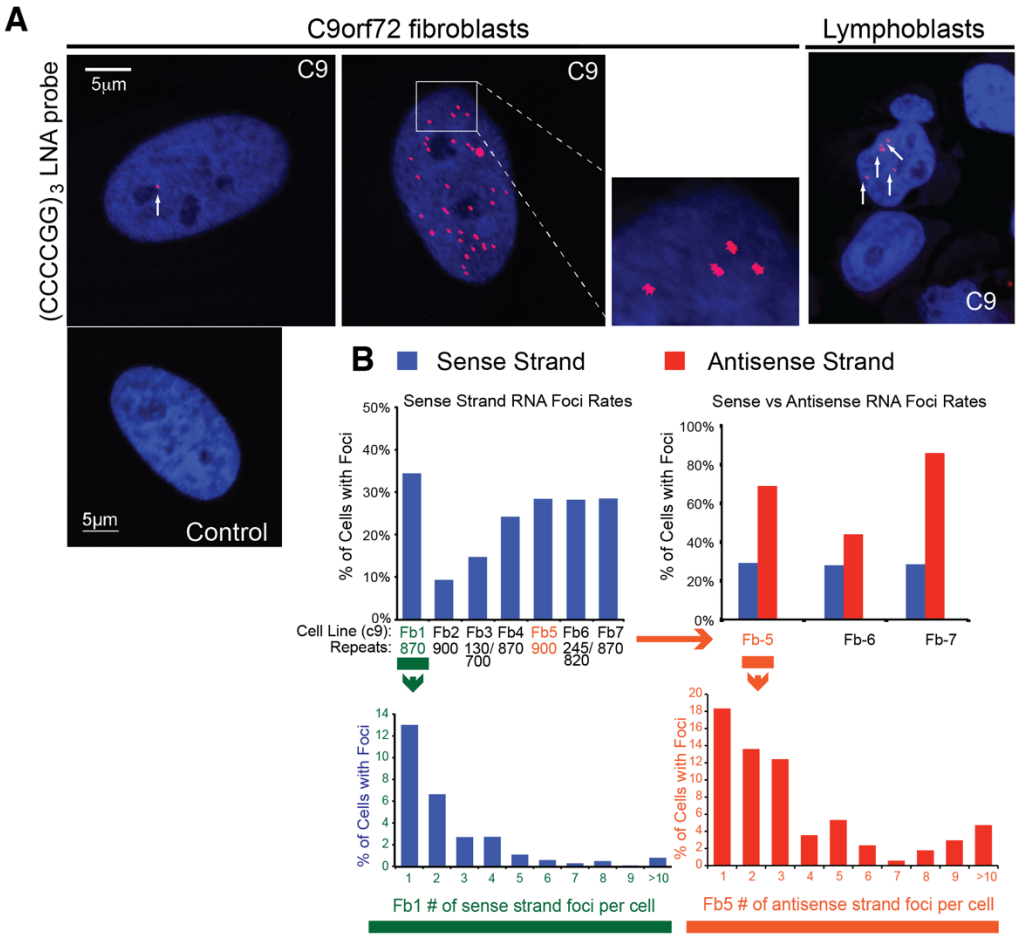

Figure 1.2 Abundant RNA foci are common to C9ORF72 patient fibroblasts and lymphoblasts
(A) Fluorescent in-situ hybridization detects abundant RNA foci in patient fibroblast cell lines and lymphoblasts, but not in unaffected controls. (sense-strand revealing RNA foci probes shown in red, DAPI staining shown in blue). (B) RNA foci quantifications across multiple fibroblast lines from affected patients reveals most lines contain nuclear foci in approximately 30% of cells, with no discernable relationship between overall repeat length measured by southern blot and apparent abundance. Most cells contain few sense-strand RNA foci with few cells containing many foci, the same general distribution is observed for antisense-strand RNA foci, except that they are apparently more abundant per affected cell and have a higher prevalence rate.

As to the molecular dysfunction underlying C9ORF72 diseases, it is possible the large and persistent RNA foci might sequester crucial RNA-binding proteins[40], like in the case of muscleblind-like protein 1 (MBNL1) in myotonic dystrophy which binds and is sequestered within CUG and CCUG repeats, leading to dysregulated expression and splicing of a number of downstream RNA targets that are normal MBNL1 substrates[50]. While an RNA-binding protein sequestration hypothesis has certainly been proposed in the case of c9ALS/FTD, none of the

proposed sequestered targets seem to overlap between different publications[51-55]; so while it certainly remains possible, the field is far from a consensus on this model. The GGGGCC repeat has also been proposed to form G-quadruplex structures[51,56], of unknown significance, based primarily on (what I personally consider to be quite weak) in-vitro circular dichroism evidence. Whether these proposed nucleotide structures are real or relevant in disease is not established, but there could also exist some other undescribed primary toxicities associated with nuclear retention or problematic export and clearance of extremely long GC-containing RNA foci.

Additionally, although the repeat expansion is transcribed from a canonical intron, both sense and antisense strands are templates for non-canonical repeat-associated non-ATG initiated (RAN) translation (a repeat-RNA associated phenomenon first discovered in the context of spinocerebellar ataxia type 8[57]) in which scanning ribosomes initiate translation in the absence of an ATG codon (usually, though not always, starting at a close cognate sequence), resulting in the production of five unique di-peptide protein products from six different reading frames[49,58,59]. Of the five unique frames (sense-strand RNA encoded: poly-Glycine-Alanine and poly-Glycine-Arginine; antisense encoded: poly-Proline-Alanine and poly-Arginine-Proline; and encoded by both strands: poly-Glycine-Proline) (Figure 1.3 A) and six unique full polypeptides if translated to completion[49] (Glycine-Proline frames are internally identical but have different C-termini sequences flanking the repeat), the Arginine containing reading frame products have been proposed to be especially toxic[60-62]. I was able to detect both sense- and antisense- derived dipeptide repeat proteins in the hippocampus and cerebellum of patient brain using immunofluorescence microscopy, where they co-localized to varying degrees with the ubiquitin associated protein p62 (Figure 1.3 B-C). Further effort in post-mortem patient tissue determined that among the possible reading frames, sense-encoded poly-GR accumulation was most closely correlated to areas of neurodegeneration[63].

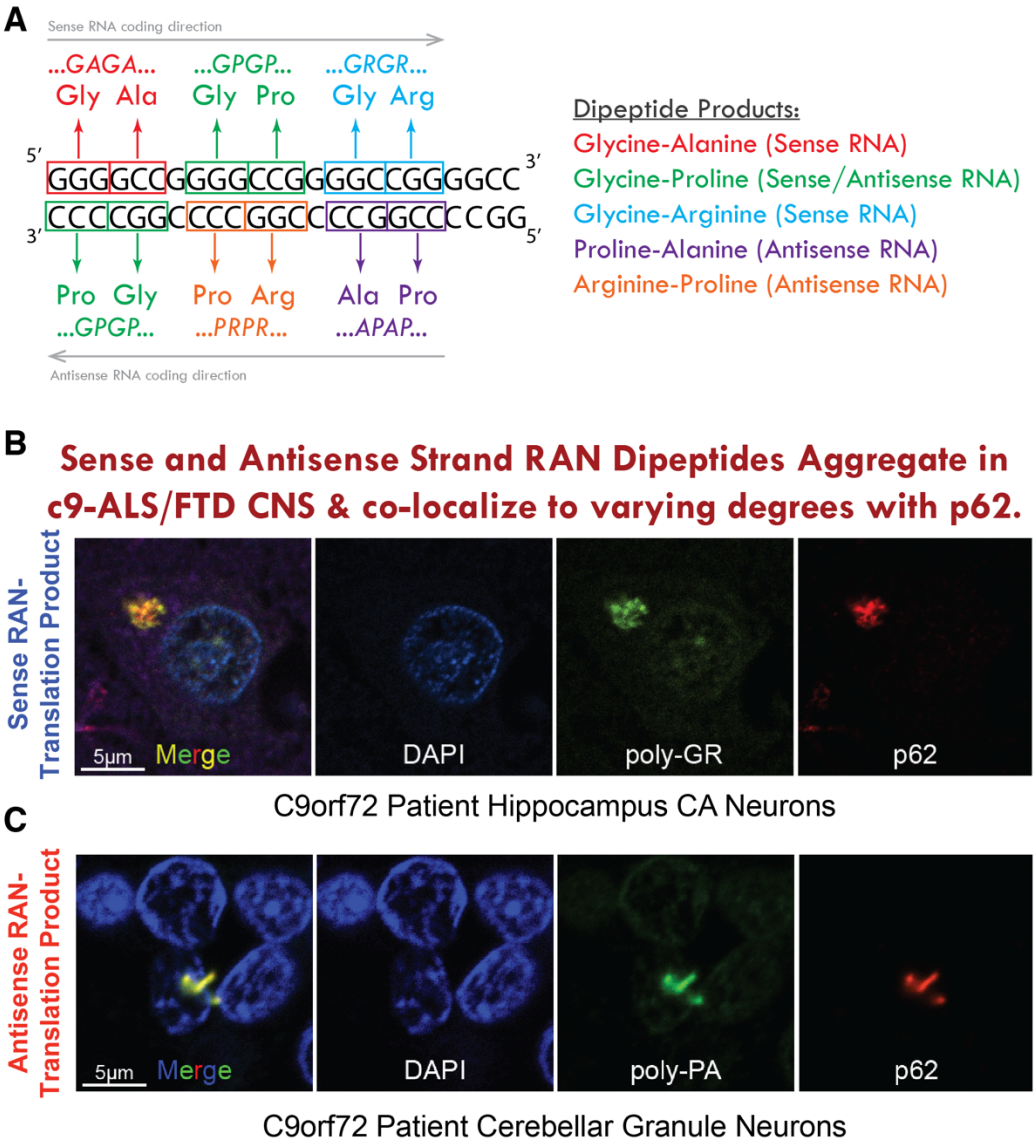

Figure 1.3 Dipeptide repeat proteins translated unconventionally from both sense- and antisense-RNAs are detected in affected C9ORF72 patient tissues

(A) Diagram depicting sense and antisense RNA stands and their respective reading frames and RAN-translation dipeptide protein products. (B) Sense-strand RNA derived poly-GR dipeptide (green) is detected by immunofluorescence staining in hippocampal Cornu Ammonis neuron of affected C9ORF72 patient, partially co-localizing with the ubiquitin-associated protein p62 (red), DAPI DNA stain shown in blue. (C) Antisense-strand RNA derived poly-PA dipeptide (green) is detected by immunofluorescence staining in Cerebellar granule neuron of affected C9ORF72 patient, fully co-localizing with the ubiquitin-associated protein p62 (red) DAPI DNA stain shown in blue.

In animal model experiments a GGGGCC expressing AAV vector composed of 66 repeats, I think quite unsurprisingly, shows ill effects when introduced within the brains of mice via intracerebroventricular injection at post-natal day zero (P0-ICV administration) and expressed at

such extraordinarily high levels that the resulting dipeptides accumulate to be approximately 2% of total brain protein[64]. One might interpret the relatively mild phenotype seen in such an experiment as an indication that the expressed poly-dipeptide protein is actually remarkably non-toxic, but this point is controversial. The AAV-injected mice accumulate RNA foci and of course RAN-translation products, and develop neuron loss and an array of behavior deficits more consistent with FTD than ALS, although they do also have a mild motor phenotype (by rotaroad analysis) and show pathologic misaccumulation of the RNA-binding protein TDP-43 (a phenomenon I will cover in greater detail in its own sub-section). A set of much better controlled experiments utilized newly produced transgenic BAC mouse models that harbored either up to 450 repeats within the authentic human gene, with C9ORF72 transgene expression at a much more physiologically relevant 2-fold level. These mice developed age dependent accumulation of RNA foci and RAN dipeptides, and similarly suffered from FTD-associated defects primarily related to cognition and memory, but without overt signs of TDP-43 pathology[47].

I (in collaboration with my colleague Clotilde Lagier-Tourenne) was also the first to demonstrate that the action of antisense oligonucleotide (ASO) drugs designed to target the C9ORF72 pre-mRNA within the nucleus of affected patient cells could reduce the levels of the RNA isoform containing the expanded repeat (Figure 1.4 A-E). Still better, by targeting the ASOs to a section of pre-mRNA immediately upstream of the repeat expansion (or partially overlapping the start of the repeat), it is possible to reduce the mutant expansion containing RNA without lowering the overall levels of normal C9ORF72 transcribed from exon 1b, a mutant RNA-specific knockdown which is the gold standard of such an approach (Figure 1.4 A, B, D).

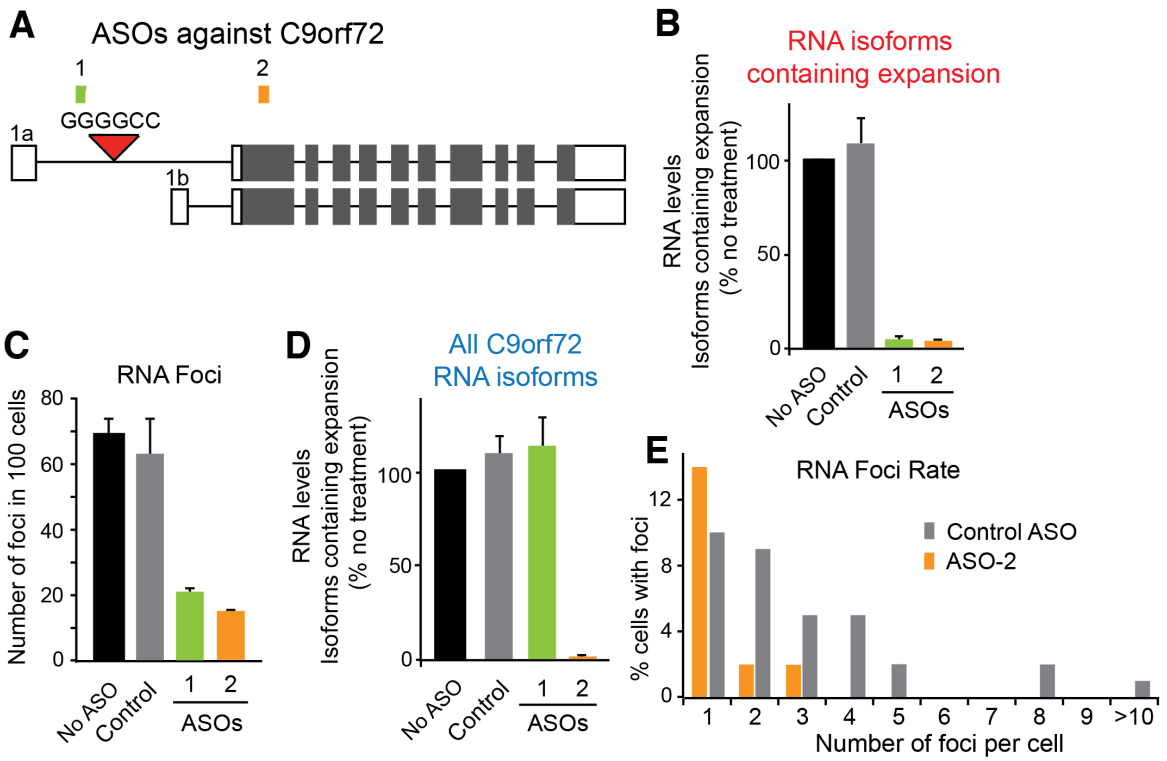

Figure 1.4 Targeted antisense oligonucleotide (ASO) treatment in patient cell lines relieves repeat-expanded RNA and sense-strand RNA foci accumulations without affecting overall C9ORF72 levels

(A) Diagram depicting C9ORF72 gene and three predicted isoforms transcribed from alternative transcription start sites upstream or downstream of the hexanucleotide repeat expansion, along with locations of targeted ASO binding and primers to detect repeat-expansion containing isoforms or total C9ORF72 RNA levels. (B) Graph depicting qRT-PCR quantification of C9ORF72 repeat-containing RNA isoforms in patient fibroblasts with and without transfection of targeted ASO drugs. (C) Graph depicting RNA foci accumulation levels in patient fibroblast with and without transfection of targeted ASO drugs. (D) Graph depicting qRT-PCR quantification of total C9ORF72 levels from all RNA isoforms in patient fibroblasts with or without transfection of targeted ASO drugs, note that ASO 1 and 2 do not reduce total C9ORF72 levels. (E) Graph depicting change in RNA foci accumulation rates per cell in patient fibroblasts transfected with a non-target control ASO or an ASO targeted to reduce levels of all C9ORF72 RNAs.

As expected, these ASO approaches were capable of substantially decreasing the prevalence of RNA foci after only 24 hours, whereas a pool of siRNAs targeting C9ORF72 with the primarily cytoplasmic RISC complex could lower overall C9ORF72 RNA levels by 75%, but without decreasing the burden of nuclear RNA foci (Figure 1.5 A-C). Extensive work in novel C9ORF72 transgenic mouse lines established that these ASO drugs were effective in-vivo in a mammalian nervous system to reduce both RNA foci accumulation and (surprisingly) to an even greater degree, dipeptide repeat proteins, and critically alleviated the FTD-like phenotypes of the mice[47]. These results established the molecular basis of mutant-specific pre-mRNA targeting ASOs in C9ORF72 repeat-expansion carrier patients[48], and an ASO drug targeting the same sequence (albeit modified by further internal chemistry development) is being administered to ALS patients in a currently ongoing clinical trial.

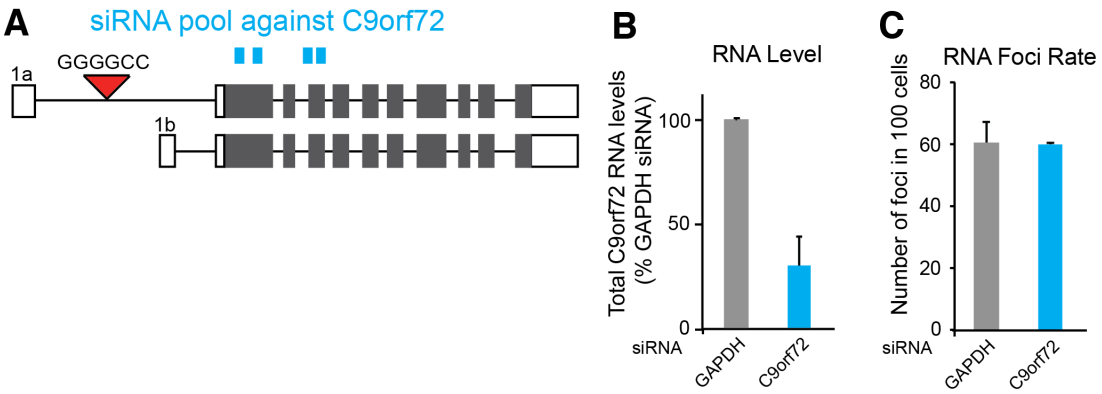

Figure 1.5 Pooled siRNA transfection into C9ORF72 patient cells reduces C9ORF72 RNA expression without relieving accumulation of sense-stand encoded RNA foci.

(A) Diagram depicting C9ORF72 gene and three predicted isoforms transcribed from alternative transcription start sites upstream or downstream of the hexanucleotide repeat expansion, along with targeting locations of four pooled siRNAs against C9ORF72 and primers to detect repeat-expansion containing isoforms or total C9ORF72 RNA levels. (B) Graph depicting qRT-PCR quantification of C9ORF72 RNA levels from all isoforms in C9ORF72 patient cells transfected with GAPDH control or C9ORF72 targeted siRNA pools. (C) Graph depicting RNA foci accumulation levels in C9ORF72 patient cells transfected with GAPDH control or C9ORF72 targeted siRNA pools.

Molecular convergence of most ALS cases on pathological TDP-43 mislocalization, largely independent of underlying genetics

Protein aggregation is a pathological finding common to many neurodegenerative diseases, including Huntington's Disease (HD), the Spinocerebellar Ataxias (SCA), Spinal-Bulbar Muscular Atrophy (SBMA), Alzheimer's disease (AD) Frontotemporal Dementias, Parkinson's disease (PD), prion diseases, and Amyotrophic Lateral Sclerosis (ALS). Pre-dating the SOD1 discovery by about two years was the pathological identification of poly-ubiquitinated aggregates as a histological hallmark in the vast majority (~97%) of ALS cases[65], and shortly thereafter a similar finding in ALS with dementia (ALS/FTD)[66,67], as well as up to half of patients with FTD[40] (termed at the time FTLD-U, or frontotemporal lobar degeneration with ubiquitinated inclusions, the second most common cause of dementia aside from Alzheimer's disease). This nearly ubiquitous (pun intended) pathological finding hinted at common physiological processes at play in these disorders, before abundant genetic evidence was available to implicate the molecular overlap.

The identity of the "missing-link" protein targeted by this poly-ubiquitination process remained mysterious for 15 years, until a seismic shift in our understanding of ALS and FTD was precipitated by the biochemical isolation and identification of transactive response DNA-binding protein 43 (TDP-43) as the major protein component of the poly-ubiquitinated aggregates[68,69]. TDP-43, encoded by the TARDBP gene, is an RNA-binding protein with a normal function(s) in pre-mRNA processing, necessitating its normal localization to the nucleus of the cell, however, in ~97% of all ALS patients (this includes essentially every patient except those with disease caused by mutations in SOD1 or FUS/TLS) and about half of FTD patients[70,71], TDP-43 is partially or fully cleared from the nucleus[69,72-74] and accumulates in cytoplasmic aggregates of the somatic compartment (by still unexplained mechanisms) where it is hyperphosphorylated. Similar TDP-43 pathology has also been found in more than half of Alzheimer's disease (AD) cases (the most

common cause of dementia), dementia with Lewy bodies (DLB)[75], and a newly described condition termed “Limbic-predominant age-related TDP-43 encephalopathy” (LATE) which is a type of frontotemporal lobar degeneration and amnesic dementia that mimics AD in many respects.[76]

It is notable that the initial discovery/identification process in this case was initiated not by traditional genetic techniques, instead utilizing monoclonal antibody generation[69] and biochemical extraction[68] of aggregated protein from patient tissue, followed in both cases by isolation and mass-spectrometry to reveal peptides whose sequence uniquely mapped to the known sequence of TDP-43. Genetic analysis later revealed that in the ~1% of all ALS patients whose disease is attributable to TDP-43 mutation[20], most of those mutations are clustered in the intrinsically disordered glycine-rich region[36] of the protein at its c-terminal end, which is thought to be crucial for its interactions with other proteins and for liquid-liquid phase separation (LLPS, a phenomenon I will not cover here but is a process presently hypothesized by many groups to be an early step in TDP-43 pathology[77,78]). This minimal genetic contribution of TDP-43 mutation to ALS is perhaps surprising given that nearly all patients at a pathologic level show nuclear clearance and aggregation of TDP-43 in affected neurons. This indicates that nearly all ALS-causing mechanisms (genetic or otherwise) converge at some point on TDP-43 function, though the initiating lesion/insult is typically caused by something other than inherited errors in the TARDBP gene sequence.

Direct therapeutic targeting of TDP-43 is highly challenged by the fact that TDP-43 tightly autoregulates its own synthesis through binding to the 3’ untranslated region of the pre-mRNA that encodes it (likely acting in a dose-dependent manner by steric binding to suppress incorporation of a cryptic exon within the untranslated region, the integration of which leads to rapid decay of the resulting RNA transcript, though it is important to note that this proposed mechanism has not been experimentally demonstrated[79]), and neither knockout/suppression nor

over-expression are well tolerated in an adult animal nervous system. TDP-43 is also an essential gene for embryonic development[80]. Since the exact molecular mechanism leading to TDP-43 disfunction is unresolved, and targeting TDP-43 at the protein or mRNA level is probably unfavorable, significant effort has been put into identifying modifiers of TDP-43 pathology, and potential neuronal gene targets of significance whose disfunction is downstream of TDP-43.

The most significant breakthrough on the first front was achieved by Aaron Gitler's laboratory at Stanford University, leveraging fundamental genetic screening techniques in yeast to identify genes capable of acting as modifiers of pathologic TDP-43 aggregation phenotypes (this phenotype being proposed as an important early step in its disfunction). From the initial identification of the yeast ortholog gene polyA-binding protein Palb1P-binding Protein (PBP1), whose dose-dependent gain or loss of expression could enhance or suppress TDP-43 overexpression toxicity, respectively, they demonstrated that the human ortholog Ataxin-2 gene (ATXN2) had a similar effect on TDP-43 toxicity in flies. The human ATXN2 gene contains a polyglutamine repeat tract that, when expanded, causes the neurodegenerative disease spinocerebellar ataxia type 2 (SCA2) which is marked by cerebellar degeneration followed by motor neuron degeneration. Gitler's team identified that polyglutamine expansions of intermediate length (not sufficiently long to trigger SCA2 disease) could be found in about 5% of familial and sporadic ALS patients in a cohort of 900 genomic DNA samples, strengthening the association of this modifier gene with ALS[81]. Most importantly though, in the context of the mammalian nervous system, Ataxin2 knockout decreases TDP-43 pathology in wild type TDP-43 overexpressing transgenic mice, and extends lifespan, improves motor function, and slows disease progression. The same study demonstrated that ASOs targeting Ataxin2 mRNA for RNase H mediated degradation had reduce accumulation of aggregated TDP-43 with a similar survival-extending effect after a single dose[82].

Given that reversal of RNA metabolism changes in affected neurons requires functional nuclear TDP-43, success of the ataxin-2 ASO approach may be dependent also on a cascade that includes restoring TDP-43 localization in addition to clearing cytoplasmic aggregation. This ASO development effort has transitioned to a full clinical development program at Ionis Pharmaceutical which, if successful in humans, would be the first effort to expand therapeutic strategies beyond known dominantly inherited causes of disease to potentially benefit "sporadic" ALS patients with no known underlying genetic lesion. ASOs to reduce Ataxin-2 levels are, of course, also being pursued outside of the ALS context for the treatment of SCA2 where there have been promising results in mammalian models of that neurodegenerative disease[83].

Beyond the identification of genetic modifiers of TDP-43 pathology, the second alternative strategy of engaging dysregulated downstream TDP-43 gene targets is potentially a more challenging and complex route for therapeutic advance, as TDP-43 has been proposed to have many roles including pre-mRNA processing, including regulation of RNA-metabolism, microRNA biogenesis[84], alternative splicing[73,85-87], translation[88], and RNA transport[89]. The contribution of each possible mechanistic role in disease and its key gene players has not reached such a point of maturity that obvious downstream gene targets are readily apparent, a challenge that stymied the field for 13 years after the discovery of TDP-43 aggregation in ALS. For example, in work I was involved with prior to graduate school, we demonstrated that TDP-43 played an important role in the processing of genes with long introns (a set that is enriched for neuronal-associated genes), some of which are suppressed in patient neurons affected by nuclear TDP-43 clearance[87], and additionally that TDP-43 interacts with the RNA of more than six thousand RNA genes (about a 30% of the total transcriptome) in the mouse brain by binding UG rich sequence motifs (often in introns). Indeed, acute knockdown in the central nervous system using ASOs that degrade TDP-43 encoding RNA leads to changes in expression (~600 genes) or splicing (~950 genes) of around 1,500 of those targets[73] (while, as expected, also proving quite toxic to the mice). Such an

extensive list of downstream TDP-43-affected gene targets in the central nervous system presents the field with a truly Herculean task of prioritizing and testing potential leads to identify candidates for further clinical modulation. All this is of course assuming the TDP-43 dependence of such a target of interest is even conserved between the original mouse models and human neurons (or visa-versa).

Efforts to decode RNA metabolism changes in ALS using the most authentic (human patient) “model organism” are even more complex, as nervous system tissues are only available for analysis at a single (end-stage) time point, the disease etiology of ALS naturally ablates the cell types of presumably greatest interest (motor neurons) by this time, and a loss of RNA quality on the time-scale of a routine autopsy typically leaves nothing for examination. I have the great pleasure of having worked with Dr. John M Ravits on his patient-centric alternative approach to overcome these substantial obstacles and try to identifying RNA targets that are modified in actual patient disease. The multi-pronged experimental paradigm that makes such an attempt possible in the face of those major challenges is centered around the clinical observation that while the site of disease onset from patient to patient is stochastic, the spread of degeneration and disfunction is fundamentally focal and contiguous through the three-dimensional anatomy of the upper- and lower-motor neuron compartments[2] (as can be confirmed by functional clinical testing through the disease course).

With this observation in hand, it is possible to select regions of a post-mortem patient spinal cord that not only contain the desired motor neurons, but are relatively spared of late-stage pathology. Specifically, by focusing on the alpha- motor neurons of lumbar spinal cords of patients who had either a bulbar or arm onset, the anatomical spread of motor neuron disfunction and death through the three-dimensional anatomy of the lower motor system would necessarily affect respiratory muscle denervation (resulting in death) before totally destroying the motor neurons most distal lumbar compartment. This observation, combined with the utilization of a rapid-

autopsy protocol that isolates specimens within four hours of patient death, and a laser-capture dissecting microscope to isolate/enrich the content of the desired motor neurons[90], we were able to isolate and sequence preserved mRNAs from 13 sporadic ALS patients and 9 controls (ICU patients with discontinued life-support).

With the physical and physiologic challenges thus overcome, the most difficult technical aspect remaining in such an experiment (which I was mostly not involved with) is the downstream bioinformatic analysis of RNA expression and RNA metabolism changes. By correlating the degree of phosphorylated TDP-43 aggregation in these patients to their RNA expression profiles one such informatic identification was the differential expression of casein kinase 1 E (CSNK1E) which was identified as tightly correlated with the pathologic TDP-43, and was shown in turn that TDP-43 regulates expression of this gene, which reciprocally promotes phosphorylation of TDP43[90]. Given the complexity in TDP-43's function (in both mice and man) maintaining normal RNA metabolism within the transcriptome of the nervous system, it should be no mystery why it took 13 years to discover a downstream neuronal gene target that is an appropriate clinical lead for TDP-43 proteinopathies and sporadic ALS.

TDP-43 mediated Stathmin-2 loss-of-function as a key driver of axonal degeneration

The pioneering discovery of cytoplasmic protein accumulations of the RNA/DNA binding protein TDP-43 in affected neurons of almost all instances of ALS (>95%) and at least 50% of FTD profoundly changed the direction of research in amyotrophic lateral sclerosis (ALS) and frontotemporal dementia (FTD). Aside from obvious TDP-43 aggregation, nuclear clearance of TDP-43 has been widely observed in affected neurons in sporadic ALS[69] (Figure 1.6 A-C), evidence strongly supporting the proposal that TDP-43 loss of function (and by extension, loss of RNA metabolism) is a key aspect of disease mechanisms underlying ALS pathogenesis. However, a direct mechanistic link between TDP-43 dependent defects in RNA metabolism and neurodegeneration was lacking until Ze'ev Melamed from our team identified that the mRNA

encoding stathmin-2 (also called SCG10, transcribed from the STMN2 gene), a neuronal growth-associated protein involved in microtubule dynamics, is the neuronal gene most affected by reduction in TDP-43 function[91].

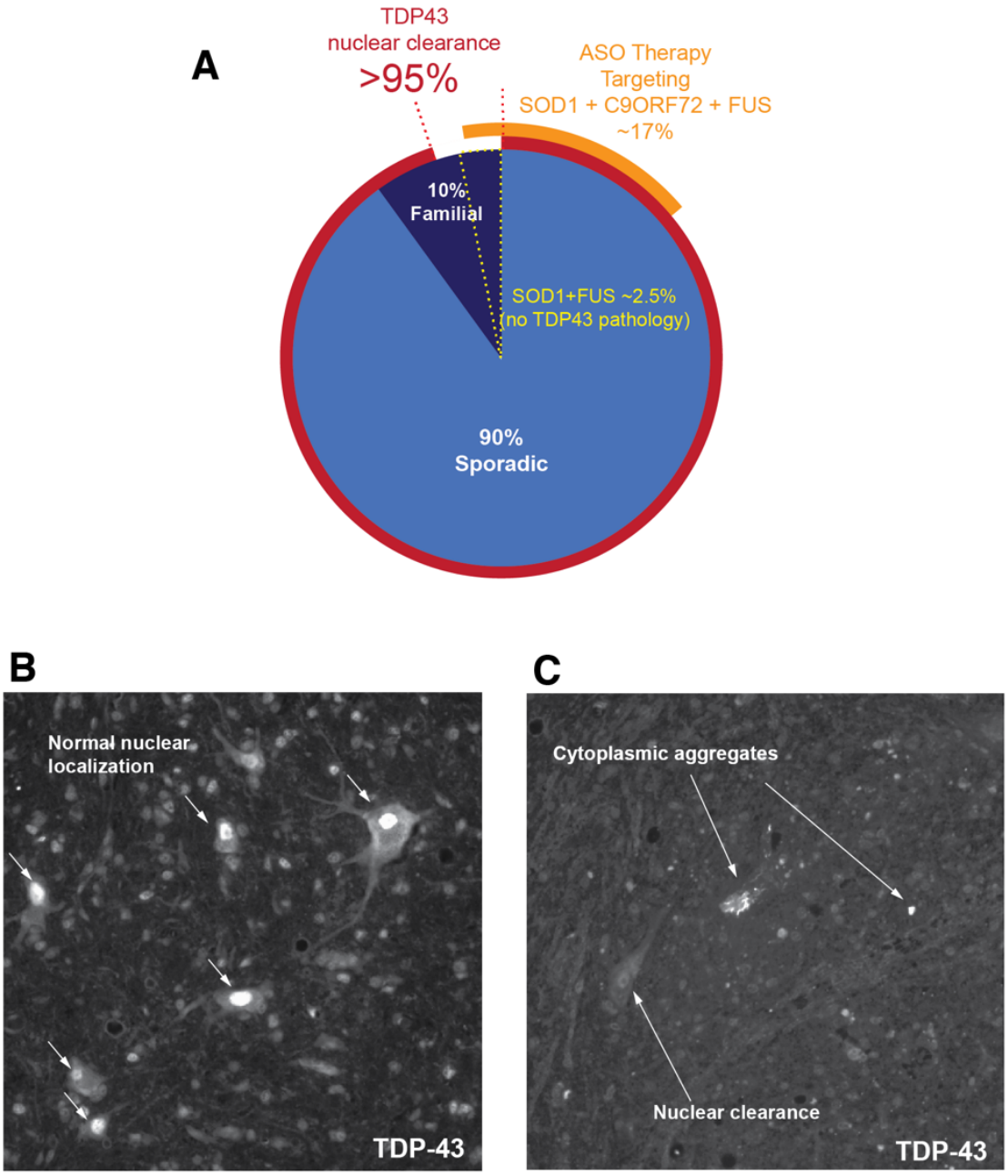

Figure 1.6 Nuclear clearance and cytoplasmic aggregation of TDP-43 is a defining pathological hallmark of Amyotrophic Lateral Sclerosis (ALS).

(A) Graphical representation of ALS heritability and pathology depicting apparent 10% familial heritability of cases versus 90% of cases with no recognizable pattern of familial heritability, present ASO therapies targeting heritable genetic causes of ALS and their combined relative proportion of all disease depicted in orange, proportion of all patients carrying SOD1 and FUS mutations which do not show nuclear clearance and aggregation of TDP-43 depicted in yellow, proportion of patients with nuclear clearance of TDP-43 depicted in red. (B) Immunofluorescence staining depicting normal nuclear localization of TDP-43. (C) Immunofluorescence staining depicting TDP-43 nuclear clearance and cytoplasmic aggregation.

Microtubules are essential components of the neuronal cytoskeleton, providing tracks for intracellular transport[92,93], a structure by which to position organelles[94], and essential for neuronal migration[95]. Correct microtubule assembly, organization and remodeling are essential for successful neuronal development and maintenance as well as maintaining the stability, shape and proper function of the neuron[92]. Accordingly, microtubule defects have long been implicated in a variety of neurodevelopmental and neurodegenerative diseases[95], but have never before been directly linked to RNA metabolism defects observed in TDP-43 proteinopathies. The microtubule core structure is built from α-tubulin and β-tubulin heterodimers, which polymerize in a head-to-tail arrangement to form a polarized cylindrical tube of approximately 25nm in diameter[96]. An intrinsic property of microtubules is their "dynamic instability" [97], i.e., the ability to switch between rapid polymerization and rapid shrinkage (known as catastrophe) at the "plus-end" of the cylinder, in a process that is largely dampened by microtubule-associated proteins[98].

The stathmin gene family, so named from the Greek "stathmos" for relay, was originally identified through stathmin-1, a small protein whose phosphorylation in pituitary and insulinoma cells was regulated by extracellular factors[99-101]. Sequence similarity subsequently enabled identification of other members of the stathmin gene family, numbering four in total (for vertebrates): including the original stathmin-1 (also known in the literature as stathmin or Op18) which is ubiquitously expressed with 90.8% identical amino acid sequences between mice (142 residues) and human (141 residues); stathmin-2 (also known as SCG10) which is 100% identical in its 179 amino acids between mouse and man; stathmin-3 (or SCLIP) 96.4% identical between the 169 amino acid human version and 180 amino acid mouse copy; and stathmin-4 (or RB3) 99.4% identical in alignment between mouse and human but with the mouse version containing 9 additional amino acids past the 167 human gene.

Stathmin-2, -3, and -4 are almost exclusively expressed in nervous tissue[102-104]. Among these, translating ribosome affinity purification and RNA-sequencing experiments performed in

mice revealed that stathmin-2 is by far the highest expressed in neuronal cell types, with comparatively low expression in glia and oligodendrocyte cells[105]. Similarly, RNA-seq from isolated human lumbar motor neurons identified stathmin-2 to be among the top 25 highest expressed genes in this ALS-critical cell[90,91]. The human stathmin proteins are characterized by conserved "stathmin-like domains" (SLD), which present 65-75% amino acid identity to stathmin-1 and harbor two tubulin binding regions. Stathmins-2, -3 and -4 present an additional N-terminal domain, which is implicated in the membrane targeting of these proteins through two palmitoylation sites and a Golgi-targeting sequence[106].

Stathmins were initially described as microtubule destabilizing factors due to their inhibition of MT polymerization in vitro[107-109], and were later implicated in neuronal differentiation and plasticity[110]. The SLD domains of different stathmin isoforms have been shown in vitro to have distinct kinetics and affinities with tubulin heterodimers, properties altered by phosphorylation[111]. Additionally, each isoform presents distinct expression profiles during development and throughout the adult nervous system, suggesting these proteins possibly play distinct roles in vivo[103,104,110,112,113]. There is, however, some evidence for functional redundancy or compensatory mechanisms as well: homozygous knockout mice for *Stmn3* and *Stmn4* present no significant alterations in anatomy, physiology or behavior (unpublished data from Sobel & Devignot)[106]; stathmin-1 null homozygous mice also develop normally[114], but during aging present mild axonopathy[115]. Interestingly, the only stathmin-2 null mice described in the literature are reported to die shortly after birth, suggesting stathmin-2 to play a crucial role in the nervous system during development[106].

Stathmin-2 was first detected in the murine nervous system, with a strong presence in the developing embryo and in specific regions of adult tissue[112,113]. More specifically, it was found in perinuclear cytoplasm, axons (as puncta), and growth cones of cultured neurons[113], and high

levels of *Stmn2* mRNA expression were found in long-distance projecting neurons (sensory and motor) and in neurons with extensive dendritic arbors[112]. More recently, stathmin-2 was shown to be anterogradely transported along axons[116] and has been implicated as an essential component of axonal regeneration in murine sensory neurons[116,117]. Critical for the development of a stathmin-2 restoring therapeutic strategy, the role of stathmin-2 in neurite outgrowth and axonal regeneration is apparently contingent upon carefully regulated levels of this protein, as previous studies using hippocampal neurons overexpressing stathmin-2 have reported collapsing growth cones, with more "moderately" increased expression levels stimulating neurite outgrowth[118,119].

Despite the early identification of strong stathmin-2 expression in motor neurons, our current knowledge about the roles of stathmins during aging is very limited, with existing literature focusing mostly on development[106], with a smaller sub-set focusing on axonal regeneration in injured sensory neurons[116,117,120,121]. A crucial piece of evidence for the potential role of stathmin function in the maintenance of motor neuron connectivity and stability came from an experiment of the Goldstein laboratory at UCSD wherein loss of function mutations of the stathmin homolog (*stai*) in Drosophila, led to the retraction of motor neurons from previously innervated neuromuscular junctions[122].

Ze'ev Melamed started his investigation utilizing two independent unbiased experimental strategies: siRNA knockdown of TDP-43 expression in the stably diploid neuroblastoma SH-SY5Y cell line of substantial neuronal character[123], and homozygous CRISPR-Cas9 knock-in of ALS-linked N352S TDP-43 mutation into the same line, followed in both cases by RNA-seq to identify major RNA changes. In both experiments, in addition to the hundreds of previously described mRNAs that were substantially changed in expression or splicing after reduced TDP-43 expression or function, stathmin-2 was identified as the most affected RNA. Indeed, stathmin-2 RNA levels changed it from one of the top-expressed genes in that cell line to a 6-fold reduction

in overall expression upon TDP-43 suppression, surpassing even the reduction (4-fold) of TDP-43 encoded RNAs that were targeted by siRNA treatment in the first place. This stathmin-2 suppression was also true at the protein level, where western blot indicated a near total loss of the stathmin-2 protein in cells treated with TDP-43 targeted siRNA pools. Analysis of mapped reads along the stathmin-2 gene from the RNA-seq data, followed by extensive cloning and 3' end sequencing of anchored dT-primed cDNA revealed that loss of full-length stathmin-2 mRNA in cells with reduced TDP-43 expression or function was the result of truncating premature polyadenylation from within a cryptically spliced terminal exon (located within the first intron of the stathmin-2 gene), producing a non-functional short RNA with an open reading frame of only 17 codons (vs the 180 codons of the full-length gene)[91]. Correspondingly, stathmin-2 is strikingly lost from motor neurons in sporadic ALS and inherited disease from GGGGCC expansion in C9orf72. I will expand upon this and other human patient evidence in the next chapter where I describe stathmin-2 loss as a hallmark of TDP-43 proteinopathy.

Stathmin-2 is similarly lost from iPSC derived motor neurons in a TDP-43 dose-dependent manner, with stathmin-2 reduction levels again far outpacing TDP-43 reduction. To assess the functional consequences of stathmin-2 depletion in the axonal regeneration process, motor neuron precursors were seeded into the proximal somatic compartment of a microfluidic device (Figure 1.7 A). Over a seven-day maturation period, axons extended through micro-groove-embedded channels (830 μm in length) that exclude neuronal cell bodies but allow axonal extension into the distal compartment. Matured motor neurons were treated for 20 days with ASOs added to the somatic compartment to reduce synthesis and accumulation of either TDP-43 or stathmin-2 (Figure 1.7 A, B). Axons were maintained after loss of either protein. After axons in the distal compartment were mechanically axotomized, axonal regrowth of motor neurons treated with non-targeting, control ASOs initiated within 24 hours. Stathmin-2 appeared in a punctate pattern along these regenerating axons and accumulated in the growth cones, consistent with a

role in promoting axonal regrowth (Figure 1.7 B, C). Remarkably, following ASO-mediated reduction in stathmin-2 or TDP-43, axonal regeneration after axotomy was almost completely suppressed, and this regeneration was restored by the restored expression of lentiviral delivered stathmin-2 protein coding sequence (Figure 1.7 C, right panels). These data demonstrate a reversable increased vulnerability of motor neurons upon reduced accumulation of the neuronal-growth factor stathmin-2, and establish stathmin-2 restoration as an attractive therapeutic target for sporadic ALS and TDP-43 proteinopathy.

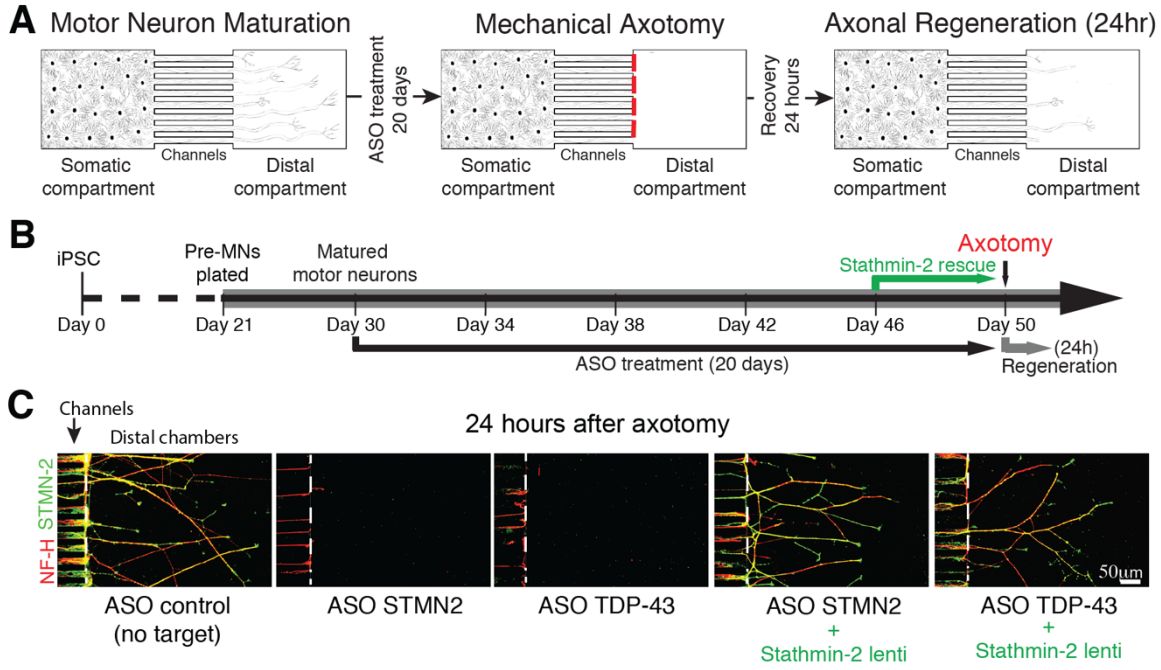

Figure 1.7 Stathmin-2 expression is essential for axonal regeneration capacity in human cultured motor neurons, and its restoration upon TDP-43 depletion restores axonal regrowth.
(A) Schematic of human iPS-derived motor neurons grown in microfluidic chambers before and after axotomy. (B) Timeline of differentiation in-vitro showing TDP-43 or stathmin-2 targeted ASO reduction starting at day 30, and lentiviral transduction of stathmin-2 coding sequence at day 46, with axotomy and 24hr re-growth starting at day 50. (C) Immunofluorescence staining of axons emerging from microfluidic channels into distal compartment 24 hours after axotomy, depicting stathmin-2 protein in green and neurofilament heavy protein marking mature axons in red, ASO treatment and lentiviral stathmin-2 restoration indicated by labels below images.

Challenges of drugging inherited diseases of the central nervous system and the promise of present and future nucleic acid therapeutics

Though work by geneticists over the past few decades has identified the genetic basis of many inherited (and some aging related) neurodegenerative and diseases, the exact downstream mechanisms and molecular drivers of toxicity in these conditions often remain elusive and/or controversial, thwarting small molecule (and monoclonal antibody) drug development for these conditions, as few agreed upon mechanistic targets mean few practical readouts by which to design a drug screen and poor efficacy in those molecules advancing to patient trials. This is evidenced by the fact that no effective treatments have been found to date to substantially slow disease onset or progression in ALS, though lack of substantial effect has not prevented the US FDA from approving two woefully inadequate drugs for use in ALS patients. The first, Riluzole (approved in 1995) is not only very costly to patients and their families but is associated with only a 2-3 month overall survival benefit[124]. Still worse, the drug Radicava (edaravone), (approved by the FDA in 2017) based upon a claim of modest change in ALS functional rating score[125] (ALSFRS) is controversial in retrospective analysis of the trial data as to whether it showed any actual benefit in the first place[126] (and comes with its own risks of infusion-related complications and side effects). These drugs are widely seen in the scientific and medical community as a costly false hope for patients, who (lacking superior alternatives) also sometimes fall victim to unevaluated or anecdotal “snake-oil” treatments or seek out stem cell infusions (of dubious authenticity) or other such interventions overseas. There is, however, reason for cautious optimism at the emergence of both new gene targets and the application of new technological advancements capable of engaging those implicated genetic lesions within the central nervous system.

Early first-generation gene silencing using virally delivered shRNAs or microRNAs and direct siRNA infusion, though on-target mechanistically, were limited in utility by effecting gene expression in only a small vicinity around the site of administration, and (at the time) had limited therapeutic utility (without substantial further development[127]). Initial delivery options via direct injection to the brain were both limited in efficiency and risky, and disease pathology is often broadly distributed. By comparison, while peripherally infused antisense oligonucleotide (ASO) drugs do a poor job of penetrating the blood-brain barrier, intrathecal (IT) administration into the cerebrospinal fluid (CSF) via lumbar puncture (quite unexpectedly) results in broad delivery to cells throughout the brain and spinal cord[128-130]. As to whether an IT route of infusion is practical and feasible in a clinical context, more than 11,000 patients have been dosed with ASO drugs by intrathecal route in clinical trials to date, with minimal occurrence of adverse events. CSF-sampling time-course data from humans suggest that most of the detectable ASO drug is cleared from the spinal fluid within 24 hours of dosing[130], indicating that whatever yet unexplained cellular uptake pathway being utilized by the drug acts rapidly upon administration. In spite of this apparently rapid clearance, ASO molecules can persist within non-dividing cells for weeks or months and even very small amounts within the active compartments of a cell can exert a sustained and dramatic effect on RNA abundance[48,128,131-133]. Once taken up into their active compartment in a cell, modified Antisense Oligonucleotide drugs (ASOs) utilize Watson-Crick base pairing to sterically bind their specific RNA target molecules effect RNA processing, maturation, and translation (by denying access to splicing factors, RNA binding proteins and/or ribosomal machinery) or by serving as a substrate to activate RNase H recognition of RNA-DNA heteroduplexes, leading to catalytic degradation of the RNA molecule. The mechanism of action, “steric binder versus substrate” is determined by internal chemistry design considerations (discussed below). The ability of ASO drugs to target the product of a primary genetic lesion, irrespective of the precise mechanism of downstream underlying toxicity, and to do so broadly

and durably across a range of cell types after a single site of administration sets them apart as a potential game changing approach for genetic diseases of the central nervous system, especially those that display non-cell autonomous onset and progression[134].

Starting with the first proof-of-concept experiments lowering mutant SOD1 in transgenic rats starting in 2006[135], culminating in a first-in-man trial of ASOs in the central nervous system to lower SOD1 levels in patients[136], followed by a major effort to lower levels of mutant expanded Huntington in animal models and then human patients[128], and more recently demonstrating the ability to lower repeat-expanded C9ORF72 in an allele-specific manner[47,48] (the gold standard of such a mutant gene targeting strategy, and an effort that I was heavily involved in), as well as the initial proof-of-concept experiments to lower mutant FUS protein with an ASO in the adult nervous system (unpublished), and most recently astrocyte-to-neuron conversion with PTB-reducing ASOs[137], the Cleveland Laboratory has played a central role in the inception and development of ASO therapies for use in the central nervous system.

To date, eight ASO drugs have been approved by the FDA: Formivirsen for viral infection, Mipomersen for familial hypercholesterolemia, Eteplirsen for Duchenne Muscular Dystrophy, Patisiran and Inotersen for TTR polyneuropathy, Volanesorsen for familial chylomicronemia syndrome, Givosiran for acute hepatic porphyria, and finally Spinraza/Nusinersen, which is the only currently approved antisense drug with a CNS target. There are presently more than 50 additional antisense drugs in human trials, including many for central nervous system targets (which began on the benches of the Cleveland team)[47,48,91,128,138-141] including the culmination of this thesis project. This class of nucleic acid drugs is proving to be a powerful tool for combating previously incurable inherited diseases of the central nervous system and could revolutionize the treatment of neurological disorders.

ASO drugs require utilization of adaptive internal chemical modifications for durability, and tolerability as natural (or unmodified) single-stranded RNA and DNA molecules are susceptible to

nuclease cleavage, making them inherently unstable. Peripherally administered unmodified nucleic acids are also rapidly excreted by the kidney, rapidly degraded in-vivo by ubiquitously expressed endo- and exonucleases, and compete poorly for binding with structured RNA targets. While most mammalian cells will readily accumulate single stranded oligos, in most cases the nucleic acids do not escape endosomal compartments, and likely end up in lysosomes. Single stranded antisense oligonucleotide drugs contain phosphorothioate (PS) modifications in which one nonbridging phosphate oxygen is replaced with a sulfur, which allows increased binding to plasma proteins when peripherally administered and cell surfaces allowing them to be retained and distributed in the body for longer periods.

Unlike small-molecule drugs, ASOs have a comparatively enormous typical size (usually 18-20 bases) around 4,500-18,000 Da, and high formal charge (-19) rendering them incapable of free diffusion across a lipid bilayer[142,143]. Surprisingly, single-stranded PS oligonucleotides make it into the cytoplasm and nucleoplasm of some cell types in the absence of transfection reagents[144], even though under current paradigms of size and charge constraints, these molecules ought not gain entry into the cytoplasmic compartment[143,145], as is seen in a wide variety of cell types and tissues[144,146] including all neurons tested thus far[129]. Indeed, all ASO strategies involving central nervous system targets rely upon free cellular uptake of 18-20mer single-stranded oligonucleotides[48,128,136,139,140].

Phosphonothioate modifications to the oligo backbone, critical for uptake and durability, are certainly not the only site of chemical enhancement utilized in the design of ASOs. Just as important are chemical modifications made to the ribose sugar ring, as the location and number of these 2' modifications are carefully chosen to determine the ultimate mechanism of action of the ASO on the target RNA molecule (steric binding or catalytic RNA degradation). Sugar modifications increase nuclease protection and binding affinity while decreasing inflammation-inducing interactions within the cell, and most commonly involve methoxy-ethyl (MOE) additions

to the 2' position of the sugar ring, but can also include constrained ethyl (cEt), locked nucleic acid (LNA), 2-O-methyl modifications (especially at the second base of the 2' unmodified deoxy-nucleotide span[147]) to reduce toxicity related to off-target protein binding, or 2-fluoro additions (less common, but sometimes used in drugs like Eteplirsen are sugar-phosphate morpholino modifications)[147,148]. Since 2'-positions are not compatible with RNase H recognition, ASOs designed to catalytically degrade their target molecules leave a "core" of 8-10 base pairs free of 2' modifications (typically using normal deoxynucleotides at these positions) to retain this enzymatic recognition capacity, while "wings" of 2'-modified bases are included but restricted in location to the outer 4-6 bases at the 5' and 3' ends, respectively. ASOs designed to act via steric binding, by contrast, may contain modifications to the 2' position of the ribose sugar at all bases, as enzymatic recognition is undesirable in these applications.

To illustrate these different uses and design pathways in the context of two inherited nervous system disorders, consider FDA-approved Spinraza splice modifying ASO versus the Ionis-C9RX ASO0 (presently in trial to degrade repeat-expanded C9ORF72). Spinraza was designed for the treatment of spinal muscular atrophy (SMA), an autosomal recessive disorder that is the most common genetic cause of infant death, caused by inherited homozygous loss of function mutations in the SMN1 gene which encodes the 294 amino-acid "survival of motor neuron" protein on chromosome 5. As would be logically suggested by inverse-eponym, a lack of SMN protein leads to early-life (though not congenital) death of the motor neurons of the spinal cord, leading to atrophy of the voluntary muscles of the limbs and trunk, and what is described clinically as a "failure to thrive" as infants fail to reach developmental motor milestones (self-support of the head and neck, ability to sit unassisted, crawl or walk).

The longevity for these patients depends largely on the copy-number of a modifier gene (SMN2, discussed momentarily) with "Type 0 and 1" patients dying before 1 year of age of respiratory failure (like ALS, SMA is a truly sinister disease), Type 2 mostly living beyond 25 years,

and Type 3/4 being unaffected in lifespan but affected by weakness or dystrophy. The genetic modifier of disease, and key to the ASO rescue strategy, is an inverted duplication of the SMN1 gene, SMN2, which (freed from evolutionary selective pressure post-gene duplication) has acquired a C to T mutation in the sixth position of exon 7. This mutation, though translationally silent in terms of resulting polypeptide sequence, is necessary to maintain proper splicing and inclusion of exon 7 to the full-length transcript. The C to T mutation reduces proper splicing frequency by approximately 90%. As tandem duplications of SMN2 are common, the 10% of functional transcripts produced by each duplicated allele gene encode a polypeptide that compensates for the loss of the SMN1 protein, setting the stage for a dose- and thus SMN2 copy-number dependent gradient of disease severity in the affected kids.

Spinraza, an 18-mer full phosphonothioate modified, and critically, full 2'-methoxy-ethyl modified (full, meaning modified at every available base or backbone phosphate position) of sequence 5'-UCACUUUCAUAAUGCUGG-3', which binds a complementary splice repressor site starting 9 bases into intron 7. Since the Spinraza ASO drug is designed with 2' sugar modifications throughout its length, it is not a substrate for RNase H mediated RNA cleavage, and therefore simply binds and sterically blocks the access and coordination of normal RNA binding proteins on the pre-mRNA. In this case ASO binding sterically blocks the normal binding site for hnRNPA1 and hnRNPA2 proteins which mediate the exclusion of Exon 7 from the SMN2 pre-mRNA. The result is a mature mRNA product that, instead of excluding exon 7 at a rate of 90%, now conversely includes exon 7 at that rate, encoding a functional SMN polypeptide[130,148,149].

By contrast, the patient-facing version of the Ionis-C9RX ASO (as opposed to "research grade" oligos used in proof-of-concept experiments in c9ALS/FTD cell lines I described previously) contains far greater internal complexity, taking significant advantage of "Generation 2.5" combinational chemistries pioneered by Ionis medicinal chemists. Allele specific targeting is achieved with an ASO whose 18 base sequence is 5'- GCCCCTAGCGCGCGACTC -3' allowing

the oligo partly bind the 5' end of the repeat expanded $GGGGCC_{(n)}$ (though, critically, not targeting the repeat sequence exclusively and directly as this has significant off-target toxicity). While the basic "rough-draft" RNase H recruiting ASO design principles remain, such as restricting 2' sugar modifications to 4-6 bp on the 5' and 3' flanking ends for sustained RNase H recognition of a deoxynucleoside core sequence, and including phosphorothioate modifications especially at either end for exonuclease resistance and in the deoxy-core for endonuclease protection, the combinational chemistry compositions applied in this case incorporate novel strategies regarding how phosphorothioates, methylcytosines, and constrained methoxyethyls, and normal phosphodiesters are utilized throughout the molecule along with (occasionally) other modifications to maximize target engagement and tolerability, with the final compound used in human trials being an asymmetric 4-8-6 MOE gapmer with phosphodiesters at linkages 2, 3, 13, 14, 15, and irregularly interspersed constrained MOEs in the wings. This is a truly chaotic looking molecule compared with the relative internal simplicity of Spinraza.

Of course, as antisense technology has advanced, so have the technological underpinnings of competing gene silencing techniques, especially the "gene therapy" field centered around Adeno-Associated Virus (AAV) delivery of gene replacement and RNAi-activating cargos. In the central nervous system these gene therapy advances have been driven recently primarily by improvements in administration[150,151], production, and payload design[152-155]. Additionally, the field is positioned to gain substantially in the coming 5-10 years from the advent of discovery pipelines for the identification of novel viral capsids[156], capable of greater cell or tissue targeting specificity and efficiency[157].

This ASO-AAV duality of nucleic acid drug advance is perhaps best exemplified by the examples of Spinraza vs Zolgensma (Onasemnogene abeparvovec). Spinraza, already covered in detail, was the first ASO drug approved by the FDA for use in the central nervous system[130]

and the first FDA-approved treatment for Spinal Muscular Atrophy. Zolgensma is an AAV-transduced single-dose gene-replacement approach targeting the same condition, delivering a replacement copy of the SMN1 gene administered at 1.1x10^14 vector genomes per kilogram of body weight into infants via intravenous infusion (along with a regimen of immune-suppressing corticosteroids). Compared with the dosing schedule of Spinraza, which is (12mg [5ml] per administration via lumbar puncture into the cerebral spinal fluid starting with four loading doses and then a maintenance dose once every 4 months for the entire life of the patient), it is clear that there is a significant advantage to a one-shot cure. By contrast, the fact that Spinraza is reversable means that should toxicity arise there is an option to discontinue treatment, the same cannot be said of an AAV approach, where overexpression toxicity is a realistic concern[158]. In terms of cost, both drugs have been widely criticized for their exorbitant price tags, with Spinraza costing about $750,000 for the first year of treatment and around $375,000 per year after, and Zolgensma holding the record for the costliest drug in the world at a price of $2,125,000 for that one shot infusion.

Correspondingly for ALS caused by mutant SOD1, there is competition in the nucleic acid therapy space between Torfersen (BIIB067 or formerly IONIS-SOD1Rx, but could just as rationally be called UCSD-Rx1) the original application of ASO use in the central nervous system to silence mutant SOD1 by RNase H recruitment[135,136,138], versus an AAV-delivered small RNA to silence mutant SOD1 synthesis[159]. Although Novartis (who purchased Avexis, the company developing the AAV approach) has decided, to the disappointment of much of many in the scientific community involved in the development process, to discontinue pursuit of that approach or undisclosed reasons. (I might speculate it may have to do with a combination of anticipated dosing complexity with anticipated incomplete administration by a simple intrathecal or cisternal infusion, the total cost associated with an adult-scale viral vector dose versus the relative ease of intravenous administration for Zolgensma, or perhaps contributing could be a failed similar

approach[160].) Phase 3 data from Torfersen are not disclosed yet, but widely reported anecdotal evidence is positive thus far, including stabilization of disease for three carriers of the most aggressive mutation in SOD1 (A4V), and media coverage of an open-label extension patient with apparently stabilized bulbar onset disease (the normal course of which would have killed him about 1 year prior to the report).

Not all applications of nucleic acid drugs in the central nervous system have seen positive outcomes. One report (with only 2 patients) of a microRNA mediated SOD1-suppressing AAV resulted in one patient with no clinical benefit, and another with substantial chronic post-operative pain[160]. A long-anticipated phase 3 ASO trial for Tominersen to lower synthesis mutant Huntington, despite quite positive phase 2 data showing good target engagement and tolerability, was also recently discontinued by recommendation of an independent data monitoring board after review of ongoing trial data showed an apparent worsening of the treated group versus control (final data still being analyzed)[161].

That ASO drugs enjoy some yet-unknown (and unexpected by first-principles) path into cells of the central nervous system vs their nucleic acid drug contemporaries is a double-edged sword: fortuitous if targeting a cell population and structure that enjoys robust free-uptake from the cerebral spinal fluid[129], but also inherently difficult to steer levels of target engagement in specific cell types of the central nervous system by rational design, and difficult or impossible (in the event of a trial failure) to determine directly what dose of drug arrived at the active compartment of an affected cell to determine molecular failure modes or possible paths forward. Conversely AAV-mediated gene therapy approaches, while understood in their pathways of targeting and delivery (with target cell tropism options well positioned to expand in the coming years), remain irreversible in their action and are not presently amenable to the possibility of re-dosing.

Chapter 2: Stathmin-2 RNA Misprocessing is a Hallmark of TDP-43 Proteinopathies

Abstract:

Amyotrophic lateral sclerosis, frontotemporal dementia, dementia with Lewy bodies and limbic-predominant age-related TDP-43 encephalopathy are all associated to with mislocalization of the RNA binding protein TDP-43. Ze'ev Melamed identified that the most consequential downstream RNA change within a neuron upon loss or mutation of nuclear TDP-43 was aberrant splicing and premature polyadenylation of the pre-mRNA transcript encoding stathmin2, a gene essential for normal axonal regeneration and neuromuscular junction maintenance. Here I utilize reverse-transcriptase polymerase chain reactions, RNA chromogenic in-situ hybridization, and laser-capture microdissection RNA-sequencing to establish that stathmin-2 pre-mRNA misprocessing and truncation are hallmarks of amyotrophic lateral sclerosis in both the upper and lower motor neuron compartments or patient post-mortem tissues.

Introduction:

Fifteen years ago, Neumann and Arai discovered that the normally nuclear RNA binding protein TDP-43 was the key polyubiquitinated component of cytoplasmic protein aggregates common to 97% of ALS and about half of FTD[68,69], a fundamental discovery that changed the field of neurodegenerative disease research, particularly for those two diseases. Today it is accepted that nuclear clearance of functional TDP-43 is a key point of pathophysiologic convergence for nearly all forms of ALS, and remains the primary finding that links inherited and sporadic forms of the disease. In spite of this pathology observation, perhaps the most important question in the field – or at least the one with the greatest potential to shape new therapeutic advances – the identification of a direct mechanism linking TDP-43 nuclear loss to a disruption in

neuronal homeostasis and axonal degeneration at the molecular level, has proven elusive for thirteen of those fifteen years since that founding discovery. Since TDP-43's central function is in RNA processing activities including transport, splicing and transcription, with thousands of nascent RNA targets, it is anticipated that nuclear TDP-43 loss in disease drives processing perturbation in many genes.

A discovery initiated in July of 2017 (published in 2019) by Ze'ev Melamed identified that siRNA suppression or homozygous mutation of TDP-43 in a human neuron-like cell line resulted in the near total loss of expression of the typically five-exon mRNA that encodes an alpha-beta tubulin heterodimer binding protein, stathmin-2. Stathmin-2 plays a critical role in microtubule dynamics, as microtubules are key components of the cytoskeleton that allows large motor neurons to maintain their enormous axonal projections (up to a meter). Microtubule associated proteins dampen the dynamic instability of microtubule structures, which normally switch between rapid catastrophe and polymerization. The only essential mammalian stathmin, stathmin-2 is one such protein that is primarily neuronally expressed, and (though still unclear) is thought to be important of neuronal outgrowth by affecting microtubule dynamics at growth cones either by sequestering tubulin to prevent microtubule assembly or by directly promoting catastrophe.

Melamed identified that loss of the mRNA encoding stathmin-2 was due to the incorporation of a short cryptic exon within the normal first intron of the stathmin-2 gene, which, when spliced into the elongated transcript utilized an alternative polyadenylation signal to truncate the RNA, resulting in a short mRNA encoding only 16-amino acid (vs 179). I here use various methodologies and rapid-autopsy acquired patient post-mortem tissues to determine that the accumulation of truncated stathmin-2 RNA with a cryptic truncating exon in both upper and lower motor neuron compartments is a hallmark of TDP-43 proteinopathy-driven ALS cases, but is not detected in the small fraction of non-TDP-43 driven cases or in unaffected control individuals. This hallmark of TDP-43 proteinopathies is an important emerging molecular biomarker of early TDP-

43 disfunction in disease and establishes stathmin-2 pre-mRNA misprocessing as a general disease feature.

Results:

RT-PCR analysis using primers spanning the splice junctions of normal stathmin-2 exon-1 and the cryptic exon2A in RNAs extracted from anterior horn grey matter in thoracic spinal cord from 13 sporadic ALS patients and three familial ALS patients carrying inherited hexanucleotide GGGGCC expansion in C9orf72 revealed in all cases robust cryptic exon incorporation and premature polyadenylation of stathmin-2 mRNA in all cases. This RNA signature was notably absent from eight healthy individuals and three familial ALS patients with SOD1 mutations (Fig 2.1 A,B), consistent with premature polyadenylation of stathmin-2 mRNA being triggered by TDP-43 dysfunction, as TDP-43 pathology is found in sporadic-ALS of unknown origin as well as both sporadic- and familial-ALS linked to C9orf72 expansion[64,162] but not SOD1-mediated ALS[163]. This indicates that loss of stathmin-2 expression by cryptic exon splicing and polyadenylation is a marker specific to TDP-43 dependent neuronal disfunction, as opposed to a general biomarker of neurodegenerative disease.

Figure 2.1 TDP-43 dependent stathmin-2 RNA truncation by cryptic splicing and polyadenylation in affected patient nervous system tissues is a hallmark of TDP-43 proteinopathy.
(A) Schematic of human gene encoding stathmin-2, depicting normal constitutive five exons in grey and cryptic exon in red along with the normal and truncated RNA products. (B) RT-PCR of RNA isolated from the grey matter of human patient thoracic spinal cord using primers specific to misprocessed truncated RNA containing cryptic terminal exon2a reveals accumulation of truncated RNA in the lower motor compartment of patients with TDP-43 proteinopathy, but not in control patients or ALS patients with mutations that precipitate disease without TDP-43 disfunction. (C) RT-PCR of RNA isolated from human patient motor cortex grey matter using primers specific to misprocessed truncated RNA containing cryptic terminal exon 2a reveals accumulation of truncated RNA in the upper motor compartment in most sporadic and familial ALS patients, but not in unaffected control patients. (D) RT-PCR of RNA isolated from frontal cortex grey matter of patients with clinical frontotemporal dementia using primers specific to misprocessed truncated RNA containing cryptic terminal exon 2a reveals accumulation of truncated RNA in that tissue, but not in unaffected control patients. (E) Schematic of tissues isolated for this experiment.

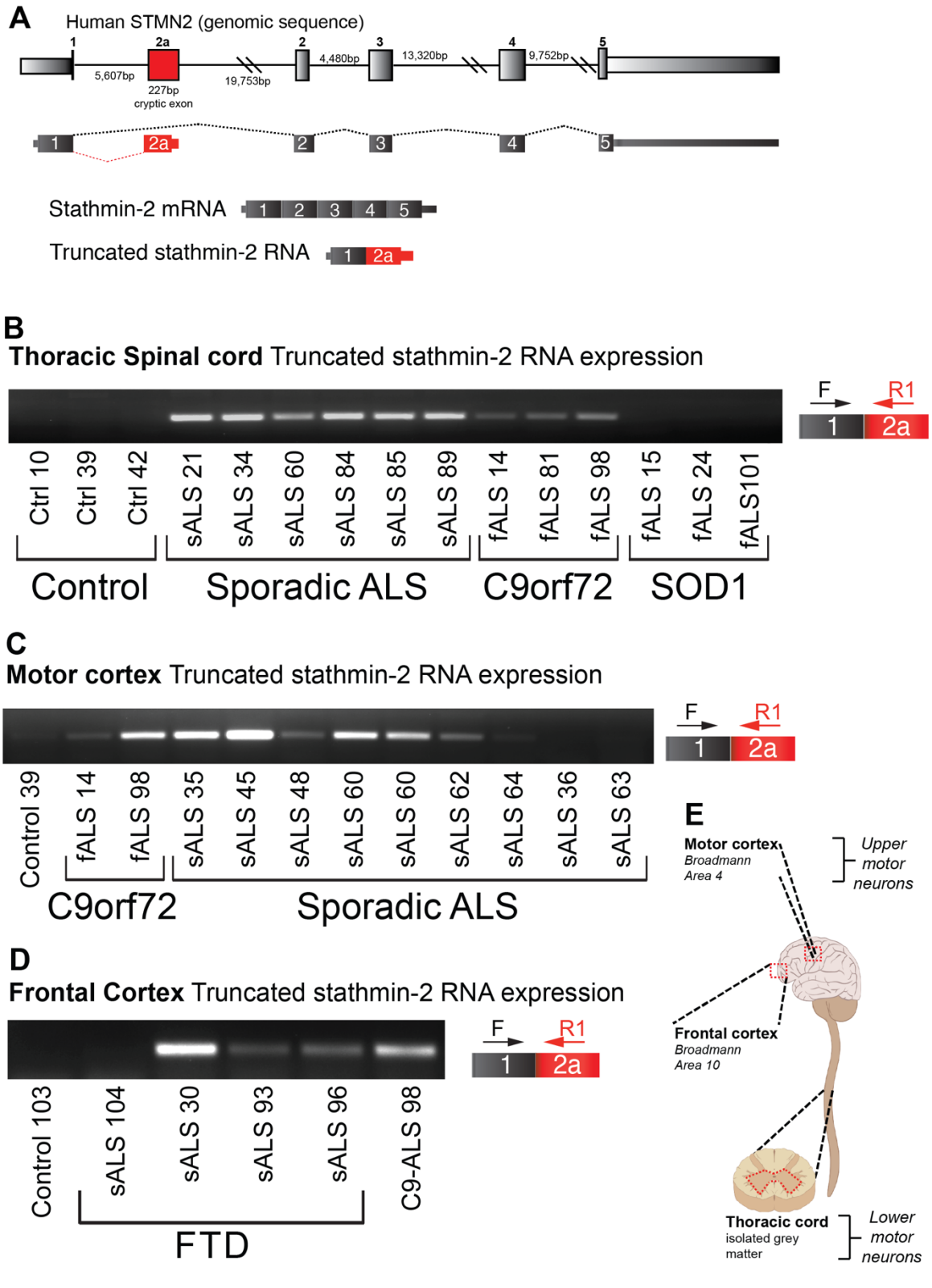
A
Human STMN2 (genomic sequence)
1
2a
2
3
4
5
5,607bp
227bp
cryptic exon
19,753bp
4,480bp
13,320bp
9,752bp
Stathmin-2 mRNA
Truncated stathmin-2 RNA
B
Thoracic Spinal cord Truncated stathmin-2 RNA expression
F
R1
Ctrl 10
Ctrl 39
Ctrl 42
sALS 21
sALS 34
sALS 60
sALS 84
sALS 85
sALS 89
fALS 14
fALS 81
fALS 98
fALS 15
fALS 24
fALS101
Control
Sporadic ALS
C9orf72
SOD1
C
Motor cortex Truncated stathmin-2 RNA expression
Control 39
fALS 14
fALS 98
sALS 35
sALS 45
sALS 48
sALS 60
sALS 60
sALS 62
sALS 64
sALS 36
sALS 63
C9orf72
Sporadic ALS
D
Frontal Cortex Truncated stathmin-2 RNA expression
Control 103
sALS 104
sALS 30
sALS 93
sALS 96
C9-ALS 98
FTD
E
Motor cortex
Broadmann
Area 4
Upper
motor
neurons
Frontal cortex
Broadmann
Area 10
Thoracic cord
isolated grey
matter
Lower
motor
neurons

Analysis of the RNA sequencing reads mapping to the stathmin-2 gene from sets of human motor neurons, which I isolated by microscopic laser microdissection from the Rexed laminae 9 of lumbar spinal cords of sporadic ALS patients who met the El Escorial criteria for definite ALS, and were followed in their clinical course of disease. The tissues were selected from patients who had either an arm or bulbar onset of disease with a caudally progressing phenotype thus preserving lumbar motor neurons for post-mortem isolation), or from unaffected control patient tissues identically collected. Examination of aligned sequencing reads revealed a clear segregation between the two phenotypes at a locus within the normal stathmin-2 intron 1. All analyzed sporadic ALS patients (n=13) contained an included cryptic exon 2a (Figure 2.2 C) as the chief terminating exon (with polyadenylation apparent at the individual read level). By contrast, RNA-seq reads aligning within the same exon 2a locus were absent in all tested (n=7) non-ALS individuals (Figure 2.2 B). The sporadic ALS patients showed an overall loss of full-length stathmin-2 expression of about two-fold compared with the unaffected control group, while ranked overall gene expression in the lumbar motor neurons of control individuals placed stathmin-2 expression among the top-20 most expressed genes of this cell type (proximal in ranking to the hyper-abundant neuronally expressed neurofilament genes).

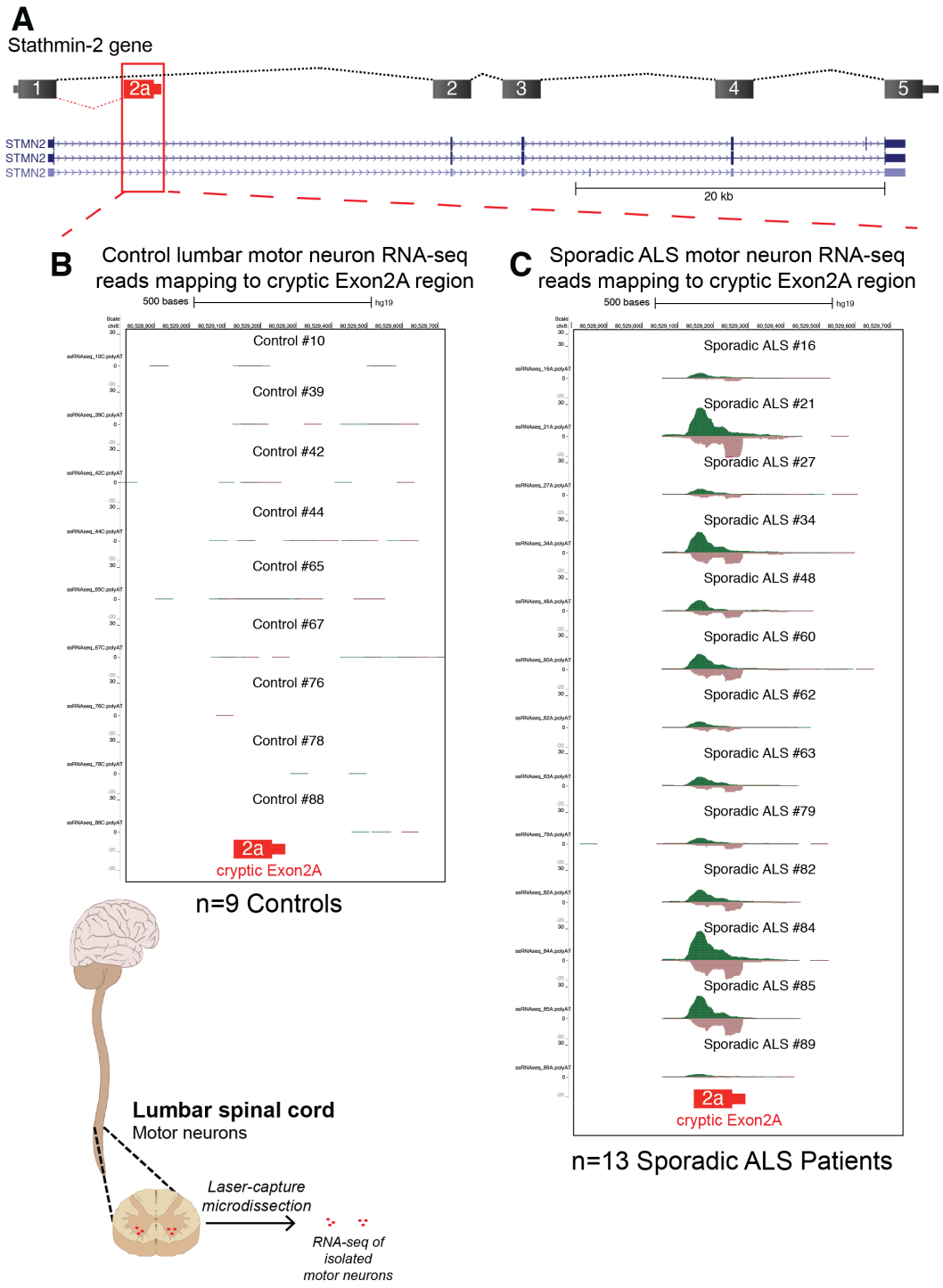

Figure 2.2 RNA-seq reads mapping to cryptic exon2a perfectly delineate spoadic ALS patients from unaffected controls in laser-capture microdissected lumbar motor neurons.

(A) Schematic of human gene encoding stathmin-2, depicting cryptic exon2a expanded view. (B) RNA-seq reads mapping to cryptic exon2a region are absent in lumbar motor neuron enriched isolated RNAs of unaffected control individuals. (C) RNA-seq reads mapping to cryptic exon2a are detected in lumbar motor neuron enriched isolated RNAs all 13 sporadic ALS patients examined.

Having established that stathmin-2 is cryptically spliced and polyadenylated in the lower motor neuron compartments of ALS patients with TDP-43 pathology, I next examined RNA isolated from grey matter of the upper motor neuron compartment within Brodman area 4. Using RT-PCR I detected the truncated stathmin-2 RNA in six out of nine sporadic ALS motor cortex samples examined (correlating with upper motor neuron dysfunction), and both of two familial C9orf72, but not in aged controls, again consistent with TDP-43 pathology in these patients (Figure 2.1 C). Since TDP-43 is also known to be mislocalized from the nucleus and aggregated in about half of frontotemporal dementia cases, I next examined the frontal cortex samples of four unlucky sporadic ALS patients who also experienced clinical symptoms of dementia during the course of their ALS (as is common to about 15% of ALS patients[41,164]) along with one patient carrying a familial C9orf72 expansion who presented with frontotemporal dementia. Three of the four sporadic ALS patients with FTD symptoms and the one C9orf72 FTD patient showed clear expression of truncated stathmin-2 RNA by RT-PCR, which was not detected in frontal cortex from an unaffected control (Fig2.1 D). Intriguingly, I was able to detect the misprocessed RNA in one patient that would typically be considered a “non-neurologic control”, but who had been undergoing ionizing radiation therapy prior to his death for the treatment of a brain tumor. Although the histologic samples were not available for this patient tissue to confirm TDP-43 abnormalities by immunostaining, the appearance of the cryptically spliced stathmin-2 mRNA in this individual probably reflected loss of function of nuclear TDP-43 probably arising from the extreme stress of DNA damage in his course of treatment.

To determine the extent of stable accumulation of truncated stathmin-2 RNA at the individual neuron level, I next utilized chromogenic in-situ hybridization in matched serial pairs of thinly cut (7 micron) tissue sections. Serial sectioning of large neurons including the Betz cells of motor cortex Layer V and the gigantic alpha motor neurons within Rexed lamina IX of the spinal

cord (both primary motor neuron types affected in ALS) allowed for examination of different cross-sections of the same neuron using two different hybridization probes. By probing motor cortex and spinal cord sections with highly specific locked-nucleic acid probes designed to hybridize to either the stathmin-2 exon2A sequence or the 3' untranslated region of the mature full length stathmin-2 mRNA (Fig 2.3 A), I was able to evaluate slide scans of the resulting stained tissues as an observer blinded to the phenotype of the individual, prior to decoding phenotype information. As expected, probes hybridizing normal stathmin-2 mRNA were highly enriched in neurons of both the motor cortex and spinal cord in all normal unaffected controls examined, while probes hybridizing exon2A of truncated stathmin-2 were nearly undetectable above background in those serial sections (what little signal is present is likely attributable to binding the elongating stathmin-2 pre-mRNA) (Fig 2.3 B, C left panels). In agreement with prior RNA analysis by laser microdissection and bulk RNA RT-PCR, the opposite staining result was readily apparent in all five sporadic ALS patients examined, where normal full-length stathmin-2 encoding mRNA was nearly undetectable above background, but serial section hybridization for truncated stathmin-2 RNA produced striking signals in all neurons examined from both motor cortex and spinal cord (Fig 2.3 B, C right panels). Hybridization of the truncated stathmin-2 RNA in sporadic ALS patient neurons also revealed that it was robustly detectable in the somatic compartment of the neuron, consistent with the truncated stathmin-2 mRNA to be capped, cryptically spliced and polyadenylated and exported from the nucleus.

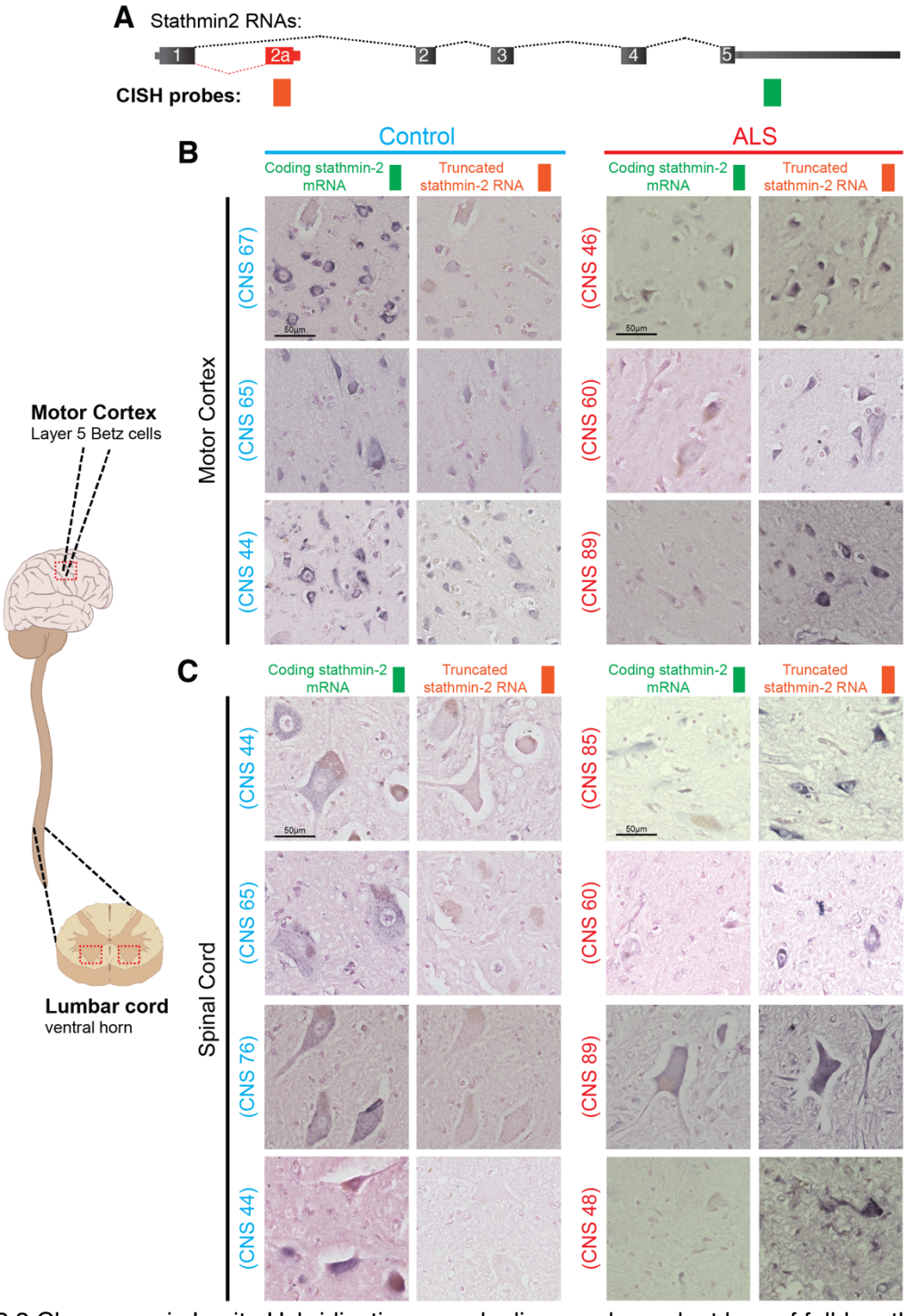

Figure 2.3 Chromagenic In-situ Hybridization reveals disease-dependent loss of full-length stathmin-2 RNA accompanied by robust accumulation of truncated RNA.

(A) Schematic of human gene encoding stathmin-2 depicting probe locations. (B) Motor cortex hybridizations of thin-cut serial sections showing matched neurons and full-length or truncated probe staining in controls and ALS tissue. (C) Lumbar spinal cord hybridizations of thin-cut serial sections showing matched neurons with full-length or truncated probe staining in controls and ALS tissue.

Discussion:

Melamed originally uncovered in a neuronal cell line that direct reduction or mutation of TDP-43 leads to a loss of full length stathmin-2 and accumulation of a truncated cryptically spliced and prematurely polyadenylated RNA transcript. I have extended this finding into ALS and FTD patients using three different approaches: 1) bulk grey matter RNA extraction and RT-PCR with tissues from upper and lower motor neuron compartments of sporadic and familial ALS and FTD patients and unaffected controls, 2) cell acquisition and analysis of RNA-seq from laser-capture micro-dissected lumbar motor neurons of sporadic ALS patients with bulbar or arm onset versus unaffected controls, and 3) chromogenic RNA in-situ hybridization of histologic sections from both upper and lower motor neuron compartments in sporadic ALS patients and controls. With these approaches I demonstrated that this RNA misprocessing event is a genuine hallmark of the majority of ALS and FTD disease (with TDP-43 proteinopathy), including all tested sporadic ALS patients (who make up the largest fraction of all ALS patients), and in patients harboring the most common genetic cause of ALS or FTD: inherited expansion in C9orf72. Of critical pathophysiologic relevance, I demonstrated that stathmin-2 pre-mRNA misprocessing is not a feature of the minority of familial ALS patients who carry SOD1 mutations known not to provoke TDP-43 pathogenesis. Thus, misprocessing and loss of full length stathmin-2 RNA is a specific hallmark of TDP-43 proteinopathy and not a generic result of neurodegeneration.

TDP-43 dysfunction and nuclear clearance is hypothesized to be an early event in disease pathogenesis, and logically so, since the protein cannot aggregate in the cytoplasm without either a failure to import newly synthesized TDP-43 protein into the nuclear compartment, and/or a clearance of existing TDP-43 from the nucleus. Irrespective of the precise chronological order and mechanism of TDP-43 nuclear clearance and aggregation in the lead-up to symptomatic ALS and FTD, it is uncontroversial that this pathologic dysfunction must necessarily precede neuronal

death. By simple inspection then, TDP-43-dependent stathmin-2 pre-mRNA misprocessing by cryptic splicing and polyadenylation, must also precede neuronal death.

This pathophysiologic chronology stands in contrast to the pharmaceutical and biomedical community's current standard prognostic biomarkers for neuron loss use in clinical trials: the intermediate filament proteins neurofilament-light and neurofilament-heavy. The neurofilament proteins are useful neuronal biomarkers thanks to their extreme abundance in large caliber myelinated axons that are so commonly affected in neuromuscular degenerative disorders, and their detectable levels within the cerebrospinal fluid and blood proportionally increase as these axons are damaged. However, because the release of these proteins into the CSF and blood are a direct consequence of physical degeneration, they are downstream of the primary sources of pathology and are lagging indicators of damage that has already occurred, not direct readouts of underlying molecular disfunction. Like the genes encoding neurofilament proteins, stathmin-2 RNA is one of the most abundantly expressed transcripts within normal human motor neurons, but unlike the neurofilament genes, stathmin-2 is entirely dependent upon functional TDP-43 for correct processing of its pre-mRNA. The same is true of exon2A mapped reads in the RNA-seq dataset, which were also a perfect indicator of disease in all thirteen sporadic ALS patients examined.

Misprocessed stathmin-2 RNA has since been validated by other research groups[165] as a post-mortem marker of TDP-43 dysfunction in FTD, but the next key conceptual advance as a prognostic biomarker of TDP-43 status in living patients would require the detection of stathmin-2 truncated RNA or its translation product within blood or cerebral spinal fluid. Preliminary unpublished data from multiple groups using a very limited number of patient spinal fluid samples has already indicated that the abundant truncated RNA can be recovered and detected by quantitative reverse-transcriptase polymerase chain reaction from exosomes in patient cerebral spinal fluid. However, the reported detection efficiency currently does not match the known

prevalence in post-mortem tissues, perhaps indicating that 1) the purported exosomes are not a common export feature of these neurons, 2) their isolation is not efficient using current techniques, or 3) heterogeneity in sample handling may contribute to instability and detection issues (or a combination of the above). Significant additional research is necessary to determine whether truncated stathmin-2 RNAs can serve as an earlier indicator of molecular pathology than neurofilament proteins.

In case of both laser-capture microdissection RNA-seq and chromogenic RNA in-situ hybridization, the presence and specificity of exon2a-terminated RNAs to delineate disease vs non-neurologic controls in sporadic and familial ALS is truly striking, allowing an otherwise blinded observer to perfectly delineate ALS patient tissues using only the presence of the truncated RNA. The persistence of the cryptically spliced and polyadenylated stathmin-2 RNA, which is not predicted to be a substrate for nonsense-mediated decay because of a lack of downstream exons beyond the terminal exon2a), within the cytoplasm of affected neurons raises the serious question of whether its 16-amino acid coding sequence is abundantly translated in the cytoplasm of cells with TDP-43 abnormalities. The small predicted size of this peptide would make it impossible to detect by traditional SDS-PAGE, and thus far unpublished efforts by multiple teams to raise a successful antibody against the peptide for efficient detection (either by ELISA or immunostaining) have failed. In terms of molecular pathology, the 16 amino acid peptide would be free to diffuse between nuclear and cytoplasmic compartments, potentially accumulating and interfering with any number of critical compartmented systems along the way. Additional efforts beyond the standard antibody-based techniques will be necessary to determine whether such a peptide is produced, and what influence it might have on disease progression.

Methods:

Patient Tissue Acquisition:

All nervous systems were acquired through a process approved by the Investigational Review Board and in compliance with the Health Insurance Portability and Accountability Act compliant process. Brain and spinal cord of ALS patients who met El Escorial criteria for definite ALS[4] and were followed during the clinical course of their illness were collected rapidly upon death, usually within 4 hours and processed for immediate embedding and freezing for RNA or fixed in 10% formalin for immunohistochemistry and cytology with later embedding in paraffin wax for sectioning, with alternating sections going to each respective process. For laser-capture experiments frozen embedded lumbar spinal cord sections were selected from patients who had bulbar or arm onset of disease, caudally progressing. Consented control nervous systems were processed identically and acquired from patients from the hospital's intensive care unit when life support was withdrawn.

Bulk spinal cord grey matter and motor cortex grey matter RNA extraction:

Frozen human spinal cord samples were freed of embedding OCT material by washing three times in 50ml of room-temperature sterile phosphate buffered saline, before scalpel excision of grey matter was performed under a dissection microscope. White and grey matter were separated into labeled tubes and immediately homogenized in Trizol, using an Omni International mechanical tissue homogenizer, and RNA was chloroform extracted and ethanol precipitated according to the Trizol reagent instructions. RNA was quantified on a Nanodrop (Thermo). Upper motor strip samples were collected at autopsy by region and flash frozen with liquid nitrogen in pre-labeled pathology cassettes before being transferred to storage at -80ºC. For RNA extraction, tissue samples were thawed at room temperature and similarly dissected to obtain grey matter sections which were placed directly into an appropriate volume of Trizol reagent and homogenized with a mechanical tissue homogenizer. Grey matter dissection was performed in both cases to prevent overloading of lipid fractions within the trizol reagent, and to enrich for the

desired neuronal somatic cellular compartments. For cDNA synthesis, 1-5 micrograms of recovered total RNA was reverse transcribed using MMLV-RT derived Superscript III (Invitrogen) according to the manufacturers' instructions. RT–PCR reactions were performed using Q5 High-Fidelity DNA polymerase (NEB) in a T100 thermocycler PCR machine (Bio-Rad). For splicing analyses, RT–PCR products were separated on 1.8% or 2.0% polyacrylamide gels and then incubated with SYBR gold (Invitrogen) for ultraviolet imaging and analysis. Quantitative real-time PCR was carried out in triplicates, using iTaq Universal SYBR green (Bio-Rad) in a CFX384 real-time PCR machine. mRNA expression of transferrin receptor protein-1 (TFRC) and glyceraldehyde-3-phosphate dehydrogenase (GAPDH) were used as endogenous control genes.

Laser capture microdissection and RNA isolation:

Thirty-five to fifty-five sections of frozen OCT-embedded human lumbar spinal cord were cut at a thickness of 9-11 μm in a -18C cryotome and placed onto uncharged glass slides. The sections were returned immediately to dry ice and maintained at that temperature for a minimum of three hours to aid proper adhesion in downstream processes. Staining with cresyl violet acetate was accomplished in a 10-step, timed, nuclease-free immersion process. Motor neurons were laser-microdissected from each slide using a Pixcell IIe Laser Capture Microdissection (LCM) System (Arcturus Bioscience) and CapSureTM Macro LCM Caps (Applied Biosystems). Each LCM session took no greater than 2.5 hours in order to preserve RNA from endogenous nucleases. RNA isolation was carried out in each using an RNeasy Micro kit (Qiagen) and RNA pools were quantified and analyzed for quality on a Bioanalyzer RNA Pico microfluidic chip (Agilent) such that only samples of sufficient quality were advanced to library preparation with random priming using the Ovation® RNA-Seq System (NuGEN) before RNA-sequencing.

In situ hybridization of STMN2 RNA isoforms:

Short locked nucleic acid (LNA) probes with 5′-digoxigenin detection labels were designed by QIAGEN. The LNA base positions are not disclosed, but the probe sequences utilized were as follows: Truncated Exon2A isoform probe: TCACACAGAGAGCCAAATTCTT; Normal STMN2 mature mRNA probe binding the 3′UTR region: ATCCTGATATCGCATGATCCAT). For each tissue, two serial FFPE tissue sections (7 µm) were cut onto charged glass slides for comparison of adjacent sections from the same cells. Each of the two sections was hybridized with one of the STMN2 probes using standard ISH protocols and revealed with a commercial anti-DIG antibody and NBT developer kit. Slides were inspected under brightfield microscopy and serial sections of individual neurons were identified and imaged at ×40 magnification on a Keyence BZ-X700 fluorescent microscope. For quantification, spinal motor neurons were identified by their large cytoplasm and/or nucleus, the presence of lipofuscin, and their position within Rexed lamina IX of the spinal cord. Neurons of the motor cortex were identified by their shape and relative size and position within cortical layering, with special attention to layers 3 and 5.

Chapters 2, 3, 4, and 5 were supported in part by an institutional award to the UCSD Genetics Training Program from the National Institute for General Medical Sciences, T32 GM008666.

Chapter 3: Normal Stathmin-2 pre-mRNA Processing is Primarily Determined by Steric Blockage of a Cryptic Splice Acceptor Site via TDP-43

Abstract:

Reduced nuclear TDP-43 drives abnormal use of cryptic splice and polyadenylation sites in the stathmin-2 pre-mRNA, leading to loss of stathmin-2 protein (also known as SCG10, transcribed from the STMN2 gene), which is required for axonal recovery after injury. I here demonstrate that removal of three TDP-43 GU binding motifs within intron 1 of the stathmin-2 pre-mRNA drives constitutive use of cryptic splicing and polyadenylation sites, demonstrating this as the normal site of TDP-43 interaction. TDP-43 binding to the stathmin-2 pre-mRNA sterically blocks usage of both cryptic sites, as synthetically targeting other RNA binding proteins, including MCP or dCasRx, to (or near to) the TDP-43 binding locus restores correct stathmin-2 pre-mRNA maturation. Genome editing to eliminate either cryptic processing site is used to determine that cryptic splicing, not cryptic polyadenylation, primarily drives abnormal stathmin-2 pre-mRNA processing.

Introduction:

The extreme sensitivity of normal stathmin-2 pre-mRNA maturation upon normal nuclear TDP-43 presence and function was discovered and described in previous work from our group[91]. Although a site for predicted TDP-43 interaction was proposed in our initial report (based on the presence of a cluster of GU binding motifs), the precise locus of TDP-43 binding was never directly confirmed by experiment. Also unresolved was determination of how TDP-43's interaction with the stathmin-2 pre-mRNA determined the pathway of RNA maturation. Although we initially hypothesized polyadenylation to be the key component, these unresolved questions are of critical

importance for devising a mechanistically “on target” therapeutic intervention, to replace TDP-43’s normal molecular role on the nascent stathmin transcript and correct endogenous stathmin-2 pre-mRNA processing in neurons affected by TDP-43 proteinopathy. I here apply sophisticated molecular techniques to address these questions and determine how TDP-43 controls stathmin-2 levels.

The breakthrough discovery of CRISPR-Cas9 genome engineering, applying the central molecular nuclease machinery of bacterial immunity to modify sequences encoded in human cells, enables precise DNA editing in cellular models with greater speed and efficiency than ever before. This technique allows for direct molecular hypothesis testing by comparing the RNA processing outcomes from edited and wildtype diploid human cell lines harboring precisely selected and engineered changes in their genomic sequence (which can differ by as little as a single nucleotide out of their approximately six billion bases of a diploid human genome). Applying this technique to the human diploid neuron-like cell line (SH-SY5Y) that we had utilized in the initial discovery effort for the stathmin-2 gene as an ALS target gene, I here demonstrate that removal of a hypothesized TDP-43 GU binding site from the first intron of stathmin-2 results in constitutive misprocessing of the stathmin-2 pre-mRNA, even though TDP-43 levels remain normal, demonstrating this as the authentic TDP-43 binding locus. By replacement of this TDP-43 binding site with a hairpin sequence bound by a bacteriophage RNA-binding protein (the MS2 coat protein [MCP]), I demonstrate that the tethering of an MCP-TDP-43 fusion-protein or simply MCP alone relieves constitutive misprocessing of stathmin-2 pre-mRNA. I confirm that simple steric binding is sufficient to rescue stathmin-2 misprocessing in an SH-SY5Y cell line harboring a homozygous disease causing TDP-43 N352S/N352S mutation by targeting the cryptic exon sequence with a large nuclease-inactivated RNA-targeted CRISPR effector dCasRx. These findings demonstrate that TDP-43 binding to the stathmin-2 pre-mRNA acts to sterically block

utilization of cryptic splice and polyadenylation site (or the binding of other RNA processing proteins that act in RNA splicing or polyadenylation).

To determine whether the cryptic splice-acceptor or cryptic alternative polyadenylation signal is the primary determinant of stathmin-2 misprocessing upon reduction in functional TDP-43, I again utilize CRISPR-Cas genome engineering to mutate each cryptic element individually, converting each into a non-functional sequence. Ablation of the cryptic splice acceptor, but not the cryptic polyadenylation site fully blocks utilization of both cryptic sites upon TDP-43 reduction, establishing that misprocessing is primarily driven cryptic pre-mRNA splicing.

Results:

Recognizing that reduced levels or mutation in TDP-43 drive aberrant splicing[91,166] and polyadenylation[91] within the first intron of the stathmin-2 pre-mRNA, I used CRISPR-Cas9 genome engineering to mechanistically test whether TDP-43 binding to the stathmin-2 pre-mRNA blocks use of either cryptic misprocessing site, and if so whether this requires its direct RNA binding at the three predicted GU-rich TDP-43 binding motifs [91]. To this end, I first replaced the three GU-motifs with the 19 nucleotide MS2 aptamer sequence that adopts an RNA stem-loop structure which can be bound with high affinity ($K_d = 2 \times 10^{-10}$ M [167]) by the MS2 coat protein (MCP) (Fig 3.1 A-C). In human neuronal SH-SY5Y cells carrying the MS2-binding site replacement in one allele and expressing normal levels of functional TDP-43, steady state stathmin-2 RNA levels were reduced by 50%, accompanied by appearance of abundant truncated, prematurely polyadenylated stathmin-2 RNA (Fig 3.1 B), thus demonstrating that the GU motif is the site of TDP-43 interaction on the stathmin-2 pre-mRNA.

Figure 3.1 Human GU-motif removal and MS2-directed tethering demonstrate TDP-43 binding locus within stathmin-2 exon2a, while cryptic site mutaitons identify TDP-43 dependent misprocessing is primarily driven by cryptic splicing

(A) Schematic of CRISPR-engineering strategy for conversion of GU motif in exon2a to MS2 aptamer sequence in SH-SY5Y neuroblastoma cells. (B) qRT-PCR demonstrating that SH-SY5Y cells carrying heterozygous GU to MS2 conversion misprocess stathmin-2 RNA from edited allele, leading to 50% loss of full-length gene product compared with wildtype cells, and simultaneously accumulate truncated RNA. (C) Schematic depicting MS2:MCP directed strategy to replace MCP-tethered cargos at normal TDP-43 binding locus. (D-F) Plots showing qRT-PCR measurement of (D) truncated stathmin-2 RNA, (E) full-length stathmin-2 RNA, (F) endogenous TDP-43 RNA levels, with and without induction of MCP-fusion protein expression in SH-SY5Y cells carrying heterozygous MS2 aptamer knock-in. GAPDH expression used as an endogenous control gene. (G-I) Plots showing qRT-PCR measured expression of TDP-43, full-length stathmin-2, and truncated stathmin-2 RNAs 96 hours after siRNA treatment with a control siRNA pool or TDP-43 targeting pool in (G) wildtype SH-SY5Y cells, (H) SH-SY5Y cells harboring a homozygous mutation of the human exon2a cryptic premature polyadenylation sequence to the murine sequence AGGAAA, and (I) SH-SY5Y cells harboring homozygous mutation of the human exon2a cryptic 3' splice acceptor site. GAPDH expression was used as an endogenous control gene.

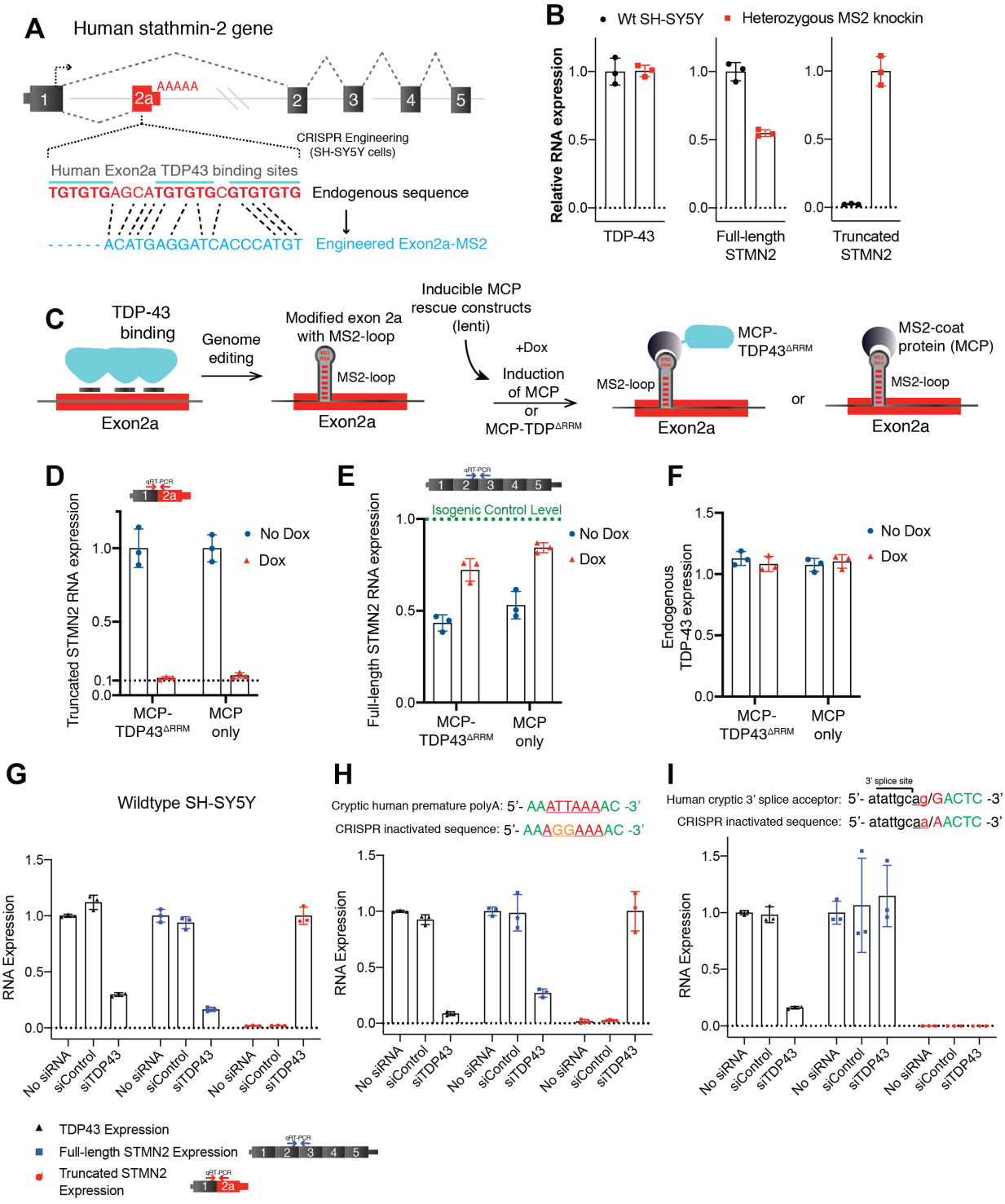
A
Human stathmin-2 gene
1
2a
AAAAA
2
3
4
5
CRISPR Engineering
(SH-SY5Y cells)
Human Exon2a TDP43 binding sites
TGTGTGAGCATGTGTGCGTGTGTG
Endogenous sequence
ACATGAGGATCACCCATGT
Engineered Exon2a-MS2
B
Wt SH-SY5Y
Heterozygous MS2 knockin
Relative RNA expression
TDP-43
Full-length STMN2
Truncated STMN2
C
TDP-43 binding
Exon2a
Genome editing
Modified exon 2a with MS2-loop
MS2-loop
Inducible MCP rescue constructs (lenti)
+Dox
Induction of MCP or MCP-TDP^ΔRRM
MCP-TDP43^ΔRRM
MS2-coat protein (MCP)
or
D
qRT-PCR
Truncated STMN2 RNA expression
No Dox
Dox
MCP-TDP43^ΔRRM
MCP only
E
Isogenic Control Level
Full-length STMN2 RNA expression
F
Endogenous TDP-43 expression
G
Wildtype SH-SY5Y
RNA Expression
No siRNA
siControl
siTDP43
TDP43 Expression
Full-length STMN2 Expression
Truncated STMN2 Expression
H
Cryptic human premature polyA: 5'- AAATTAAAAC -3'
CRISPR inactivated sequence: 5'- AAAGGAAAAC -3'
I
3' splice site
Human cryptic 3' splice acceptor: 5'- atattgcag/GACTC -3'
CRISPR inactivated sequence: 5'- atattgcaa/AACTC -3'

To further determine whether steric TDP-43 binding to exon 2a is sufficient to prevent use of either the cryptic splice acceptor or polyadenylation site, I transduced the MS2-knockin cells with a lentivirus encoding a human TDP-43 RNA binding deficient variant [missing both RNA-recognition motifs (ΔRRM)] and fused to an MS2 coat protein (MCP-TDP-43$^{\Delta RRM}$) with the fusion construct expressed from an inducible promoter (Fig 3.1 C). The MCP (enhanced with an N55K mutation enabling increased affinity [167] to direct binding of the fusion construct to the MS2 aptamer) is the natural binding partner of the bacteriophage-derived, 19 base MS2 RNA aptamer that was substituted for the 24 base GU rich TDP-43 binding site(s) in the stathmin-2 pre-mRNA (Fig 3.1 C).

Within 24h of doxycycline induction, levels of truncated stathmin-2 RNA were reduced by 90% (Fig 3.1 D, left), demonstrating that TDP-43 binding within exon 2a prevents cryptic splicing and polyadenylation. To test whether the observed repression of cryptic elements is mediated by simple steric interaction, I alternatively induced expression of MCP without fusion to TDP-43 (Fig 3.1 C, right), which resulted in comparable suppression of the truncated stathmin-2 RNA (Fig 3.1 D). Levels of full-length stathmin-2 mRNA (measured by quantitative real-time PCR (qPCR)) confirmed near complete restoration of correct stathmin-2 RNA processing mediated by either MCP-TDP-43$^{\Delta RRM}$ or MCP alone (Fig 3.1 E), while endogenous TDP-43 RNA levels were unaltered (Fig 3.1 F). This evidence provides strong support for a simple steric model in which TDP-43 binding to exon 2a of the stathmin-2 pre-mRNA blocks utilization of cryptic splicing and polyadenylation.

Having determined that steric occupancy within exon 2a at the normal TDP-43 binding locus is critical for stathmin-2 pre-mRNA processing, I sought to determine which of the two cryptic cis-regulatory sequences are responsible for initiating misprocessing when TDP-43 levels were reduced. To that end, I again used genome editing in SH-SY5Y cells to eliminate either the

alternative polyadenylation motif or the 3' splice acceptor site within exon 2a. In cells homozygously edited to carry a non-functional premature polyadenylation signal [by converting the ATTAAA sequence to AGGAAA (Fig 3.1 H)], a 92% reduction of TDP-43 levels by siRNA resulted in suppression of properly processed stathmin-2 mRNA by 73%. By comparison, a 70% reduction in TDP-43 in wildtype SH-SY5Y cells resulted in 85% reduction of normal stathmin-2 (Fig 3.1 G), suggesting that elimination of the normal premature polyadenylation signal was not protective against pre-mRNA misprocessing. However, downstream within Intron 1 in stathmin-2 pre-mRNA, I identified twenty-two AUUAAA sequences and thirty-nine occurrences of the more commonly utilized sequence AAUAAA, which – if utilized – could explain the continuous suppression of full length stathmin-2 mRNA.

I homozygously CRISPR-edited the 3' splice acceptor sequence of the cryptic splice site within intron 1 of the stathmin-2 pre-mRNA from a functional AG/GA to a non-functional AAAA sequence. In this cell line, siRNA reduction of TDP-43 levels by 84% resulted in no significant loss of full-length stathmin-2 mRNA compared with non-targeting siRNA treatment (Fig 3.1 I) and a cryptically polyadenylated stathmin-2 RNA remained undetectable, indicating that simply blocking the exon1-2a splice recognition/resolution is protective against altered processing of stathmin-2 pre-mRNA when TDP-43 level is reduced.

The ability of a relatively small 29 kDa RNA-binding protein of bacteriophage origin (MCP) to restore normal human stathmin-2 pre-mRNA processing through simple steric occupancy of the TDP-43-binding locus raised the possibility that engineered RNA binding protein strategies may have broad therapeutic utility in TDP-43 proteinopathies. To test this idea, I utilized a recently identified RNA-targeting CRISPR effector of bacterial origin RfxCas13d (CasRx)[168]. Mutation of the two RNase-activity conferring higher eukaryotes and prokaryotes nucleotide-binding **(**HEPN) domains of CasRx produces a "nuclease-dead" (dCasRx) protein that retains its RNA-binding (but

not enzymatic cleavage) capacity and can be targeted to pre-mRNA molecules to affect alternative splicing[168]. Given the reported versatility of dCasRx-binding to its RNA target, independent of a typical protospacer adjacent motif (PAM) requirement, I designed twelve separate guide RNAs that tile across the exon2A region of the stathmin-2 intron (Fig 3.2 A).

SH-SY5Y cells carrying a homozygous TDP-43 $^{N352S/N352S}$ mutation in the gene encoding TDP-43, which results in 50% reduction of the normal stathmin-2 levels[91] (Fig 3.2 B), were transduced to stably express dCasRx with individual gRNAs, and RNA was collected after one week of puromycin selection to eliminate non-transduced cells. Expression of four of the twelve gRNAs demonstrated marked reduction in the levels of prematurely polyadenylated stathmin-2 RNA relative to the no-guide control (Fig 3.2 C, D). Consistent with the CRISPR genome engineering results (Figure 3.1 H), direct dCasRx targeting of the premature polyadenylation site (Fig 3.2 C-D, Guide 4) was not sufficient to restore normal processing of full-length stathmin-2 mRNA, although a reduction in levels of truncated stathmin-2 RNA was detected. Instead, direct targeting of dCasRx to the 3' splice acceptor site of exon 2a (Fig 3.2 C-D, Guide 2) showed partial stathmin-2 mRNA restoration. Less pronounced outcome was achieved by targeting an adjacent upstream intronic sequence (Fig 3.2 C-D, Guide 1), whereas full dCasRx mediated rescue of normal stathmin-2 mRNA processing was achieved by targeting an RNA sequence approximately equidistant between the TDP-43 binding sites and the canonical 3' end of exon 2a (Fig3.2 C-D, Guide 3).

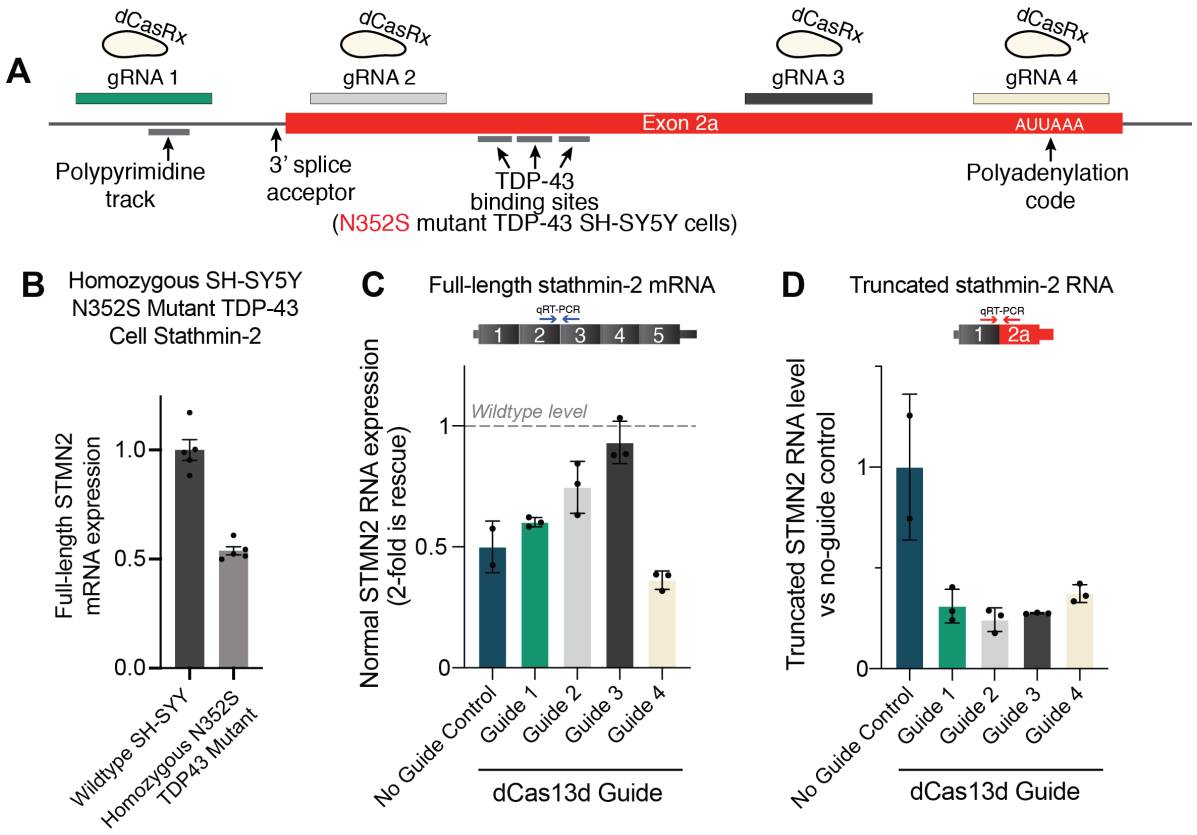

Figure 3.2 Exon2a binding by nuclease-inactivated RNA-targeting bacterial CRISPR effector protein dCasRx is sufficient to alleviate misprocessing of stathmin-2 in cells carrying mutated TDP-43

(A) Schematic of the guide RNA design approach, tiling dCasRx guides across the stathmin-2 intron 1 and exon2a regions. (B) qRT-PCR shows SH-SY5Y cells carrying homozygous TDP-43 N352S disease causing mutations misprocess stathmin-2 mRNA leading to a 50% loss of total gene product compared with wildtype cells. (C) Plot showing qRT-PCR expression of full-length stathmin-2 RNA levels for each guide RNA expressing cell line, in SH-SY5Y cells with a homozygous TDP-43 mutant background, relative to a no-guide control expressing only the untargeted CRISPR effector protein. GAPDH used as an endogenous control gene. (D) Plot showing qRT-PCR expression measures of truncated stathmin-2 RNA levels for each guide RNA-expressing cell line in SH-SY5Y cells with a homozygous TDP-43 mutant background, relative to a no-guide control expressing only the untargeted CRISPR effector protein. GAPDH used as an endogenous control gene.

SH-SY5Y cells carrying an homozygous TDP-43 $^{N352S/N352S}$ mutation in the gene encoding TDP-43, which results in 50% reduction of the normal stathmin-2 levels [91] (Fig 3.2 B), were transduced to stably express dCasRx with individual gRNAs, and RNA was collected after one week of puromycin selection to eliminate non-transduced cells. Expression of four of the twelve gRNAs demonstrated marked reduction in the levels of prematurely polyadenylated stathmin-2 RNA relative to the no-guide control (Fig 3.2 C, D). Consistent with the CRISPR genome engineering results (Figure 3.1 H), direct dCasRx targeting of the premature polyadenylation site (Fig 3.2 C-D, Guide 4) was not sufficient to restore normal processing of full-length stathmin-2 mRNA, although a reduction in levels of truncated stathmin-2 RNA was detected. Instead, direct targeting of dCasRx to the 3' splice acceptor site of exon 2a (Fig 3.2 C-D, Guide 2) showed partial stathmin-2 mRNA restoration. Less pronounced outcome was achieved by targeting an adjacent upstream intronic sequence (Fig 3.2 C-D, Guide 1), whereas full dCasRx mediated rescue of normal stathmin-2 mRNA processing was achieved by targeting an RNA sequence approximately equidistant between the TDP-43 binding sites and the canonical 3' end of exon 2a (Fig3.2 C-D, Guide 3).

Discussion:

Two key questions for the development of stathmin-2 corrective strategies in TDP-43 proteinopathy are identification of the essential cryptic elements that govern TDP-43 binding and function in stathmin-2 pre-mRNA maturation, and how does TDP-43 binding interact with these elements to direct pre-mRNA processing? We previously determined that reduction or mutation in TDP-43 promotes truncation and premature polyadenylation within the first intron of the stathmin-2 encoding pre-mRNA, leading to a striking loss of the normally encoded stathmin-2 mRNA and protein product within affected cells. We had proposed in that initial report that this process is mediated chiefly through co-transcriptional utilization of a cryptic polyadenylation signal

that is normally blocked by TDP-43 binding at a suggested trio of GU-rich sites that lie 127 bases 5' to the site of premature polyadenylation[91]. Utilizing CRISPR-mediated genome editing to introduce three sets of individual targeted mutations into the human stathmin-2 intronic sequence of neuron-like SH-SY5Y cells, I have identified that suppression of cryptic splicing within intron 1 is the dominant determinant of the TDP-43 mediated processing of stathmin-2 pre-mRNA.

The removal of the 24 base GU-rich motif from the human stathmin-2 gene leads to constitutive misprocessing while TDP-43 levels are normal, solidifying this locus as the authentic site or TDP-43 interaction with stathmin-2. This result was not unexpected, as RNA binding protein cross-linking immunoprecipitation and sequencing by another group using the same cell line had identified TDP-43 binding peaks in the vicinity of Exon2A[74,91], and the site I targeted for modification was the only sensible GU-rich motif for use as a probable binding locus. In order to extend this experiment, I replaced the 24 base GU stretch with a 19 base MS2 aptamer sequence to allow forced tethering of factors to this locus via fusion with the MS2 natural binding partner MCP (the MS2 coat protein).

With this approach, I discovered that forced binding to this site by a 29 kDa RNA binding protein of bacteriophage origin is largely sufficient to restore normal pre-mRNA processing, with or without direct fusion to a TDP-43 variant. The TDP-43 fusion variant utilized in this case contained a large deletion of the RNA recognition motifs, the resulting sequence comprising only 256 amino acids of the normal 414 encoded in normal human TDP-43, making its interaction with RNA molecules completely dependent on the MS2:MCP system (Fig. 3.3 A-C). The design was chosen to prevent induced TDP-43 fusion protein expression from inducing acute toxicity by interactions with thousands of normal TDP-43 RNA targets in the transcriptome. The design was successful, as endogenous TDP-43 RNA levels are not altered by induced expression of the mutant fusion protein, despite known autoregulation functions (Figure 3.1 F). While more sophisticated RNA binding null mutants of TDP-43 that convert specific RNA-critical residues

while retaining the authentic polypeptide length have since emerged from our laboratory[78], the RRM deletion mutant was conceptually the simplest and most self-evident version.

The MCP tethering fusion protein was designed as a head-to-tail dimer of N55K high-affinity binding mutants to ensure robust binding at a stoichiometric ratio of one RNA molecule per one MCP-TDP-43 or MCP-only binding partner (Fig. 3.3 C). Since two monomeric MCPs can simultaneously bind either side of the MS2 stem loop, utilization of a dimer accounts for and prevents a scenario where multiple TDP-43 fusion molecules would be directed to the same locus. The functional equivalence of MCP- and MCP-TDP-43 to divert stathmin-2 pre-mRNA from misprocessing strongly supports a steric blinding role for normal TDP-43 at this locus.

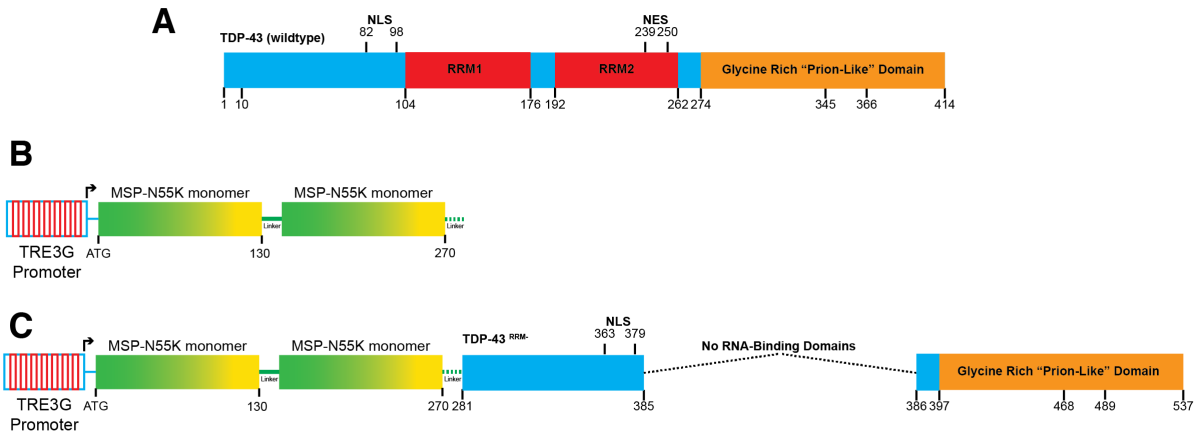

Figure 3.3 TDP-43 RNA Recognition Motif deletion prevents inducible MCP fusion protein from binding normal TDP-43 RNA targets

(A) Schematic wildtype TDP-43 with normal RNA-Recognition Motif (RRM) domains intact. (B) Schematic of inducible head-to-tail dimeric MCP protein with N55K high-affinity binding mutation. (C) Schematic of MCP-TDP43 fusion construct with deleted RRM domains to prevent normal RNA interactions and govern RNA tethering by MCP binding.

Recognizing that the TDP-43 mediated cryptic element suppression mechanism within Exon2A may involve additional cis-regulatory elements in addition to the GU rich TDP43 binding sites, I screened the approximately 350 nucleotide region for additional elements with a cutting-edge CRISPR-effector approach. While the bacterial Class 2 CRISPR-Cas adaptive immunity system has sparked a revolution in genomic research, enabling the types of (comparatively) fast and inexpensive genome editing experiments I describe in this very chapter testing functions of genomic elements, or toward investigating disease-causing mutations like the founding work identifying dysregulation of stathmin-2 by a disease-causing mutant TDP-43, the therapeutic application of this system to correct disease causing mutations has faced challenges related to its overall size (~1200 amino acids) and cellular deliverability and tolerability, plus recent reports of off-target genomic editing rates that are higher than originally anticipated[169-173].

Recently, Cas13d, part of a new class of CRISPR Cas system (type VI-D) which targets RNA instead of DNA, was computationally identified and characterized in human iPS neurons[168,174]. RNA targeting CRISPR systems allow gene product targeting while eliminating the risk of unintended permanent genome mutagenesis[175]. One such Cas13d enzyme, CasRx, at 972 amino acids is the smallest Class 2 CRISPR yet identified. CasRx processes its own guide arrays, has no flanking protospacer-adjacent sequence requirements (making it targetable to any arbitrary single-stranded RNA sequence), and has reportedly exquisite target-specificity versus comparable RNAi systems achieving better than 90% target reduction with no detectable off target effects measuring across the entire transcriptome (versus hundreds of significant unintended changes detectable from a comparable shRNA)[168]. Importantly, cis-element targeting of a nuclease-inactive mutant dCasRx has been demonstrated to manipulate pre-mRNA processing and alternative splicing in the context of 3- and 4-repeat Tau[168].

My thinking with dCasRx in the stathmin-2 context was that this system might enable a platform for targeting of specific pre-mRNA sequences to explore their cis-regulatory roles in RNA

(mis)processing and trans-element binding. This idea relies heavily on the somewhat naive assumption of uniform on-target activity of every possible guide RNA (from first principles, even considering RNA accessibility and secondary structures, this is certainly not the case) (Fig 3.4 C-D).

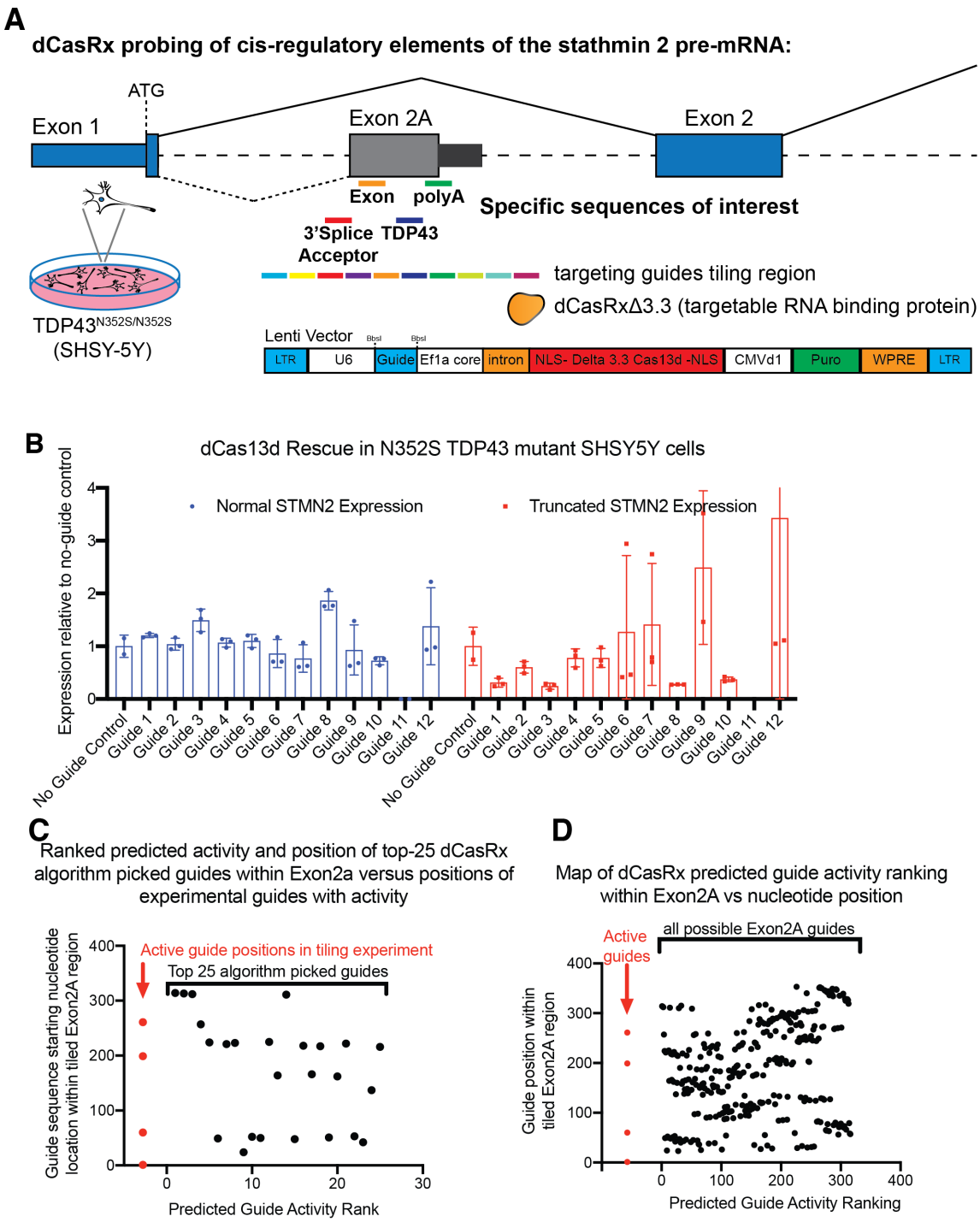

Figure 3.4 dCasRx tiling to probe cis-regulatory elements by steric inhibition and binding of an RNA-targeted CRISPR effector

(A) Schematic of guide tiling approach to identify sequence regions of cis-regulatory relevance within the exon2a region (B) qRT-PCR results for each guide RNA expressing line, showing normal and truncated stathmin-2 RNA levels vs a no-guide control line, for all 12 guides tested. GAPDH was used as an endogenous control gene. (C-D) Graphical representation of in-silico ranked guide activity predictions versus guide position along exon2a for top 25 (C), and all possible (D) guide designs, guides with in-vitro activity are shown in red and cluster near predicted active sites.

Even so, I leveraged the dCasRx system, targeting the nuclease-inactivated Cas enzyme to the STMN2 pre-mRNA using a collection of unique 22-nucleotide guide sequences distributed across the pre-mRNA region starting 50bp upstream of Exon 2A's splice acceptor site and spanning to 50bp downstream of the AUUAAA polyadenylation sequence (an approximate 350bp span for a total of 12 tiled custom dCasRx guide RNAs) (Fig 3.4 A,B). While the experiment clearly successfully corroborated the MCP-binding data indicating that TDP-43's likely role on the stathmin-2 pre-mRNA is mediated by simple steric binding, this success is somewhat limited in scope. However, the site of dCasRx rescue I identified may not actually be the locus for additional cis-regulatory elements or trans-acting factors that govern use of the cryptic sites, as a post-hoc in-silico analysis ranking all potential guides across the exon2A region for their predicted in-vitro Cas13 activity scored the only fully restorative guide at the top of the list. I interpret this to mean the tiling assay I employed in this case was perhaps most efficient at simply identifying efficient Cas13 guide RNAs.

Additionally, I can say with great certainty that this experiment did not serve, as I initially envisioned, an alternate role to identify potential antisense oligonucleotide targeting sites of interest. Having seen the precise placement of hits from the exhaustive single nucleotide resolution rescue antisense oligonucleotide lead candidate screen from exon 2A all the way 5' to exon 1, there exist excellent oligo rescue hits densely populating most of the exon 2a region (particularly on its 5' end, but also from the site of the most active dCasRx guide) that do not correspond to sites of any notable dCasRx rescue (exact data withheld here out of respect for trade secrets). It is clear that ASO and Cas13 guide kinetics differ for this pre-mRNA molecule, with ASOs winning the day in every respect for their broad efficacy of rescue at many loci (ASOs favored in a ratio of at least 33:1, with >14 ASOs demonstrating accompanying in-vivo tolerability profiles to be useful in clinical development, vs only one active dCasRx guide identified).

That TDP-43's action on the stathmin-2 pre-mRNA is largely interchangeable with such highly dissimilar steric binding factors as MCP and dCasRx indicates that TDP-43's normal binding within exon2A functions primarily to deny occupancy by components of the splicing/polyadenylation machineries that would otherwise drive usage of cryptic splicing and polyadenylation sites. Correspondingly, I propose that stathmin-2 pre-mRNA processing is likely amenable to rescue using a wide array of potential trans-acting interventions that interact with nucleic acids, including small molecules, synthetic RNA binding proteins, RNA-targeted CRISPR effector systems, and steric binding antisense oligonucleotides.

I identified that removal of the exon2a cryptic splice acceptor site (but not the cryptic polyadenylation site) provided significant protection against aberrant pre-mRNA processing when TDP-43 is suppressed, proposing cryptic splice resolution as the primary factor suppressed by TDP-43 binding (Fig 3.1 G-I). This result overturned an initial the model that the cryptic exon truncation of stathmin-2 is primarily driven by the uncovered polyadenylation site. By contrast to the splice acceptor mutation outcome, removal of the alternative polyadenylation sequence had only a weak protective effect, visible mostly by comparing the relative rate of reduction of TDP-43 (targeted directly by siRNA treatment) versus stathmin-2 (Fig 3.1 G, H). In every other case examined with wildtype cells stathmin-2 loss ought to be more profound than TDP-43 reduction. The reversal in the polyadenylation signal mutant suggests a slight protective effect of the full-length stathmin-2 allele, but in any case, the results are broadly suggestive that although 3' cleavage/polyadenylation and splicing are co-transcriptionally coupled[176,177], within this stepwise process splicing is required and presumably precedes 3' cleavage and polyadenylation, which are potentially resolved by use of additional downstream sites.

Methods:

SH-SY5Y cell culture

ATCC derived neuroblastoma cells were cultured in DMEM/F12 (Gibco) supplemented with 10% v/v fetal-bovine serum except for during FACS sorting and recovery when twice this fraction was utilized (Omega), and 1% v/v penicillin-streptomycin (Gibco) except for one week prior to electroporation when antibiotic-free media was utilized. Cells were grown in a 37ºC incubator with 5% carbon dioxide. For knockdown experiment conditions see siRNA conditions below.

CRISPR genome editing

A plasmid expressing a single guide RNA alongside an RNA encoding Cas9-T2A-GFP (based upon the backbone plasmid Addgene plasmid# 48138) was linearized by digestion with BbsI-HF enzyme to completion and purified after gel electrophoresis. Software-designed protospacer motif sequences were cloned into the linearized plasmid from annealed commercial DNA oligonucleotides and the resulting plasmids verified by Sanger sequencing to produce: Plasmid MB-sgRNA-133-134 (guide protospacer sequence: GGCTTGTGGCACAGTTGACA, off-target score: 88, activity score: 66, PAM: AGG, 1150ng/ul, overall length 9289bp) for editing of the polyadenylation signal sequence and TDP-43 binding site, and Plasmid MB-sgRNA-143-144 (guide protospacer: TATATTCATATTGCAGGACT, off-target score: 85, activity score: 53, PAM: CGG) for editing of the 3' splice acceptor site of exon2A. The activity of each guide was confirmed by transfection into 293T cells followed by gDNA isolation, PCR, and Surveyor nuclease assay with PCR primers Fw: 5'-CAATACATCTGGCTTGAGGCAGAC-3', Rev: 5'-AAAGGTGGTAATGGCTGCATGG-3' (795bp product) (Fig 3.5 A).

A

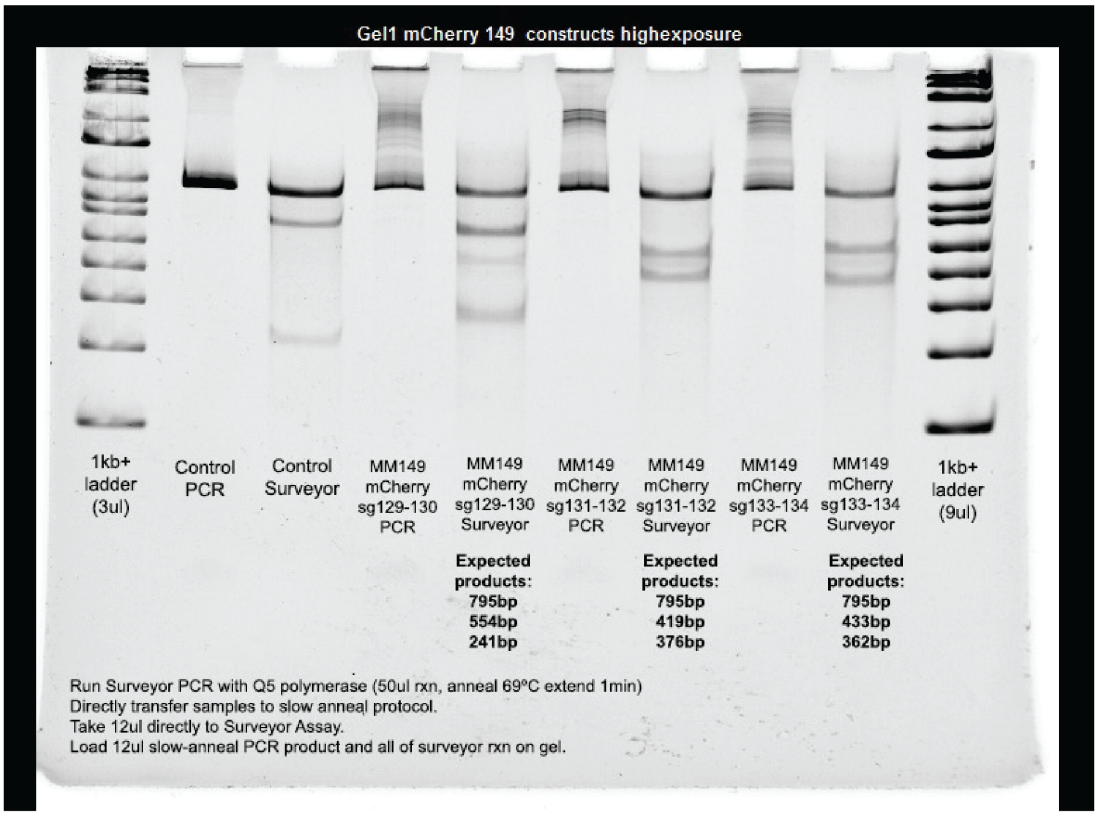

Figure 3.5 Surveyor assay validating activity of Cas9 guides for engineering exon2a
(A) Lanes showing surveyor-assay digestion products versus undigested PCR product controls indicate activity of all sgRNA designs tested.

A single homology directed repair (HDR) double-stranded donor template of 1630bp in length was designed from sequence spanning the region of the stathmin-2 intron including all of cryptic exon2A, with an EcoRI restriction site added to the 5' end and a NotI restriction site added to the 3' end. The double stranded DNA was ordered as a gBlock gene fragment from Integrated DNA technologies, however the manufacturer was unable to complete the assembly successfully, so the component fragments were provided free-of-charge and were ultimately joined using overlap-extension PCR with a Q5 high-fidelity DNA polymerase. The fragment was cloned into a bacterial plasmid backbone for production and mutagenized by site-directed mutagenesis with phosphorylated primers to incorporate either the cryptic polyadenylation site mutation ATTAAA to AGGAAA (plasmid MBSP10) with screening for converted clones based on the deletion of a BtsCI-HF type II restriction enzyme cut site within Exon2A (50^{o}c incubation temperature), or the TDP-43 binding site to MS2 aptamer conversion TGTGTGAGCATGTGTGCGTGTGTG to ACATGAGGATCACCCATGT (plasmid MBSP11), with screening for converted clones enabled by direct PCR assay with a reverse primer located within the MS2 stem loop knock-in sequence (Figures 3.6- 3.8).

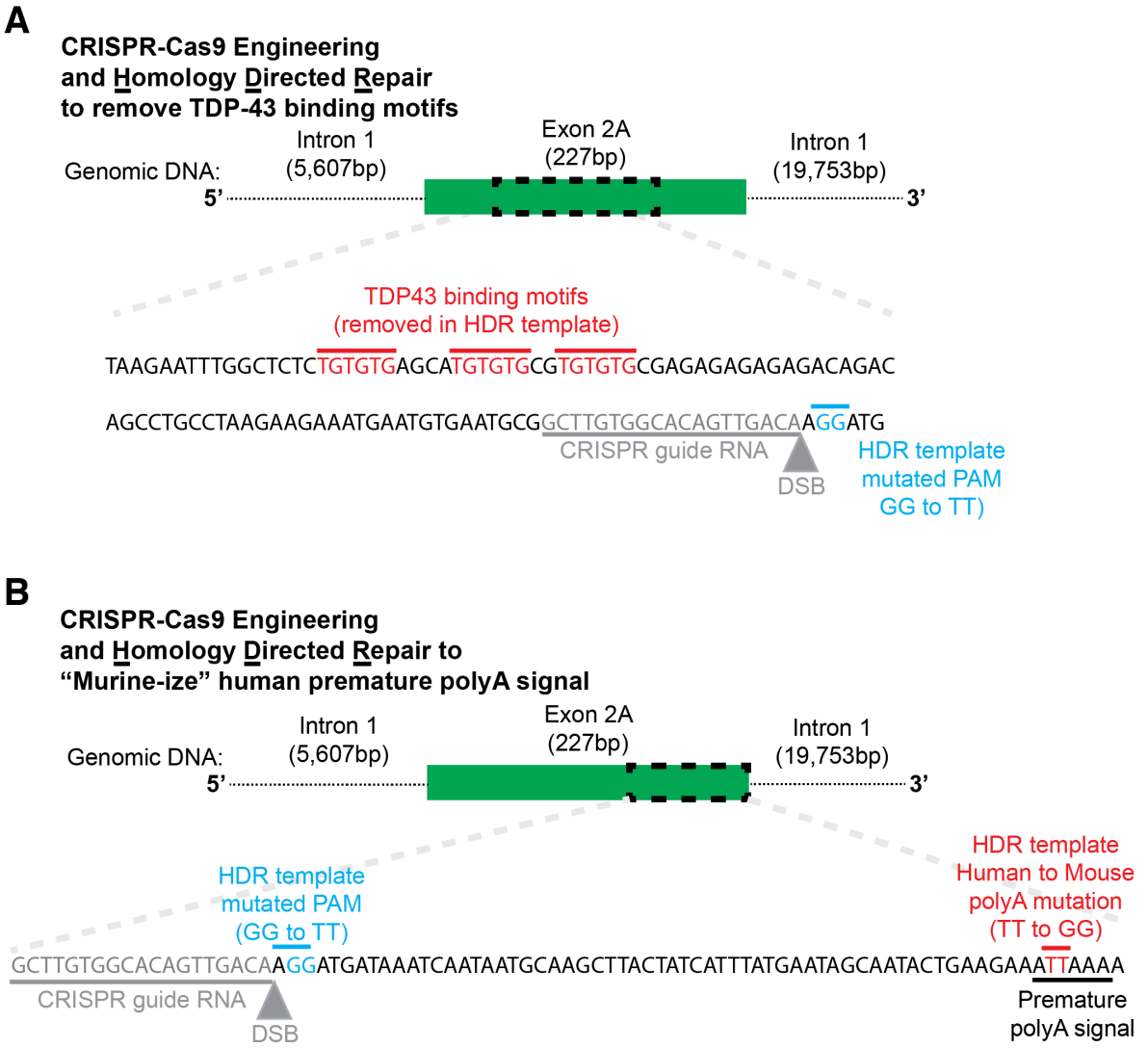

Figure 3.6 Knockin strategy for large homology repair template variants with difficult distal cut site targeting

(A) Precise schematic outlining CRISPR-engineering to replace GU motif with MS2 aptamer sequence. (B) Precise schematic outlining CRISPR-engineering to mutate human alternative polyadenylation sequence.

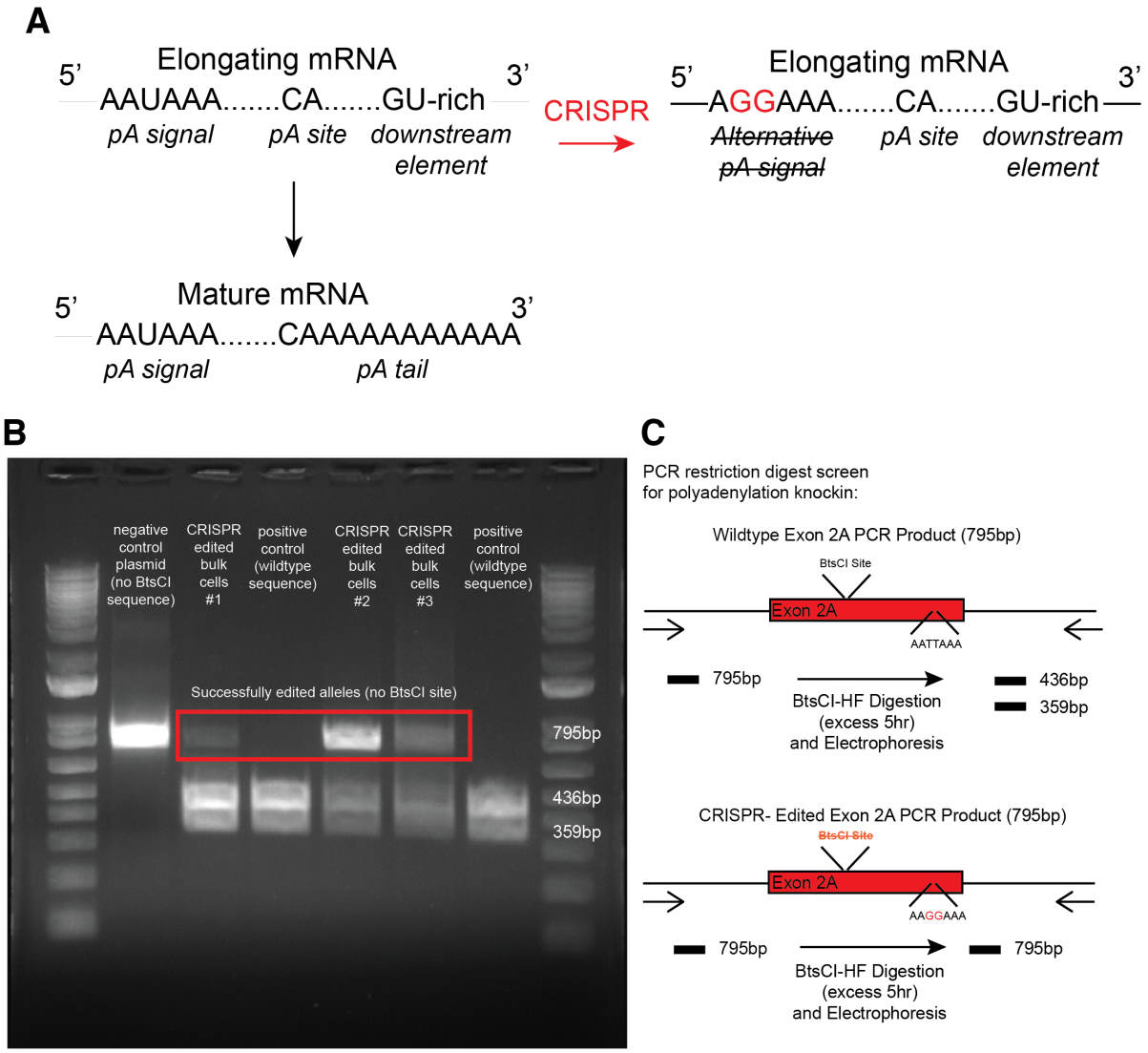

Figure 3.7 Outline of screening process to identify CRISPR-engeineered alternative polyadenylation mutants

(A) Schematic diagramming normal cis-regulatory elements of polyadenylation and the desired mutation of the alternative polyadenylation site. (B) Representative electrophoresis gel of bulk-sorted SH-SY5Y cells after Cas9 and guide transfection identifying the sorted populations amenable for single-cell screening to identify mutants. (C) Schematic of PCR and restriction digest-based assay to identify positive clones before TOPO cloning and Sanger sequencing to confirm genotyping.

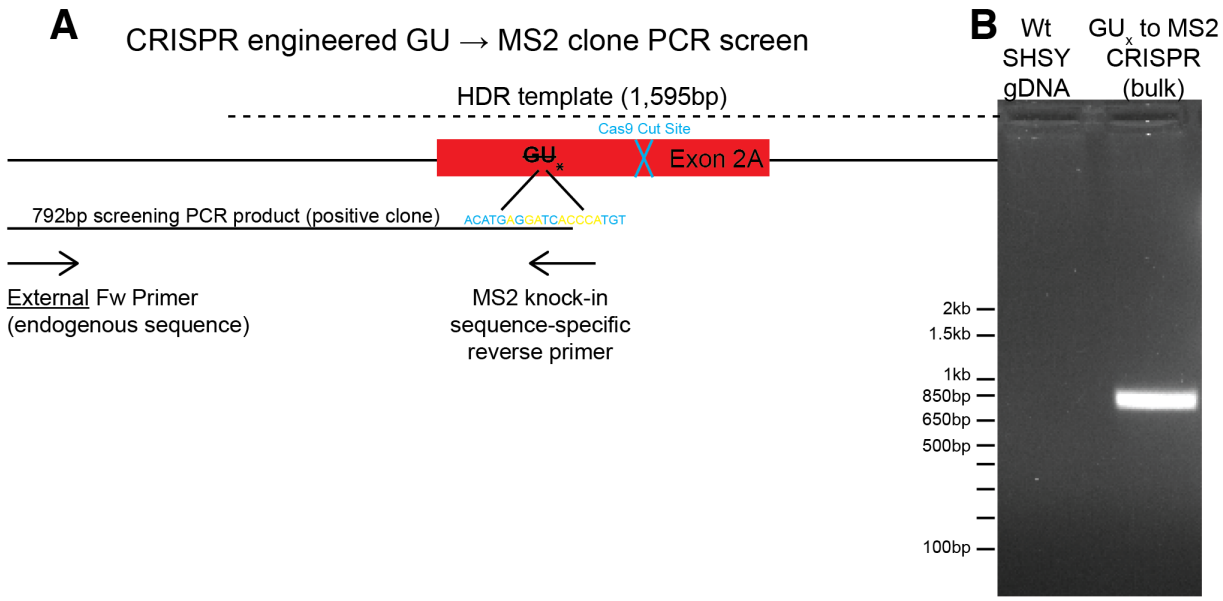

Figure 3.8 Outline of PCR screening strategy to identify GU-to-MS2 engineered SH-SY5Y clones
(A) Schematic of knock-in straddling PCR with internal primer in MS2 sequence and external primer placed outside homology repair template to identify successfully edited clones. (B) Representative PCR of positive and negative screening result using bulk-sorted cells (step before single clone screening) confirming efficient knock-in events.

After Sanger sequencing of completed HDR plasmids, 30 micrograms of each homology template plasmid were linearized to remove the bacterial gene portion by digestion with NotI-HF and EcoRI-HF enzymes for 4.5 hours at 37C. The digestion was stopped with an SDS containing DNA loading dye and size-separated on an agarose gel. The band was cut and gel purified. The linear template DNA is frozen at a concentration of 1336ng/ul (1607bp overall length). MBSP19 TDP to MS2 homology directed repair final concentration of 690ng/ul. These templates were designed for use with the CRISPR plasmid MB-sgRNA-133-134. The Cas9/guide plasmid is about 5.7 times larger than the HDR template, so to exceed the guideline ratio of guide plasmid to HDR template (1:10), an electroporation ratio of 1000ng CRISPR plasmid to 10,000ng template was selected for these two templates.

By contrast, the 3' splice acceptor mutant homology directed repair template was prepared as a commercial single-strand oligo of sequence:

5'CGAACTCATATACCTGGGGATTTTATTACTCTGGGAATTATGTGTTCTGCCCCATC ACTCTCTCTTAATTGGATTTTTAAAATTATATTCATATTGAAAAACTCGGCAGAAGACCTTCG AGAGAAAGGTAGAAAATAAGAATTTGGCTCTC3' from Integrated DNA Technologies (ordered as a 4nmole "Ultramer" format) with the 5'- and 3'- direction selected to be the negative DNA strand so as to be incompatible with direct identification by the Cas9+sgRNA complex (Fig 3.9 A-B). Additionally, the induced mutation encoded by this oligonucleotide disrupts the protospacer seed region of the single guide RNA, and is not predicted to enable cutting of the repair template or repaired edited allele (Fig 3.9 B). Clones successfully edited with this construct are lacking the normal HinfI restriction site located directly adjacent to the edited splice acceptor site and can be screened by PCR across the region followed by digest with HinfI enzyme to identify enzymatic digest-resistant PCR products that retain their full length (Fig 3.9 B-E). The resulting 4nmole of dried 100 base oligonucleotide was resuspended in 100ul of PBS, and 2ul of this was utilized directly for electroporation with 1ug of MB-sgRNA-143-144 (guide protospacer:

TATATTCATATTGCAGGACT, off-target score: 85, activity score: 53, PAM: CGG) in a 100ul reaction volume of Lonza Kit V electroporation reagent in a 2mm cuvette and an equivalent of one 100mm plate of SH-SY5Y cells (ATCC)

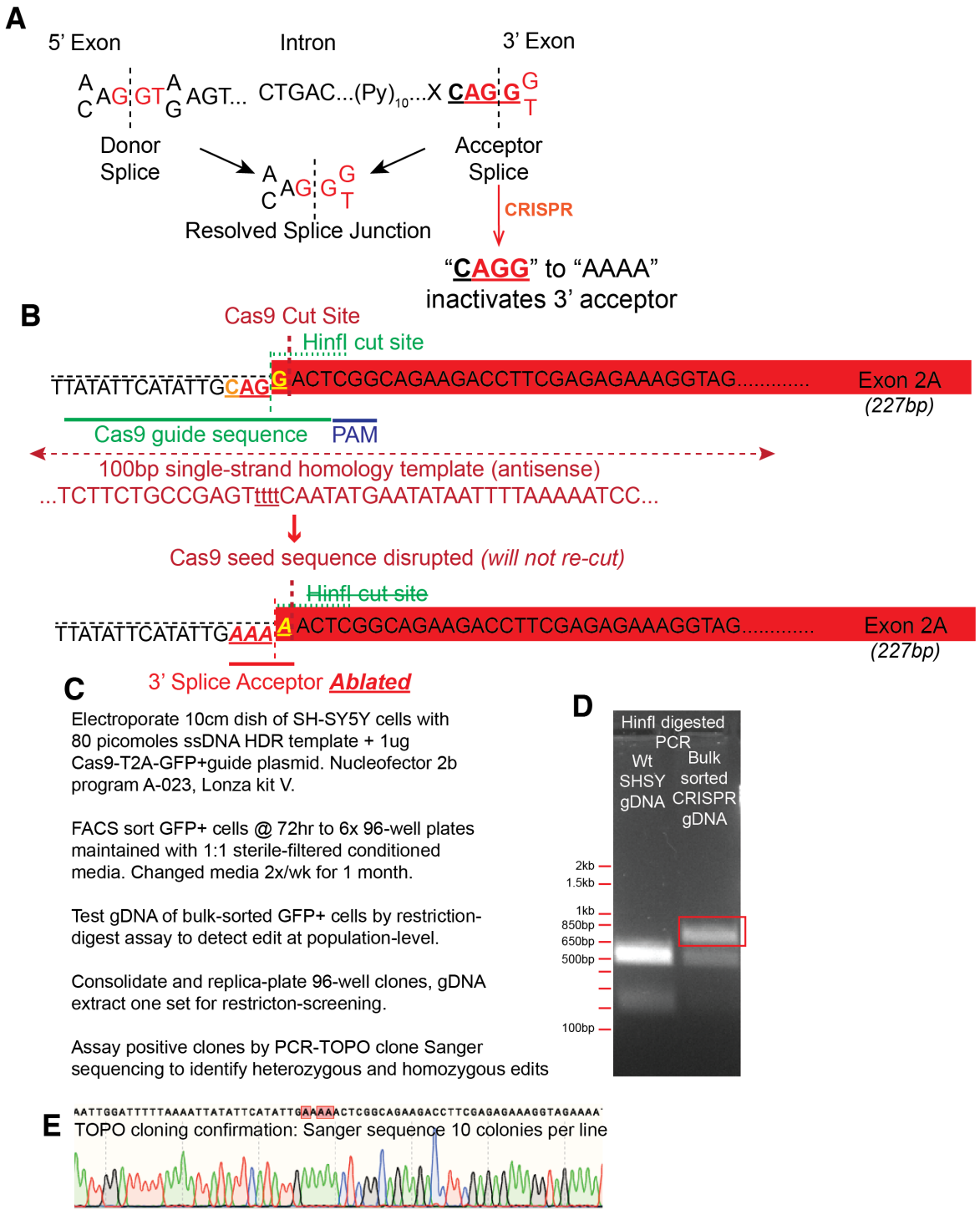

Figure 3.9 Knock-in CRISPR engineering strategy to mutate cryptic 3' splice-acceptor sequence in SH-SY5Y cells

(A) Schematic highlighting functional location of desired knock-in relative to other cis-regulatory elements of splicing. (B) Nucleotide-specific schematic of CRISPR engineering edit strategy, including disruption of a restriction for identification of edited clones. (C) Technical outline of engineering steps utilized. (D) Representative PCR and DNA gel electrophoresis image demonstrating the presence of restriction-digest resistant clones in a bulk population before single-cell isolation and sequencing. (E) Representative Sanger sequencing result from homozygous clone with two edited splice acceptor alleles.

For editing in the target cell line, one 150mm plate of early passage (7) ATCC-sourced Wildtype SHSY-5Y cells grown without antibiotic treatment to ~70% confluence was detached by DPBS wash and brief treatment in 0.05% trypsin, half of the cells were taken for electroporation, replating the rest. Cells were pelleted by centrifugation and resuspended in 350ul Lonza Kit V electroporation solution (100ul per electroporation, or about 2/3 to 1 full confluent plate per electroporation). 100ul of cells resuspended in this mix were added to the premixed homology repair template and Cas9+guide plasmid DNA combination required for each respective edit, and pipetted directly into a sterile electroporation cuvette (2mm). Electroporation with Nucleofector 2b program A-023 was performed and cells were immediately resuspended in 1ml of fresh media and placed in a 15ml tube with 5 ml of normal media. To increase viability, cells were then re-pelleted by centrifugation once again to remove media containing trace amounts of electroporation solution. Pellets were resuspended in 3ml of fresh media, and cells were plated in one well of a 6-well dish per electroporation condition.

The following day the cells were checked for bright GFP fluorescence (which appeared approximately equivalent across electroporation conditions) and cells were passaged to allow further proliferation. 72 hours post-transfection cells were sorted by GFP fluorescence by Fluorescence-Activate Cell Sorting on a SONY SH800 cell sorter. Sorting parameters were devised using a wildtype SH-SY5Y non-fluorescent control cell sample, and sorting gates were set at a minimum of 10-fold higher fluorescent gating over the wildtype background signal level. Sorting to single-cells was performed into 6x 96 well plates per condition, plated with 100ul per well of 20% FBS containing media completed with 1%AA and 1% PenStrep. The remaining GFP positive cells were then bulk-sorted into 15ml conical tubes (14,000 cells per condition, or as allowed by total cell number allowed, and about 5,000 cells for lines where cells ran out while sorting). The bulk-sorted cells were centrifuged and re-plated in a 24 well plate. Between 5-15% of the cells in the parental CRISPR electroporated populations were positive for GFP fluorescence

at 72 hours, with the lowest was the 3' Splice acceptor mutation cells at 5%, indicating an inefficient electroporation process overall for all lines. A sample of bulk-sorted GFP+ cells for each respective edit were replica plated and one replicate lysed for PCR and restriction digest analysis (as indicated for the edit detection protocol) to confirm desired edits were available to find at the bulk-population level before proceeding to individual clone screening, using the screening paradigm previously described.

The day after sorting (after attachment was confirmed by brightfield microscopy), the 100ul of initial media per well was supplemented with another 100ul of 1:1 v/v mixed fresh:sterile-filtered SHSY5Y cell conditioned media. Media was changed (100ul out 100ul conditioned media in) twice a week until colonies filled their wells. (Our incubator evaporates media very quickly on my top shelf assigned position, so I added an additional water dish to the rear side of the shelf where the gas outlets are and change media often to prevent death by osmotic stress.)

Proliferating cells (approximately one third of all wells) were consolidated to new plates to remove gaps wells between proliferating colonies, and during the process were simultaneously replica-plated to new plates during passaging to new 96-well dishes. One replicate plate was seeded with higher density cells for genomic DNA extraction and screening, and the other lower density plate maintained for eventual expansion and characterization. Genomic DNA was extracted from the high-density replicate plate by direct lysis and isolation in a 96-well format gDNA column kit from Zymo research (Cat# D3011). gDNA was eluted in 12ul nuclease free water for direct loading into previously described PCR assays utilizing a Q5 high-fidelity polymerase (New England Biolabs Cat# M0491). A handful of negative clones at this step were selected as isogenic control lines for continued passaging and use, and positive clones from the first screening step were passaged into larger culture plates for an independent genomic DNA isolation and secondary screening by PCR across the edited region with validated primers and the same Q5 polymerase, the resulting PCR product was TOPO cloned into a TOPO blunt kit

(processive polymerases like Q5 leave blunted ends). 10 colonies from each plated TOPO product were grown by bacterial plasmid mini-prep and sent to Sanger sequencing to confirm hetero- vs homo-zygosity calls made in the initial screening. Secondary screening by TOPO cloning was crucial to identify false-positives. Positive heterozygous and homozygous clones and their respective isogenic controls were further characterized for their endogenous expression of overall stathmin-2 and TDP-43 by qRT-PCR, and clones with levels closest to the parental wildtype line were selected for characterization in downstream experiments.

Lentiviral transduction of tetracycline activated expression vectors

MS2 knock-in cells, once identified, were transduced with lentivirus stably expressing the doxycycline-binding Tet3g transcriptional activator from an EF1alpha promoter, along with an internal ribosome entry site and aminoglycoside phosphotransferase gene for selection. A stable expressing population of cells was then split and further transduced with lentivirus carrying a construct under control of the tetracycline responsive element third generation promoter controlling either MCP-dimer expression or the dimer fused to the described TDP-43 (Fig 3.3 B-C). It is notable that no homozygous knock-in clones were recovered from the GU to MS2 conversion CRISPR editing effort, which may indicate that a double knockout of exon 2A TDP-43 binding is non-viable (at least under the selective pressure of FACS sorting stress). With this possible viability constraint in mind and given that MCP expression can rescue stathmin-2 pre-mRNA processing, an alternative future approach to obtain homozygous clones would be to first transduce the parental wildtype line with these two lentiviruses and induce expression with doxycycline for the duration of CRISPR genome engineering to alleviate stathmin-2 related cellular stress.

siRNA transfections

50nM of siRNA “smart pools” from Dharmicon targeting either human TDP-43 (Cat# L-012394-00-0020) or control sequences (Cat# D-001810-10-20) were reverse-transfected into each well of a 50% confluent 12 well plate with RNAiMax transfection reagent following manufacture instructions, and then forward-transfected with a second dose of the same concentration 24 hours later, with cells collected for analysis 96 hours after the initial transfection.

RNA extractions and qRT-PCR:

Cells were collected in Trizol reagent (Invitrogen) and RNA was chloroform extracted per manufacturers protocol, with RNA pellets resuspended in water and evaluated on a NanoDrop machine (Thermo). 1-5ug of RNA (depending on the experiment) was loaded into a 20ul SuperScript-III first-strand cDNA synthesis reaction (Invitrogen) to generate cDNA. cDNA was diluted 1:50 or 1:100 in water and loaded in technical triplicates into 10ul reactions of Bio-Rad iTaq Universal Probes Supermix (Cat# 1725134) and evaluated on a 384 well Bio-Rad C1000 qPCR thermocycler. Primers were as follows:

Full-length stathmin-2: Fw 5’-AGCTGTCCATGCTGTCACTG, Rev 5’-GGTGGCTTCAAGATCAGCTC, Probe 5’-FAM-ATTTGCTTCACTTCCATATCATCGTAAGTATAGATG

GAPDH: Fw 5’- GAAGGTGAAGGTCGGAGTC, Rev 5’- GAAGATGGTGATGGGATTTC, Probe 5’-FAM- CAAGCTTCCCGTTCTCAGCC

Truncated stathmin-2: Fw 5’- CTTTCTCTAGCACGGTCCCAC, Rev 5’-ATGCTCACACAGAGAGCCAAATTC, Probe 5’-FAM- CTCTCGAAGGTCTTCTGCCG

TDP-43: Fw 5’- TCATCCCCAAGCCATTCAGG, Rev 5’- TGCTTAGGTTCGGCATTGGA, Probe 5’-HEX- TCCTCTCCACAAAGAGACTGC

Expression analysis was performed with delta-delta-CT calculations utilizing GAPDH as an endogenous control gene.

Chapters 2, 3, 4, and 5 were supported in part by an institutional award to the UCSD Genetics Training Program from the National Institute for General Medical Sciences, T32 GM008666.

Chapters 3, 4, and 5, in part, are being prepared for publication as “Therapeutic restoration of stathmin-2 expression in TDP-43 proteinopathies.” 2021, and also include co-authored unpublished work. Other authors are: Zevik Melamed, Jone Lopez-Erauskin, Mariana Bravo-Hernandez, Haiyang Yu, Melinda Beccari, Melissa Mcalonis, John Ravits, Karen Ling, Paymann Jafar-nejad, Frank Rigo, Aamir Zuberi, Max Presa, Cat Lutz, C. Frank Bennett, Martin Marsala, Clotilde Lagier-Tourenne, Don W. Cleveland. The dissertation author was the primary investigator and author of this material.

Chapter 4: Steric Antisense Oligonucleotide Binding Restores Endogenous Stathmin-2 Expression and Rescues Axonal Re-Growth in Human Neurons

Abstract:

Previous work demonstrated the vulnerability of motor neurons upon reduction in stathmin-2, a factor we established to be essential for axonal recovery after injury. However, our earlier efforts relied upon AAV to drive additional synthesis of stathmin-2, an approach with multiple practical hurdles that limits its practicality for use as a disease therapy in ALS or FTD, including the potential damage from overexpression of stathmin-2. Recognizing this, I now demonstrate a therapeutically feasible approach through use of ASOs to correct stathmin-2 pre-mRNA splicing. I show that ASO-mediated therapy can restore normal stathmin-2 pre-mRNA processing and protein levels in cells with dysfunctional or depleted TDP-43, thereby restoring axonal regeneration in those cells without exogenous gene transfer.

Introduction:

Antisense oligonucleotide (ASO) therapy for neurodegenerative disease, established by the Cleveland laboratory and developed in collaboration with Ionis Pharmaceuticals, leverages either catalytic RNA degradation (with ASOs formulated for RNase H substrate recognition) or steric alteration of pre-mRNA splicing (with ASOs formulated for RNase H incompatibility). Trials to degrade disease-causing mutant genes with the RNase H strategy are currently underway in SOD1-ALS, C9orf72-ALS (initiated in September, 2018 for targeting hexanucleotide-containing RNAs, see also Fig 1.4), and Alzheimer's disease (initiated October, 2017 for reducing tau). The already FDA-approved ASO therapy Spinraza utilizes the steric binding mechanism of action to

correct pre-mRNA processing in the SMN2 gene, effectively curing the developmental motor neuron disease spinal muscular atrophy (SMA) by preventing degeneration of motor neurons.

Recognizing these precedents for successful use of ASOs for therapy in a neurodegenerative disease context, including by reversal of aberrant splicing, and our evidence establishing stathmin-2 pre-mRNA misprocessing as a new hallmark in ALS mediated by loss of TDP-43, I now identify rescue ASOs (rASOs) capable of restoring stathmin-2 pre-mRNA maturation and stathmin-2 protein levels. Critically, these rASOs restore axon regeneration capacity of cultured human motor neurons when TDP-43 level is suppressed, establishing the use of such rASOs as an attractive translational approach for sporadic ALS and TDP-43 proteinopathies.

Results:

Antisense oligonucleotides (ASOs) chemically formulated to correct RNA processing defects have become an attractive and promising therapeutic approach for neurodegenerative diseases [130]. Such ASOs and constitute the first FDA-approved use in the central nervous system. More than 50 additional ASO applications are currently in clinical trials. Based on my preliminary success using rescue ASOs (rASOs) that bind the stathmin-2 pe-mRNA and induce its processing, 200 ASOs tiling across the exon 2a region were designed. Each was electroporated into SH-SY5Y cells harboring a homozygous ALS-causing TDP-43^{N352S} mutation. More than 34 were identified to increase correct stathmin-2 pre-mRNA processing. From this initial screen, I further validated the four most efficacious rASOs, establishing their capacity to restore normal stathmin-2 mRNA expression (Fig 4.1 A). Assay (by qRT-PCR) of RNA collected 24 hours following rASO introduction (by lipid transfection) demonstrated dose-dependent reduction in levels of the accumulated truncated stathmin-2 RNA variant (Fig 4.1 B) and restoration of stathmin-2 mRNA levels comparable to that of wildtype cells (Fig 4.1 C).

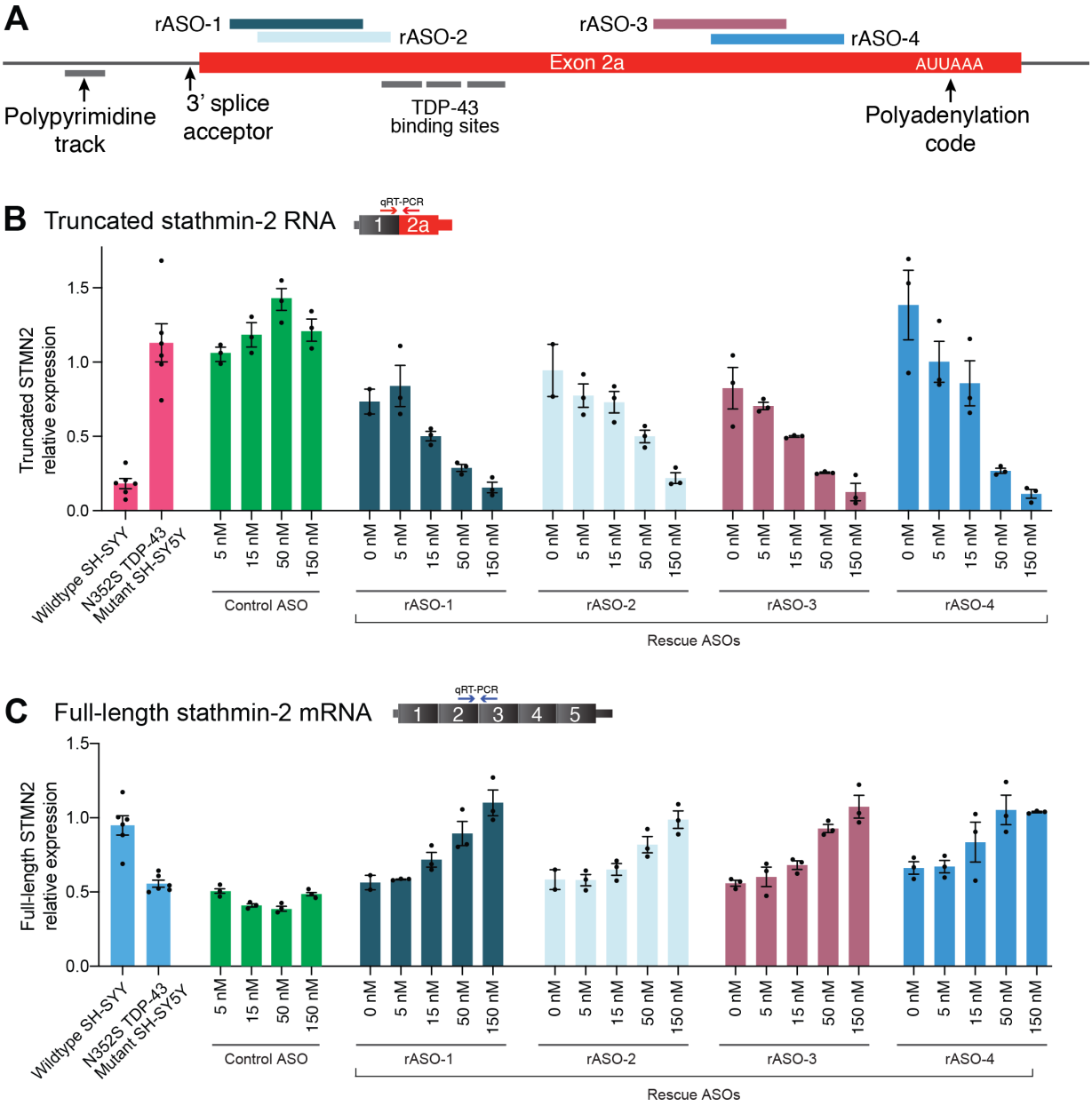

Figure 4.1 Rescue antisense oligonucleotide (rASO) screening identifies steric binding ASOs that suppress missplicing and restore full-length-stathmin-2 RNAs in a dose-dependent manner in cells carrying homozygous N352S mutaiton of TDP-43

(A) Schematic representation of the exon2a region of the human stathmin-2 gene, with the identified locus of TDP-43 binding and 4 representative rASOs that show splice-modifying activity. (B) Graph showing truncated stathmin-2 RNA dose-dependent suppression compared with untreated wildtype and TDP-43 mutated SH-SY5Y cells, as measured by qRT-PCR using GAPDH as an endogenous control gene, each dot is one independent biological replicate. Error bars plotted as SEM. (C) Graph showing stathmin-2 mRNA dose-dependent restoration upon ASO treatment by qRT-PCR using GAPDH as an endogenous control, each dot is an independent biological replicate. Error bars plotted as SEM.

Motor neurons were then induced from pluripotent stem (cells as previously described[91]) matured in cell culture for 30 days followed by rASO addition to culture media for 20 days, followed by TDP-43 depletion (by addition of an ASO targeting TDP-43 mRNA through RNase H-dependent catalytic RNA degradation (Fig 4.2 A). In motor neurons not treated with rASOs, reduction of TDP-43 for 20 days resulted in reduction in stathmin-2 mRNA level to 25% of the original level (Fig 4.2 A, left bar) and accumulation of the cryptically spliced and polyadenylated, truncated RNA variant (as measured with qPCR) (Fig 4.2 B, left bar). Of the four tested rASOs, rASO-3 yielded the greatest (70% of normal) restoration of stathmin-2 mRNA (Fig 4.2 A), accompanied by the corresponding suppression of accumulation of the truncated stathmin-2 RNA (Fig 4.2 B). In agreement with our previous report[91], partial reduction in TDP-43 (by addition of an RNase H active ASO targeting TDP-43 mRNA) resulted in a larger degree of suppression of stathmin-2 RNA and protein level (Fig 4.2 C). Stathmin-2 mRNA levels were fully reversed by addition to neuronal culture media of either rASO-3 or rASO-4 (Fig 4.2 C), demonstrating the therapeutic potential of the splice-rescuing ASO approach for the restoration of endogenous stathmin-2 processing in TDP-43 proteinopathies.

To determine the functional consequence(s) of rASO-mediated endogenous stathmin-2 correction on the axonal regeneration capacity of motor neurons challenged with chronic TDP-43 suppression, we utilized an iPSC-motor neuron axotomy and regrowth assay within microfluidic chambers, as previously described [91]. Sustained lowering of TDP-43 levels in the somatic compartment was achieved for 20 days via addition of targeted RNase H recruiting ASOs to the cell media (Fig 4.2 D). The corresponding loss of stathmin-2 produced complete inhibition of axonal regeneration capacity after mechanically induced axotomy, compared with motor neurons treated with non-targeting control ASOs (Fig 4.2 E, left and middle panels). Importantly, rASO-3 added by free uptake to the somatic compartment 5 days after addition of ASOs to reduce TDP-43 level (Fig 4.2 D), was sufficient to restore expression of stathmin-2 protein (Fig 4.2 E). As

importantly, rASO-3 also reversed the inability of motor neurons to regenerate into the distal compartment.

These results provide evidence supporting the potential of stathmin-2 splice-rescuing ASOs to restore the regenerative capacity of motor neurons that have been damaged as a direct molecular consequence of TDP-43 proteinopathy.

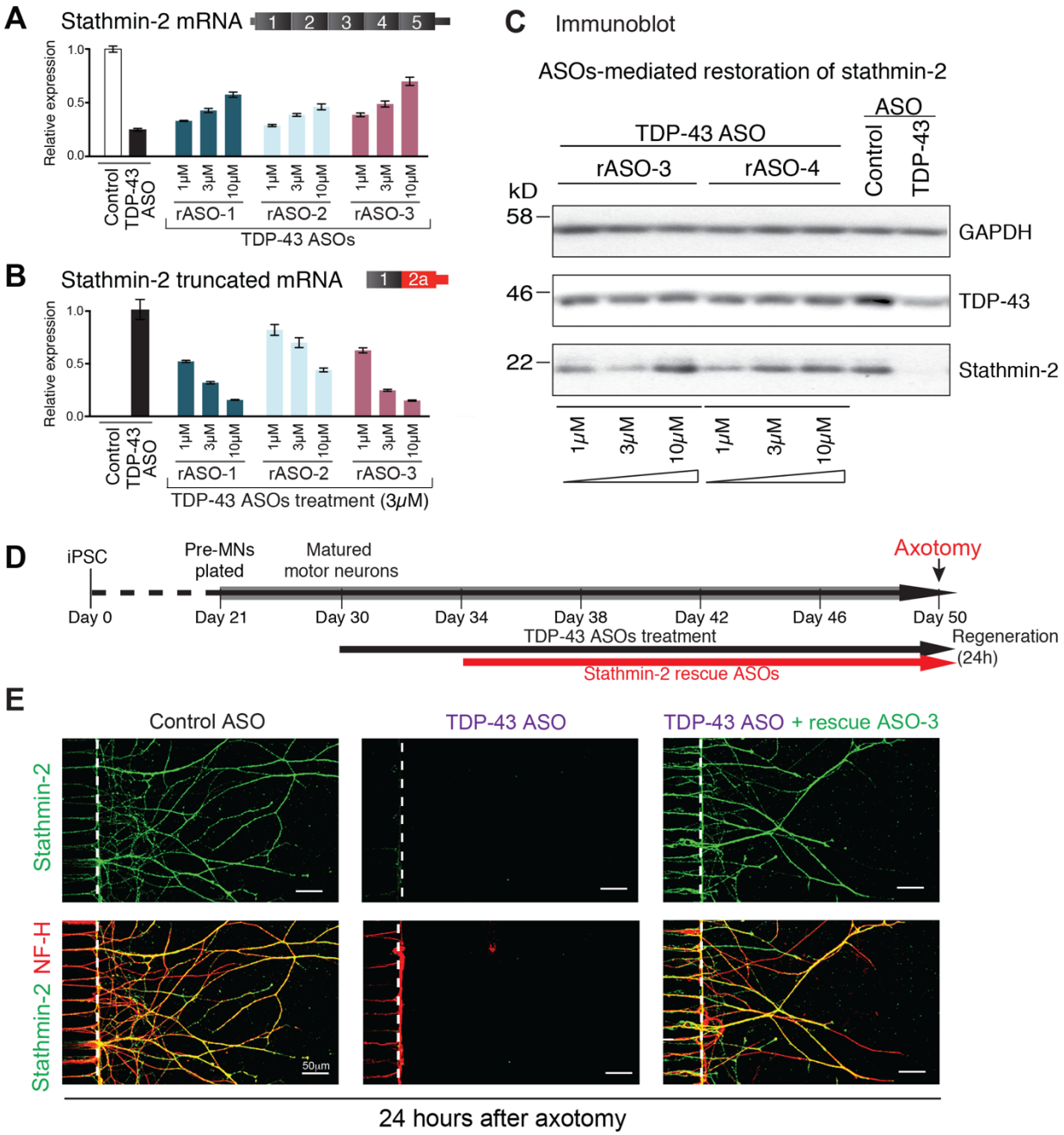

Figure 4.2 Restoration of axonal regeneration capacity using rASOs that alleviate pre-mRNA missplicing and rescue stathmin-2 levels in iPSC-derived motor neurons under conditions of sustained TDP-43 reduction

(A) Stathmin-2 mRNA restoration analyzed by qRT-PCR after treatment with 4 representative rASOs in iPSC-derived motor neurons depleted of TDP-43. Expression of TFRC mRNA was used as endogenous control gene. (B) qRT-PCR analysis of truncated stathmin-2 RNA levels after treatment with 4 representative rASOs in iPSC-derived motor neurons depleted of TDP-43. Expression of TFRC mRNA was used as an endogenous control. (C) Immunoblotting of TDP-43 and stathmin-2 in iPSC-derived motor neurons treated with TDP-43 suppressing ASO and stathmin-2 rASOs by dose-response. GAPDH blotting is shown as an endogenous loading control. (D) Timeline of iPSC-derived motor neuron maturation, and ASO/rASO treatment and axotomy. (E) Immunofluorescence images of distal microgrooves (left of dotted line) and distal compartments (right), 24 hours post-axotomy. Axonal regeneration and growth cones observed b immunofluorescence of stathmin-2 (green) and NF-H (red) in terminals of motor neurons.

Discussion:

Cytoplasmic accumulation coupled with nuclear clearance of the RNA binding TDP-43 is found in affected neurons of most ALS patients[68,69,163], strong evidence that nearly all ALS-causing mechanisms converge on TDP-43 loss of function. However, direct therapeutic targeting of TDP-43 at the protein or mRNA level is challenged by many factors, including 1) unresolved primary molecular mechanisms that provoke its initial misaccumulation and altered intracellular localization, 2) apparently exquisite sensitivity to TDP-43 expression changes in healthy neurons, and 3) an autoregulatory mechanism that is proposed to gate TDP-43 levels by TDP-43 dependence in processing the its own pre-mRNA. These challenges have given rise to two alternative approaches: 1) the targeting of genetic modifiers of TDP-43 pathology and 2) identification of targetable genes and processes downstream of TDP-43 primary dysfunction.

Currently, the major therapeutic effort for the first of these approaches is ASO-mediated suppression of the gene encoding ataxin-2, an ALS risk factor gene and potent modifier of TDP-43 pathology, whose reduction decreased TDP-43 aggregation and extended lifespan in transgenic mice *overexpressing* human TDP-43 [82]. Success of the ataxin-2 ASO approach to reverse RNA metabolism changes in affected neurons may require a cascade of events downstream of ataxin-2 reduction, including restoring nuclear TDP-43 localization and clearance of cytoplasmic aggregation. Therapy efforts for the second approach are complicated by TDP-43's prolific role in the transcriptome, with thousands of binding sites affecting thousands of identified mRNA targets upon TDP-43 pathologic dysfunction, the identification of viable gene targets has proven elusive [73,74,87]. Correspondingly, our identification of stathmin-2 1) to be an essential factor for axonal regeneration after injury, 2) to be one of the most abundantly expressed genes in human spinal motor neurons, and 3) to undergo sustained loss when nuclear TDP-43 levels fall TDP-43-dependent loss, has made it perhaps the most attractive gene target for therapy in sporadic ALS [91].

The use of a non-RNase active ASO to alter pre-mRNA splicing has been proven to be a viable strategy in neurodegenerative disease, exemplified by the FDA-approval of Spinraza (Nusinersen) for spinal muscular atrophy. Spinraza was formulated to bind the pre-mRNA of the SMN2 gene, simultaneously blocking binding of splice-suppressing proteins hnRNPA1 and hnRNPA2 so as to promote inclusion of exon 7 into the final SMN2 mRNA and production of a final mRNA encoding the SMN protein to compensate for inherited loss SMN1 [130,148,178]. From this founding example, I and my colleagues have developed non-RNase H active rescue ASOs (rASOs) whose Watson-Crick base pairing within or near to "exon 2a" of the stathmin-2 pre-mRNA can sterically block utilization of a cryptic splice site that at the 5' border of exon 2a. Our approach enables restoration of normal level of stathmin-2 in neurons affected by TDP-43 pathology.

I note that the rASO approach can restore stathmin-2 without any possibility of a potentially adverse effect of stathmin-2 overexpression, making it a much more therapeutically attractive approach to alternative approaches, including AAV-mediated gene delivery which is likely to overexpress stathmin-2 in neurons (and non-neurons) regardless of TDP-43 status (or bolster expression in non-neuronal cells). Moreover, with my colleague Dr. Erauskin-Lopez, we have established that in human motor neurons a rASO therapy rescues axonal regrowth after injury, demonstrating proof of principle for rASO utilization as a safe, durable, reversible method for correcting TDP-43 pathology-induced stathmin-2 loss in human ALS/FTD. The approach to rescue stathmin-2 using ASOs may also have relevance in a broader spectrum of TDP-43 proteinopathies.

Further validation of the attractiveness of rASO-mediated restoration of stathmin-2 expression in ALS is needed to determine 1) how chronic reduction or loss of stathmin-2 affects an otherwise normal adult nervous system and 2) whether chronic loss of stathmin-2 is sufficient to initiate the age-dependent neurodegeneration seen in ALS, FTD, and other TDP-43 proteinopathies. I undertake efforts to answer these two points in Chapter 5.

Methods:

SH-SY5Y cell culture

ATCC derived neuroblastoma cells were cultured in DMEM/F12 (Gibco) supplemented with 10% v/v fetal-bovine serum except for during FACS sorting and recovery when twice this fraction was utilized (Omega), and 1% v/v penicillin-streptomycin (Gibco) except for one week prior to electroporation when antibiotic-free media was utilized. Cells were grown in a 37ºC incubator with 5% carbon dioxide. For ASO transfection experiments Xfect transfection reagent (Clontech) was utilized. Stock ASO concentrations were confirmed by Absorbance at 260 nanometers on a Nanodrop (Thermo) and known extinction coefficient, dilutions were made based on the final transfection concentration desired and ASO was added to supplied Xfect dilution buffer and mixed by vortexing (50ul total volume of buffer + ASO + transfection reagent per well of a 12 well plate, scaled for the number of biological replicates per concentration), 1.05ul transfection reagent was used per 50ul total transfection volume added directly to the ASO and dilution buffer mix and vortexed again. Volume was collected at the bottom of the tube by brief centrifugation and allowed to stand at room temperature for 15 minutes before being added dropwise to the 12-well plate. Plates were agitated side-to-side before being placed in the incubator. 24 hours post transfection media was removed from all wells and cells were lysed in Trizol reagent (Invitrogen) for 10 minutes at room temperature. Trizol reagent was then diluted 1:1 v/v in ethanol, mixed by pipetting and added directly to a DirectZol-96 column plate (Zymo Research) for direct isolation of RNA and on-column DNase I digestion before being eluted in nuclease free water. RNA concentrations were measured with a NanoDrop (Thermo) and one microgram of cDNA synthesized with SuperScript-III using manufacturer's instructions on a 384-well plate using a C1000 thermocycler (BioRad) for temperature control. cDNA was diluted 1:100

and 4 microliters loaded per 10 microliter reaction for qPCR with hydrolysis probes (as previously described in prior chapters).

Induced pluripotent cells (iPSC) and motor neuron differentiation

The iPSC line was derived from peripheral blood mononuclear cells donated by a 58-year-old healthy male, by introducing episomal DNA expressing Oct4, Sox2, Klf4, L-Myc, Nanog, and shRNAs against p53. The selected clone was fully characterized and demonstrated normal karyotype with normal self-renewal and differentiation capacity comparable with H9 human embryonic stem cells. Next generation sequencing data shows that no modifications occurred in ALS related genes. iPS cells were then differentiated into motor neurons using the proprietary differentiation protocol patented by iXCells Biotechnologies (see provisional application 14359-001-888 for further details).

Antisense Oligonucleotide treatments

All ASO molecules were from Ionis Pharmaceuticals (some manufactured at Ionis and others at Integrated DNA Technologies, Inc under license from Ionis) ASOs mediating RNase H dependent degradation of TDP-43 encoding mRNA: (5'-AAGGCTTCATATTGTACTTT), stathmin-2 encoding mRNA: (5'-GGTCTTAGTCAAGCTCAGAG), murine MALAT1 long-noncoding RNA as a control ASO: (5'-GGGTCAGCTGCCAATGCTAG) were all designed as 5-10-5 gapmers with methoxy-ethyl 2' sugar modifications on the outer 5 bases on either end and 2'deoxynucleotides in the 10 core bases, along with full phosphorothioate modifications at every position throughout with the exception of the stathmin-2 targeting ASO which has phosphodiester linkages in the wings of the ASO and 5'-methylcytosines at all cytosine residues. These ASOs were added to the iPSC motor neuron culture media at day 29 of maturation. Media was changed every 3-4 days with additional ASO added. RNA was collected after 12 days of treatment (day 41

total). The rescue ASOs (rASOs) each were 18-mer oligonucleotides which had phosphorothioates at every linkage and methoxyethyl modifications at the 2' position of every ribose sugar, the sequences were as follows: rASO1 (5'-AGCCAAATTCTTATTTTC), rASO2 (5'-CACACAGAGAGCCAAATT), rASO3 (5'-ATTCATTTCTTCTTAGGC), rASO4 (5'-TCACATTCATTTCTTCTT).

Compartmentalized microfluidic chamber devices and axotomy

Master molds for microfluidic devices were fabricated by photolithography by the Bioengineering Department at the University of California San Diego Nano3 cleanroom facility. Two compartment devices were molded by soft lithography using Sylgard 182 (Ellsworth Adhesives, Germantown WI). Each compartment of the device was 108 microns tall, separated by microgrooves that are 3.1 microns tall, 16.28 microns wide and 830 microns long. The proximal compartment contained one hole on either end 8 millimeters in diameter cut by a biopsy punch while distal holes were 4 millimeters in diameter. After curing the cut devices were bath sonicated in water, then washed in 70% ethanol and sterilized under ultraviolet lamps before being mounted onto glass coverslips. The devices were coated in Matrigel (Corning 356230) for an hour at 37ºC and rinsed with DMEM before plating cells. Five hundred thousand iPSC-derived motor neuron precursor cells were plated in the proximal comatic compartment and axonal growth to distal compartments was achieved during eight days of maturation. ASOs were then added to the somatic compartment for 20 days of treatment, with half the media changed every 4 days and a second dose of ASO added at day 12. For aspiration axotomy media was simultaneously aspirated from one side of the distal compartment and added back to the opposing distal compartment side to create shear forces that removed axons (the process was completed until the distal compartment total axotomy was confirmed.

Chapters 2, 3, 4, and 5 were supported in part by an institutional award to the UCSD Genetics Training Program from the National Institute for General Medical Sciences, T32 GM008666.

Chapters 3, 4, and 5, in part, are being prepared for publication as “Therapeutic restoration of stathmin-2 expression in TDP-43 proteinopathies.” 2021, and also include co-authored unpublished work. Other authors are: Zevik Melamed, Jone Lopez-Erauskin, Mariana Bravo-Hernandez, Haiyang Yu, Melinda Beccari, Melissa Mcalonis, John Ravits, Karen Ling, Paymann Jafar-nejad, Frank Rigo, Aamir Zuberi, Max Presa, Cat Lutz, C. Frank Bennett, Martin Marsala, Clotilde Lagier-Tourenne, Don W. Cleveland. The dissertation author was the primary investigator and author of this material.

Chapter 5: Mouse and Adeno-Associated Virus Models of Stathmin-2 Misprocessing and Loss

Abstract:

My colleagues and I have previously demonstrated in humans that the pathological loss of function and/or nuclear localization of the RNA binding protein TDP-43 that is observed in ALS and other age-associated TDP-43 proteinopathies leads to misprocessing and profound loss of the mRNA encoding neuronal stathmin-2, a protein essential for axonal regeneration. However, even though the human and mouse protein products are 100% identical, I have identified that the genomic elements mediating the TDP-43 dependence of stathmin-2 in humans are not conserved in mice. The impact of sustained stathmin-2 loss in an aged adult mammalian nervous is unknown. Here using novel AAV9 RNAi vectors I designed and produced, loss of murine stathmin-2 has been achieved within neurons of the lumbar spinal cord of adult animals after delivery by subpial administration[150,151]. Chronic loss of stathmin-2 produces loss of neuromuscular junctions and onset of progressive motor and sensory phenotypes that are specific to the targeted lower limbs. These efforts provide powerful support for rescue ASO-mediated restoration of stathmin-2 as an attractive therapeutic approach in sporadic and C9orf72-mediated ALS.

As the endogenous mouse stathmin-2 pre-mRNA does not contain the TDP-43 binding sites found in human exon2a, nor the cryptic elements that mediate pre-mRNA misprocessing, and is thus not processed in a TDP-43-dependent manner, with my colleagues at the Jackson Laboratory I demonstrate a strategy to “humanize” intron 1 of the murine stathmin-2 gene by introduction of a 394bp segment of the human sequence containing the cryptic exon 2a resulting in a successfully TDP-43 state-sensitized murine stathmin-2 gene in-vivo. Indeed, my RNAi AAV vectors were then delivered to deplete TDP-43 in the nervous system of mice with the humanized

stathmin-2 gene and I verified that addition of this human cryptic exon is sufficient to confer sensitivity of mouse stathmin-2 to TDP-43 loss of function. Finally, for the clinical development of stathmin-2 splice-rescuing antisense oligonucleotides (ASOs), I designed and executed a second "humanization" strategy in which I combined the exon 2a humanization with inactivation of the TDP-43 binding site demonstrated in Chapter 3. With this strategy and my colleagues at Jax, I produced a mouse that constitutively misprocesses stathmin-2 pre-mRNAs from the humanized, TDP-43-binding-null allele. This mouse line provides an essential in-vivo screening platform for identification of lead rescue ASOs that will have the highest in-vivo potency and the lowest toxicity in therapy development for sporadic ALS.

Introduction:

ALS is marked by premature denervation and death of upper and lower motor neurons, leading to fatal paralysis, and has clinical, genetic, and pathological overlap with the neurodegenerative disorder FTD, which involves neuron loss affecting changes in behavior and language. While motor neuron death is one feature of ALS, the loss of neuromuscular junctions is widely recognized as one of the earliest clinically measurable pathological events in both sporadic and familial forms of ALS[15,179,180]. Neuromuscular junctions are the sophisticated synapses formed between motor neuron terminals and the muscle cells they innervate, and their disruption occurs prior to disease onset and eventual motor neuron degeneration[179-182].

The landmark discovery in 2019 of stathmin-2 disruption as a hallmark of these TDP-43 proteinopathies[91] has opened new avenues for understanding the mechanisms by which TDP-43 dysfunction can initiate a disease cascade leading from neuromuscular junction disruption to axonal degeneration and neuronal loss. Upon axonal injury, stathmin-2 is upregulated and recruited to growth cones of regenerating axons[117] where we have demonstrated it plays an indispensable role in regrowth[91]. Microtubule destabilization is known to mediate axon branch

loss in neuromuscular synapse elimination during development[183], and stathmin-2 is thought to directly affect this process either by directly promoting catastrophe[184] or preventing tubulin assembly[106]. Additionally, immunofluorescence staining in adult animals reveals that stathmin-2 localizes to neuromuscular junctions in mice, and evidence from Drosophila shows the only stathmin ortholog of that organism is required for neuromuscular junction stability[122]. Of the four mammalian stathmin proteins, the contribution of stathmin-2 toward long term maintenance and stability of adult neuromuscular junction synapses is unknown.

As first direct link between RNA metabolism defects and impaired microtubule dynamics, stathmin-2 has emerged as arguably the most relevant therapeutic target in sporadic ALS[91] and FTD[91,165], with additional unexplored potential in dementia with Lewy bodies and Alzheimer's disease. Indeed, multiple ongoing efforts by both academic and industry groups seek to restore normal stathmin-2 levels or pre-mRNA processing in TDP-43 proteinopathy. Having established in human motor neurons that splice-correcting antisense oligonucleotide drugs can restore normal stathmin-2 expression and reverse axonal regeneration defects brought on by TDP-43 loss or mutation, our team is well positioned to develop an ASO-based stathmin-2 restorative therapy. However, because in-vivo efficacy is indispensable to the success of a clinical development program, and murine stathmin-2 is not conserved in cryptic elements necessary for misprocessing of the stathmin-2 pre-mRNA, the advancement of this strategy now requires the creation of new and innovative in-vivo animal models.

Constraining this advance, it is not established whether the identified cryptic elements mediating stathmin-2 mis-splicing and premature polyadenylation in humans will translate to the machinery of the mouse transcriptional environment. Even if such a "humanized" stathmin-2 mouse carrying these cryptic elements were to perfectly recapitulate the profound TDP-43 pre-mRNA processing dependence of the human gene, mouse TDP-43 levels are notoriously difficult

to modulate without inducing severe acute toxicity, casting serious doubt on the ultimate utility of a TDP-43 gated stathmin-2 mouse model for ASO drug development.

Here, to first determine the functional consequences of chronic stathmin-2 loss from the adult mammalian central nervous system, I design and build a series of novel adeno-associated virus (AAV) vectors leveraging RNA polymerase II-regulated microRNA-based RNA interference techniques[185] to profoundly suppress murine stathmin-2 RNAs. Together with Drs. Jone Erauskin-Lopez and Mariana Bravo-Hernandez, stathmin-2 suppression is achieved focally within the lumbar spinal cord following subpial surgical AAV administration[150,151], achieving chronic reduction of stathmin-2 lumbar expression to only 6% of its initial level and triggering neuromuscular junction loss along with focal, progressive, sensory and motor phenotypes.

I next designed AAV-RNAi vectors to modestly reduce brain TDP-43 levels in newborn transgenic mice containing a murine stathmin-2 gene “humanized” by a 394-base knock-in fragment containing the human stathmin2 cryptic exon 2a. With these, I determine that the human cryptic elements when inserted into the mouse gene are sufficient to mediate murine-TDP-43-dependent disruption in stathmin-2 pre-mRNA (in support of stathmin-2 humanized mouse models for the study of TDP-43 molecular pathogenesis). Finally, based upon the corpus of molecular evidence presented in previous chapters presented here, we develop a proof-of-concept murine neuron-like cell line carrying an approximately three kilobase segment of the first intron of human stathmin-2, but with the human TDP-43 binding locus replaced by an MS2 aptamer sequence, and demonstrate this produces constitutive misprocessing and a chimeric truncated RNA product. Utilizing this platform and my colleagues at the Jackson Laboratory, we build a knock-in stathmin-2 misprocessing mouse model for rescue ASO drug clinical development which I demonstrate can be utilized without upstream modulation of TDP-43 expression.

Results:

Recognizing that expression of mutant stathmin has been reported to cause retraction of motor neuron axons from innervated neuromuscular junctions in *Drosophila*[122], I utilized a non-traditional RNA polymerase II regulated RNAi system[185] based on the structural elements of a microRNA (normally processed from the third intron of a novel long non-coding RNA[186] mir30a) to develop adeno-associated virus (AAV) vector that, by targeting its 3' untranslated region, could efficiently reduce mouse stathmin-2 levels in neuron-like N2A cells (Figure 5.1 A-C).

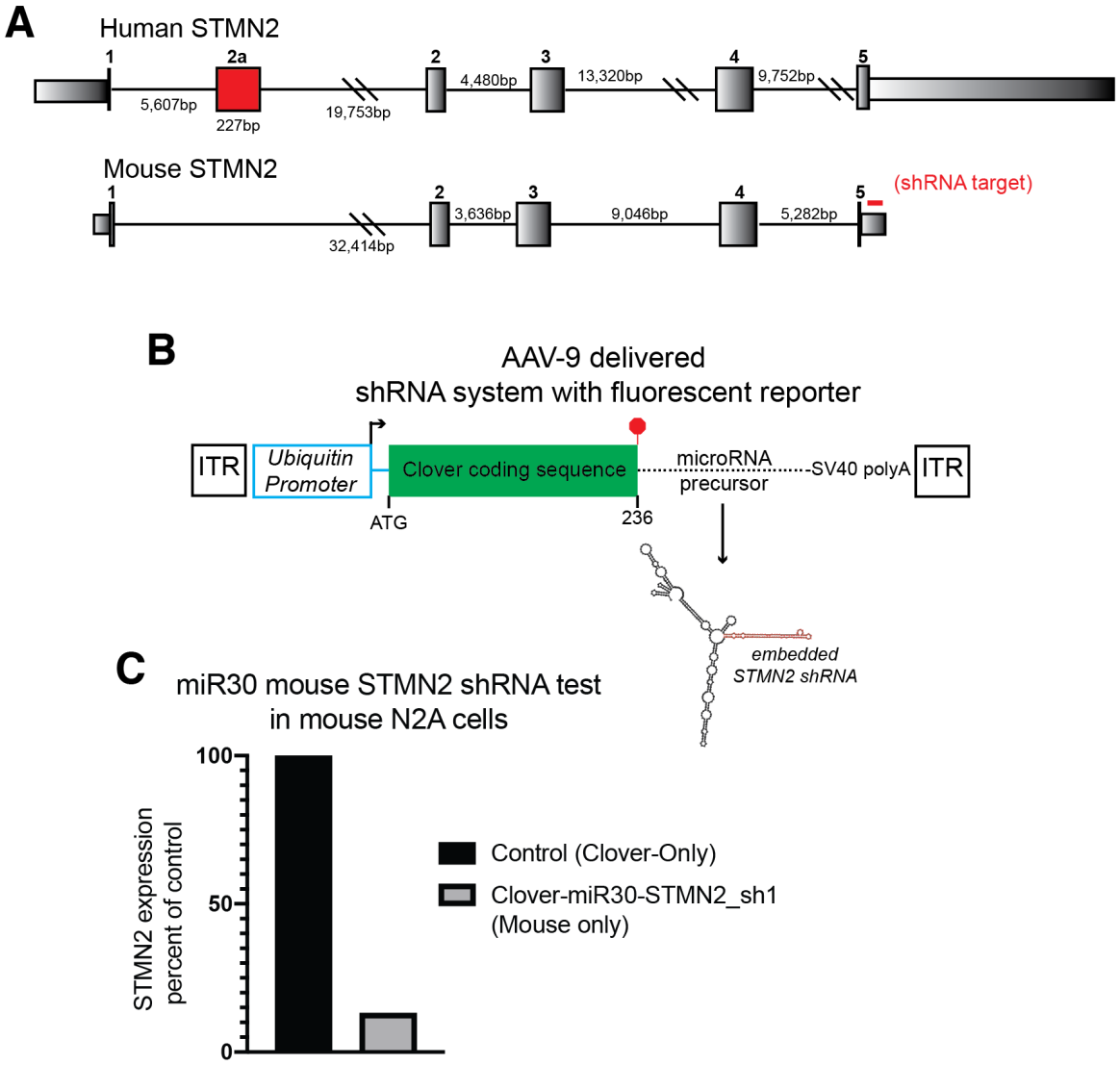

Figure 5.1 Design and in-vitro testing of an RNA polymerase II driven RNAi system to reduce murine stathmin-2 expression

(A) Schematic of human stathmin-2 gene with cryptic exon 2a and mouse stathmin-2 gene without cryptic element conservation, RNAi target within 3' untranslated region of mouse stathmin-2 indicated at right. (B) Schematic of AAV transfer vector payload encoding a ubiquitin pol II promoter, a clover fluorescent protein coding sequence, followed by the microRNA precursor sequence with embedded stathmin-2 targeting hairpin, followed by an SV40 polyadenylation sequence. (C) Proof of concept testing of stathmin-2 RNA suppression using simple payload transfection into mouse neuron-like N2A cells and measuring RNA levels by qRT-PCR with mouse GAPDH as an endogenous control gene.

To determine the consequences of chronic, focal, specific and profound reduction of stathmin-2 levels in an adult mouse, I packaged this viral vector and a control vector targeting the non-expressed gene beta-galactosidase into AAV9n capsids which is capable of efficiently transducing spinal neurons[187], and our team administered the vectors into the lumbar spinal cord of aged (1 year old) mice via surgical sub-pial administration[150,151] (beneath the inner-most layer pia mater) to allow focal administration to deep gray matter cells of that spial cord region, but importantly, without targeting cells of the upper spinal cord that control motor function of forelimbs or respiratory muscles (Figure 5.2 A, B).

Figure 5.2 Subpial lumbar administration of AAV9 stathmin-2-targeting RNAi system in adult animals results in focal, chronic, and specific depletion of mouse stathmin-2 within neurons of the lumbar spinal cord and dorsal root ganglion cells

(A) Schematic of mouse stathmin-2 gene without cryptic element conservation, RNAi target within 3' untranslated region of mouse stathmin-2 indicated at right. (B) Schematic of focal AAV administration to via subpial injection to transduce cells of the lumbar spinal cord controlling hindlimb function, but spare cervical spinal cord controlling forelimbs. (C) Measurement of mouse stathmin-2 levels in non-target control AAV and stathmin-2 reducing AAV injected animals at cervical, thoracic, and lumbar levels at 4- and 32-weeks post-administration. Measurements made on extracted RNA by qRT-PCR using GAPDH as an endogenous control gene. Each data point is an individual mouse. Error bars are plotted as SEM. (D) Measurement in lumbar spinal cord segments at 32 weeks post injection of control or stathmin-2 targeting AAV of RNA expression by qRT-PCR with a panel of genes including mouse stathmin1-4 and potential off-target genes confirms focal stathmin-2 suppression is specific to the intended RNAi target. GAPDH used as an endogenous control gene. Each data point is an individual mouse. Error bars are plotted as SEM. (E) Measurement of stathmin-2 RNA levels in dorsal root ganglion 32 weeks post-injection comparing uninjected animals, control non-target RNAi injected animals and animals injected with RNAi targeting stathmin-2. GAPDH is used as an endogenous control gene. Each data point is an individual mouse. Error bars plotted as SEM.

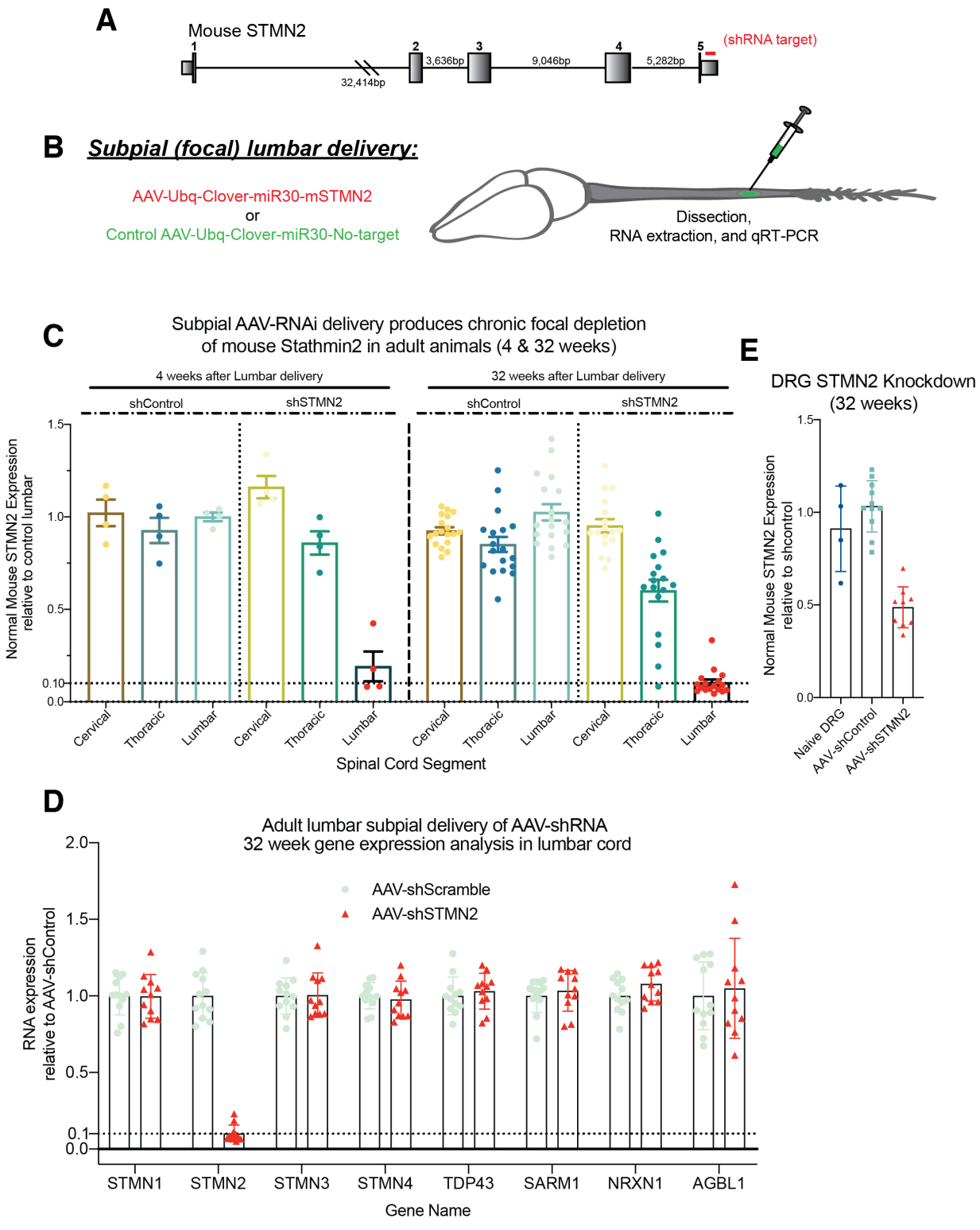
A
Mouse STMN2
1
2
3
4
5
(shRNA target)
32,414bp
3,636bp
9,046bp
5,282bp
B
Subpial (focal) lumbar delivery:
AAV-Ubq-Clover-miR30-mSTMN2
or
Control AAV-Ubq-Clover-miR30-No-target
Dissection,
RNA extraction, and qRT-PCR
C
Subpial AAV-RNAi delivery produces chronic focal depletion
of mouse Stathmin2 in adult animals (4 & 32 weeks)
4 weeks after Lumbar delivery
32 weeks after Lumbar delivery
shControl
shSTMN2
shControl
shSTMN2
Normal Mouse STMN2 Expression
relative to control lumbar
1.5
1.0
0.5
0.10
0.0
Cervical
Thoracic
Lumbar
Cervical
Thoracic
Lumbar
Cervical
Thoracic
Lumbar
Cervical
Thoracic
Lumbar
Spinal Cord Segment
E
DRG STMN2 Knockdown
(32 weeks)
Normal Mouse STMN2 Expression
relative to shcontrol
1.5
1.0
0.5
0.0
Naive DRG
AAV-shControl
AAV-shSTMN2
D
Adult lumbar subpial delivery of AAV-shRNA
32 week gene expression analysis in lumbar cord
AAV-shScramble
AAV-shSTMN2
RNA expression
relative to AAV-shControl
2.0
1.5
1.0
0.5
0.1
0.0
STMN1
STMN2
STMN3
STMN4
TDP43
SARM1
NRXN1
AGBL1
Gene Name

My expression analysis by qRT-PCR on RNA extracted from cervical, thoracic, and the targeted lumbar spinal cords collected 4- and 32-weeks after subpial administration showed a robust reduction of murine stathmin-2 at both time points, with an average of 80% reduced expression after 4-weeks versus the non-targeting control virus injected animals, and an average of 90% reduction by 32-weeks with some animals with reduction to only ~6% of the normal murine lumbar stathmin-2 level (Figure 5.2 C-D). Of key importance to this surgical administration strategy, the murine stathmin-2 reduction remained almost entirely focal at both time points with no indication of knockdown in the cervical spinal cord level, and only four animals at 32-weeks showing knockdown at the thoracic cord level (probably due to virus leaking up into this compartment after administration) (Figure 5.2 C). Lumbar spinal cord RNA from the 32-week timepoint was further analyzed to detect either potential off-target effects of the RNAi system or endogenous compensatory expression changes in the other murine stathmin genes, with no expression differences found (aside from the targeted murine stathmin-2) between targeting- and control-AAV injected groups (Figure 5.2 D).

This outcome demonstrates efficient, focal, and specific depletion of stathmin-2 was achieved using this system. In contrast to typical reports wherein AAV administered via lumbar intrathecal or cisternal injection results in high levels of dorsal root ganglion transduction but relatively poor targeting of deeper grey matter cells[150], qRT-PCR analysis of RNA from dorsal root ganglion at the 32-week time point indicated only 50% reduction of murine stathmin-2 (Fig 5.2 E).

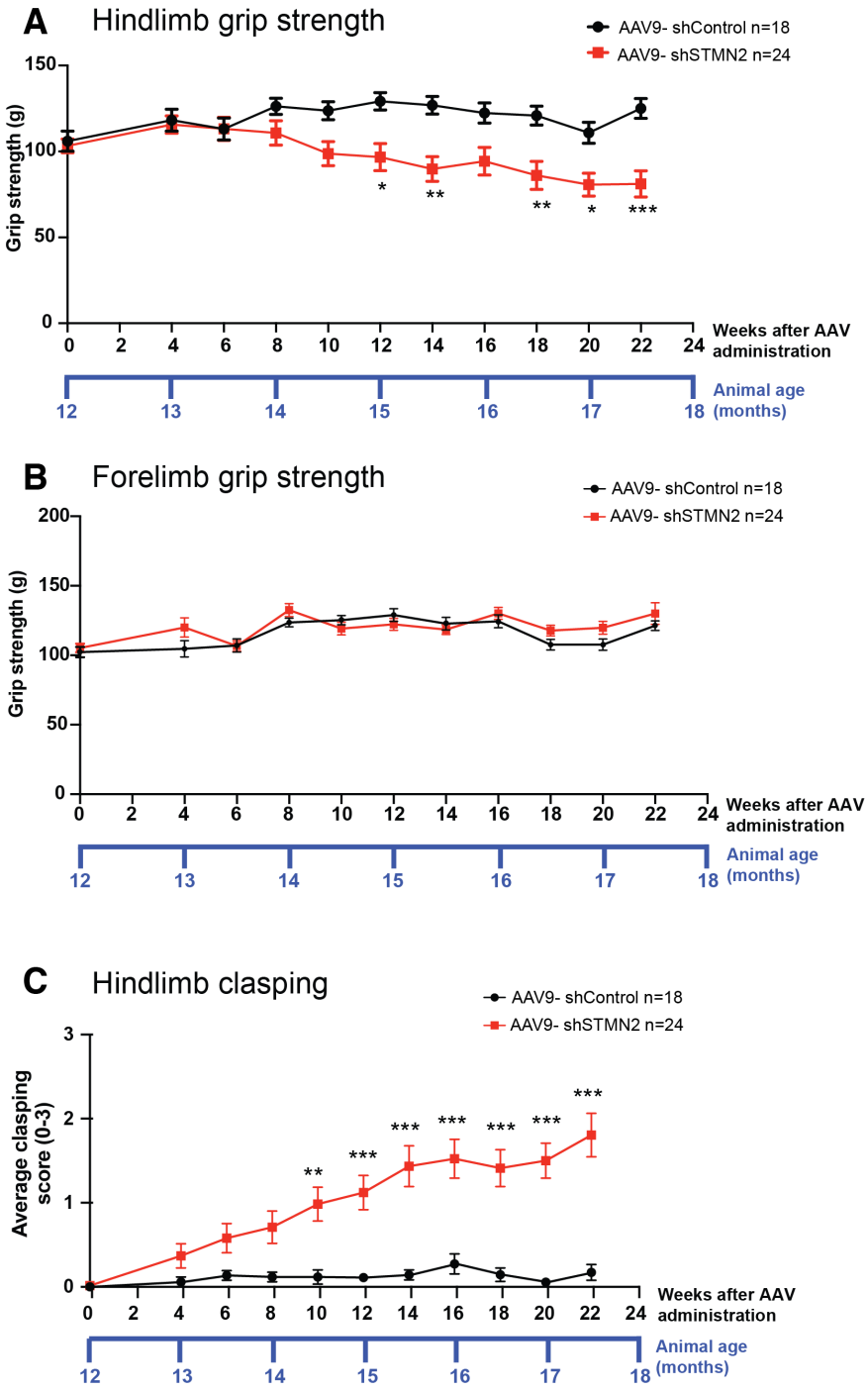

Figure 5.3 Subpial lumbar administration of AAV9 RNAi system results in focal, targeted, and specific depletion of mouse stathmin-2 within neurons of the lumbar spinal cord and dorsal root ganglion cells

(A) Time course of measurements of hindlimb grip strength in 12-month-old animals treated by subpial administration of AAV9 encoding stathmin-2 reducing or non-target control RNAi payloads. (B) Time course of measurements of forelimb grip strength in 12-month-old animals treated by subpial administration of AAV9 encoding stathmin-2 reducing or non-target control RNAi payloads. (C) Time course of measurements scoring hindlimb clasping in 12-month-old mice treated by subpial administration of AAV9 encoding stathmin-2 reducing or non-target control RNAi payloads.

Consistent with the lumbar-targeted stathmin-2 reduction, phenotypic analysis showed no detectable changes in grip strength to the forelimbs (Fig 5.3 B), but apparent hindlimb grip strength loss began starting 8 weeks post-injection and progressed slowly for the duration of the experiment (Fig 5.3 A). This was accompanied by early and progressive indications of hindlimb clasping (Fig 5.3 C), which is a common early indicator in mouse models of ataxic neurodegenerative disease[188,189] including TDP-43 mouse models [80]. These motor phenotypes were accompanied by an apparent loss of protective sensation response (touch and pain) in the hindlimbs, which was evaluated by Von Frey tactile sensitivity testing. Von Frey testing utilizes individual calibrated plastic filaments with bending forces ranging from 0.02 grams to 2 grams are applied to the plantar surface of the hind paw to determine the amount of force required on the filament for the mouse to retract their paw. Increasing control mouse response to increasing filament force is attenuated upon stathmin-2 suppression, indicating reduced touch sensitivity in this group (Fig 5.4).

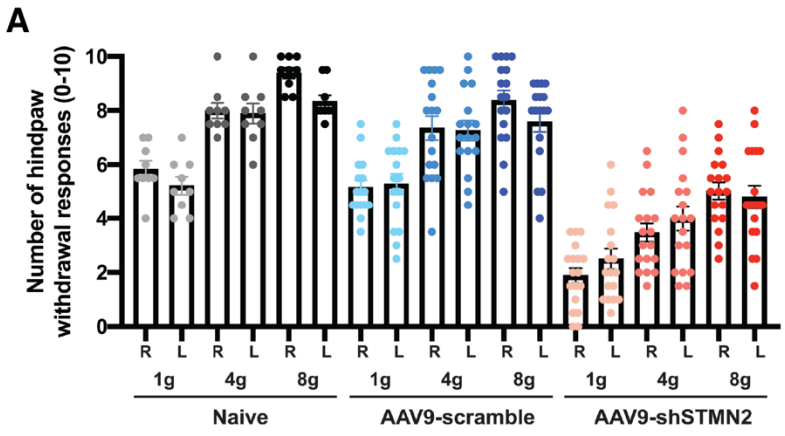

Figure 5.4 Chronic suppression of stathmin-2 by subpial AAV9 RNAi results in reduced touch sensitivity in affected hindpaws

(A) Von Frey hair testing of AAV9 subpial lumbar stathmin-2 RNAi depleted animals indicates a reduced sensitivity to touch in the plantar surface of the hind-paw, indicated by a lower frequency of hindpaw withdrawal responses compared with non-target and uninjected control animals. Testing was performed 30-32 weeks post AAV administration.

To determine whether the human-specific cryptic elements contained within the stathmin-2 exon 2a region of intron 1 are sufficient to confer TDP-43 sensitivity in the context of an otherwise murine stathmin-2 gene and transcriptional environment, I modified the AAV RNAi vector backbone from the murine stathmin-2 reduction experiment for targeted reduction of the gene encoding mouse TDP-43. I designed and tested five new microRNA elements targeting elements against the 3' untranslated region of TARDP and selected the two elements that showed the greatest activity in mouse neuron-like N2A cells to produce two new AAV9 viral vectors (Fig 5.5 A-B). To test the activity of these vectors in the mouse central nervous system a dose-response experiment was performed in P0 pups with delivery (by ICV injection) of either undiluted virus or dilutions of 1:10 or 1:100, in phosphate buffered saline, and measuring cortical TDP-43 RNA levels versus a set of three control animals (Fig 5.5 C). The dose response reflected the relative effectiveness seen in the N2A cells, although the in-vivo efficacy of the vectors was greatly diminished compared with the in-vitro result (Fig 5.5 B). This may reflect that in-vivo TDP-43 reduction is complicated by tight autoregulatory mechanisms involving processing of the targeted 3' untranslated region. It is possible that coding exon targeted microRNA vectors would have shown greater effect, but this was not attempted. Given the limited knockdown capacity of these vectors in-vivo, I additionally packaged the same transfer vectors into AAV-PHP.eB serotype capsids[157], which have a slightly higher transduction efficiency in-vivo by P0 ICV administration[190].

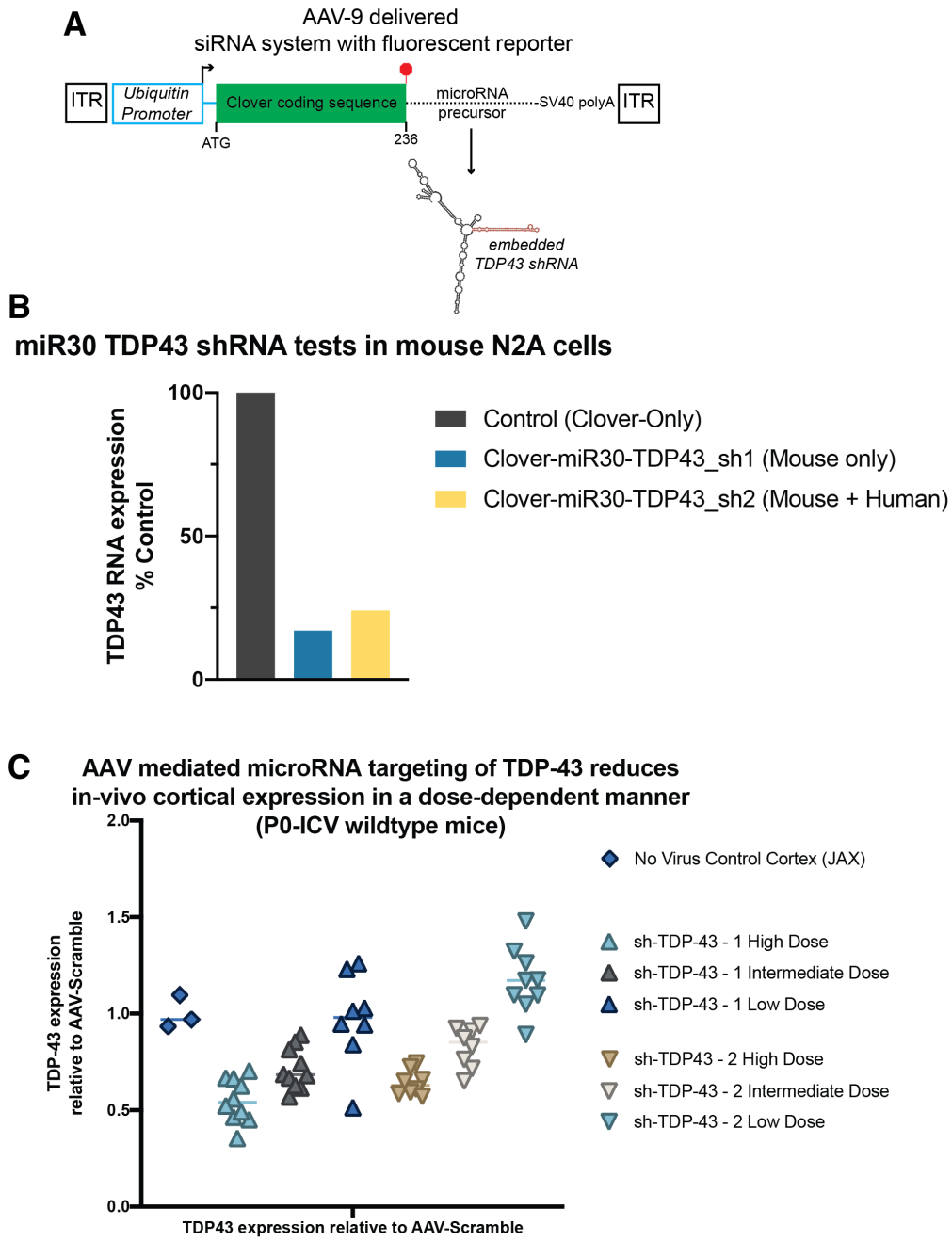

Figure 5.5 Design and testing of AAV9 RNAi vectors targeting mouse TDP-43, in-vitro and in-vivo
(A) Schematic of AAV transfer vector payload encoding a ubiquitin pol II promoter, a clover fluorescent protein coding sequence, followed by the microRNA precursor sequence with embedded TDP-43 targeting hairpin, followed by an SV40 polyadenylation sequence. (B) Proof of concept testing of two TDP-43 RNA suppression vectors using simple payload transfection into mouse neuron-like N2A cells and measuring RNA levels by qRT-PCR with mouse GAPDH as an endogenous control gene. (C) Proof of concept testing of two TDP-43 RNA suppression vectors in-vivo utilizing P0 ICV injection into newborn pups with a 1:1 1:10 and 1:100 dose response of each vector or a no-virus control, measuring RNA levels from cortex collected at 4 weeks post-transduction by qRT-PCR with mouse GAPDH as an endogenous control gene. Each data point is an individual mouse.

Next, CRISPR-Cas9 genome engineering was used to cut at two adjacent loci within the first intron of the murine stathmin-2 gene, removing 479 bases of mouse sequence and inserting a 394-base segment of human sequence (not counting mouse sequence homology arms used for homology-directed repair), with the human sequence containing the full 227 base exon 2a element. With this strategy, the insertion site positioned the human sequence starting 5466 bases into the murine intronic sequence (producing the same positioning of the human cryptic element as it is in the human gene) (Fig 5.6 A).

Homozygous lines of stathmin-2 “humanized” mice carrying this minimalist human exon 2a stathmin-2 insertion were generated and pup cohorts injected at birth with AAV9 with 1) a non-targeting RNAi control sequence, 2) vehicle control (phosphate buffered saline), 3) the top preforming TDP-43 reducing vector, or 4) a no-injection control cohort (to detect whether cellular stress induced by injections caused TDP-43 disruption) (Fig 5.6 B-F). AAV-PHP.eB capsid vectors were identically administered but without the no-injection control cohort (Fig 5.6 B-C, G-I). qRT-PCR analysis that I performed on RNA extracted from cortical tissues 4 weeks post-injection revealed that despite very modest reductions in mouse TDP-43 expression achieved by both virus serotypes (Fig 5.6 E, H), a truncated chimeric RNA containing mouse exon 1 ligated to the humanized exon 2a was detectable exclusively in the animals dosed with TDP-43 disrupting RNAi (Fig 5.6 D, G).

Thus, the mouse stathmin-2 pre-mRNA, when humanized with a small fragment of human sequence (containing the cryptic elements I identified and characterized in previous chapters), is rendered exquisitely sensitive to TDP-43 dependent misprocessing. No overall reduction of total full-length mouse stathmin-2 RNA was detected (Fig 5.6 F, I), probably due to the very modest level of TDP-43 dysregulation.

Figure 5.6 Mice with stathmin-2 humanized by knock-in of a small human exon 2a fragment show high sensitivity in pre-mRNA processing to very modest TDP-43 suppression

(A) Schematic showing knock-in of a small human exon 2a fragment inserted into the first intron of the mouse stathmin-2 gene. (B-C) Schematics showing AAV payload design and P0 ICV route of administration. (D) Measurement of chimeric RNA consisting of mouse exon-1 spliced to human exon-2a in mice injected with non-target control RNAi vector, naïve mice, mice injected with a vehicle (PBS) control treatment, and mice injected with a TDP-43 targeting RNAi vector, 4-weeks post administration by P0 ICV injection with AAV9 serotype capsid. Measurements made on extracted RNA extracted from cortex by qRT-PCR using GAPDH as an endogenous control gene. Each data point is an individual mouse. Error bars are plotted as SEM. (E) Measurement of endogenous TDP-43 encoding RNA in mice injected with non-target control RNAi vector, naïve mice, mice injected with a vehicle (PBS) control treatment, and mice injected with a TDP-43 targeting RNAi vector, 4-weeks post administration by P0 ICV injection with AAV9 serotype capsid. Measurements made on extracted RNA extracted from cortex by qRT-PCR using GAPDH as an endogenous control gene. Each data point is an individual mouse. Error bars are plotted as SEM. (F) Measurement of full-length mouse stathmin-2 RNA in mice injected with non-target control RNAi vector, naïve mice, mice injected with a vehicle (PBS) control treatment, and mice injected with a TDP-43 targeting RNAi vector, 4-weeks post administration by P0 ICV injection with AAV9 serotype capsid. Measurements made on extracted RNA extracted from cortex by qRT-PCR using GAPDH as an endogenous control gene. Each data point is an individual mouse. Error bars are plotted as SEM. (G) Measurement of chimeric RNA consisting of mouse exon-1 spliced to human exon-2a in mice injected with non-target control RNAi vector, mice injected with a vehicle (PBS) control treatment, and mice injected with a TDP-43 targeting RNAi vector, 4-weeks post administration by P0 ICV injection with AAV-PHP.eB capsid. Measurements made on extracted RNA extracted from cortex by qRT-PCR using GAPDH as an endogenous control gene. Each data point is an individual mouse. Error bars are plotted as SEM. (H) Measurement of mouse TDP-43 RNA levels in mice injected with non-target control RNAi vector, mice injected with a vehicle (PBS) control treatment, and mice injected with a TDP-43 targeting RNAi vector, 4-weeks post administration by P0 ICV injection with AAV-PHP.eB capsid. Measurements made on extracted RNA extracted from cortex by qRT-PCR using GAPDH as an endogenous control gene. Each data point is an individual mouse. Error bars are plotted as SEM. (I) Measurement of mouse full-length stathmin-2 RNA in mice injected with non-target control RNAi vector, mice injected with a vehicle (PBS) control treatment, and mice injected with a TDP-43 targeting RNAi vector, 4-weeks post administration by P0 ICV injection with AAV-PHP.eB capsid. Measurements made on extracted RNA extracted from cortex by qRT-PCR using GAPDH as an endogenous control gene. Each data point is an individual mouse. Error bars are plotted as SEM.

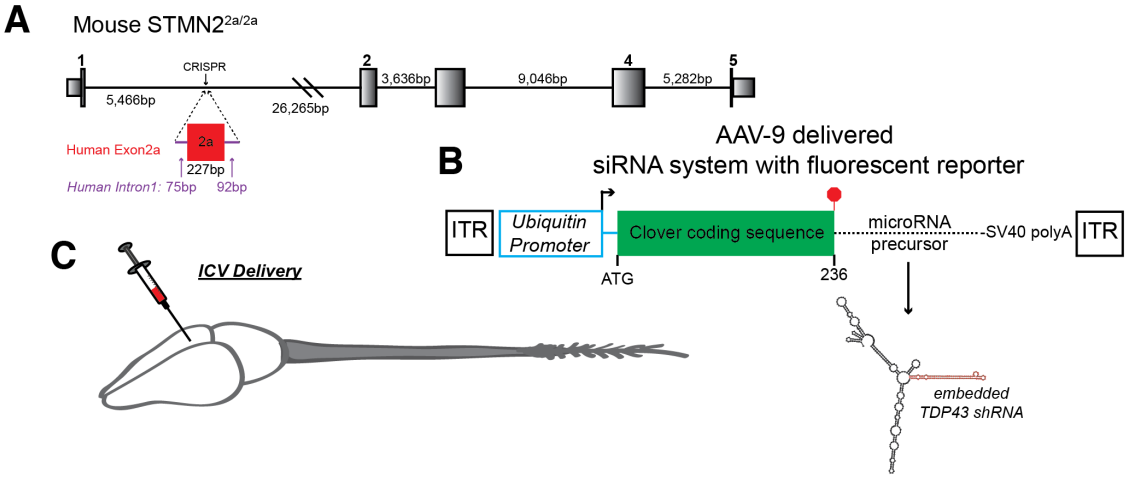

AAV9 Capsid ICV P0 Injection (4 weeks)

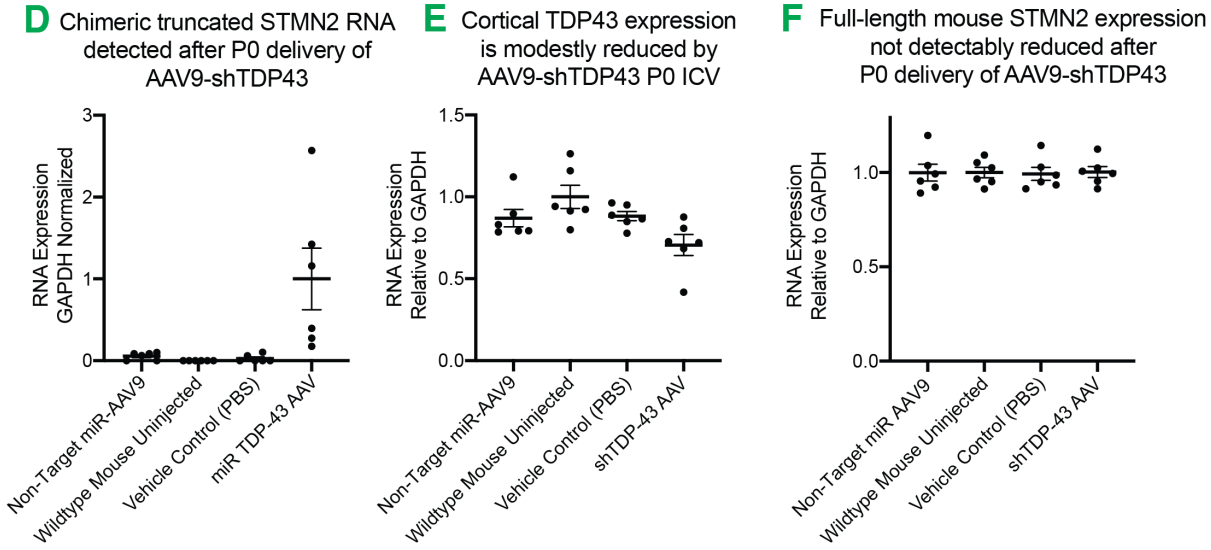

PHP.eB Capsid ICV P0 Injection (4 weeks)

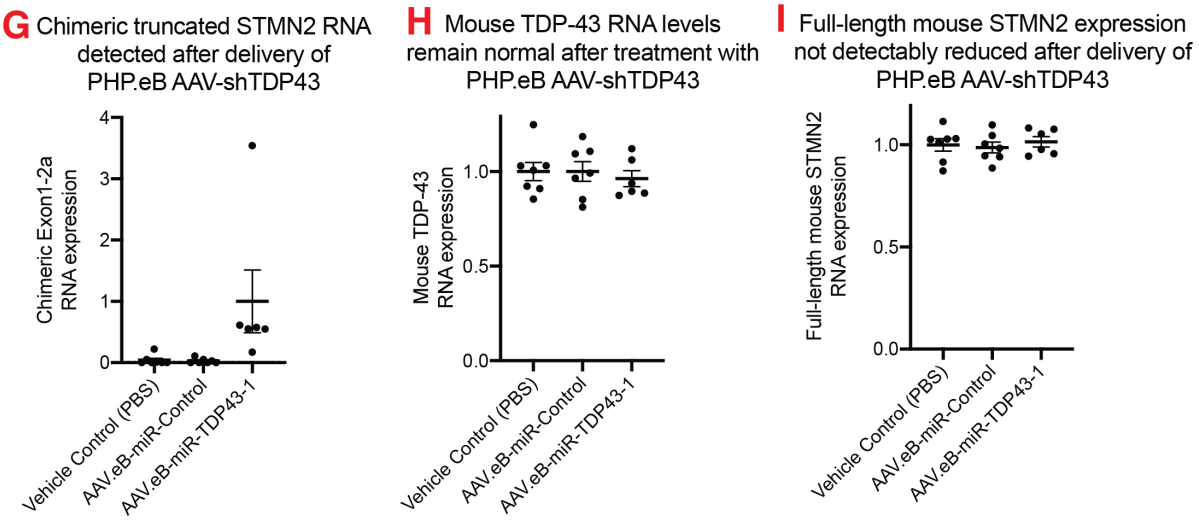

Existing models of TDP-43 depletion (by Cre recombinase induced gene deletion) are severely toxic[80,191]. Moreover, since our success in lowering TDP-43 (at least by P0 ICV administration) was extremely limited (even when utilizing the same RNAi system that was extremely efficient against the murine stathmin-2 gene target by subpial administration), the directly humanized stathmin-2 mouse had little to no utility as an in-vivo model for advancing splice-rescue antisense oligonucleotide (rASO) clinical development or other stathmin-2 restorative therapeutics. Recognizing this, I designed a more aggressive approach to producing a mouse model of induced stathmin-2 pre-mRNA misprocessing in which I removed TDP-43 binding dependence altogether. To accomplish this, I leveraged a strategy I described in Chapter 3, replacing the normal human TDP-43 GU binding motif with an MS2 aptamer, an edit that I demonstrated in the human context leads to constitutive misprocessing of the stathmin-2 pre-mRNA by outright eliminating TDP-43 interaction. Having already demonstrated with the previous humanized mouse experiment that the core pre-mRNA determinants of stathmin-2 misprocessing from the human gene can functionally transfer to the mouse stathmin-2 genomic context, it was plausible that such a system could work.

Testing was first carried out in mouse neuron-like N2A cells (Fig 5.7 A-F). CRISPR-Cas9 knock-in of a 3 kilobase fragment of human stathmin-2 with homology arms each around 800 bases in length into the corresponding intronic coordinates of the mouse gene (Fig 5.7 B). Knock-in to the non-diploid N2A cell line resulted in multiple clones confirmed to carry the correct insertion by PCR screening (representative clones shown in Fig 5.7 C), resulting in a knock-in copy-number-dependent reduction of full-length endogenous stathmin-2 by qRT-PCR (Fig 5.7 D) including near total loss of stathmin-2 in clones with knock-in at all alleles, and corresponding reduction of total stathmin-2 protein by immunoblot (Fig 5.7 E). This was accompanied by robust RT-PCR detection of a chimeric RNA containing mouse exon 1 ligated to human exon2A (Fig 5.7 F). As hoped for in my initial design, after production of mice heterozygous for my humanized

allele, in both brain and spinal cord (compared with wildtype littermate controls), half of the stathmin-2 RNAs made from the two endogenous alleles are misprocessed (Fig 5.7 I), generating truncated chimeric stathmin-2 RNAs from utilization of exon 2a cryptic splice and polyadenylation sites within the humanized allele (Fig 5.7 J) despite endogenous TDP-43 levels remaining normal (Fig 5.7 H).

Figure 5.7 Mice humanized by insertion of a TDP-43-binding-null human cryptic exon2a constitutively misprocess endogenous stathmin-2 pre-mRNA, creating a robust platform for in-vivo testing of splice-rescuing therapy

(A) Measurement by qRT-PCR of endogenous wildtype mouse TDP-43 and stathmin-2 RNA expression in neuron-like N2A cells after treatment with non-target control pool or TDP-43 targeting siRNAs demonstrate no dependence of mouse stathmin-2 expression on TDP-43 level. GAPDH was used as an endogenous control gene. (B) Scheme of murine stathmin-2 gene and knock-in strategy placing 3 kilobases of human intron including exon2a at the equivalent locus of the mouse intron in N2A cells. Human exon2a fragment is modified to replace GU binding sequence of TDP-43 with an MS2 RNA aptamer. (C) Genotyping PCR of genomic DNA showing homozygous and heterozygous N2A cell line clones using primers spanning the site of sequence insertion. (D) Measurement of expression in humanized N2A cells shows knock-in allele number dependent reduction of full-length endogenous murine stathmin-2 gene by qRT-PCR. GAPDH used as an endogenous control gene. (E) Immunoblot measuring murine stathmin-2 protein level versus GAPDH protein as an endogenous loading control demonstrates knock-in allele number dependent loss of murine stathmin-2. (F) RT-PCR with primers for exon 1 from murine stathmin-2 and human exon-2a show accumulation of a chimeric RNA in cell lines with one or more knock-in humanized allele, but not in wildtype N2A cells. (G) Schematic of TDP-43 binding-null (MS2) 3 kilobase human intron1/exon2a knock-in to the equivalent locus of mouse stathmin-2 intron 1. (H) Measurement of endogenous mouse TDP-43 RNA expression by qRT-PCR in heterozygous and wildtype littermates for two different knock-in lines derived from the strategy outlined in G, in brain and spinal cord, reveals no change to mouse TDP-43 levels between lines. GAPDH was used as an endogenous control gene. (I) Measurement of endogenous mouse full-length stathmin-2 mRNA expression by qRT-PCR in heterozygous and wildtype littermates for two different knock-in lines derived from the strategy outlined in G, in brain and spinal cord, reveals consistent loss of half the normal level of stathmin-2 mRNA in heterozygote knock-in animals versus wildtype control animals. GAPDH was used as an endogenous control gene. (J) Measurement of chimeric truncated stathmin-2 RNA expression by qRT-PCR with a forward primer in mouse exon 1 and a reverse primer in human exon 2a, in heterozygous and wildtype littermates for two different knock-in lines derived from the strategy outlined in G, in brain and spinal cord, reveals consistent accumulation of truncated chimeric stathmin-2 RNA in heterozygote knock-in animals versus wildtype control animals. GAPDH was used as an endogenous control gene. (K) Schematic showing in-vivo proof-of-concept efficacy and target-engagement testing of rescue ASOs (or other splice rescuing therapeutics) in knock-in mice without the need to manipulate levels of endogenous mouse TDP-43.

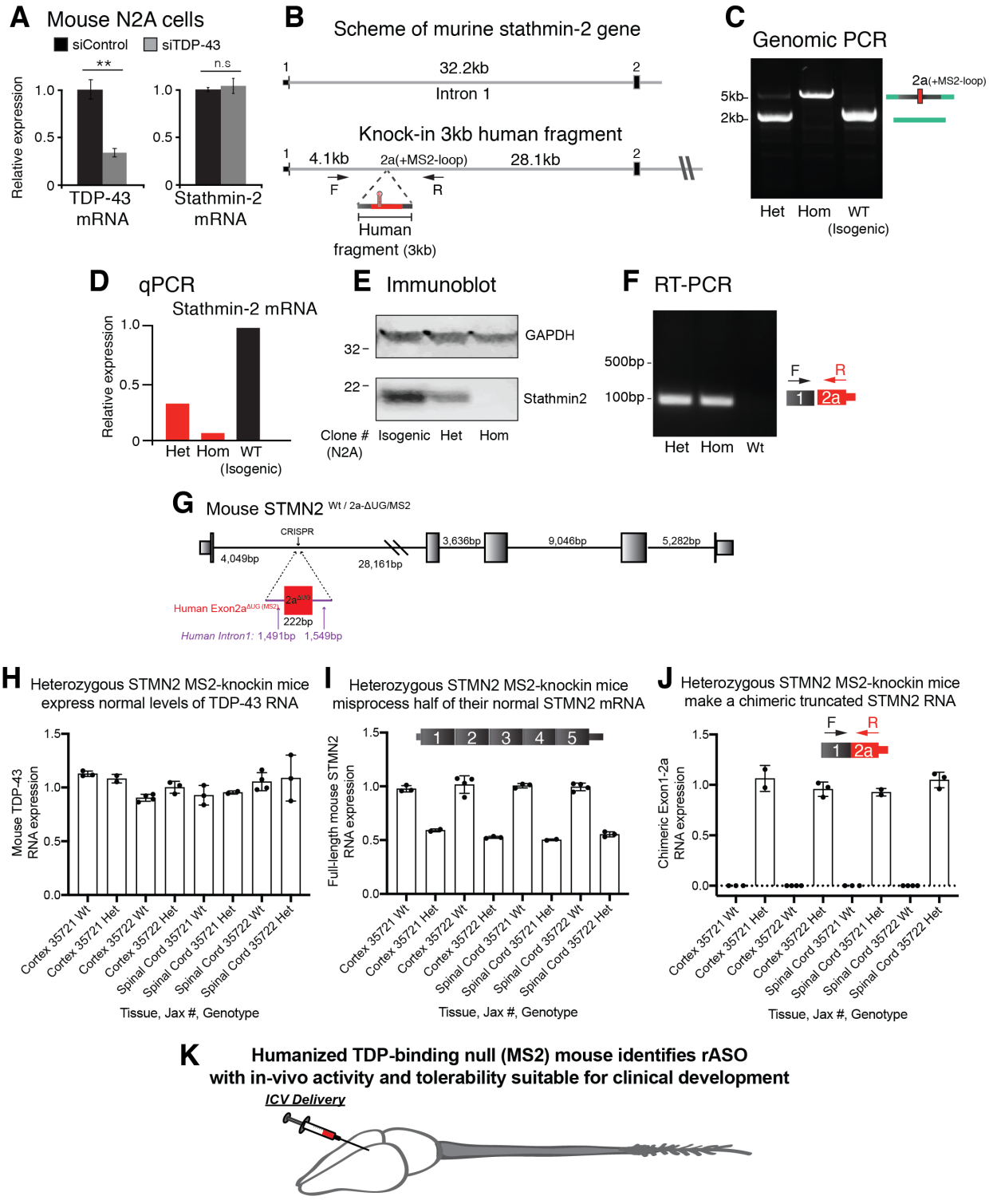
A
Mouse N2A cells
siControl
siTDP-43
**
n.s
Relative expression
1.0
0.5
0
TDP-43 mRNA
Stathmin-2 mRNA
B
Scheme of murine stathmin-2 gene
1
32.2kb
2
Intron 1
Knock-in 3kb human fragment
4.1kb
2a(+MS2-loop)
28.1kb
F
R
Human fragment (3kb)
C
Genomic PCR
5kb
2kb
2a(+MS2-loop)
Het Hom WT
(Isogenic)
D
qPCR
Stathmin-2 mRNA
Relative expression
Het Hom WT
(Isogenic)
E
Immunoblot
32
22
GAPDH
Stathmin2
Clone # (N2A)
Isogenic Het Hom
F
RT-PCR
500bp
100bp
F
R
1
2a
Het Hom Wt
G
Mouse STMN2 Wt / 2a-ΔUG/MS2
CRISPR
4,049bp
28,161bp
3,636bp
9,046bp
5,282bp
Human Exon2a ΔUG (MS2)
2a ΔUG
222bp
Human Intron1: 1,491bp 1,549bp
H
Heterozygous STMN2 MS2-knockin mice express normal levels of TDP-43 RNA
Mouse TDP-43 RNA expression
1.5
1.0
0.5
0.0
Cortex 35721 Wt
Cortex 35721 Het
Cortex 35722 Wt
Cortex 35722 Het
Spinal Cord 35721 Wt
Spinal Cord 35721 Het
Spinal Cord 35722 Wt
Spinal Cord 35722 Het
Tissue, Jax #, Genotype
I
Heterozygous STMN2 MS2-knockin mice misprocess half of their normal STMN2 mRNA
Full-length mouse STMN2 RNA expression
1 2 3 4 5
Tissue, Jax #, Genotype
J
Heterozygous STMN2 MS2-knockin mice make a chimeric truncated STMN2 RNA
F
R
1
2a
Chimeric Exon1-2a RNA expression
Tissue, Jax #, Genotype
K
Humanized TDP-binding null (MS2) mouse identifies rASO with in-vivo activity and tolerability suitable for clinical development
ICV Delivery

Discussion:

Key challenges for the development of stathmin-2 restoration strategies as a clinical development program in sporadic ALS and other TDP-43 proteinopathies turn on the question of whether (and to what extent) stathmin-2 loss from an adult nervous system recapitulates ALS-like disease and/or the failure of axonal regeneration after injury we observed using in-vivo motor neuron culture experiments[91]. This question is essential to therapy development since, for all the advantages of modeling human motor neurons in culture, TDP-43 proteinopathies are diseases of aging. This was already an issue with modeling age-dependent disease in mice, whose life-span of about two years requires disease to be modeled about 25 times faster than it does in actual human disease. It is even more of a problem for the idea that in-vivo cultures of cells with mixed neuronal maturity developed over a mere handful of weeks. It ought to be uncontroversial that such cultures may not fully recapitulate the consequences of gene loss from an adult animal. To paraphrase George E. P. Box, “Essentially all models are wrong, but some are useful.”

Here, by applying new technologies and molecular tools, I and my colleagues have demonstrated that the answer to that key question is, yes. Profound chronic focal loss of stathmin-2 expression from motor and sensory neurons of an adult animal produces signs of synaptic dysfunction that are consistent with the early neuromuscular junction loss clinically observed in ALS[179-182], as well as observations from Drosophila (an organism with only a single stathmin gene)[122]. This demonstrates the predictive value of our initial motor neuron culture models and produced new lines of evidence suggesting stathmin-2 mediated dysfunctions could be an early feature of TDP-43 proteinopathy.

Despite the clear signs of focal synapse loss that were detected in both motor and sensory systems, alteration in motor neuron survival, along with microglia and astroglia densities appeared unchanged for the time period we evaluated. Since stathmin-2 is primarily expressed in neurons,

it is unsurprising that reduction of stathmin-2 levels (which amount to a cell-autonomous neuronal insult) should not fully recapitulate non-cell-autonomous aspects of disease[192-203]. Stathmin-2 is only one of many TDP-43 targets in human neurons, and it is fully expected in TDP-43 proteinopathy that other disrupted target genes contribute to the overall disease pathophysiology, likely including affected gene targets in non-neuronal cells. Additionally, it is important to keep in perspective that mouse stathmin-2 is not normally regulated by TDP-43, reflecting possible broader divergence between the transcriptome landscapes of mouse and human nervous systems.

Emerging (still unpublished) evidence from our group and others looking at new knockout models of mouse stathmin-2 indicate that while neonatal lethality is a feature of this model (as first reported)[106], about 5% of knockout pups survive to adulthood without any discernable phenotype (at least in our analysis thus far). This strongly suggest that, on top of profoundly different pre-mRNA regulation of stathmin-2, mice may have unique genetic compensatory mechanisms to deal with stathmin-2 loss, possibly involving other members of the four-gene stathmin family, or via some yet unknown genetic modifier(s) (studies are already underway to determine whether such modifiers exist). The ultimate experiment to determine the contribution of stathmin-2 loss in human TDP-43 proteinopathy will be initiated with the commencement of anticipated Ionis/Biogen clinical trials (presently undisclosed) testing stathmin-2 rescue ASOs in sporadic ALS patients.

Perhaps the most significant barrier we have faced in driving stathmin-2 forward as an ASO clinical development target, since our team first disclosed the discovery to Ionis on June 8th, 2017, has been the eventual development of in-vivo models suitable for rescue ASO testing. Mice lack the key cryptic elements governing human TDP-43 dependent pre-mRNA misprocessing, and humanization of the mouse gene with the proposed cryptic elements could be challenged by factors including lack of conservation of mouse TDP-43 function, lack of conservation of the

transcriptional processing environments of the two species including trans-acting factors, by unanticipated additional cryptic elements of the human intron 1 influencing human-specific misprocessing, or any number of other possible mechanisms. Had additional elements of human intronic sequence (outside those I identified proximal to exon 2a) been characterized as necessary to create a functional mouse platform, a BAC mouse carrying the complete human stathmin-2 gene over a background of mouse stathmin-2 knockout would be utilized. The 100% amino-acid level conservation between the two species indicates this could be a successful approach, with the advantage of providing 100% of the possible oligo sequence screening space of the full human gene, though with the shortcoming of continued TDP-43 gated pre-mRNA processing which might require additional crosses (to TDP-43 mutant mice) or manipulations.

Anticipation of the technical challenges with reducing in-vivo levels of murine TDP-43 prompted me to select an entirely RNA Polymerase II controlled RNAi system and adapt it for use in an AAV gene therapy platform. Recognizing that TDP-43 autoregulates its own pre-mRNA processing to provide precise control over its accumulation, and additionally that acute TDP-43 loss is reported to be extremely toxic in mice, I designed a system that could offer more fine-tuned control over TDP-43 engaging RNAi elements. To avoid compounding acute toxicity from loss of TDP-43 expression with the weakened state of mice post-surgery (both AAV delivery and ASO injections are quite invasive surgical procedures for a mouse that typically involve direct stereotaxic injection into the brain), my original strategy was to leverage tools in the “RNA Polymerase II Toolbox” to control the timing of TDP-43 knockdown after AAV delivery via an inducible Pol-II promoter, allowing mice to recover from AAV and ASO delivery surgeries before triggering acute TDP-43 disfunction. Consistent with the engineering philosophy of removing unnecessary parts to increase simplicity and reliability, an all-Pol-II strategy also seemed easier than deploying Cre-recombinase dependent timed gating of RNA polymerase III driven RNAi elements, and potentially less toxic than ASO-mediated reduction of TDP-43 (without the potential

interference with uptake) while retaining the ability to mark transduced/induced cells with green fluorescence from the same RNA molecule. It was gratifying that this decision led to a very successful stathmin-2 reducing RNAi outcome in the chronic lumbar depletion experiment.

Nevertheless, the capacity of RNAi to reduce TDP-43 levels in-vivo were ultimately quite limited. It is possible, from a technical perspective, that application of the original tetracycline-inducible promotor system to the TDP-43 targeting RNAi could substantially boost expression compared with the relatively mild ubiquitin promotor I ultimately selected, and thus further deplete TDP-43 levels. I suspect, however, that the system is either inherently limited by TDP-43 autoregulation, by the selection of a 3'UTR targeted RNAi sequence, and/or by the P0 ICV route of vector administration. I know the latter factor is a major contributing component, as I have directly compared subpial delivery knockdown efficiency of the stathmin-2 reducing RNAi vectors (~90% efficient) to the same vector delivered by ICV injection (~20% efficient), consistent with the level of observed engagement of the TDP-43 targeted RNAi delivered by this route (Fig 5.6 E, H).

Technical considerations aside, even with a limited TDP-43 knockdown capacity, our humanized stathmin-2 exon2a mouse was successful, demonstrating that the small inserted fragment of human exon2a does in fact contain all of the cryptic pre-mRNA processing elements needed to confer stathmin-2 sensitivity to TDP-43 dysfunction. Equally important to the in-vivo modeling goal, the experiment demonstrated that there exists sufficient conservation of any involved trans-acting splicing factors to confer misprocessing of the human sequence fragment in a mouse cell. The only real shortcoming of this experiment was a lack of effect on overall mouse stathmin-2 levels, though this is likely achievable in future experiments which will utilize an inducible deletion mouse model of TDP-43 to more severely impact processing of the humanized pre-mRNA.

Of perhaps greatest importance in the advancement of the stathmin-2 finding from bench to bedside is the design and creation of a TDP-43 binding null exon2a humanized murine

stathmin-2 mouse. ASO drug development pipelines proceed by the following rough outline: high-throughput screening in cell lines at single molecule resolution of hundreds or thousands of tiled ASO designs to identify sites of high activity, followed by a dose-response to determine IC-50 values and narrow leads, followed by tolerability studies in wildtype mice where a massive 700ug dose of the best lead ASOs are delivered by ICV injection and functional observation battery scoring to determine acute and delayed toxicity.

In order for the process to proceed past this point, since about half of the ASO leads that show activity in culture will have no useful activity in-vivo (for reasons that are not well understood), in-vivo efficacy proof-of-concept studies are required. I am immensely gratified that my application of principles of molecular and RNA biology led to the successful design (simply mutating 24 bases of DNA!) and construction of a cellular model and then a true in-vivo system in mice with a humanized stathmin-2 allele that confers constitutive mis-splicing and truncation of stathmin-2 pre-mRNAs while retaining a large 3 kilobase sequence space for increased screening utility. Sixty of these mice are presently being dosed in an initial experiment with 15 separate rASO leads (four mice per ASO), including 3 of the leads demonstrated in this thesis for in-vivo proof-of-concept testing to develop leads for additional rational design screening, which will eventually (> 2 years) culminate in a human trial.

From initial proof-of concept[135] to human trial[136], the SOD1 ASO effort for the first identified ALS gene took 12 years. The C9ORF72 ASO approach for the most common genetic cause of ALS took 7 years. My colleagues and I anticipate that for stathmin-2 in sporadic and C9orf72-mediated ALS we will further reduce that number to 5 years, with a rescue ASO targeting a mechanism common to 97% of ALS.

Methods:

miR30 based RNAi vector production and validation

97-mer hairpin oligos were designed using the Hannon Lab RNAi Central siRNA design tool (http://katahdin.mssm.edu/siRNA/RNAi.cgi?type=shRNA) selecting “shRNA psm2 Design” as the oligo type, requesting 100 separate oligo designs, and selecting “mouse” as the desired species. Input sequences were restricted to the annotated 3’ untranslated region of the RefSeq version of the targeted gene (accessed via the UCSC Genome Browser) to enable future exogenous expression restoration experiments utilizing gene transfer with untargeted cDNA-cloned coding sequences. From the 100 oligo designs output by the tool, designs were hand-sorted based upon the following criteria (looking at the “22mer” line sequence, not the 97bp oligo sequence): selected oligos contained two blocks (minimum of three bases) of G/C, with one block starting at the 5’ end of the 22mer sequence and the other in the middle of the sequence, and low GC content at the 3’ end, blocks of four uninterrupted G/C blocks were automatically rejected, as were 22-mers with strings of 5 G/C bases or 5 A/T bases. After hand-sorting the list with these criteria, the top 5 best matching 22-mer sequences were BLAST-searched with NCBI nucleotide blast for potential off targets, and results indicating E-values greater than 1 corresponding to any gene other than the intended target were rejected. The resulting 3-5 candidate designs were ordered as 97mer single-stranded DNA oligonucleotides from Integrated DNA Technologies (IDT Ultramer Single Stranded Oligo product selection). Single stranded oligonucleotides were amplified using Vent Polymerase (New England Biolabs) and primers that add XhoI and EcoRI restriction sites at either end for cloning Forward primer: (5'-GATGGCTGCTCGAGAAGGTATATTGCTGTTGACAGTGAGCG), Reverse primer: (5'-GTCTAGAGGAATTCCGAGGCAGTAGGCA), amplification reactions were performed in 50 microliters total volume with final concentrations as follows: 1x ThermoPol Buffer, 2 millimolar Magnesium Sulfate, 5% DMSO, 200 micromolar dNTPs, 100 nanograms of template oligo (equal to 1ul of 4nanomole Ultramer resuspended in 1.2ml Tris), 0.5 micromolar forward primer, 0.5 micromolar reverse primer (1ul of 25 micromolar stock), and 1Unit per reaction of VENT

Polymerase. All components were added on ice to the reaction and cycled with the following thermocycler program: 94ºC 5 minutes, 94ºC 30 seconds, 54ºC 30 seconds, 75ºC 30 seconds, repeat steps 2-4 for 12 cycles, 75ºC 2 minutes, 4ºC Hold. Following PCR amplification products were fully loaded and run on an 8% acrylamide gel, with bands cut and incubated 1-2 hours at 55ºC in TE buffer to allow the PCR product to diffuse out of the gel into buffer, remaining gel was spun down and TE moved to a new tube for restriction digestion with XhoI and EcoRI for three hours (to completion). Post-restriction digest fragments were purified on a QIAquick PCR purification column (Qiagen). Ligation of the hairpin into a miR30[185,186] based backbone vector I previously modified by insertion of a Clover coding sequence upstream of the microRNA was performed at insert ratio of 10:1 or 3:1 ratio (depending on how much digested hairpin insert was recovered), or approximately 4.2 nanograms of hairpin insert to 100 nanograms of vector backbone, in a reaction volume of 10 microliters. After ligation, vectors were transformed using half the reaction (5 microliters) into Stbl3 chemically competent bacteria and plate on Carb or Amp plates. All hairpin or repetitive plasmids (including downstream AAV) were amplified in stable lines at 30ºC. When transferring a hairpin from one vector to another by restriction digest, melting of the agarose gel prior to column purification was performed at room temperature or 4ºC overnight to prevent hairpin denaturation. Resulting vectors were sub-cloned into an AAV backbone plasmid containing only ITR sequences and a transcript terminating SV40 polyadenylation signal sequence by digesting the backbone with SalI-NheI and inserting two fragments: a 1212 base pair RNA polymerase-II regulated Ubiquitin promoter digested with XhoI-BmtI, and the subcloned Clover-miR30 sequence. Screening for positive clones was performed by restriction digest with EcoRV/MluI/KpnI in a triple digestion to identify plasmids that drop out three appropriate bands. Sanger sequencing reactions were run with 10% DMSO added to the sequencing reaction to allow opening of the shRNA secondary structure by the sequencing polymerase. Five vectors with different 97-mer hairpin sequences were cloned and tested per target gene, with efficacy tests

performed on the final AAV transfer plasmid vector by simple transfection (Trans-IT X2 or Trans-IT LT1, Mirus Bio) into mouse N2A cells, with RNA isolation and qRT-PCR performed 48-72 hours post-transfection. For a non-targeting control vector, an existing shRNA design targeting the beta-galactosidase gene was adapted to the miR30 based vector system using the same Hannon Lab tool which optionally accepts 21-mer shRNA sequences as inputs and adapts an appropriate 97-mer sequence. 97-mer sequences utilized in AAV transfer vectors are as follows:

Non-targeting sequence (based on beta-galactosidase): TGCTGTTGACAGTGAGCG**CGAAATCGCTGATGTGTAGTCG**TAGTGAAGCCACAGATGTA**C GACTACACATCAGCGATTTCA**TGCCTACTGCCTCGGA

Targeting murine stathmin-2 (but not human): TGCTGTTGACAGTGAGCG**AGAAGTGTATGACATGGTTTAA**TAGTGAAGCCACAGATGTA**TT AAACCATGTCATACACTTCC**TGCCTACTGCCTCGGA

Targeting Human stathmin-2 (but not murine): TGCTGTTGACAGTGAGCGA**GGAATGTATGACATGGTTTAA**TAGTGAAGCCACAGATGTA**TT AAACCATGTCATACATTCCC**TGCCTACTGCCTCGGA

Targeting Murine TDP-43 (but not human, sometimes noted as TDP-43-1): TGCTGTTGACAGTGAGCG**CGCAAATAACGTACGAATGTTT**TAGTGAAGCCACAGATGTA**A AACATTCGTACGTTATTTGCT**TGCCTACTGCCTCGGA

Targeting both Human and Murine TDP-43 (sometimes noted as TDP-43-2): TGCTGTTGACAGTGAGCG**CGGCATGAAAGGCTAGTATGAG**TAGTGAAGCCACAGATGTA**C TCATACTAGCCTTTCATGCCT**TGCCTACTGCCTCGGA

Adeno-associated virus generation and purification

Fully sequenced and tested transfer plasmids were seeded in LB containing Carbenicillin selection and shaken at 155 RPM at 30ºC while passaged into 2 liters of broth which were shaken

over-night. First thing the next morning the bacteria were pelleted at 4000 RCF for 30 minutes at 4ºC with a large refrigerated centrifuge (BD). Pellets were resuspended and purified using a Giga kit from Zymo Research, with careful attention paid to the endotoxin removal step at the end of the protocol. 400 micrograms of purified transfer plasmid, along with the tropism AAV9n (Addgene plasmid 112865) or, for other experiments PHP.eB (Addgene plasmid 103005), or AAV-retro (Addgene plasmid 81070) encoding Rep/Cap plasmids and the Adenovirus helper plasmid (Addgene plasmid 112867) into 293T cells using VirusGen transfection reagent (Mirus Bio), and cells lysed, sheered, and benzonase treated and purified by gradient centrifugation as previously described[204]. Titration of resulting virus was performed by qPCR with primers specific to the viral genome payload and a standard dilution curve of AAV for absolute quantification versus a precisely diluted transfer vector where the number of plasmid copies was known.

AAV administration in mice

For P0 injections, timed mating was setup and pregnant females were monitored every 12 hours for pups. Newborn pups were ICV injected with (depending on the experiment) 1ul or 3ul of undiluted AAV (titers measured as ~1x10^13 viral genomes per milliliter) either as unilateral or bilateral hemisphere dosing. For AAV titration experiments with the TDP-43 reducing vectors, 1 microliter injections were utilized with dilutions of 1:1, 1:10, or 1:100 into phosphate buffered saline made as indicated. Mice were monitored for 4 weeks before collection and freezing of tissues. Subpial injections were performed as previously described[151], with virus diluted 1:1 in phosphate buffered saline prior to administration.

Chapters 2, 3, 4, and 5 were supported in part by an institutional award to the UCSD Genetics Training Program from the National Institute for General Medical Sciences, T32 GM008666.

Chapters 3, 4, and 5, in part, are being prepared for publication as “Therapeutic restoration of stathmin-2 expression in TDP-43 proteinopathies.” 2021, and also include co-authored unpublished work. Other authors are: Zevik Melamed, Jone Lopez-Erauskin, Mariana Bravo-Hernandez, Haiyang Yu, Melinda Beccari, Melissa Mcalonis, John Ravits, Karen Ling, Paymann Jafar-nejad, Frank Rigo, Aamir Zuberi, Max Presa, Cat Lutz, C. Frank Bennett, Martin Marsala, Clotilde Lagier-Tourenne, Don W. Cleveland. The dissertation author was the primary investigator and author of this material.

Chapter 6: A Vision for the Future

Detection of truncated stathmin-2 RNA as an early biomarker of TDP-43 proteinopathy

Since TDP-43 dysfunction and nuclear clearance is thought to be an early event in the pathogenesis of TDP-43 proteinopathies, it follows that TDP-43-dependent stathmin-2 misprocessing must also be an early disease event. This cascade, if discernible via detection of misprocessed truncated stathmin-2 transcripts in accessible biofluids (specifically, cerebrospinal fluid or blood) could be a valuable early biomarker for these proteinopathies. Full-length stathmin-2 mRNA is abundantly transcribed (among the top 25 gene list in a motor neuron), and similarly the truncated RNA product appears to be both abundantly produced in affected cells, and (based upon robust CISH detection in human tissues Fig 2.3 B-C) exported to the cytoplasmic compartment where it is apparently not rapidly cleared (as steady-state accumulation is determined by degradation rate). Though protocols are divergent, early unpublished evidence from multiple groups suggests that it is possible to detect the truncated misprocessed stathmin-2 RNA in cerebrospinal fluid using the same sensitive primer-probe based qRT-PCR method I have already used in this study. The mechanism by which the truncated RNA reaches this extracellular medium is unknown, although some of the more successful isolation and detection protocols suggests possible exosome encapsulation (further study is required to more precisely determine the route of escape from the neuron somatic compartment).

The collection of cerebrospinal fluid from patients is not routine for clinical diagnostics in the management of ALS, and while the collection procedure is technically unsophisticated it is invasive and often produces painful after-effects (frequently causing headaches post-lumbar-puncture). This makes rapid, regular, and routine laboratory access to homogeneously collected and handled clinical cerebrospinal fluid samples infeasible outside of a clinical trial setting. Likely

for this reason, unpublished data based on voluntary ad-hoc clinical collection show great heterogeneity of truncated stathmin-2 detection between patients. Extracellular RNA stability is likely a major limiting factor in the absence of uniform and rigorous collection, chain-of-custody, and processing protocols. Fortunately, the field can overcome these challenges by simply integrating stathmin-2 truncated RNA biomarker detection experiments into the existing cerebrospinal fluid sampling that is now a routine aspect of the lumbar puncture protocol utilized in current ASO trials for treatment of C9ORF72 patients. In these protocols cerebrospinal fluid is sampled prior to ASO dosing to track levels of circulating ASO and the biomarker neurofilament. Post-hoc analysis of already collected cerebrospinal fluid samples, properly collected and stored from the C9-ASO trial could answer this question. Critically, the ASO trial for SOD1 would be an inappropriate channel by which to determine the utility of truncated stathmin-2 RNA as a biomarker, as SOD1 patients do not have TDP-43 pathology. Resolution of this question via integration with existing clinical trial protocols is also not unlikely, as the major biotech companies behind the C9ORF72 ASO trial (Ionis and Biogen) also have a major interest in ASO strategies to rescue stathmin-2 expression.

Determining whether there is a polypeptide translation product produced from the truncated stathmin-2 RNA

The truncated, cryptically spliced and prematurely polyadenylated stathmin-2 RNA produced upon reduction or loss of TDP-43 function in humans contains an ATG start codon initiating within the normal exon 1 sequence, with an open reading frame that continues into cryptic exon 2a for a total of 16 encoded amino acids before reaching a stop codon. Since the prematurely polyadenylated cryptic exon 2a is the terminal exon of this short RNA transcript, the RNA is not predicted to be a substrate for degradation by the activation of nonsense-mediated decay pathways. Additionally, because this resulting RNA proceeds through all of the normal

steps of mRNA processing, being spliced, capped, polyadenylated, and apparently exported from the nucleus to accumulated in the cytoplasmic compartment (Fig 2.3, right panels), there is no evidence based upon first-principles upon which to believe the 17-codon message encoded by this short RNA would not serve as a substrate for translation.

The diminutive size of the reading frame alone does not rule out translation[205] or possible biological significance[206-208]. To the contrary, emerging techniques have enabled the identification of evolutionarily conserved micropeptides (also known as short open reading frames), proteins with fewer than 100 amino acids including some down to the scale of single-digit codon-counts. Setting aside upstream open reading frames (uORFs) whose ribosome occupancy and translation in turn affect translation rates of the adjacent downstream reading frames (stathmin-2 cryptic processing does not fit this category), important functional small open reading frame examples include the “tarsal-less” or “polished rice” (tal/pri) from Drosophila, which encodes four small open reading frames which translate one 32- and three 11-amino acid microproteins, conserved in metazoans, that regulate development of that organism[206,207] allowing it to grow normal legs. Additionally the mammalian small open reading frame CYREN[208] (Cell Cycle Regulator of Non-Homologous End Joining) is an NHEJ inhibitor expressed in S and G2 phases of the cell cycle to reduce chromosomal rearrangements and preserve DNA integrity. Finally, the knockout of a muscle-expressed 46 amino acid small open reading frame encoding myoregulin (encoded by a previously annotated non-coding RNA) in mice enables striking improvement of treadmill performance, allowing them to run a full 30% longer, a phenotype produced by impeding sarcoplasmic reticulum calcium uptake[209].

While we have demonstrated already with AAV-delivered RNAi knockdown that full-length stathmin-2 depletion on its own is sufficient to mediate neuromuscular junction loss, that does not rule out a possible truncated stathmin-2 micropeptide contribution in disease pathology. It is highly unlikely that, were such a peptide stable enough to persist, the open reading frame encoded by

the truncated stathmin-2 RNA product has any real functional role in a TDP-43 depleted cell, but a toxic gain-of-function for such a peptide may contribute to neuronal dysfunction and disease. The likely unstructured nature of many micropeptides also leaves open the possibility that many may interact or interfere with intracellular condensate formation (also known as liquid-liquid phase separation), or fail to be filtered by intracellular gatekeepers like the nuclear pore complexes. Micropeptides with toxic properties also have precedent in a variety of animal venoms, including scorpions, water bugs, and funnel-web spiders.

Experimental challenges for the identification and study of a potential stathmin-2 derived micropeptide include the inability to resolve such a small putative protein by SDS-polyacrylamide gel electrophoresis, difficulty in identifying the single tryptic peptide by mass-spectroscopy (whereas most protein targets contain many tryptic peptide products to allow high-confidence unique identification, irrespective of individual transmission profiles through the apparatus or loading column), and the difficulty in raising a suitable detecting antibody against such a short and inherently unstructured amino acid sequence (the diminutive predicted polypeptide would be dwarfed by an IgG antibody, likely made inaccessible by fixation, and easily washed out of an unfixed cell, and the unstructured conformation makes it unsuitable for camelid nanobody production). Accordingly, unpublished efforts by our group and others to identify suitable antibodies for use in human patient sample immunohistochemistry experiments have (so far) all proven unsuccessful, as have preliminary detection efforts using mass spec from neuron-like cell lysates.

One approach that has proven successful for the identification of non-canonical translated open reading frames[210] is the utilization of translating ribosome affinity purification (TRAP)[211,212]. In classical applications, transgenic mice expressing a BAC-TRAP system utilize a bacterial artificial chromosome containing a cell-type-specific promoter that drives expression of a GFP-tagged L10a ribosomal protein. Tissues are collected in the presence of cycloheximide, which

halts translation and freezes ribosomes in-place on their bound mRNA, ribosomes incorporating the GFP-tagged subunit are then affinity purified using two anti-GFP monoclonal antibodies bound to magnetic beads to capture and identify RNAs that are actively translated in the target cell type. Variations on this concept include substitution of the GFP fusion segment with an anti-GFP nanobody, to allow neuron connectivity gated profiling using retrograde transport of GFP-expressing viruses[213], or biotin ligase ribosomal subunit fusions[210], even CRISPR based methods have proven successful in this context[214].

To determine whether, and to what extent, the stathmin-2 truncated RNA product is ribosome-associated, I engineered my own improved lentivirus-encoded variant of the TRAP system for the efficient ribosome characterization of neuron like cells in-vitro (Fig 6.1 A,B). This ribosome labeling strategy, while largely similar to the layout of the original BAC-TRAP construct (Fig 6.1 A) with a tagged L10a ribosomal subunit, contains four important improvements: 1) most importantly, the construct has two tandem Strep-TagII affinity tag peptides for highly-specific direct affinity purification using commercial “Streptactin” magnetic beads (versus capture mediated by anti-GFP monoclonal antibodies), 2) the GFP used in the original construct is replaced with a superior (brighter with shorter maturation time) monomeric green fluorescent protein, Clover, derived from Branchiostoma lanceolatum[215] to aid in Fluorescence Activated Cell Sorting, 3) the construct is codon-optimized for expression in human cells (instead of mouse), and 4) it is encoded in a lentiviral transfer plasmid for fast and easy transduction into relevant human cell lines.

Figure 6.1 Enhanced Lenti-TRAP translating-ribosome affinity purificaton system in neuron like cells carrying homozygous TDP-43 mutations show enriched ribosomal binding to truncated stathmin-2 RNA

(A) Schematic of comparing features of BAC-TRAP and Lenti-TRAP translated gene capture systems. (B) Schematic depicting transduction and ribosome-bound RNA pulldown workflow with human neuron-like cells using the Lenti-TRAP system. (C) Graph depicting relative gene expression enrichment compared to GAPDH endogenous control gene using isoform-specific primer-probe qRT-PCR to measure RNA isoform abundance in ribosome-bound affinity purified RNA. Three biologic replicates are depicted per condition.

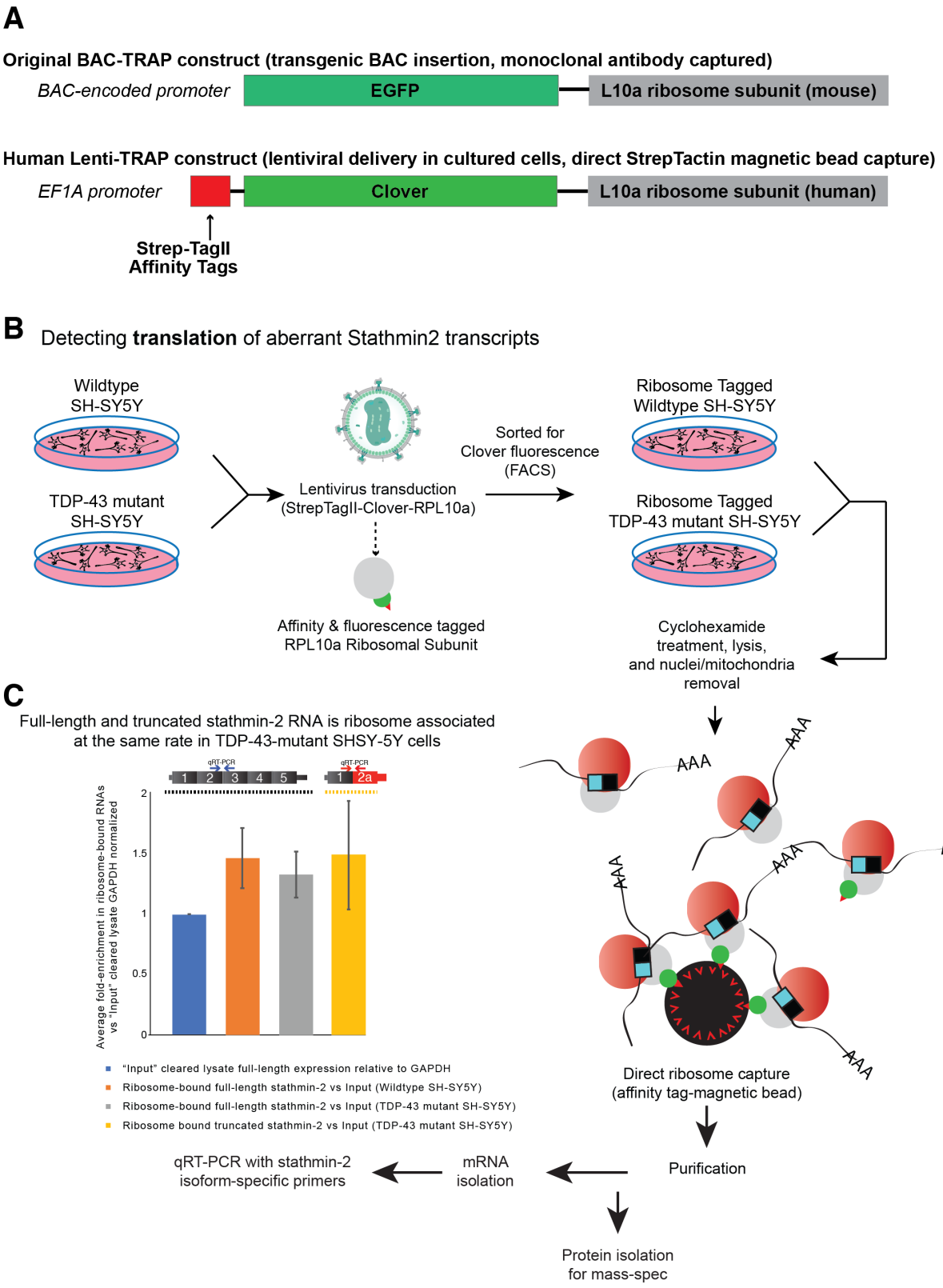
A
Original BAC-TRAP construct (transgenic BAC insertion, monoclonal antibody captured)
BAC-encoded promoter
EGFP
L10a ribosome subunit (mouse)
Human Lenti-TRAP construct (lentiviral delivery in cultured cells, direct StrepTactin magnetic bead capture)
EF1A promoter
Clover
L10a ribosome subunit (human)
Strep-TagII
Affinity Tags
B
Detecting translation of aberrant Stathmin2 transcripts
Wildtype
SH-SY5Y
TDP-43 mutant
SH-SY5Y
Lentivirus transduction
(StrepTagII-Clover-RPL10a)
Affinity & fluorescence tagged
RPL10a Ribosomal Subunit
Sorted for
Clover fluorescence
(FACS)
Ribosome Tagged
Wildtype SH-SY5Y
Ribosome Tagged
TDP-43 mutant SH-SY5Y
Cyclohexamide
treatment, lysis,
and nuclei/mitochondria
removal
C
Full-length and truncated stathmin-2 RNA is ribosome associated
at the same rate in TDP-43-mutant SHSY-5Y cells
qRT-PCR
1 2 3 4 5
qRT-PCR
1 2a
Average fold-enrichment in ribosome-bound RNAs
vs "Input" cleared lysate GAPDH normalized
2
1.5
1
0.5
0
"Input" cleared lysate full-length expression relative to GAPDH
Ribosome-bound full-length stathmin-2 vs Input (Wildtype SH-SY5Y)
Ribosome-bound full-length stathmin-2 vs Input (TDP-43 mutant SH-SY5Y)
Ribosome bound truncated stathmin-2 vs Input (TDP-43 mutant SH-SY5Y)
AAA
Direct ribosome capture
(affinity tag-magnetic bead)
Purification
mRNA
isolation
qRT-PCR with stathmin-2
isoform-specific primers
Protein isolation
for mass-spec

I delivered this lentivirus into wildtype and homozygous TDP-43$^{N352S/N352S}$ mutant SH-SY5Y neuron-like cells, with the mutant line normally misprocessing about half its normal stathmin-2 to produce the truncated RNA product (Fig 3.2 B). Stably transduced clones were isolated by FACS, gating on the bright clover protein fluorescence, and sorted cells were grown to confluence. Prior to lysis, cells were treated with cycloheximide for 20 minutes, and lysis, pulldown, and ribosome-bound transcript isolation was performed in cycloheximide-containing media using buffers previously described[211] in combination with commercial StrepTactin magnetic beads. The ribosome-bound RNA fraction along with 10% of the unpurified sample input, and unbound RNA fraction were isolated for cDNA generation and further analysis (Fig 6.1 B). With specific primer-probe sets for qRT-PCR and utilizing GAPDH (a highly translated RNA) as an endogenous control RNA, I compared the ribosome-bound fraction enrichment versus input for wildtype and TDP-43 mutant lines (Fig 6.1 C). I identified that normal full-length stathmin-2 RNAs are enriched in the ribosome-bound fraction versus their respective representation in the sample input, indicating that, as expected for a highly translated gene product, normal stathmin-2 RNA is highly ribosome-associated. Intriguingly, when I performed the same analysis with primer-probes specific to the truncated stathmin-2 RNA in the mutant cells, I found this truncated RNA was on average comparably enriched in the ribosome-bound RNA fraction versus the full-length stathmin-2 RNA (Fig 6.1 C). Thus, translating ribosome affinity purification indicates ribosome occupancy enrichment of truncated RNA approximately equal to that of full-length RNA, suggesting the truncated stathmin-2 RNA product is indeed a substrate for translation.

To my knowledge this is the first experimental result supporting such a model of small open reading frame translation in truncated stathmin-2 RNAs, however, this is a technically challenging experiment to follow-up with additional study for all the reasons I previously enumerated. Substantial additional research focus is needed to determine whether the translation product of the truncated RNA is stably accumulated in affected patient neurons, including

technologies (antibody or otherwise) for micropeptide detection. A logical next step would be gradient centrifugation and polyribosome fractionation, and endogenous small open reading frame tagging by CRISPR-Cas9 genome engineering, a strategy with implications for identifying small molecules to rescue both TDP-43 and stathmin-2 dysfunctions.

A truncated stathmin-2 RNA reporter system to enable high-throughput screening TDP-43 function modifying and/or stathmin-2 splice-rescuing small molecules

Forward genetic screening techniques, like the yeast system that identified Ataxin2 as a modifier of TDP-43 pathology[82], now augmented in the modern era of CRISPR-Cas9 genome-scale libraries[216-219], are powerful tools that enable rapid gene interrogation in relevant cell types to identify genetic pathways and modifier genes relevant to production or alleviation of specific pathologies. Similarly, high-throughput small molecule screening for splice-modifying compounds, like the recently FDA approved selective small molecule effector of SMN2 splicing Risdiplam[220], are an attractive potential therapeutic avenue that deserves further development in the context of stathmin-2 splicing restoration. These screening technologies both require robust, quantitative, easy to measure readouts in order to identify potential gene or small molecule candidates. The sensitivity of stathmin-2 pre-mRNA processing to normal TDP-43 function makes that RNA molecule an attractive potential basis for a reporter readout in genetic and small molecule screening assays, which could help identify genes and compounds capable of preventing or reversing primary TDP-43 related dysfunction(s). Similarly, this molecular indicator has potential utility in an assay for the identification and development of stathmin-2 pre-mRNA splice-modifying molecules, a necessary next-step for the field of classical medicinal chemistry. To enable advances utilizing these technologies, the design and development of new molecular sensors of stathmin-2 pre-mRNA processing dysfunction are now required.

The normal stathmin-2 open reading frame initiates 19 bases from the end of the first exon, and upon stathmin-2 pre-mRNA misprocessing it terminates with a stop codon 32 bases into exon 2a, well upstream of the normal TDP-43 binding site (Fig 6.2 A). One of the simplest potential readouts of stathmin-2 pre-mRNA misprocessing would be to extend and tag this open reading frame with a fluorescent protein coding sequence, which would produce a potentially greater dynamic range of readout than alternative strategies encoding survival-screening factors (such as an antibiotic resistance gene). Since I have previously demonstrated TDP-43's action on the stathmin-2 pre-mRNA is primarily to block utilization of the cryptic 3' splice acceptor site of exon 2a, which is the primary cis-regulatory determinant of exon 2a inclusion, it would likely be advantageous to preserve the respective TDP-43-bound and 3'splice acceptor sequence positioning in a knock-in reporter construct. Thus, to target a gene insertion 3' to the TDP-43 binding site and utilize the endogenous open reading frame of stathmin-2, it is necessary to mutate two in-frame stop codons within exon 2a leading up to an appropriate Cas9 cut site (Fig 6.2 A, sequences in green and purple). In addition to preserving the spatial relationship between the two most critical exon 2a regulatory elements, it is likely advantageous to minimize the overall size of the gene insertion, as the overall length of the endogenous truncated stathmin-2 transcript is a mere 628 bases. Ranking the popular non-antibody based endogenous protein-tagging polypeptides by overall size (Fig 6.2 B), the three smallest are the GCN4 peptide, NanoBiT/HiBiT, and GFP11.

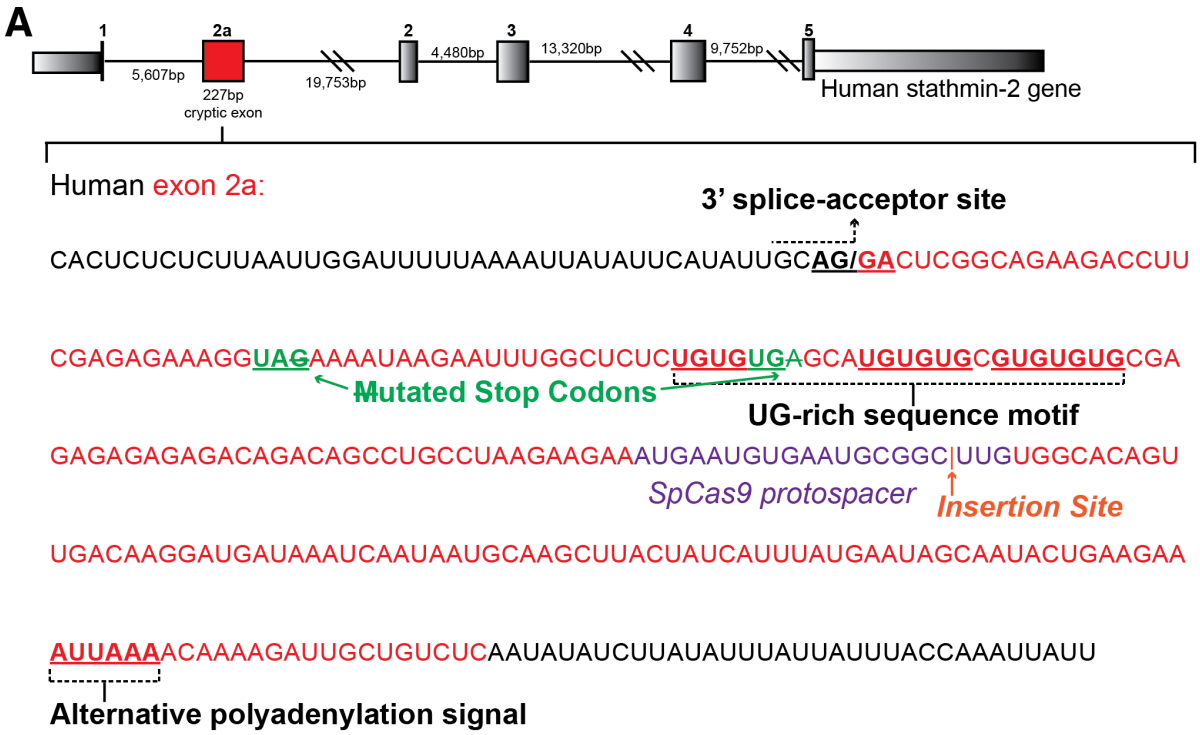

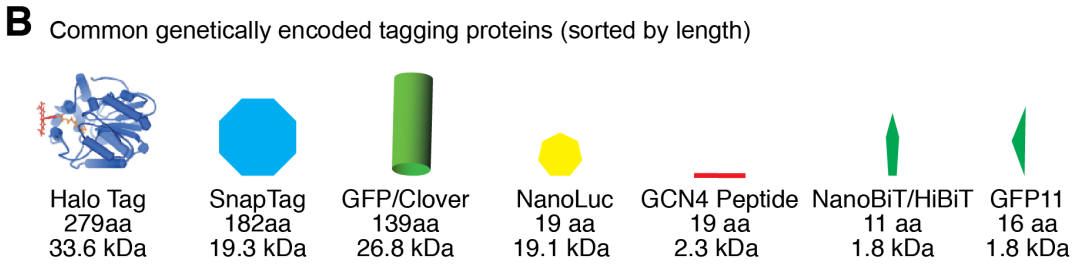

Figure 6.2 Endogneous tagging of truncated stathmin-2 exon 2a by CRISPR knock-in enables high-throughput screening applications

(A) Schematic depicting the human cryptic exon 2a sequence in red, with relevant pre-mRNA processing elements underlined, open reading frame extending codon mutations indicated in green, and SpCas9 targeting elements indicated in purple. (B) Size-ranked comparison of commonly utilized endogenous gene knock-in tagging polypeptide sequences.

The GCN4 peptide is an epitope bound by a single-chain variable fragment (scFv) antibody which can be used to physically tether two separately translated proteins (Fig 6.X A). This the GCN4/scFv system has been used to great effect in the SunTag fluorescent imaging paradigm, wherein a tandem polycistronic reading frame of 24 consecutive GCN4 epitope repeats is bound by scFv-GFP fusion proteins to tag the GCN4-labled protein of interest with a high level of fluorescence (Fig 6.3 A,B), enabling single-molecule live cell protein tracking, and also in a CRISPR-activation system to bind a large number of transcriptional activators to a GCN4-repeat tagged Cas9 protein to direct transcriptional activation at a genomic locus of interest[221]. That the GCN4 peptide itself has no fluorescent properties (and is typically used in a tandem repeat) rules it out as an appropriate candidate in the exon 2a knock-in context, as separately expressed scFv-GFP fusion molecules would fluoresce independent of stathmin-2 expression states.

By contrast, the HiBiT system[222,223], a split luciferase adapted from the NanoBiT[224] system (which was originally designed as a reporter for protein-protein interaction but had low affinity of binding between the split luciferase molecules, K_D>100uM,) has much higher binding affinity to its partner molecule (K_D 700pM) with the scalability and sensitivity of a luciferase-based detection assay. HiBiT is presently the smallest such luminescence-based knock-in protein reporter, but the overall advantages in sensitivity of a luciferase-based assay are likely unnecessary for assays using a properly neuron-like host cell, which will naturally express high levels of stathmin-2 RNA. While HiBiT is an appropriate option, the benefits of this system may not justify the additional substrate costs and screening complexity.

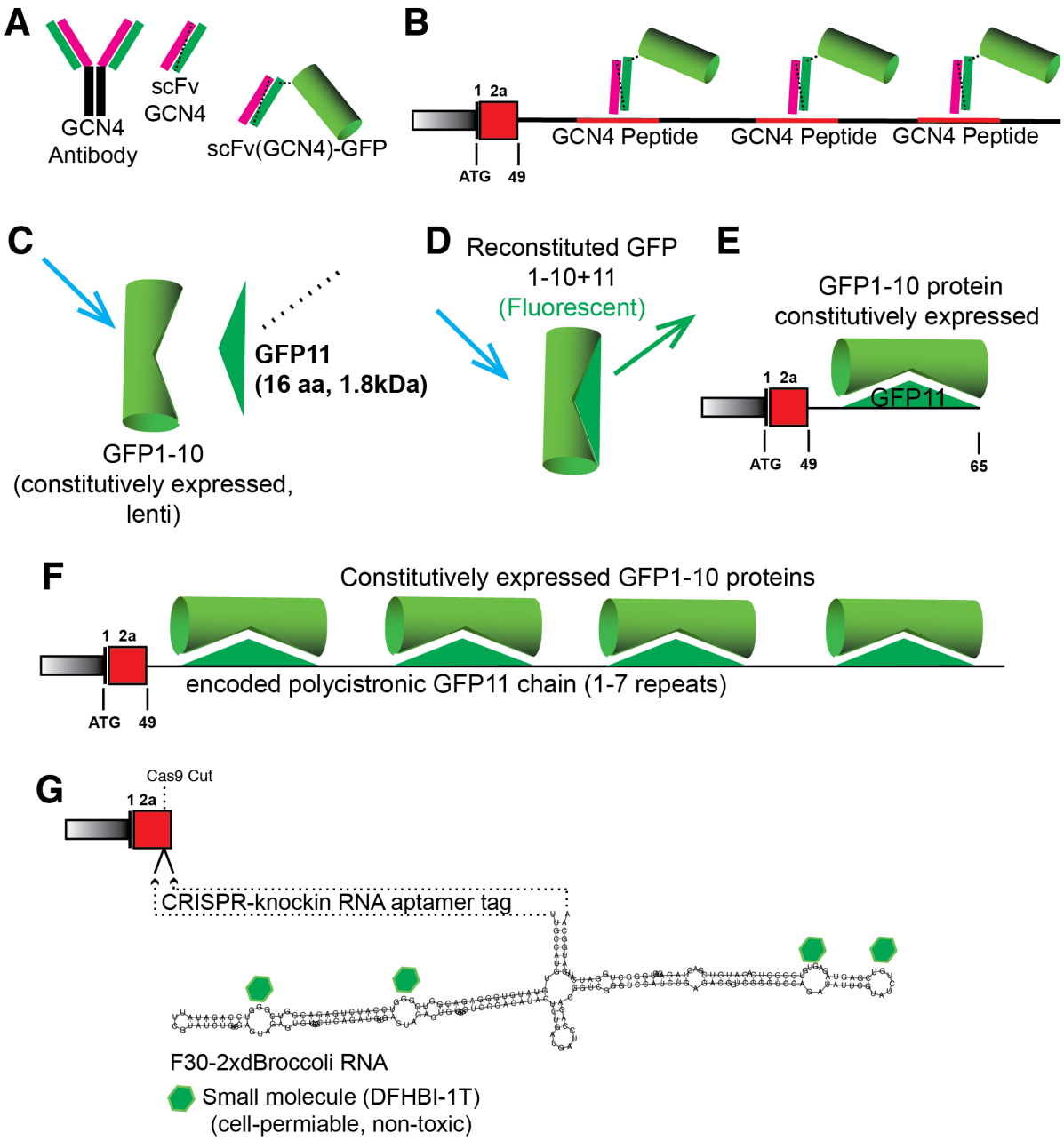

Figure 6.3 Split-fluorescent molecule tagging and directly fluorescent engineered RNA aptamer knockin strategies provide quantitative readouts of truncated stathmin-2 levels for small molecule and genome-scale CRISPR screening applications

(A) Schematic depicting the molecular lineage of scFv-GFP fusion reporters for epitope tag visualization. (B) Schematic of GCN4 polycistronic epitope CRISPR tagging and scFv-GFP fusion protein based fluorescent molecule visualization. (C) Schematic of split-GFP tagging strategy for low molecular weight knock-in fluorescent tagging of endogenous open reading frames depicting separated non-fluorescent component molecules. (D) Schematic depicting reconstituted fluorescent split-GFP. (E) Schematic depicting single-repeat GFP11 endogenous open reading frame knock-in tagging of stathmin-2 cryptic exon 2a, and fluorescent visualization by separate expression of GFP1-10 protein. (F) Schematic depicting polycistronic GFP11 endogenous knock-in tagging for enhanced fluorescent signal with multimeric reconstituted GFP molecules. (G) Schematic depicting F30-2xdBroccoli RNA aptamer knock-in to cryptic exon 2a RNA sequence and direct detection with conjugate binder DFHBI-1T [((Z)-4-(3,5-difluoro-4-hydroxybenzylidene)-2-methyl-1-(2,2,2-trifluoroethyl)-1H-imidazol-5(4H)-one)].

Finally, the 16-amino acid green fluorescent protein fragment GFP11[225] is essentially one polypeptide “wrap” removed from the normal “wrapped-barrel” structure of green fluorescent protein. While each separate polypeptide component on its own is non-fluorescent, when co-expressed with the complementary portion of the GFP molecule (GFP1-10), GFP11 binds back to the parent structure and produces a complete and fluorescent GFP molecule (Fig 6.3 C-E). GFP11 is an attractive knock-in strategy for this gene and application because (if needed) it has semi-scalable fluorescence potential via the same GCN4 polycistronic chain methodology without the off-target fluorescence issues (Fig 6.3 B, F), in this context it would also be translated from a highly expressed RNA, which should make signal detection straightforward. Additionally, the intended application does not depend on an extremely rapid fluorescence maturation time, or luciferase addition, reducing cost and complexity.

In addition to the endogenous fluorescent tagging of truncated stathmin-2, it will also be necessary to counter-tag the full-length stathmin-2 polypeptide, either in the same line using a fluorescent protein sequence with emission in a distinct wavelength, or in a distinct cell line, to enable secondary/counter screening experiments. Such a knock-in strategy should be easily achievable using normal fluorescent protein systems without the practical constraints arising from a limited overall knock-in construct size (there is no expectation that knock-in to the fifth exon of stathmin-2 would affect cryptic element utilization, the premise driving the proposal of small split-fluorescent elements described above), and thus does not require detailed strategic discussion here.

To be clear, tagging the open reading frame of the truncated exon1-2a RNA product by CRISPR knock-in of a fluorescent tag (or variant system) is unlikely to be a viable strategy unless the truncated stathmin-2 RNA is already a cellular substrate for translation. I have presented evidence that this short RNA is indeed ribosome-associated and thus likely translated, suggesting a knock-in to the truncated reading frame (slightly extended by stop codon mutation) ought to be

successful. However, this need not be the only strategy, as translation-independent direct visual readouts using specially engineered RNAs have also been enabled by recently described advances.

Bacteriophage viral RNA aptamer knock-in approaches using PP7[226] or MS2[227] recognition sequences, a strategy I demonstrated within the exon 2a context in experiments throughout my thesis, are unlikely to be favorable in this specific application context, as I have shown interactions between these RNA aptamer sequences and their protein binding partners are sufficient to inhibit pre-mRNA misprocessing of stathmin-2 when targeted to the exon 2a region.

A strategy further reducing overall complexity would be to knock-in a direct RNA fluorescent reporter tag, encoding either the engineered RNA aptamers of the Spinach/Spinach2 sequence, or the more stable (not a substrate for intracellular cleavage) multimeric 234-base F30-2xdBroccoli[228], which is transcribed into stem-loop structures that, upon addition of its non-toxic, cell-permeable, conditional, small molecule conjugate binder DFHBI-1T [((Z)-4-(3,5-difluoro-4-hydroxybenzylidene)-2-methyl-1-(2,2,2-trifluoroethyl)-1H-imidazol-5(4H)-one)], produces detectable fluorescent signal with excitation/emission at 472/507nm (similar to GFP) in living cells. Use of this direct-detection RNA knock-in would enable quantitative fluorescent readout of truncated stathmin-2 RNA levels, fully independent of translation (Fig 6.3 G). Critically, the F30-2xdBroccoli repeat, when delivered as a multimeric repeat sequence has been demonstrated to function in differentiated neurons, producing bright fluorescence from the tagged gene upon expression[228], demonstrating the utility and viability of such an approach for reporter-tagging the truncated stathmin-2 RNA. These endogenous stathmin-2 tagging strategies are now part of the toolkit necessitated to enable applied research and development of small molecule and advanced genome-scale screening approaches.

Genetic tools to determine whether therapeutic restoration of stathmin-2 synthesis might restore axonal regrowth in-vivo and lead to the restoration of functional neuromuscular synapses

SOD1 mouse models of ALS demonstrate that many neuromuscular junctions are already lost by the time of disease onset in that system. Between post-embryonic days 14-25, 20% and 40% of neuromuscular junctions are already lost in the gastrocnemius and tibialis anterior, respectively, with earliest detection of muscle weakness apparent only later on day 29[229]. This early junction loss is consistent with human patient electromyography measurements, which establish this dysfunction as one of the earliest features of disease[179-182]. Since clinical diagnosis of symptomatic disease is thus apparently quite late on the insidious timeline underlying pathological changes, a crucial question to every potential therapeutic approach involving stathmin-2 restoration is, "to what extent can restored stathmin-2 expression halt (or reverse) the synaptic/neuromuscular junction loss phenotype" observed in the context our AAV mouse model of chronic stathmin-2 suppression, and ultimately in a TDP-43 proteinopathy patient after disease onset/diagnosis.

Since stathmin-2 disfunction is associated with defects in axonal transport, and our team and others have identified stathmin-2 localization at the sites of acute axonal damage as a key mediator of regenerative capacity, it remains an open question whether transport of either restored stathmin-2 mRNA (assuming local translation can effect axonal stathmin-2 levels) or protein (stathmin-2 is Golgi-sorted for fast axonal transport to axons via palmytoilation-mediated post-translational modification) can be sufficiently delivered through an already disrupted axonal transport system to its site of action and mediate recovery of a damaged neuron. Given these unknowns, and the fact that all ongoing studies to date have focused only on the consequences of suppressing normal stathmin-2 levels, the tipping point between a potential stathmin-2 restoration-mediated recovery and permanent axonal loss has not been established. Resolution

of this next question is key to the prognosis for a stathmin-2-restorative therapy program for TDP-43 proteinopathies.

In order to more precisely establish the effective therapeutic window for stathmin-2 restoration in an adult nervous system, I designed a simple Cre-LoxP system modification of my already proven AAV9 RNAi payload, which I previously demonstrated is highly effective at chronic reduction of murine stathmin-2 expression (Fig 5.1-5.3). The Cre-LoxP system is site-specific recombination scheme originally derived from the P1 bacteriophage[230] which has seen extensive use within inducible genetic model systems. Implementing a modern variant of the Cre-LoxP strategy, in which sets of so-called FLEX sites (also known as DIO or Double-floxed inverted open reading frame) are arranged around the RNAi payload reading frame, I can produce a vector with an inducible, efficient, and irreversible RNAi kill-switch (Fig 6.4 A). FLEX switches involve use of two sets of wildtype LoxP sequences alongside two mutant sequences, which are arranged such that two pairs of mis-matched sites first invert the intervening DNA sequence orientation, before a subsequent excision step removes a site and prevents re-inversions[231] (Fig 6.4 A-C). In order to include a fluorescent color-change indicator of successful FLEX inversion, my implementation additionally takes advantage of the fact that the mCherry fluorescent protein coding sequence contains a naturally stop-codon-free reverse reading frame, allowing its inverted positioning in a pre-recombination payload without interference in downstream clover marker or RNAi expression.

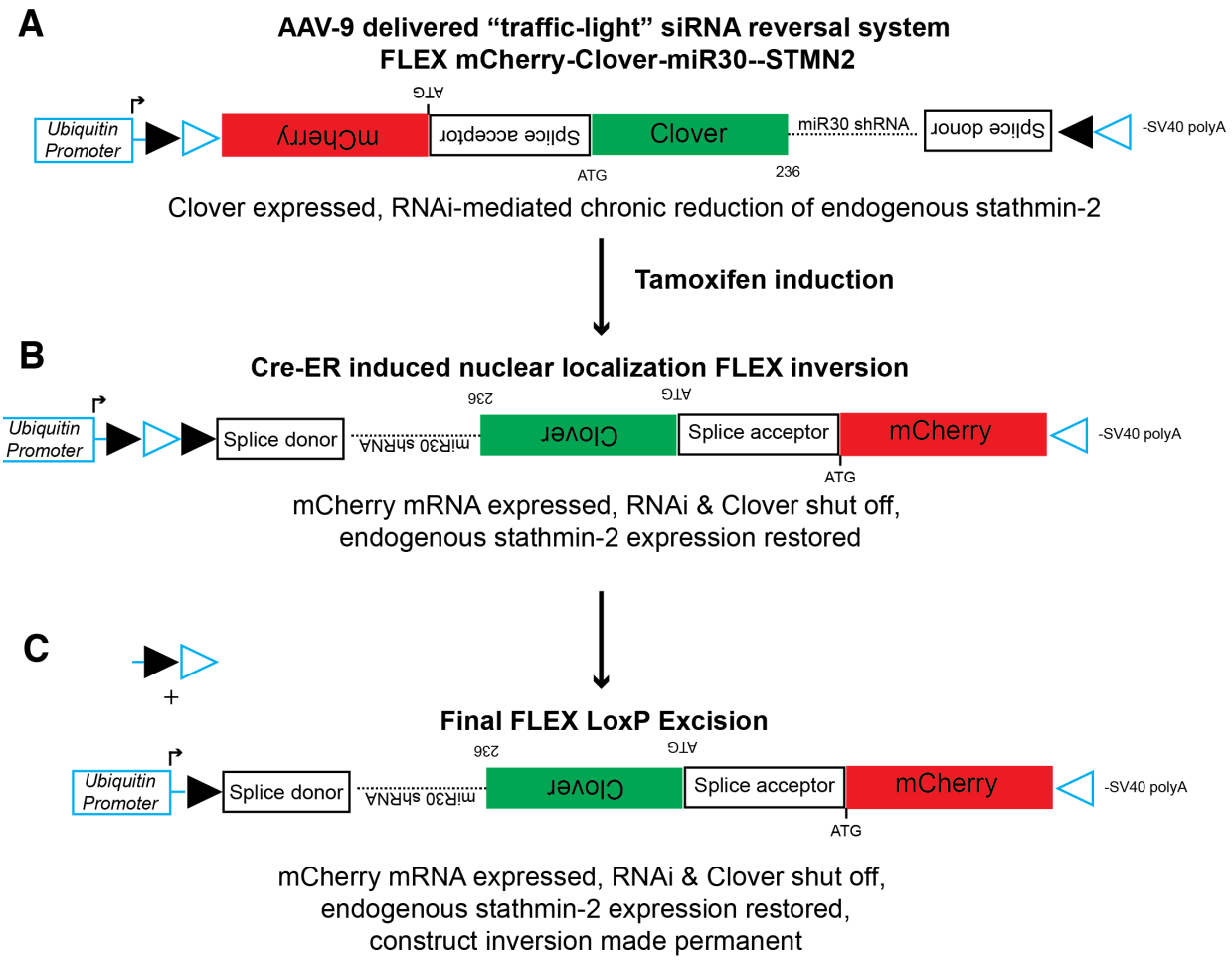

Figure 6.4 AAV FLEX-RNAi and stoplight reporter payload to determine time-dependent changes in axonal restoration capacity by inducible and permanent Cre-dependent RNAi inactivation

(A) Schematic depicting the initial encoded features of the AAV-FLEX RNAi vector before Cre-ER dependent inversion, RNA polymerase II transcription produces an RNA encoding a fluorescent Clover protein open reading frame and a miR30 embedded shRNA hairpin targeting the 3'UTR of endogenous murine stathmin-2 encoding RNAs. (B) Schematic depicting intermediate step of FLEX inversion, with swapped DNA strand orientation relative to promoter and un-excised LoxP sites, expressing in-frame mCherry fluorescent protein. (C) Schematic depicting permanently inverted FLEX-RNAi system with inactivated stathmin-2 targeting RNAi and Clover expression, accompanied by activated expression of red mCherry fluorescent protein.

Administration of the resulting AAV9 vector by subpial delivery to the lumbar spinal cord of mice expressing Cre-recombinase fused to the estrogen receptor should enable a robust initial RNAi mediated knockdown of endogenous murine stathmin-2 (equivalent to Fig 5.1-5.3) while simultaneously marking successfully transduced neurons with the green fluorescent clover protein. Upon treatment of mice with tamoxifen, the Cre-recombinase-estrogen receptor fusion protein will translocate from the cytoplasmic compartment into the nucleus and (via the FLEX LoxP sites) invert the orientation of the RNAi expression construct, shutting off the stathmin-2 suppression system to allow restored expression of endogenous stathmin-2 mRNA and marking converted cells with expression of red fluorescent mCherry protein (turning the transduced recombinant cells from green to red). This allows for inducible restoration of endogenous stathmin-2 expression after experimentally defined period(s) of RNAi-mediated knockdown in parallel cohorts of mice, such that detailed molecular and phenotypic consequences with respect to axonal recovery can be determined after pulsed suppression of endogenous stathmin-2 synthesis.

Utilizing this genetic tool to adjust the timing of RNAi-mediated stathmin-2 suppression and subsequent relief allows for simulation of therapeutic outcomes for stathmin-2 restoration after an investigator-defined period of neuronal stathmin-2 deprivation, all without relying upon TDP-43 dependent pre-mRNA misprocessing or chronic ASO (be it knockdown or rescue) dosing. By carefully following both the resulting mouse phenotypes established in the ongoing stathmin-2 knockdown experiment (EMG, grip test, von Frey test, etc.) and resulting effects on neuromuscular junction innervation, this system should enable a quantitative answer to identify the “point of no return” for a stathmin-2 depleted neuron.

A negative outcome for this open question, wherein the window of possible neuronal repair is rapidly closed after onset, does not doom a therapeutic stathmin-2 restoration approach. To the contrary, recognizing the focal onset and progressive compartmented nature of disease

spread in ALS, the protection of neurons still naive to TDP-43 disfunction is essential to halting progression of the disease throughout the upper and lower motor compartments. That said, the tantalizing possibility that restoration of a protein involved in axonal repair and regrowth could lead to some functional restoration in affected patients after onset certainly warrants investigation. A FLEX-RNAi AAV payload is one genetic tool I have built that could be utilized to answer this question.

Does a lack of stathmin-2 cryptic exon conservation explain a common lack of motor neuron disease phenotype in ALS mouse models?

Evidence supporting the hypothesis that enabling TDP-43 regulation of murine stathmin-2 processing might in turn enable better mouse models of sporadic ALS include data from the ongoing experiment in Chapter 5, wherein I demonstrate that chronic focal murine stathmin-2 suppression alone in spinal cord of adult animals leads to progressive neuromuscular junction loss and motor and sensory phenotypes (Fig 5.2, 5.3). Additionally, my demonstration that murine stathmin-2 pre-mRNAs humanized by insertion of the corresponding fragment of human exon2A are sensitized to TDP-43 perturbations (Fig 5.6) builds a logical foundation and molecular system to test whether TDP-43-dependent stathmin-2 disruption contributes to pathophysiology of ALS/FTD mouse models.

In order to determine how stathmin-2 contributes to neuronal function and to develop therapeutic approaches based on restoration of stathmin-2 levels in ALS and FTD, the field needs more faithful animal models where processing of the stathmin-2 transcript is dependent on TDP-43 function, as we have demonstrated to be true in human. We built such a model system (described in detail in Chapter 5, see also Fig 6.5 A, B, D) by knocking in a 394bp segment of human exon 2a into the corresponding mouse intron 1 locus, and demonstrated that it confers

pre-mRNA processing sensitivity of mouse stathmin-2 to even modest perturbations of TDP-43 levels (achieved by AAV-RNAi mediated reduction of TDP-43 after administration into the brains of newborn pups). However, the low relative efficiency of knockdown I observed in the initial P0 ICV AAV-RNAi administration studies (and with other RNAi gene products points similarly dosed at this early post-natal time point) compared with the striking knockdown observed after adult subpial administration of the exact same AAV virus, clarifies that an experiment to determine whether chronic TDP-43 dependent stathmin-2 pre-mRNA misprocessing in an adult animal results in synapse or neuromuscular junction consequences would be best addressed in the AAV context via adult subpial administration of this TDP-43 targeting RNAi vector. This experiment is underway with a pilot cohort of animals dosed and under evaluation for TDP-43 and stathmin-2 target engagement and resulting altered pre-mRNA processing outcomes, respectively, with a larger cohort prepared for phenotype and molecular analysis.

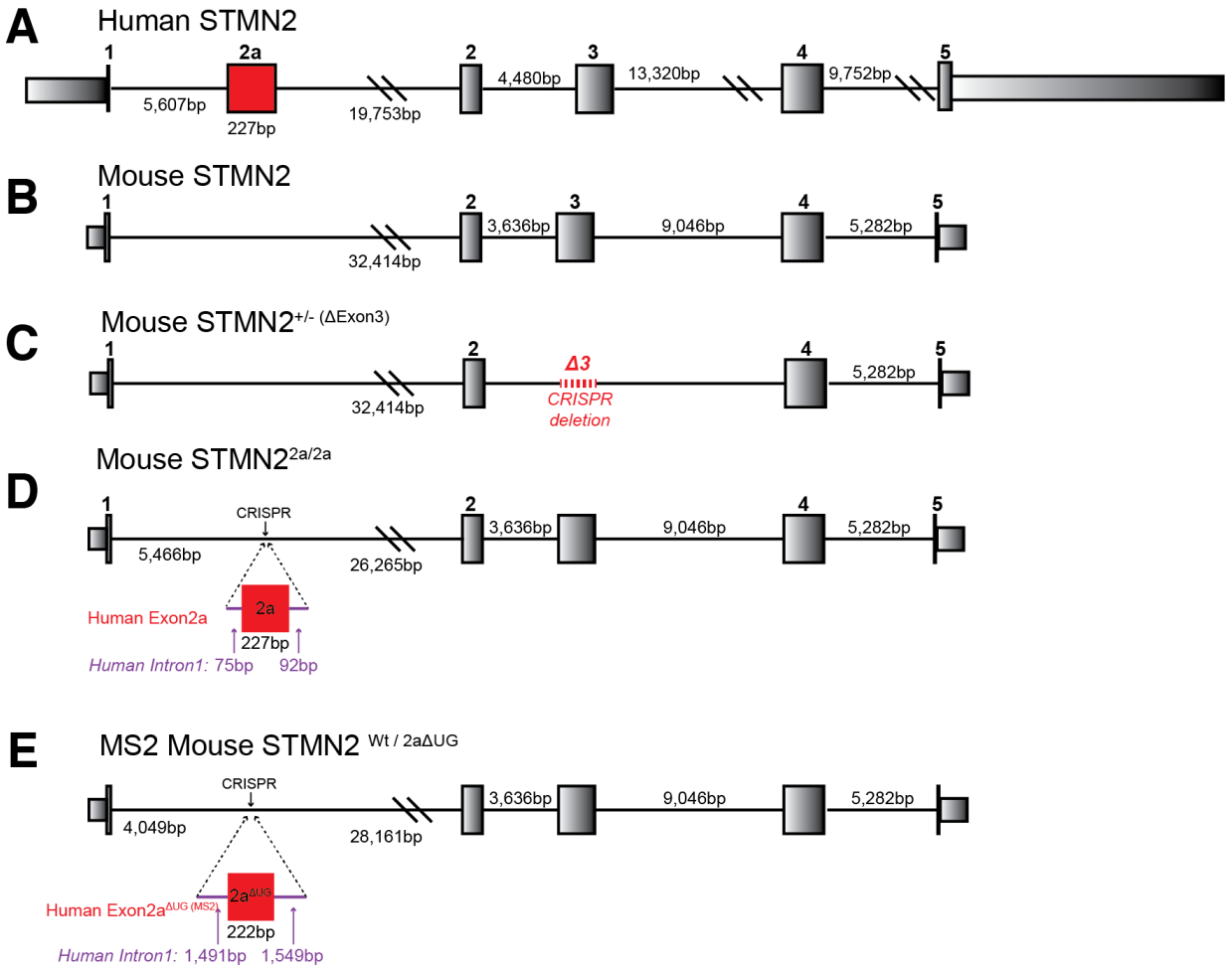

Figure 6.5 Humanized and knockout stathmin-2 mouse models enable more accurate molecular modeling of sporadic ALS pathophysiology

(A) Schematic depicting features of normal human stathmin-2 gene including cryptic exon 2a which is not conserved in mice. (B) Schematic depicting features of wildtype mouse stathmin-2 gene. (C) Schematic depicting mouse stathmin-2 gene CRISPR knockout strategy featuring deletion of exon 3 leading to a frameshift mutation and predicted nonsense mediated decay of the resulting gene product. (D) Schematic of mouse stathmin-2 gene humanized by insertion of complete human exon 2a fragment into the corresponding locus of murine stathmin-2 intron 1. (E) Schematic depicting mouse stathmin-2 gene humanized with a mutant human exon 2a in which the TDP-43 UG binding sequence is replaced with an MS2 aptamer sequence to drive constitutive misprocessing and truncation of the encoded stathmin-2 pre-mRNA.

AAV-delivered RNAi is just one molecular tool by which to disrupt normal TDP-43 function in an adult animal. Indeed, numerous transgenic rodents expressing human TDP-43 have been generated, with or without disease-causing mutations and under various promoters[232-235]. Overexpression of TDP-43 induces a severe lethal phenotype independent of the presence of mutation[232,233]. However, mice expressing levels close to endogenous TDP-43 develop mutant and age-dependent neurological phenotypes, including mild motor and cognitive deficits, motor neuron degeneration, and neuromuscular denervation, but strikingly (and disappointingly) without paralysis or reduced lifespan[236,237].

An important caveat for animal modeling of TDP-43 proteinopathies is that the repertoire of RNAs bound by TDP-43 differs between species with RNA processing alterations elicited by TDP-43 dysfunction distinct between mice and humans. Indeed, our own demonstration that the human RNA most affected by TDP-43 disruption encodes the neuronal growth-associated factor stathmin-2 was just one example[91]. The experimental paradigm in that discovery was exceptionally simple: take a human neuron-like cell and see what happens to RNA expression levels when TDP-43 function is disrupted by various means. The analogous murine investigation performed in a more sophisticated experimental design: acute TDP-43 depletion from the adult central nervous system of wild-type mice[73,87], was not capable of identifying stathmin-2 as a neuronal TDP-43 target because stathmin-2 RNAs are neither bound nor regulated by TDP-43 in rodents[73,91]. Consistently, abnormal pre-mRNA processing of stathmin-2 is not recapitulated in mice expressing TDP-43 transgenes or in TDP-43 deficient mouse models. While I have identified that this is mechanistically due to the unconserved TDP-43 binding site and the cryptic 3' splice acceptor it modulates, it raises the broader question of whether and to what extent the shortcomings regarding fatal paralysis of non-SOD1 mouse models of ALS are due to the TDP-43 independence of murine stathmin-2 pre-mRNA processing.

Recognizing that the incomplete phenotypes in TDP-43 mutant mice may reflect that neither the cryptic polyadenylation site nor the TDP-43 binding sites that provoke the loss of stathmin-2 upon TDP-43 depletion is conserved in mice[91], efforts are now underway to determine the consequences of stathmin-2 reduction in mice expressing an ALS/FTD-causing TDP-43 mutant (TDP-43^{Q331K}) previously generated by the Cleveland group[237,238] and which develop only partial motor neuron disease. The goal is to determine whether stathmin-2 loss synergizes with TDP-43 disruption to exacerbate neurodegeneration in ALS/FTD. The TDP-43^{Q331K} line expresses mutant TDP-43 throughout the nervous system in a pattern mimicking endogenous TDP-43[237]. Nonetheless, despite a level of expression twice the TDP-43 level in non-transgenic mice and development of age-dependent motor neuron disease with the degeneration of 1/3rd of the lower motor neurons by one year of age, 2/3^{rds} of motor neurons do not degenerate at any age[237].

In work currently underway in collaboration with the Jackson Laboratory, cohorts of TDP43^{Q331K} transgenic mice with zero, one, or both humanized stathmin-2 alleles (Fig 6.5 D) are being generated. These cohorts will then be aged and carefully followed by phenotypic and pathological measures to determine the ultimate impact of stathmin-2 RNA misprocessing/loss of function on ALS and FTD related phenotypes, including disease onset and degree and/or rate and/or extent of disease progression. Postmortem pathological analyses will then be used to determine – across disease course – the degree of stathmin-2 suppression and whether any stathmin-2 reduction affects the pathology developed in motor neuron perikarya/dendrites, axons, or neuromuscular junctions and/or any effects on astrocytes, microglia, or oligodendrocytes.

Since TDP43^{Q331K} transgenic develop mutant and age-dependent neurological phenotypes, including mild motor and cognitive deficits, motor neuron degeneration, and neuromuscular denervation, without apparent aggregation or loss of nuclear TDP-43 localization[236,237], an additional study is underway utilizing stathmin-2 humanization in a model of

ALS/FTD with more overt TDP-43 pathology. Expression of C9ORF72 repeats encoded by AAV following intracerebroventricular (ICV) injection into P1 wild-type mice was initially shown by our collaborator Dr. Petrucelli to induce progressive behavioral and pathological phenotypes associated with C9ORF72 disease including phospho-TDP-43 aggregates[239,240]. Notably, ICV injections lead to expression of G_4C_2 repeats predominantly in the brain and induce FTD-related behavioral phenotypes. AAV transduction remains low, however, in the spinal cord and does not lead to ALS-like spinal motor neuron death and paralysis. To overcome this limitation, we have recently extended the subpial injection approach to establish a new, reliable model for C9ORF72-repeat expansion motor neuron disease through a single subpial injection of AAV-C9ORF72-$(G_4C_2)_{66}$ into lumbar spinal cord of wild-type mice. This produces classic progressive motor neuron disease (limited to lumbar and lower thoracic cord) accompanied by complete paralysis from death of motor neurons. We are hopeful that the TDP-43 pathology of this model system, when combined with stathmin-2 humanized alleles sensitized to TDP-43 dependent pre-mRNA misprocessing (Fig 6.5 D) will produce a mouse with phenotypes that better reflect human disease. At the same time, stathmin-2 is only one TDP-43 dependent human pre-mRNA that is not conserved in mice, it is not necessarily the case that among unconserved TDP-43 targets between mice and humans that stathmin-2 is the only contributing factor necessary for a true ALS-like neurodegenerative disease phenotype, so these experiments will determine whether and to what extent stathmin-2 loss contributes uniquely to human TDP-43 proteinopathy.

As a potential alternative approach to mouse models, the African Turquoise Killifish is an intriguing emerging rapid model organism for the rapid (short life cycle) study of aging, which critically, includes the time-dependent aggregation of TDP-43, and has a stathmin-2 ortholog gene with a long first intron containing a partly conserved Exon2a sequence with is 45% similarity to the human cryptic exon sequence including a GU binding motif. The fact that the killifish naturally

has detectable TDP-43 proteinopathy as a natural consequence of its aging process could set it apart from the murine model as an alternative system in which to test stathmin-2 dependent neurodegenerative disease. A great deal of additional work will be required to produce such a disease model in this organism.

What is the molecular mechanism that allows 5% of stathmin-2 homozygous knockout mice to survive?

Chauvin & Sobe reported in a review[106] (but without accompanying supportive evidence) that mice with complete loss of the Stmn2 gene were not viable. They did not comment on the fate of mice with heterozygous reduction in stathmin-2. The stathmin-2 knock-out mouse they referenced in that review has not been published or further characterized, so our collaborators, the Lutz group at The Jackson Labs utilized CRISPR/Cas9 to inactivate one allele of an endogenous Stmn2 gene in the C57BL/6J inbred mouse strain by deleting exon 3 (Fig 6.5 C). The loss of this 173nt coding exon is predicted to cause a frameshift mutation at Asp-38 followed by premature termination 46 amino acids later, producing an unstable RNA that is a substrate for nonsense mediated decay. Consistent with this prediction, we determined that heterozygous $Stmn2^{+/-}$ mice are viable and fertile despite expressing stathmin-2 protein to 50% of normal levels. In characterization work presently still in early stages, we have not (so far) detected motor abnormalities in these mice, although a separate experiment performed with ICV delivery of a stathmin-2 reducing ASO in wildtype mice demonstrated a loss of neuromuscular junctions after 8 weeks of stathmin-2 suppression accompanied by decreased axonal conduction velocity measured by compound Muscle Action Potential (cMAP) amplitude[241,242]. It remains to be seen whether the heterozygous mice developmentally escape neuromuscular consequences observed by direct acute stathmin-2 knockdown in an adult animal, and if so, what is the tipping point of stathmin-2 expression that would explain a phenotypic difference.

By the same token, in contrast to the report of Chavin & Sobel[106], mating of our stathmin-2 heterozygotes (to produce homozygous loss of that gene) has demonstrated that complete loss of Stmn2 produces viable stathmin-2 deletion progeny, albeit only at 1/5 the Mendelian rate. Of 89 progeny screened from a $Stmn2^{+/-}$ x $Stmn2^{+/-}$ mating, five homozygous deletion mice were recovered (5%). This means that stathmin-2's role in development is substantial, as 95% of mice lacking this gene product will die as a consequence, however, equally interesting are the developmental mechanisms for survival of a subset (5%) of $Stmn2^{-/-}$ mice that escaped pre- and postnatal lethality and went on to live for at least 1 year of age without apparent motor phenotype (before being taken down for necropsy and molecular analysis). Three efforts to identify the compensatory mechanism(s) are underway 1) embryonic development analysis for neurogenesis/innervation and careful observation and necropsy after birth of homozygous stathmin-2 null animals to determine a common cause of death, 2) comparative RNA-sequencing between surviving and non-surviving littermates to identify compensatory genes and pathways that might enable escape from post-natal mortality, and 3) backcrossing experiments to determine comparative mortality rates of this genetic lesion in different mouse lines and similarly start to identify genetic compensatory mechanisms. Such genes and mechanisms, if identified, could provide additional therapeutic insights for the treatment of TDP-43 proteinopathy, while furthering our understanding of basic stathmin biology.

Direct AAV supplementation of stathmin-2 expression to physiologically tolerable levels in the CNS as a neuroprotective treatment in TDP-43 proteinopathy

Restored pre-mRNA processing of the endogenously expressed stathmin-2 encoding RNA transcript, which I have demonstrated using splice-rescuing antisense oligonucleotides and RNA-targeted CRISPR effectors (likely also achievable with small molecules and other means), is undoubtedly the safest current therapeutic avenue for stathmin-2 restoration in TDP-43

proteinopathy. Aside from what is perhaps the most difficult “high risk” molecular therapeutic alternative solution for in-vivo stathmin-2 misprocessing (suggested by the results of my genome editing experiments): the utilization of transient CRISPR base editing to ablate the exon 2a cryptic splice acceptor from the STMN2 gene in neurons and ablate the ability of cells to misprocess their stathmin-2 pre-mRNA in neurons altogether, another intervention that carries a potential high risk/reward deserving further investigation is direct gene supplementation therapy with a stathmin-2 expressing viral payload. While the coding sequence of stathmin-2 consists of a mere 537 DNA bases and is well within the packaging limitations of a standard AAV gene therapy vector, the real technical challenge for such an AAV cargo is the prevention of supra-physiologic expression in targeted cells with TDP-43 dysfunction, while leaving stathmin-2 levels ideally unaltered within normal healthy neurons with functional nuclear TDP-43. Indeed, it has been reported that stathmin-2 moderate overexpression induces desirable neurite outgrowth while higher levels of induction causes microtubule catastrophe and axonal growth cone collapse in-vitro and in-vivo[118,119,184]. Additionally, the conservation of cryptic exon 2a pre-mRNA processing elements among primates suggests that TDP-43 expression gating mechanisms for stathmin-2 may be necessary to alleviate some stathmin-related cellular toxicities, perhaps at specific developmental or neuronal differentiation timepoints that coincide with reduced TDP-43 levels.

It is clear from the ongoing experiments I presented in Chapter 5 that the loss of stathmin-2 from the lower motor system is deleterious to the maintenance of synapses. Key questions for the viability of a gene therapy restoration approach are: whether, to what extent, and at what expression levels is stathmin-2 supplementation beneficial or detrimental for axonal maintenance and regrowth in-vivo. That stathmin-2 is already among the top-25 highest expressed genes in a transcriptionally hyper-active cell type like a neuron[91] raises the question as to whether supplementation strategies driven by moderate-expression promoters are even capable of inducing long-term toxicity. To this question, our direct lentiviral restoration of stathmin-2

expression in a microfluidic culture system, demonstrated in our initial discovery[91] achieved a moderately higher level of restored stathmin-2 expression using the PGK promoter than was initially predicted/desired based upon our preceding unpublished viral titration experiments, but without apparent deleterious effect in those human iPS motor neurons, indicating tolerance of moderate stathmin-2 overexpression. It will be important for the field to experimentally determine these expression-level “guideposts” to guide development of appropriate stathmin-2 restoring gene therapy vectors.

For an initial experiment to determine the consequences of a gene-therapy vector driving moderate expression of stathmin-2 within the adult central nervous system, I designed an AAV cassette driven by a moderate expressing Ubiquitin promoter sequence, encoding both the red fluorescent marker protein mScarlet and the human stathmin-2 protein from the same RNA. The two peptides are co-translationally cleaved at a viral T2A sequence which triggers the failure of a translating ribosome to incorporate an amino acid between the two polypeptide sequences (Fig 6.6 A). The result is moderate expression of both a red fluorescent marker to light-up transduced cells, and an untagged stathmin-2 polypeptide. A control vector expressing only mScarlet with a T2A sequence driven by the same expression promoter would be utilized as a transduction control (Fig 6.6 B). mScarlet-stathmin2 or mScarlet-only AAV vectors introduced into the mouse lumbar spinal cord of wildtype animals via subpial delivery (Fig 6.6 C) would achieve broad neuron transduction[150,151] and mice would be aged to determine axonal conduction velocity measured by compound Muscle Action Potential (cMAP) amplitude[241,242], clasping, and neuromuscular junction and axon cross-section quantification over time to determine the effects of moderate stathmin-2 overexpression in wildtype animals.

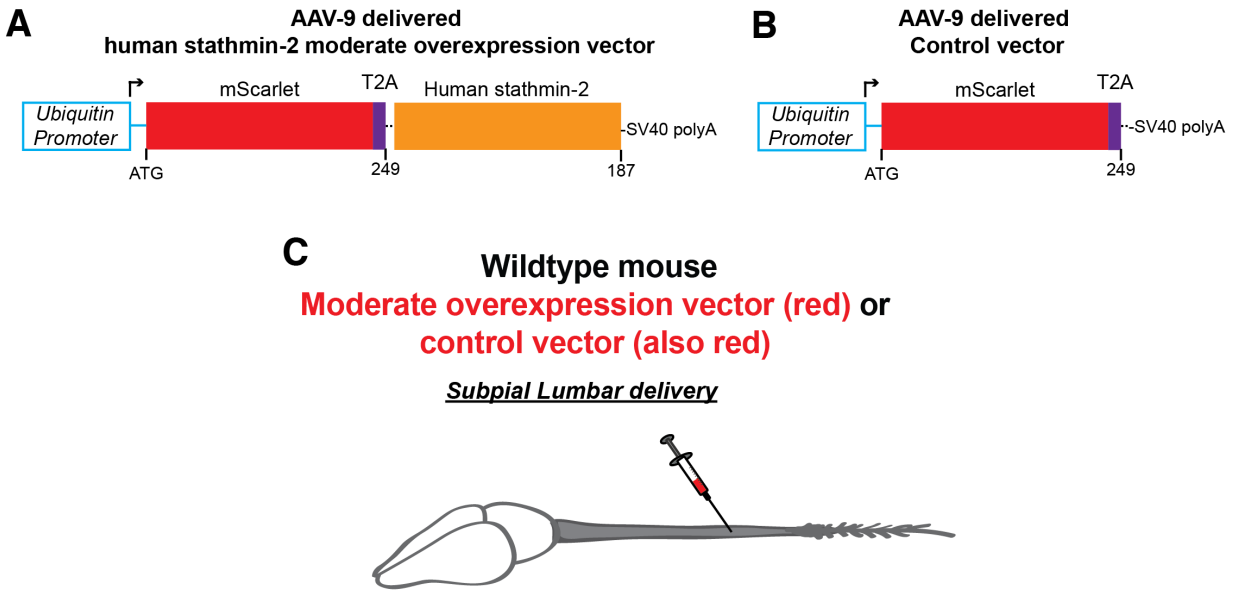

Figure 6.6 Subpial delivery of AAV encoding stathmin-2 gene payload and fluorescent transduction marker, to determine the in-vivo consequences of focal moderate stathmin-2 overexpression in the lumbar spinal cord

(A) Schematic depicting features of an AAV payload delivering a moderately and ubiquitously expressed stathmin-2 coding sequence and mScarlet fluorescent protein transduction marker. (B) Schematic depicting features a control AAV payload expressing only the mScarlet fluorescent protein transduction marker. (C) Schematic depicting focal subpial lumbar AAV administration strategy to determine the consequences of chronic stathmin-2 gene expression supplementation in the lumbar spinal cord of adult mice.

Given the focal onset and spread within and between compartments in ALS and other TDP-43 proteinopathies, within the central nervous system of any given patient there must necessarily be a heterogeneous mixture of neurons either with or without normal functioning TDP-43 (especially early in disease when many neurons outside the initial site of onset are apparently unaffected). Thus, a significant challenge facing stathmin-2 restorative gene therapy approaches is the potential for unintended, cumulative, combined overexpression of endogenous and exogenous stathmin-2 in otherwise healthy neurons with normal nuclear TDP-43 (and thus unaltered high expression of endogenous stathmin-2). This is due the fact that a normal gene therapy payload cannot differentiate between healthy neurons with functional TDP-43 and diseased neurons. The ideal stathmin-2 restoring gene therapy payload design must be engineered to adaptively gate its own expression based on the actual TDP-43 status of whatever neuron it might be transduced into, activating only in the absence of functional TDP-43.

The best way to achieve this desired expression pattern is to leverage what is already known about other human genes with TDP-43-expression-gated RNA expression, borrowing those processing elements and their molecular mechanisms from nature, and engineering these features into a stathmin-2 encoding AAV payload. With this in mind, I have already tested the two most obvious natural TDP-43 gated RNA systems: 1) utilizing the cryptic human stathmin-2 exon2a elements and their partner TDP-43 binding sites to control inclusion of a stathmin-2 encoding alternative exon, and 2) leveraging TDP-43's own somewhat ill-defined autoregulatory mechanism, which involves binding to sites on its own pre-mRNA 3’ untranslated region, to reverse-gate the expression of a chimeric stathmin-2 coding-sequence fused to the full TDP-43 3’UTR sequence.

The first approach is fitting in its apparent simplicity: recycle the same endogenous stathmin-2 pre-mRNA elements that mediate cryptic exon 2a splicing and polyadenylation upon reduction of normal TDP-43 pre-mRNA binding (the molecular mechanism of endogenous

stathmin-2 loss we are trying to reverse in the first place) and fuse those elements to a stathmin-2 coding sequence to generate a TDP-43 loss-dependent stathmin-2 supplementation with an expression profile that should perfectly match (with inversion) the primary defect. There are two primary routes to build such a system, the first is to use an exon 2a variant in which the five normal in-frame stop codons encoded within exon 2a (and premature polyadenylation signal) have been mutated to allow translational read-through to an alternative reading frame of a downstream exon encoding a T2A co-translational cleavage signal followed by the stathmin-2 coding sequence (Fig 6.7 A,B). This system allows exon 2a gating of expression of an untagged stathmin-2 polypeptide, reversing the normal TDP-43 dependent silencing. Testing of this TDP-43 inverted expression system is already underway.

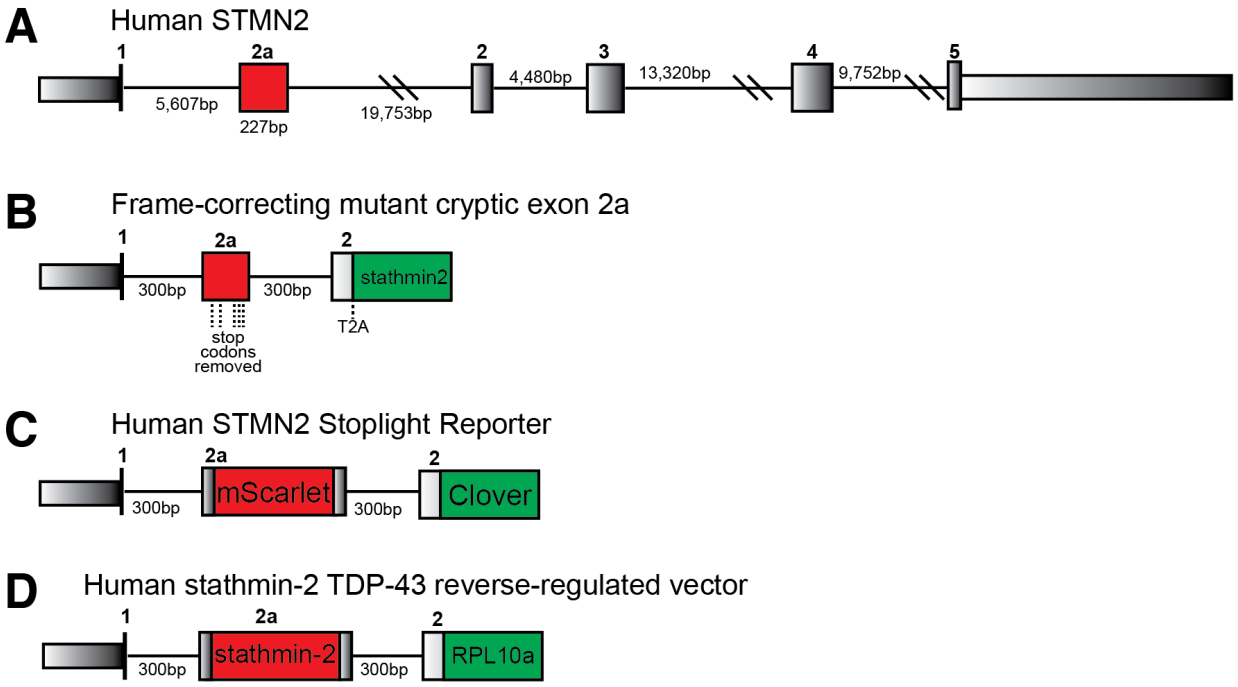

Figure 6.7 TDP-43-reverse-regulated expression of stathmin-2 coding sequence via embedded exon 2a cis-regulatory elements enables safe AAV gene transfer by limiting supplemental expression to neurons lacking functional TDP-43.

(A) Schematic depicting normal human stathmin-2 encoding gene, including TDP-43 regulated cryptic exon 2a. (B) Schematic of an expression payload in which inclusion of an intervening cryptic exon 2a, modified to mutate the five endogenous in-frame stop codons and restore a contiguous open reading frame, is upstream from an otherwise out-of-frame T2A-stathmin-2 coding sequence, enabling co-translational cleavage from the upstream polypeptide. In the absence of TDP-43 the cryptic exon is included, putting the stathmin-2 coding sequence in-frame for translation. (C) Schematic depicting a stoplight reporter sequence utilizing the cis-regulatory elements of exon 2a to express either the coding sequence for the red mScarlet fluorescent protein from cryptic exon 2a upon loss of normal TDP-43 function, or alternatively the clover fluorescent protein coding sequence embedded in the normal exon 2 of the stathmin-2 gene when TDP-43 function is normal. (D) Schematic depicting a gene therapy strategy for TDP-43-reverse-gated expression of the stathmin-2 gene coding sequence embedded within cryptic exon 2a cis-regulatory elements.

The second variation on this strategy is to fully insert the desired alternative coding sequences into the cryptic exon 2a reading frame (and downstream normal exon 2, if desired) (Fig 6.7 C,D). An initial test of this system, also underway, utilizes a “stoplight reporter” with alternative reading frames in exon 2a and normal exon 2, encoding a red mScarlet fluorescent protein and a green fluorescent Clover protein, respectively (Fig 6.7 C). If successful, restriction cloning will be used to insert the coding sequence of stathmin2 and the ubiquitously expressed endogenous ribosomal protein RPL10a into the respective reading frames to encode two alternative gene products (Fig 6.7 D). Since normal TDP-43 binding and RNA processing function is highly enriched in distal intronic regions, with particular enrichment on very long introns[73], it is possible that this mini-gene like strategy will be challenged by an overall short intron length that may be insufficient for efficient TDP-43 dependent pre-mRNA processing (and misprocessing).

An alternative strategy, which does not depend on TDP-43’s action at a variant of an endogenous distal intron, takes advantage of the fact that TDP-43’s complete 3’ untranslated region is only 2110 bases in total length (well suited for AAV packaging limits) while apparently harboring cis-regulatory elements for TDP-43 dependent pre-mRNA processing. While the proposed mechanistic action(s)[79] of TDP-43 protein binding to its own pre-mRNA are not precisely established, it is well known that TDP-43 is capable of negatively regulating its own synthesis via binding and influencing the alternative processing of the 3’ UTR of the pre-mRNA. It is possible that this protein:RNA autoregulatory relationship contributes to a feed-forward loop in TDP-43 aggregation pathology whereby cytoplasmic aggregation and nuclear clearance of TDP-43 alters pre-mRNA processing to disinhibit new TDP-43 synthesis, and in-turn newly translated cytoplasmic TDP-43 is captured into cytoplasmic aggregates, with pre-mRNA maturation rates increasing as normal TDP-43 is progressively cleared from the nucleus, unable to be replenished (Fig 6.8 A-C). Normally, a natural early consequence accompanying this depletion of nuclear

TDP-43 would be the misprocessing and loss of normal full-length stathmin-2 mRNA, however, by merging parts of the RNAs encoding each protein (TDP-43 and stathmin-2) into a single chimeric transcript (Fig 6.8 D) it should be possible to create a novel stathmin-2 encoding pre-mRNA whose correct maturation and expression is, conversely, activated by the loss of normal nuclear TDP-43. Such a chimeric encoded pre-mRNA payload should attain an opposite TDP-43 regulatory relationship versus endogenous stathmin-2, with maturation suppressed by normal TDP-43 levels and high mRNA expression only possible in the pathologic absence of nuclear TDP-43. (Fig 6.8 E-G). This AAV payload design will enable broad delivery in the central nervous system, to both sick and normal neurons of the brain and spinal cord, without risking over-expression of stathmin-2 in healthy neurons that are not yet affected by TDP-43 dysfunction.

Figure 6.8 Fusion of stathmin-2 gene coding sequence to the autoregulated 3' untranslated region of the TDP-43 mRNA produces a stathmin-2 AAV payload activated by loss of TDP-43.
(A) Schematic depicting a neuron with normal nuclear TDP-43 protein binding the 3'UTR of its own pre-mRNA to prevent maturation and silence expression. (B) Schematic depicting a neuron with partial depletion of nuclear TDP-43 protein, resulting in decreased binding to the 3'UTR of its own pre-mRNA, reducing autoregulation and allowing maturation of additional TDP-43-encoing mRNAs. (C) Schematic depicting a neuron with nuclear clearance of TDP-43 protein, resulting in disinhibited TDP-43 pre-mRNA maturation. (D) Schematic of "StathminSafe" AAV payload consisting of a ubiquitously expressed RNA encoding the fluorescent transduction reporter protein mScarlet and a T2A co-translationally cleaved human stathmin-2 coding sequence, fused to the 3'UTR sequence from the TDP-43 mRNA. (E) Schematic depicting a transduced healthy neuron with normal nuclear TDP-43 protein and silenced AAV payload expression via TDP-43 binding and altered pre-mRNA maturation. (F) Schematic depicting an AAV-transduced motor neuron under stress, with reduced nuclear TDP-43 levels partly disinhibiting AAV payload RNA maturation and allowing partial expression of supplemental stathmin-2 protein. (G) Schematic depicting a sick AAV-transduced motor neuron with nuclear clearance of TDP-43, disinhibiting normal payload mRNA maturation and expression of supplemental stathmin-2 protein.

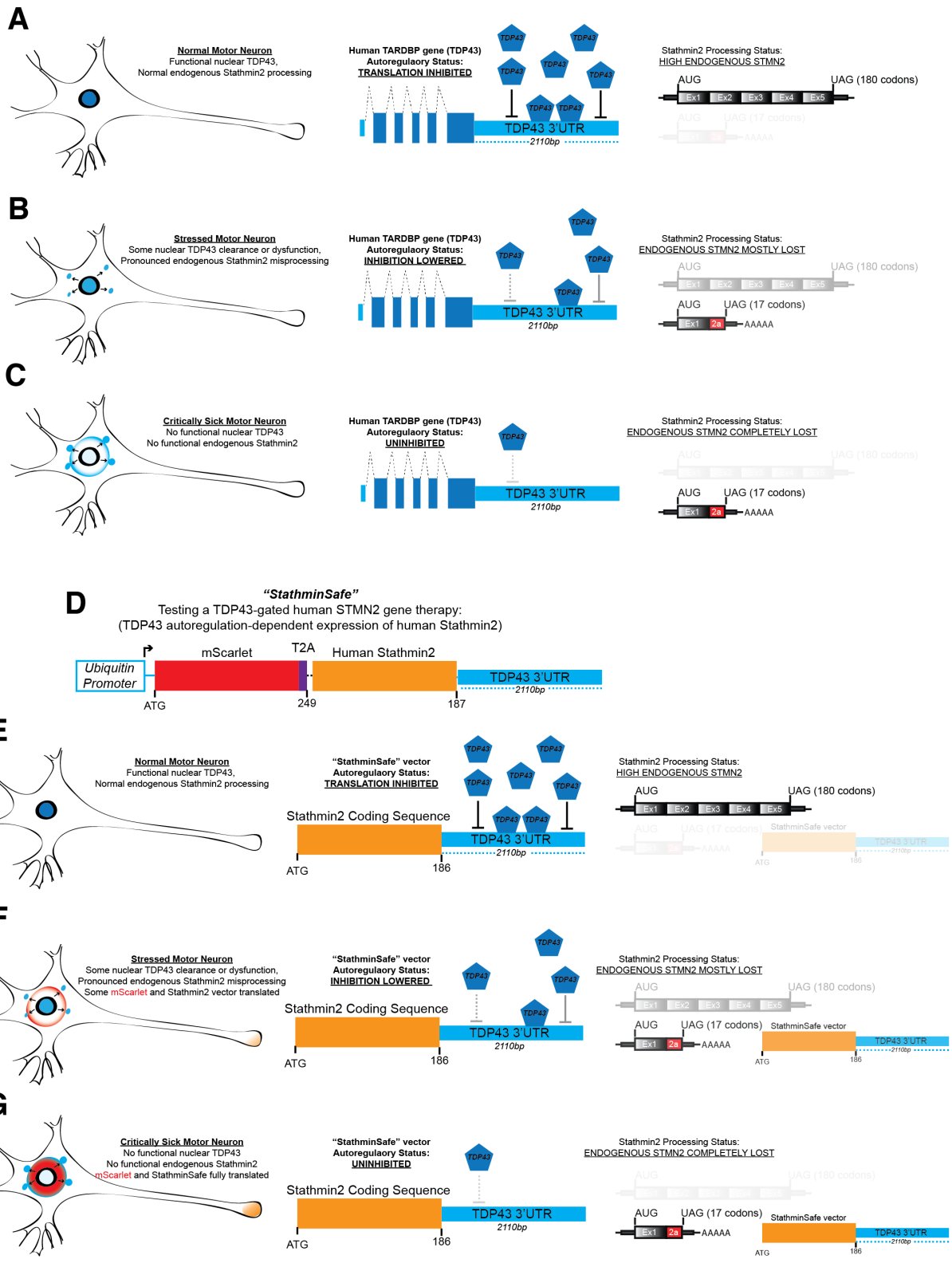
A
Normal Motor Neuron
Functional nuclear TDP43,
Normal endogenous Stathmin2 processing
Human TARDBP gene (TDP43)
Autoregulaory Status:
TRANSLATION INHIBITED
TDP43 3'UTR
2110bp
Stathmin2 Processing Status:
HIGH ENDOGENOUS STMN2
AUG
UAG (180 codons)
Ex1 Ex2 Ex3 Ex4 Ex5
UAG (17 codons)
2a
AAAAA
B
Stressed Motor Neuron
Some nuclear TDP43 clearance or dysfunction,
Pronounced endogenous Stathmin2 misprocessing
Human TARDBP gene (TDP43)
Autoregulaory Status:
INHIBITION LOWERED
Stathmin2 Processing Status:
ENDOGENOUS STMN2 MOSTLY LOST
C
Critically Sick Motor Neuron
No functional nuclear TDP43
No functional endogenous Stathmin2
Human TARDBP gene (TDP43)
Autoregulaory Status:
UNINHIBITED
Stathmin2 Processing Status:
ENDOGENOUS STMN2 COMPLETELY LOST
D
"StathminSafe"
Testing a TDP43-gated human STMN2 gene therapy:
(TDP43 autoregulation-dependent expression of human Stathmin2)
Ubiquitin Promoter
mScarlet
T2A
Human Stathmin2
TDP43 3'UTR
2110bp
ATG
249
187
E
Normal Motor Neuron
Functional nuclear TDP43,
Normal endogenous Stathmin2 processing
"StathminSafe" vector
Autoregulaory Status:
TRANSLATION INHIBITED
Stathmin2 Coding Sequence
TDP43 3'UTR
2110bp
ATG
186
Stathmin2 Processing Status:
HIGH ENDOGENOUS STMN2
AUG
UAG (180 codons)
Ex1 Ex2 Ex3 Ex4 Ex5
UAG (17 codons)
2a
AAAAA
StathminSafe vector
F
Stressed Motor Neuron
Some nuclear TDP43 clearance or dysfunction,
Pronounced endogenous Stathmin2 misprocessing
Some mScarlet and Stathmin2 vector translated
"StathminSafe" vector
Autoregulaory Status:
INHIBITION LOWERED
Stathmin2 Coding Sequence
TDP43 3'UTR
2110bp
ATG
186
Stathmin2 Processing Status:
ENDOGENOUS STMN2 MOSTLY LOST
AUG
UAG (180 codons)
Ex1 Ex2 Ex3 Ex4 Ex5
UAG (17 codons)
2a
AAAAA
StathminSafe vector
G
Critically Sick Motor Neuron
No functional nuclear TDP43
No functional endogenous Stathmin2
mScarlet and StathminSafe fully translated
"StathminSafe" vector
Autoregulaory Status:
UNINHIBITED
Stathmin2 Coding Sequence
TDP43 3'UTR
2110bp
ATG
186
Stathmin2 Processing Status:
ENDOGENOUS STMN2 COMPLETELY LOST
AUG
UAG (17 codons)
Ex1 2a
AAAAA
StathminSafe vector

I have demonstrated in a preliminary proof-of-concept experiment, expressing the chimeric vector design (Fig 6.8 D, “StathminSafe”) in neuron-like SH-SY5Y cells, that this predicted inverted-expression relationship between the chimeric mRNA and endogenous TDP-43 is observable after acute depletion of normal TDP-43. Electroporation was used to introduce the AAV transfer plasmid into SH-SY5Y cells, which were then immediately plated into reverse-transfection media containing 50nM pooled control or TDP-43 siRNAs encapsulated in RNAiMax transfection reagent. After 24 hours cells were once again forward-transfected with the same siRNA reagents, and cells were collected in Trizol reagent for RNA extraction at 96 hours (Fig 6.9 A). qRT-PCR with primers specific to the chimeric RNA, endogenous TDP-43 and GAPDH as an endogenous control gene were utilized to determine that substantial depletion of TDP-43 occurred in the siRNA dosed cells (~20% of control expression) (Fig 6.9 B), which was accompanied by a substantial increase in “stathmin-safe” encoded transcripts (Fig 6.9 C). Two limitations of this experiment were the selection of a relatively weak promoter to drive expression of the “stathmin-safe” chimeric RNA, and the lack of an antibiotic selection strategy to enrich the otherwise low efficiency of electroporation in this cell-type (~30%). However, this experiment is sufficient to demonstrate the desired regulatory pre-mRNA maturation relationship between the chimeric stathmin-2:TDP-43 fusion construct and endogenous TDP-43 levels.

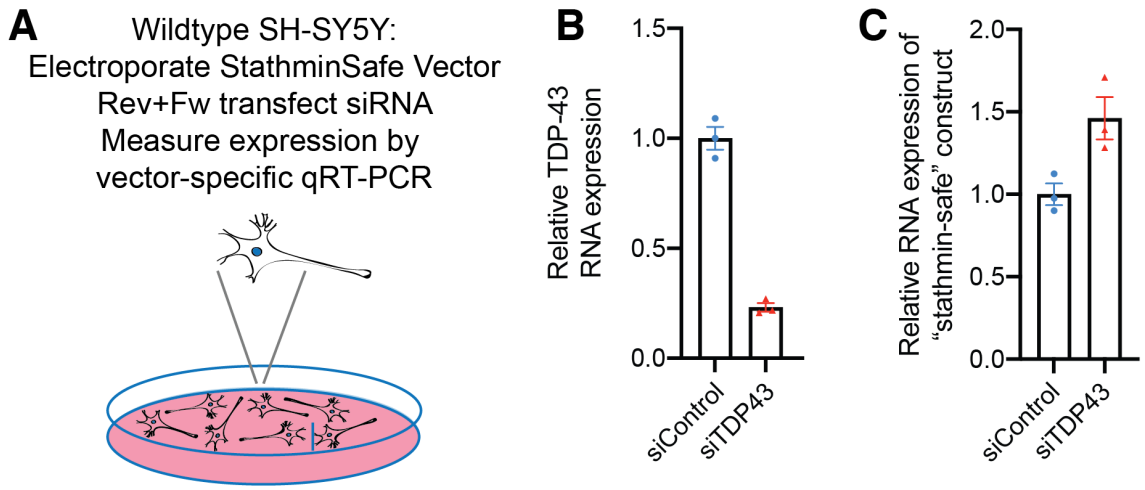

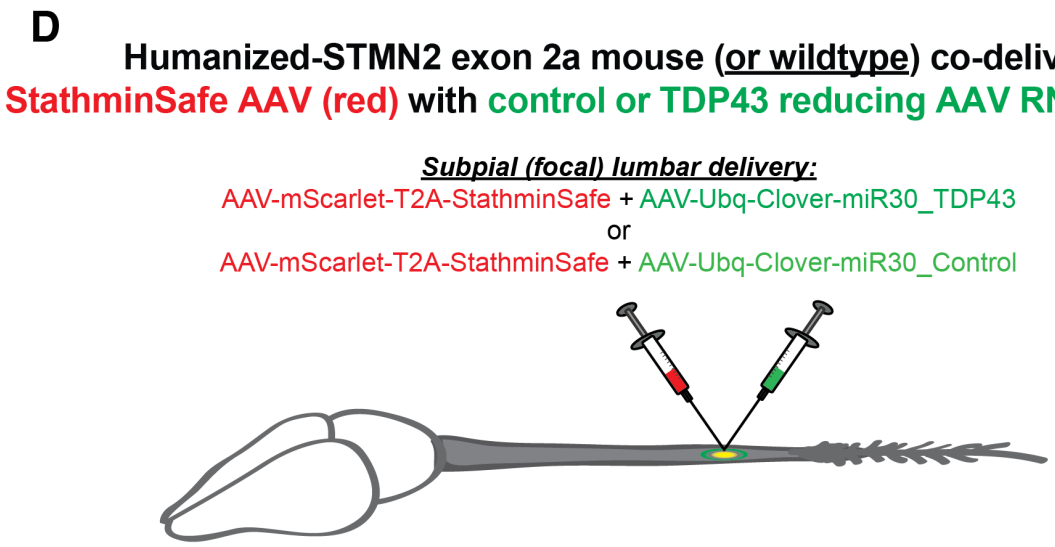

Figure 6.9 StathminSafe AAV payload expression is enhanced after TDP-43 depletion in neuron-like cells

(A) Schematic describing StathminSafe vector expression and siRNA gene depletion in neuron-like cells, followed by isoform-specific expression analysis with qRT-PCR. (B) Graph showing TDP-43 expression relative to the endogenous control gene GAPDH after siRNA treatment. n=3 biological replicates, SEM plotted. (C) Graph showing StathminSafe payload expression relative to the endogenous control gene GAPDH after siRNA treatment. n=3 biological replicates, SEM plotted. (D) Schematic of in-vivo StathminSafe AAV payload expression trial via sub-pial co-delivery of StathminSafe vector alongside either a control Clover-RNAi AAV or TDP-43 depleting Clover-RNAi AAV.

The next experimental step is to determine whether this chimeric Stathmin-Safe construct maintains the same TDP-43-loss-dependent pre-mRNA maturation and expression pattern in-vivo within an adult mammalian spinal cord. The ideal mouse model in which to test this gene therapy approach has been humanized by insertion of human stathmin-2 exon 2a into the corresponding region of the mouse stathmin-2 first intron (Fig 5.6 A, Fig 6.5 D), however a wildtype mouse would also be suitable for an initial in-vivo test of the basic molecular mechanism. After modifying the original construct with a stronger promoter and packaging the improved payload into an AAV9 capsid, I will co-deliver the virus by surgical subpial administration with either an AAV encoding a Clover-only control and non-targeting RNAi element, or an AAV encoding a Clover fluorescent marker and RNAi element uniquely targeting endogenous murine TDP-43 (critically, without targeting the human TDP-43 3'UTR sequence utilized in the chimeric Stathmin-Safe construct); contemporaneously injecting control cohorts of humanized stathmin-2 exon 2a mice with only AAV-Clover-non-target RNAi or AAV-Clover-RNAi-TDP43 virus, for contemporaneous comparative phenotyping of effects on progressive TDP-43 dependent loss of humanized stathmin-2 expression (Fig 6.9 D).

Mice will be followed for 8 months of phenotyping to compare scores of hindlimb clasping, accelerating-rotarod performance, grip strength, and axonal conduction velocity measured by compound Muscle Action Potential (cMAP) amplitude[241,242]. Spinal cords will be collected 8 months post-AAV administration for direct fluorescent imaging, protein expression analysis, and isoform-specific qRT-PCR of endogenous TDP-43, Stathmin-Safe, Clover, and GAPDH. Muscle will be collected for neuromuscular junction analysis and quantification, and motor roots will be prepared for electron microscopy analysis of axonal diameter and number. Neurons transduced by subpial AAV administration will all be marked by green fluorescence, while red fluorescence (Stathmin-Safe RNA-encoded mScarlet) should mark only the cells with correctly maturing chimeric mRNAs.

If expression of the Stathmin-Safe chimeric AAV payload is, as expected, gated by the loss of normal nuclear TDP-43 expression, I expect to visualize both red and green fluorescence co-expression in the spinal neurons of StathminSafe/RNAi-TDP-43 injected animals, and only green fluorescence in StathminSafe/non-target RNAi animals (with qRT-PCR expression analysis following suit). Alternatively, a failure of autoregulation would be indicated at the cellular level by neurons marked with red fluorescence in the absence of green. Most critically, though, will be the experimental determination of whether 1) administration of the StathminSafe AAV without modulation of TDP-43 prevents stathmin-2 overexpression and possible related toxicity in control animals, and 2) whether StathminSafe AAV administration is sufficient to rescue neuromuscular junction integrity and associated motor phenotypes initiated by TDP-43-dependent misprocessing of the humanized stathmin-2 allele. The eagerly anticipated answers to these questions will be critical to the further clinical development of a safe, effective, and permanent gene therapy strategy to restore stathmin-2 expression in diseases with TDP-43 proteinopathy.

References

1 Charcot, J. M. Sclérose latérale amyotrophique. *Oeuvres Complétes* **2**, 249-266 (1897).

2 Ravits, J. M. & La Spada, A. R. ALS motor phenotype heterogeneity, focality, and spread: Deconstructing motor neuron degeneration. *Neurology* **73**, 805-811, doi:10.1212/wnl.0b013e3181b6bbbd (2009).

3 Mehta, P., Kaye, W., Raymond, J., Wu, R., Larson, T., Punjani, R., Heller, D., Cohen, J., Peters, T., Muravov, O. & Horton, K. Prevalence of Amyotrophic Lateral Sclerosis — United States, 2014. *MMWR Morb Mortal Wkly* **67**, 216-218 (2018).

4 Brooks, B. R. El Escorial World Federation of Neurology criteria for the diagnosis of amyotrophic lateral sclerosis. Subcommittee on Motor Neuron Diseases/Amyotrophic Lateral Sclerosis of the World Federation of Neurology Research Group on Neuromuscular Diseases and the El Escorial "Clinical limits of amyotrophic lateral sclerosis" workshop contributors. *J Neurol Sci* **124 Suppl**, 96-107, doi:10.1016/0022-510x(94)90191-0 (1994).

5 Masland, R. L. & Wigton, R. S. NERVE ACTIVITY ACCOMPANYING FASCICULATION PRODUCED BY PROSTIGMIN. *Journal of Neurophysiology* **3**, 269-275, doi:10.1152/jn.1940.3.3.269 (1940).

6 Leite, M. A. A., Orsini, M., De Freitas, M. R. G., Pereira, J. S., Gobbi, F. H. P., Bastos, V. H., De Castro Machado, D., Machado, S., Arrias-Carrion, O., De Souza, J. A. & Oliveira, A. B. Another perspective on fasciculations: when is it not caused by the classic form of amyotrophic lateral sclerosis or progressive spinal atrophy? *Neurology International* **6**, doi:10.4081/ni.2014.5208 (2014).

7 Gowers, W. *Manual of Diseases of the Nervous System*. (Churchill, 1886).

8 Isaacs, J. D., Dean, A. F., Shaw, C. E., Al-Chalabi, A., Mills, K. R. & Leigh, P. N. Amyotrophic lateral sclerosis with sensory neuropathy: part of a multisystem disorder? *Journal of Neurology, Neurosurgery & Psychiatry* **78**, 750-753, doi:10.1136/jnnp.2006.098798 (2006).

9 Pugdahl, K., Fuglsang-Frederiksen, A., De Carvalho, M., Johnsen, B., Fawcett, P. R. W., Labarre-Vila, A., Liguori, R., Nix, W. A. & Schofield, I. S. Generalised sensory system

abnormalities in amyotrophic lateral sclerosis: a European multicentre study. *Journal of Neurology, Neurosurgery & Psychiatry* **78**, 746-749, doi:10.1136/jnnp.2006.098533 (2006).

10 Hammad, M., Silva, A., Glass, J., Sladky, J. T. & Benatar, M. Clinical, electrophysiologic, and pathologic evidence for sensory abnormalities in ALS. *Neurology* **69**, 2236-2242, doi:10.1212/01.wnl.0000286948.99150.16 (2007).

11 Chiò, A., Mora, G. & Lauria, G. Pain in amyotrophic lateral sclerosis. *The Lancet Neurology* **16**, 144-157, doi:10.1016/s1474-4422(16)30358-1 (2017).

12 Goy, E. R., Carter, J. & Ganzini, L. Neurologic disease at the end of life: caregiver descriptions of Parkinson disease and amyotrophic lateral sclerosis. *J Palliat Med* **11**, 548-554, doi:10.1089/jpm.2007.0258 (2008).

13 Kawata, A., Kato, S., Hayashi, H. & Hirai, S. Prominent sensory and autonomic disturbances in familial amyotrophic lateral sclerosis with a Gly93Ser mutation in the SOD1 gene. *Journal of the Neurological Sciences* **153**, 82-85, doi:10.1016/s0022-510x(97)00176-7 (1997).

14 Shimizu, T., Kawata, A., Kato, S., Hayashi, M., Takamoto, K., Hayashi, H., Hirai, S., Yamaguchi, S., Komori, T. & Oda, M. Autonomic failure in ALS with a novel SOD1 gene mutation. *Neurology* **54**, 1534-1537, doi:10.1212/wnl.54.7.1534 (2000).

15 Cleveland, D. W. & Rothstein, J. D. From Charcot to Lou Gehrig: deciphering selective motor neuron death in ALS. *Nat Rev Neurosci* **2**, 806-819, doi:10.1038/35097565 35097565 [pii] (2001).

16 Pasinelli, P. & Brown, R. H. Molecular biology of amyotrophic lateral sclerosis: insights from genetics. *Nat Rev Neurosci* **7**, 710-723 (2006).

17 Doman, J. L., Raguram, A., Newby, G. A. & Liu, D. R. Evaluation and minimization of Cas9-independent off-target DNA editing by cytosine base editors. *Nat Biotechnol* **38**, 620-628, doi:10.1038/s41587-020-0414-6 (2020).

18 Rosen, D. R. Mutations in Cu/Zn superoxide dismutase gene are associated with familial amyotrophic lateral sclerosis. *Nature* **364**, 362, doi:10.1038/364362c0 (1993).

19 Deng, H. X., Hentati, A., Tainer, J. A., Iqbal, Z., Cayabyab, A., Hung, W. Y., Getzoff, E. D., Hu, P., Herzfeldt, B., Roos, R. P. & Siddique, T. Amyotrophic lateral sclerosis and structural defects in Cu,Zn superoxide dismutase. *Science* **261**, 1047-1051 (1993).

20 Taylor, J. P., Brown, R. H., Jr. & Cleveland, D. W. Decoding ALS: from genes to mechanism. *Nature* **539**, 197-206, doi:10.1038/nature20413 (2016).

21 Cleveland, D. W. From Charcot to SOD1: mechanisms of selective motor neuron death in ALS. *Neuron* **24**, 515-520, doi:S0896-6273(00)81108-3 [pii] (1999).

22 Gurney, M. E., Pu, H., Chiu, A. Y., Dal Canto, M. C., Polchow, C. Y., Alexander, D. D., Caliendo, J., Hentati, A., Kwon, Y. W. & Deng, H. X. Motor neuron degeneration in mice that express a human Cu,Zn superoxide dismutase mutation. *Science* **264**, 1772-1775 (1994).

23 Wong, P. C., Pardo, C. A., Borchelt, D. R., Lee, M. K., Copeland, N. G., Jenkins, N. A., Sisodia, S. S., Cleveland, D. W. & Price, D. L. An adverse property of a familial ALS-linked SOD1 mutation causes motor neuron disease characterized by vacuolar degeneration of mitochondria. *Neuron* **14**, 1105-1116, doi:0896-6273(95)90259-7 [pii] (1995).

24 Ripps, M. E., Huntley, G. W., Hof, P. R., Morrison, J. H. & Gordon, J. W. Transgenic mice expressing an altered murine superoxide dismutase gene provide an animal model of amyotrophic lateral sclerosis. *Proc Natl Acad Sci U S A* **92**, 689-693 (1995).

25 Bruijn, L. I., Becher, M. W., Lee, M. K., Anderson, K. L., Jenkins, N. A., Copeland, N. G., Sisodia, S. S., Rothstein, J. D., Borchelt, D. R., Price, D. L. & Cleveland, D. W. ALS-linked SOD1 mutant G85R mediates damage to astrocytes and promotes rapidly progressive disease with SOD1-containing inclusions. *Neuron* **18**, 327-338, doi:S0896-6273(00)80272-X [pii] (1997).

26 Cleveland, D. W., Laing, N., Hurse, P. V. & Brown, R. H. Toxic mutants in Charcot's sclerosis. *Nature* **378**, 342-343, doi:10.1038/378342a0 (1995).

27 Reaume, A. G., Elliott, J. L., Hoffman, E. K., Kowall, N. W., Ferrante, R. J., Siwek, D. F., Wilcox, H. M., Flood, D. G., Beal, M. F., Brown, R. H., Jr., Scott, R. W. & Snider, W. D. Motor neurons in Cu/Zn superoxide dismutase-deficient mice develop normally but exhibit enhanced cell death after axonal injury. *Nat Genet* **13**, 43-47, doi:10.1038/ng0596-43 (1996).

28 Bruijn, L. I., Houseweart, M. K., Kato, S., Anderson, K. L., Anderson, S. D., Ohama, E., Reaume, A. G., Scott, R. W. & Cleveland, D. W. Aggregation and motor neuron toxicity of

an ALS-linked SOD1 mutant independent from wild-type SOD1. *Science* **281**, 1851-1854 (1998).

29 Flood, D. G., Reaume, A. G., Gruner, J. A., Hoffman, E. K., Hirsch, J. D., Lin, Y. G., Dorfman, K. S. & Scott, R. W. Hindlimb motor neurons require Cu/Zn superoxide dismutase for maintenance of neuromuscular junctions. *Am J Pathol* **155**, 663-672, doi:10.1016/S0002-9440(10)65162-0 (1999).

30 Hamilton, R. T., Bhattacharya, A., Walsh, M. E., Shi, Y., Wei, R., Zhang, Y., Rodriguez, K. A., Buffenstein, R., Chaudhuri, A. R. & Van Remmen, H. Elevated protein carbonylation, and misfolding in sciatic nerve from db/db and Sod1(-/-) mice: plausible link between oxidative stress and demyelination. *PLoS One* **8**, e65725, doi:10.1371/journal.pone.0065725 (2013).

31 Fischer, L. R., Li, Y., Asress, S. A., Jones, D. P. & Glass, J. D. Absence of SOD1 leads to oxidative stress in peripheral nerve and causes a progressive distal motor axonopathy. *Exp Neurol* **233**, 163-171, doi:10.1016/j.expneurol.2011.09.020 (2012).

32 Hayes, L. R., Asress, S. A., Li, Y., Galkin, A., Stepanova, A., Kawamata, H., Manfredi, G. & Glass, J. D. Distal denervation in the SOD1 knockout mouse correlates with loss of mitochondria at the motor nerve terminal. *Exp Neurol* **318**, 251-257, doi:10.1016/j.expneurol.2019.05.008 (2019).

33 Muller, F. L., Song, W., Liu, Y., Chaudhuri, A., Pieke-Dahl, S., Strong, R., Huang, T. T., Epstein, C. J., Roberts, L. J., 2nd, Csete, M., Faulkner, J. A. & Van Remmen, H. Absence of CuZn superoxide dismutase leads to elevated oxidative stress and acceleration of age-dependent skeletal muscle atrophy. *Free Radic Biol Med* **40**, 1993-2004, doi:10.1016/j.freeradbiomed.2006.01.036 (2006).

34 Andersen, P. M., Nordstrom, U., Tsiakas, K., Johannsen, J., Volk, A. E., Bierhals, T., Zetterstrom, P., Marklund, S. L., Hempel, M. & Santer, R. Phenotype in an Infant with SOD1 Homozygous Truncating Mutation. *N Engl J Med* **381**, 486-488, doi:10.1056/NEJMc1905039 (2019).

35 Park, J. H., Elpers, C., Reunert, J., McCormick, M. L., Mohr, J., Biskup, S., Schwartz, O., Rust, S., Gruneberg, M., Seelhofer, A., Schara, U., Boltshauser, E., Spitz, D. R. & Marquardt, T. SOD1 deficiency: a novel syndrome distinct from amyotrophic lateral sclerosis. *Brain* **142**, 2230-2237, doi:10.1093/brain/awz182 (2019).

36 Lagier-Tourenne, C. & Cleveland, D. W. Rethinking ALS: the FUS about TDP-43. *Cell* **136**, 1001-1004, doi:S0092-8674(09)00263-3 [pii] 10.1016/j.cell.2009.03.006 (2009).

37 DeJesus-Hernandez, M., Mackenzie, I. R., Boeve, B. F., Boxer, A. L., Baker, M., Rutherford, N. J., Nicholson, A. M., Finch, N. A., Flynn, H., Adamson, J., Kouri, N., Wojtas, A., Sengdy, P., Hsiung, G. Y., Karydas, A., Seeley, W. W., Josephs, K. A., Coppola, G., Geschwind, D. H., Wszolek, Z. K., Feldman, H., Knopman, D. S., Petersen, R. C., Miller, B. L., Dickson, D. W., Boylan, K. B., Graff-Radford, N. R. & Rademakers, R. Expanded GGGGCC hexanucleotide repeat in noncoding region of C9ORF72 causes chromosome 9p-linked FTD and ALS. *Neuron* **72**, 245-256, doi:10.1016/j.neuron.2011.09.011 (2011).

38 Renton, A. E., Majounie, E., Waite, A., Simon-Sanchez, J., Rollinson, S., Gibbs, J. R., Schymick, J. C., Laaksovirta, H., van Swieten, J. C., Myllykangas, L., Kalimo, H., Paetau, A., Abramzon, Y., Remes, A. M., Kaganovich, A., Scholz, S. W., Duckworth, J., Ding, J., Harmer, D. W., Hernandez, D. G., Johnson, J. O., Mok, K., Ryten, M., Trabzuni, D., Guerreiro, R. J., Orrell, R. W., Neal, J., Murray, A., Pearson, J., Jansen, I. E., Sondervan, D., Seelaar, H., Blake, D., Young, K., Halliwell, N., Callister, J. B., Toulson, G., Richardson, A., Gerhard, A., Snowden, J., Mann, D., Neary, D., Nalls, M. A., Peuralinna, T., Jansson, L., Isoviita, V. M., Kaivorinne, A. L., Holtta-Vuori, M., Ikonen, E., Sulkava, R., Benatar, M., Wuu, J., Chio, A., Restagno, G., Borghero, G., Sabatelli, M., Consortium, I., Heckerman, D., Rogaeva, E., Zinman, L., Rothstein, J. D., Sendtner, M., Drepper, C., Eichler, E. E., Alkan, C., Abdullaev, Z., Pack, S. D., Dutra, A., Pak, E., Hardy, J., Singleton, A., Williams, N. M., Heutink, P., Pickering-Brown, S., Morris, H. R., Tienari, P. J. & Traynor, B. J. A hexanucleotide repeat expansion in C9ORF72 is the cause of chromosome 9p21-linked ALS-FTD. *Neuron* **72**, 257-268, doi:10.1016/j.neuron.2011.09.010 (2011).

39 Gijselinck, I., Van Langenhove, T., van der Zee, J., Sleegers, K., Philtjens, S., Kleinberger, G., Janssens, J., Bettens, K., Van Cauwenberghe, C., Pereson, S., Engelborghs, S., Sieben, A., De Jonghe, P., Vandenberghe, R., Santens, P., De Bleecker, J., Maes, G., Baumer, V., Dillen, L., Joris, G., Cuijt, I., Corsmit, E., Elinck, E., Van Dongen, J., Vermeulen, S., Van den Broeck, M., Vaerenberg, C., Mattheijssens, M., Peeters, K., Robberecht, W., Cras, P., Martin, J. J., De Deyn, P. P., Cruts, M. & Van Broeckhoven, C. A C9orf72 promoter repeat expansion in a Flanders-Belgian cohort with disorders of the frontotemporal lobar degeneration-amyotrophic lateral sclerosis spectrum: a gene identification study. *Lancet Neurol* **11**, 54-65, doi:10.1016/S1474-4422(11)70261-7 (2012).

40 Ling, S.-C., Polymenidou, M. & Don. Converging Mechanisms in ALS and FTD: Disrupted RNA and Protein Homeostasis. *Neuron* **79**, 416-438, doi:10.1016/j.neuron.2013.07.033 (2013).

41 Ringholz, G. M., Appel, S. H., Bradshaw, M., Cooke, N. A., Mosnik, D. M. & Schulz, P. E. Prevalence and patterns of cognitive impairment in sporadic ALS. *Neurology* **65**, 586-590 (2005).

42 La Spada, A. R. & Taylor, J. P. Repeat expansion disease: progress and puzzles in disease pathogenesis. *Nature Reviews Genetics* **11**, 247-258, doi:10.1038/nrg2748 (2010).

43 Rohrer, J. D., Isaacs, A. M., Mizielinska, S., Mead, S., Lashley, T., Wray, S., Sidle, K., Fratta, P., Orrell, R. W., Hardy, J., Holton, J., Revesz, T., Rossor, M. N. & Warren, J. D. C9orf72 expansions in frontotemporal dementia and amyotrophic lateral sclerosis. *Lancet Neurol* **14**, 291-301, doi:10.1016/S1474-4422(14)70233-9 (2015).

44 van Blitterswijk, M., DeJesus-Hernandez, M., Niemantsverdriet, E., Murray, M. E., Heckman, M. G., Diehl, N. N., Brown, P. H., Baker, M. C., Finch, N. A., Bauer, P. O., Serrano, G., Beach, T. G., Josephs, K. A., Knopman, D. S., Petersen, R. C., Boeve, B. F., Graff-Radford, N. R., Boylan, K. B., Petrucelli, L., Dickson, D. W. & Rademakers, R. Association between repeat sizes and clinical and pathological characteristics in carriers of C9ORF72 repeat expansions (Xpansize-72): a cross-sectional cohort study. *Lancet Neurol* **12**, 978-988, doi:10.1016/S1474-4422(13)70210-2 (2013).

45 Iyer, S., Subramanian, V. & Acharya, K. R. C9orf72, a protein associated with amyotrophic lateral sclerosis (ALS) is a guanine nucleotide exchange factor. *PeerJ* **6**, e5815, doi:10.7717/peerj.5815 (2018).

46 Suzuki, N., Maroof, A. M., Merkle, F. T., Koszka, K., Intoh, A., Armstrong, I., Moccia, R., Davis-Dusenbery, B. N. & Eggan, K. The mouse C9ORF72 ortholog is enriched in neurons known to degenerate in ALS and FTD. *Nature Neuroscience* **16**, 1725-1727, doi:10.1038/nn.3566 (2013).

47 Jiang, J., Zhu, Q., Gendron, T. F., Saberi, S., McAlonis-Downes, M., Seelman, A., Stauffer, J. E., Jafar-Nejad, P., Drenner, K., Schulte, D., Chun, S., Sun, S., Ling, S. C., Myers, B., Engelhardt, J., Katz, M., Baughn, M., Platoshyn, O., Marsala, M., Watt, A., Heyser, C. J., Ard, M. C., De Muynck, L., Daughrity, L. M., Swing, D. A., Tessarollo, L., Jung, C. J., Delpoux, A., Utzschneider, D. T., Hedrick, S. M., de Jong, P. J., Edbauer, D., Van Damme, P., Petrucelli, L., Shaw, C. E., Bennett, C. F., Da Cruz, S., Ravits, J., Rigo, F., Cleveland, D. W. & Lagier-Tourenne, C. Gain of Toxicity from ALS/FTD-Linked Repeat Expansions in C9ORF72 Is Alleviated by Antisense Oligonucleotides Targeting GGGGCC-Containing RNAs. *Neuron* **90**, 535-550, doi:10.1016/j.neuron.2016.04.006 (2016).

48 Lagier-Tourenne, C., Baughn, M., Rigo, F., Sun, S., Liu, P., Li, H. R., Jiang, J., Watt, A. T., Chun, S., Katz, M., Qiu, J., Sun, Y., Ling, S. C., Zhu, Q., Polymenidou, M., Drenner, K., Artates, J. W., McAlonis-Downes, M., Markmiller, S., Hutt, K. R., Pizzo, D. P., Cady, J., Harms, M. B., Baloh, R. H., Vandenberg, S. R., Yeo, G. W., Fu, X. D., Bennett, C. F., Cleveland, D. W. & Ravits, J. Targeted degradation of sense and antisense C9orf72 RNA foci as therapy for ALS and frontotemporal degeneration. *Proc Natl Acad Sci U S A* **110**, E4530-4539, doi:10.1073/pnas.1318835110 (2013).

49 Zu, T., Liu, Y., Banez-Coronel, M., Reid, T., Pletnikova, O., Lewis, J., Miller, T. M., Harms, M. B., Falchook, A. E., Subramony, S. H., Ostrow, L. W., Rothstein, J. D., Troncoso, J. C. & Ranum, L. P. RAN proteins and RNA foci from antisense transcripts in C9ORF72 ALS and frontotemporal dementia. *Proc Natl Acad Sci U S A* **110**, E4968-4977, doi:10.1073/pnas.1315438110 (2013).

50 Sellier, C., Cerro-Herreros, E., Blatter, M., Freyermuth, F., Gaucherot, A., Ruffenach, F., Sarkar, P., Puymirat, J., Udd, B., Day, J. W., Meola, G., Bassez, G., Fujimura, H., Takahashi, M. P., Schoser, B., Furling, D., Artero, R., Allain, F. H. T., Llamusi, B. & Charlet-Berguerand, N. rbFOX1/MBNL1 competition for CCUG RNA repeats binding contributes to myotonic dystrophy type 1/type 2 differences. *Nature Communications* **9**, doi:10.1038/s41467-018-04370-x (2018).

51 Conlon, E. G., Lu, L., Sharma, A., Yamazaki, T., Tang, T., Shneider, N. A. & Manley, J. L. The C9ORF72 GGGGCC expansion forms RNA G-quadruplex inclusions and sequesters hnRNP H to disrupt splicing in ALS brains. *Elife* **5**, doi:10.7554/eLife.17820 (2016).

52 Donnelly, C. J., Zhang, P. W., Pham, J. T., Haeusler, A. R., Mistry, N. A., Vidensky, S., Daley, E. L., Poth, E. M., Hoover, B., Fines, D. M., Maragakis, N., Tienari, P. J., Petrucelli, L., Traynor, B. J., Wang, J., Rigo, F., Bennett, C. F., Blackshaw, S., Sattler, R. & Rothstein, J. D. RNA toxicity from the ALS/FTD C9ORF72 expansion is mitigated by antisense intervention. *Neuron* **80**, 415-428, doi:10.1016/j.neuron.2013.10.015 (2013).

53 Mori, K., Lammich, S., Mackenzie, I. R., Forne, I., Zilow, S., Kretzschmar, H., Edbauer, D., Janssens, J., Kleinberger, G., Cruts, M., Herms, J., Neumann, M., Van Broeckhoven, C., Arzberger, T. & Haass, C. hnRNP A3 binds to GGGGCC repeats and is a constituent of p62-positive/TDP43-negative inclusions in the hippocampus of patients with C9orf72 mutations. *Acta Neuropathol* **125**, 413-423, doi:10.1007/s00401-013-1088-7 (2013).

54 Sareen, D., O'Rourke, J. G., Meera, P., Muhammad, A. K., Grant, S., Simpkinson, M., Bell, S., Carmona, S., Ornelas, L., Sahabian, A., Gendron, T., Petrucelli, L., Baughn, M., Ravits, J., Harms, M. B., Rigo, F., Bennett, C. F., Otis, T. S., Svendsen, C. N. & Baloh, R. H. Targeting RNA foci in iPSC-derived motor neurons from ALS patients with a C9ORF72 repeat expansion. *Science translational medicine* **5**, 208ra149, doi:10.1126/scitranslmed.3007529 (2013).

55 Xu, Z., Poidevin, M., Li, X., Li, Y., Shu, L., Nelson, D. L., Li, H., Hales, C. M., Gearing, M., Wingo, T. S. & Jin, P. Expanded GGGGCC repeat RNA associated with amyotrophic lateral sclerosis and frontotemporal dementia causes neurodegeneration. *Proc Natl Acad Sci U S A* **110**, 7778-7783, doi:10.1073/pnas.1219643110 (2013).

56 Haeusler, A. R., Donnelly, C. J., Periz, G., Simko, E. A., Shaw, P. G., Kim, M. S., Maragakis, N. J., Troncoso, J. C., Pandey, A., Sattler, R., Rothstein, J. D. & Wang, J.

C9orf72 nucleotide repeat structures initiate molecular cascades of disease. *Nature* **507**, 195-200, doi:10.1038/nature13124 (2014).

57 Zu, T., Gibbens, B., Doty, N. S., Gomes-Pereira, M., Huguet, A., Stone, M. D., Margolis, J., Peterson, M., Markowski, T. W., Ingram, M. A., Nan, Z., Forster, C., Low, W. C., Schoser, B., Somia, N. V., Clark, H. B., Schmechel, S., Bitterman, P. B., Gourdon, G., Swanson, M. S., Moseley, M. & Ranum, L. P. Non-ATG-initiated translation directed by microsatellite expansions. *Proc Natl Acad Sci U S A* **108**, 260-265, doi:10.1073/pnas.1013343108 (2011).

58 Ash, P. E., Bieniek, K. F., Gendron, T. F., Caulfield, T., Lin, W. L., Dejesus-Hernandez, M., van Blitterswijk, M. M., Jansen-West, K., Paul, J. W., 3rd, Rademakers, R., Boylan, K. B., Dickson, D. W. & Petrucelli, L. Unconventional translation of C9ORF72 GGGGCC expansion generates insoluble polypeptides specific to c9FTD/ALS. *Neuron* **77**, 639-646, doi:10.1016/j.neuron.2013.02.004 (2013).

59 Mori, K., Weng, S. M., Arzberger, T., May, S., Rentzsch, K., Kremmer, E., Schmid, B., Kretzschmar, H. A., Cruts, M., Van Broeckhoven, C., Haass, C. & Edbauer, D. The C9orf72 GGGGCC repeat is translated into aggregating dipeptide-repeat proteins in FTLD/ALS. *Science* **339**, 1335-1338, doi:10.1126/science.1232927 (2013).

60 Kwon, I., Xiang, S., Kato, M., Wu, L., Theodoropoulos, P., Wang, T., Kim, J., Yun, J., Xie, Y. & McKnight, S. L. Poly-dipeptides encoded by the C9orf72 repeats bind nucleoli, impede RNA biogenesis, and kill cells. *Science* **345**, 1139-1145, doi:10.1126/science.1254917 (2014).

61 Lee, K. H., Zhang, P., Kim, H. J., Mitrea, D. M., Sarkar, M., Freibaum, B. D., Cika, J., Coughlin, M., Messing, J., Molliex, A., Maxwell, B. A., Kim, N. C., Temirov, J., Moore, J., Kolaitis, R. M., Shaw, T. I., Bai, B., Peng, J., Kriwacki, R. W. & Taylor, J. P. C9orf72 Dipeptide Repeats Impair the Assembly, Dynamics, and Function of Membrane-Less Organelles. *Cell* **167**, 774-788 e717, doi:10.1016/j.cell.2016.10.002 (2016).

62 May, S., Hornburg, D., Schludi, M. H., Arzberger, T., Rentzsch, K., Schwenk, B. M., Grasser, F. A., Mori, K., Kremmer, E., Banzhaf-Strathmann, J., Mann, M., Meissner, F. & Edbauer, D. C9orf72 FTLD/ALS-associated Gly-Ala dipeptide repeat proteins cause neuronal toxicity and Unc119 sequestration. *Acta Neuropathol* **128**, 485-503, doi:10.1007/s00401-014-1329-4 (2014).

63 Saberi, S., Stauffer, J. E., Jiang, J., Garcia, S. D., Taylor, A. E., Schulte, D., Ohkubo, T., Schloffman, C. L., Maldonado, M., Baughn, M., Rodriguez, M. J., Pizzo, D., Cleveland, D. & Ravits, J. Sense-encoded poly-GR dipeptide repeat proteins correlate to neurodegeneration and uniquely co-localize with TDP-43 in dendrites of repeat-expanded

C9orf72 amyotrophic lateral sclerosis. *Acta Neuropathol* **135**, 459-474, doi:10.1007/s00401-017-1793-8 (2018).

64 Chew, J., Gendron, T. F., Prudencio, M., Sasaguri, H., Zhang, Y. J., Castanedes-Casey, M., Lee, C. W., Jansen-West, K., Kurti, A., Murray, M. E., Bieniek, K. F., Bauer, P. O., Whitelaw, E. C., Rousseau, L., Stankowski, J. N., Stetler, C., Daughrity, L. M., Perkerson, E. A., Desaro, P., Johnston, A., Overstreet, K., Edbauer, D., Rademakers, R., Boylan, K. B., Dickson, D. W., Fryer, J. D. & Petrucelli, L. C9ORF72 repeat expansions in mice cause TDP-43 pathology, neuronal loss, and behavioral deficits. *Science* **348**, 1151-1154, doi:10.1126/science.aaa9344 (2015).

65 Okamoto, K., Hirai, S., Yamazaki, T., Sun, X. & Nakazato, Y. New ubiquitin-positive intraneuronal inclusions in the extra-motor cortices in patients with amyotrophic lateral sclerosis. *Neuroscience letters* **129**, 233-236, doi:10.1016/0304-3940(91)90469-a (1991).

66 Wightman, G., Anderson, V. E., Martin, J., Swash, M., Anderton, B. H., Neary, D., Mann, D., Luthert, P. & Leigh, P. N. Hippocampal and neocortical ubiquitin-immunoreactive inclusions in amyotrophic lateral sclerosis with dementia. *Neurosci Lett* **139**, 269-274 (1992).

67 Okamoto, K., Murakami, N., Kusaka, H., Yoshida, M., Hashizume, Y., Nakazato, Y., Matsubara, E. & Hirai, S. Ubiquitin-positive intraneuronal inclusions in the extramotor cortices of presenile dementia patients with motor neuron disease. *Journal of Neurology* **239**, 426-430, doi:10.1007/bf00856806 (1992).

68 Arai, T., Hasegawa, M., Akiyama, H., Ikeda, K., Nonaka, T., Mori, H., Mann, D., Tsuchiya, K., Yoshida, M., Hashizume, Y. & Oda, T. TDP-43 is a component of ubiquitin-positive tau-negative inclusions in frontotemporal lobar degeneration and amyotrophic lateral sclerosis. *Biochem Biophys Res Commun* **351**, 602-611, doi:10.1016/j.bbrc.2006.10.093 (2006).

69 Neumann, M., Sampathu, D. M., Kwong, L. K., Truax, A. C., Micsenyi, M. C., Chou, T. T., Bruce, J., Schuck, T., Grossman, M., Clark, C. M., McCluskey, L. F., Miller, B. L., Masliah, E., Mackenzie, I. R., Feldman, H., Feiden, W., Kretzschmar, H. A., Trojanowski, J. Q. & Lee, V. M. Ubiquitinated TDP-43 in frontotemporal lobar degeneration and amyotrophic lateral sclerosis. *Science* **314**, 130-133 (2006).

70 Dormann, D. & Haass, C. TDP-43 and FUS: a nuclear affair. *Trends Neurosci* **34**, 339-348, doi:10.1016/j.tins.2011.05.002 (2011).

71 Giordana, M. T., Piccinini, M., Grifoni, S., De Marco, G., Vercellino, M., Magistrello, M., Pellerino, A., Buccinna, B., Lupino, E. & Rinaudo, M. T. TDP-43 redistribution is an early

event in sporadic amyotrophic lateral sclerosis. *Brain Pathol* **20**, 351-360, doi:10.1111/j.1750-3639.2009.00284.x (2010).

72 Van Deerlin, V. M., Leverenz, J. B., Bekris, L. M., Bird, T. D., Yuan, W., Elman, L. B., Clay, D., Wood, E. M., Chen-Plotkin, A. S., Martinez-Lage, M., Steinbart, E., McCluskey, L., Grossman, M., Neumann, M., Wu, I. L., Yang, W. S., Kalb, R., Galasko, D. R., Montine, T. J., Trojanowski, J. Q., Lee, V. M., Schellenberg, G. D. & Yu, C. E. TARDBP mutations in amyotrophic lateral sclerosis with TDP-43 neuropathology: a genetic and histopathological analysis. *Lancet Neurol* **7**, 409-416 (2008).

73 Polymenidou, M., Lagier-Tourenne, C., Hutt, K. R., Huelga, S. C., Moran, J., Liang, T. Y., Ling, S. C., Sun, E., Wancewicz, E., Mazur, C., Kordasiewicz, H., Sedaghat, Y., Donohue, J. P., Shiue, L., Bennett, C. F., Yeo, G. W. & Cleveland, D. W. Long pre-mRNA depletion and RNA missplicing contribute to neuronal vulnerability from loss of TDP-43. *Nat Neurosci* **14**, 459-468, doi:10.1038/nn.2779 (2011).

74 Tollervey, J. R., Curk, T., Rogelj, B., Briese, M., Cereda, M., Kayikci, M., Hortobagyi, T., Nishimura, A. L., Zupunski, V., Patani, R., Chandran, S., Rot, R., Zupan, B., Shaw, C. E. & Ule, J. Characterising the RNA targets and position-dependent splicing regulation by TDP-43; implications for neurodegenerative diseases. *Nat Neurosci* (2011).

75 McAleese, K. E., Walker, L., Erskine, D., Thomas, A. J., McKeith, I. G. & Attems, J. TDP-43 pathology in Alzheimer's disease, dementia with Lewy bodies and ageing. *Brain Pathol* **27**, 472-479, doi:10.1111/bpa.12424 (2017).

76 Nelson, P. T., Dickson, D. W., Trojanowski, J. Q., Jack, C. R., Boyle, P. A., Arfanakis, K., Rademakers, R., Alafuzoff, I., Attems, J., Brayne, C., Coyle-Gilchrist, I. T. S., Chui, H. C., Fardo, D. W., Flanagan, M. E., Halliday, G., Hokkanen, S. R. K., Hunter, S., Jicha, G. A., Katsumata, Y., Kawas, C. H., Keene, C. D., Kovacs, G. G., Kukull, W. A., Levey, A. I., Makkinejad, N., Montine, T. J., Murayama, S., Murray, M. E., Nag, S., Rissman, R. A., Seeley, W. W., Sperling, R. A., White Iii, C. L., Yu, L. & Schneider, J. A. Limbic-predominant age-related TDP-43 encephalopathy (LATE): consensus working group report. *Brain* **142**, 1503-1527, doi:10.1093/brain/awz099 (2019).

77 Gasset-Rosa, F., Lu, S., Yu, H., Chen, C., Melamed, Z., Guo, L., Shorter, J., Da Cruz, S. & Cleveland, D. W. Cytoplasmic TDP-43 De-mixing Independent of Stress Granules Drives Inhibition of Nuclear Import, Loss of Nuclear TDP-43, and Cell Death. *Neuron* **102**, 339-357 e337, doi:10.1016/j.neuron.2019.02.038 (2019).

78 Yu, H., Lu, S., Gasior, K., Singh, D., Vazquez-Sanchez, S., Tapia, O., Toprani, D., Beccari, M. S., Yates, J. R., Da Cruz, S., Newby, J. M., Lafarga, M., Gladfelter, A. S., Villa, E. & Cleveland, D. W. HSP70 chaperones RNA-free TDP-43 into anisotropic intranuclear liquid spherical shells. *Science* **371**, eabb4309, doi:10.1126/science.abb4309 (2021).

79 Tziortzouda, P., Van Den Bosch, L. & Hirth, F. Triad of TDP43 control in neurodegeneration: autoregulation, localization and aggregation. *Nat Rev Neurosci* **22**, 197-208, doi:10.1038/s41583-021-00431-1 (2021).

80 Tsao, W., Jeong, Y. H., Lin, S., Ling, J., Price, D. L., Chiang, P.-M. & Wong, P. C. Rodent models of TDP-43: Recent advances. *Brain Research* **1462**, 26-39, doi:10.1016/j.brainres.2012.04.031 (2012).

81 Elden, A. C., Kim, H.-J., Hart, M. P., Chen-Plotkin, A. S., Johnson, B. S., Fang, X., Armakola, M., Geser, F., Greene, R., Lu, M. M., Padmanabhan, A., Clay-Falcone, D., McCluskey, L., Elman, L., Juhr, D., Gruber, P. J., Rüb, U., Auburger, G., Trojanowski, J. Q., Lee, V. M. Y., Van Deerlin, V. M., Bonini, N. M. & Gitler, A. D. Ataxin-2 intermediate-length polyglutamine expansions are associated with increased risk for ALS. *Nature* **466**, 1069-1075, doi:10.1038/nature09320 (2010).

82 Becker, L. A., Huang, B., Bieri, G., Ma, R., Knowles, D. A., Jafar-Nejad, P., Messing, J., Kim, H. J., Soriano, A., Auburger, G., Pulst, S. M., Taylor, J. P., Rigo, F. & Gitler, A. D. Therapeutic reduction of ataxin-2 extends lifespan and reduces pathology in TDP-43 mice. *Nature* **544**, 367-371, doi:10.1038/nature22038 (2017).

83 Scoles, D. R., Meera, P., Schneider, M. D., Paul, S., Dansithong, W., Figueroa, K. P., Hung, G., Rigo, F., Bennett, C. F., Otis, T. S. & Pulst, S. M. Antisense oligonucleotide therapy for spinocerebellar ataxia type 2. *Nature* **544**, 362-366, doi:10.1038/nature22044 (2017).

84 Kawahara, Y. & Mieda-Sato, A. TDP-43 promotes microRNA biogenesis as a component of the Drosha and Dicer complexes. *Proc Natl Acad Sci U S A* **109**, 3347-3352, doi:10.1073/pnas.1112427109 (2012).

85 Buratti, E. & Baralle, F. E. Characterization and functional implications of the RNA binding properties of nuclear factor TDP-43, a novel splicing regulator of CFTR exon 9. *J Biol Chem* **276**, 36337-36343, doi:10.1074/jbc.M104236200 (2001).

86 Deshaies, J. E., Shkreta, L., Moszczynski, A. J., Sidibe, H., Semmler, S., Fouillen, A., Bennett, E. R., Bekenstein, U., Destroismaisons, L., Toutant, J., Delmotte, Q., Volkening, K., Stabile, S., Aulas, A., Khalfallah, Y., Soreq, H., Nanci, A., Strong, M. J., Chabot, B. & Vande Velde, C. TDP-43 regulates the alternative splicing of hnRNP A1 to yield an aggregation-prone variant in amyotrophic lateral sclerosis. *Brain* **141**, 1320-1333, doi:10.1093/brain/awy062 (2018).

87 Lagier-Tourenne, C., Polymenidou, M., Hutt, K. R., Vu, A. Q., Baughn, M., Huelga, S. C., Clutario, K. M., Ling, S. C., Liang, T. Y., Mazur, C., Wancewicz, E., Kim, A. S., Watt, A.,

Freier, S., Hicks, G. G., Donohue, J. P., Shiue, L., Bennett, C. F., Ravits, J., Cleveland, D. W. & Yeo, G. W. Divergent roles of ALS-linked proteins FUS/TLS and TDP-43 intersect in processing long pre-mRNAs. *Nat Neurosci* **15**, 1488-1497, doi:10.1038/nn.3230 (2012).

88 Neelagandan, N., Gonnella, G., Dang, S., Janiesch, P. C., Miller, K. K., Kuchler, K., Marques, R. F., Indenbirken, D., Alawi, M., Grundhoff, A., Kurtz, S. & Duncan, K. E. TDP-43 enhances translation of specific mRNAs linked to neurodegenerative disease. *Nucleic Acids Res* **47**, 341-361, doi:10.1093/nar/gky972 (2019).

89 Alami, N. H., Smith, R. B., Carrasco, M. A., Williams, L. A., Winborn, C. S., Han, S. S. W., Kiskinis, E., Winborn, B., Freibaum, B. D., Kanagaraj, A., Clare, A. J., Badders, N. M., Bilican, B., Chaum, E., Chandran, S., Shaw, C. E., Eggan, K. C., Maniatis, T. & Taylor, J. P. Axonal transport of TDP-43 mRNA granules is impaired by ALS-causing mutations. *Neuron* **81**, 536-543, doi:10.1016/j.neuron.2013.12.018 (2014).

90 Krach, F., Batra, R., Wheeler, E. C., Vu, A. Q., Wang, R., Hutt, K., Rabin, S. J., Baughn, M. W., Libby, R. T., Diaz-Garcia, S., Stauffer, J., Pirie, E., Saberi, S., Rodriguez, M., Madrigal, A. A., Kohl, Z., Winner, B., Yeo, G. W. & Ravits, J. Transcriptome-pathology correlation identifies interplay between TDP-43 and the expression of its kinase CK1E in sporadic ALS. *Acta Neuropathol* **136**, 405-423, doi:10.1007/s00401-018-1870-7 (2018).

91 Melamed, Z., Lopez-Erauskin, J., Baughn, M., Zhang, O., Drenner, K., Sun, Y., Freyermuth, F., McMahon, M. A., Beccari, M., Artates, J., Ohkubo, T., Rodriquez, M., Lin, N., Wu, D., Bennett, C. F., Rigo, F., Da Cruz, S., Ravits, J., Lagier-Tourenne, C. & Cleveland, D. W. Premature polyadenylation-mediated loss of stathmin-2 is a hallmark of TDP-43-dependent neurodegeneration *Nat. Neurosci.* **22**, 180-190 (2019).

92 Kapitein, L. C. & Hoogenraad, C. C. Building the Neuronal Microtubule Cytoskeleton. *Neuron* **87**, 492-506, doi:10.1016/j.neuron.2015.05.046 (2015).

93 Kreutzberg, G. W. Neuronal dynamics and axonal flow. IV. Blockage of intra-axonal enzyme transport by colchicine. *Proc Natl Acad Sci U S A* **62**, 722-728, doi:10.1073/pnas.62.3.722 (1969).

94 De Forges, H., Bouissou, A. & Perez, F. Interplay between microtubule dynamics and intracellular organization. *The International Journal of Biochemistry & Cell Biology* **44**, 266-274, doi:10.1016/j.biocel.2011.11.009 (2012).

95 Breuss, M. W., Leca, I., Gstrein, T., Hansen, A. H. & Keays, D. A. Tubulins and brain development - The origins of functional specification. *Mol Cell Neurosci* **84**, 58-67, doi:10.1016/j.mcn.2017.03.002 (2017).

96 Chretien, D., Metoz, F., Verde, F., Karsenti, E. & Wade, R. H. Lattice defects in microtubules: protofilament numbers vary within individual microtubules. *J Cell Biol* **117**, 1031-1040, doi:10.1083/jcb.117.5.1031 (1992).

97 Mitchison, T. & Kirschner, M. Dynamic instability of microtubule growth. *Nature* **312**, 237-242, doi:10.1038/312237a0 (1984).

98 Desai, A. & Mitchison, T. J. Microtubule polymerization dynamics. *Annu.Rev.Cell Dev.Biol.* **13**, 83-117 (1997).

99 Schubart, U. K. Regulation of protein phosphorylation in hamster insulinoma cells. Identification of Ca2+-regulated cytoskeletal and cAMP-regulated cytosolic phosphoproteins by two-dimensional electrophoresis. *J Biol Chem* **257**, 12231-12238 (1982).

100 Sobel, A. & Tashjian, A. H., Jr. Distinct patterns of cytoplasmic protein phosphorylation related to regulation of synthesis and release of prolactin by GH cells. *J Biol Chem* **258**, 10312-10324 (1983).

101 Sobel, A., Boutterin, M. C., Beretta, L., Chneiweiss, H., Doye, V. & Peyro-Saint-Paul, H. Intracellular substrates for extracellular signaling. Characterization of a ubiquitous, neuron-enriched phosphoprotein (stathmin). *J Biol Chem* **264**, 3765-3772 (1989).

102 Schubart, U. K., Banerjee, M. D. & Eng, J. Homology between the cDNAs encoding phosphoprotein p19 and SCG10 reveals a novel mammalian gene family preferentially expressed in developing brain. *DNA* **8**, 389-398, doi:10.1089/dna.1.1989.8.389 (1989).

103 Ozon, S., Maucuer, A. & Sobel, A. The stathmin family -- molecular and biological characterization of novel mammalian proteins expressed in the nervous system. *Eur J Biochem* **248**, 794-806, doi:10.1111/j.1432-1033.1997.t01-2-00794.x (1997).

104 Ozon, S., Byk, T. & Sobel, A. SCLIP: a novel SCG10-like protein of the stathmin family expressed in the nervous system. *J Neurochem* **70**, 2386-2396, doi:10.1046/j.1471-4159.1998.70062386.x (1998).

105 Sun, S., Sun, Y., Ling, S. C., Ferraiuolo, L., McAlonis-Downes, M., Zou, Y., Drenner, K., Wang, Y., Ditsworth, D., Tokunaga, S., Kopelevich, A., Kaspar, B. K., Lagier-Tourenne, C. & Cleveland, D. W. Translational profiling identifies a cascade of damage initiated in motor neurons and spreading to glia in mutant SOD1-mediated ALS. *Proc Natl Acad Sci U S A* **112**, E6993-7002, doi:10.1073/pnas.1520639112 (2015).

106 Chauvin, S. & Sobel, A. Neuronal stathmins: a family of phosphoproteins cooperating for neuronal development, plasticity and regeneration. *Prog Neurobiol* **126**, 1-18, doi:10.1016/j.pneurobio.2014.09.002 (2015).

107 Jourdain, L., Curmi, P., Sobel, A., Pantaloni, D. & Carlier, M. F. Stathmin: a tubulin-sequestering protein which forms a ternary T2S complex with two tubulin molecules. *Biochemistry* **36**, 10817-10821, doi:10.1021/bi971491b (1997).

108 Marklund, U., Larsson, N., Gradin, H. M., Brattsand, G. & Gullberg, M. Oncoprotein 18 is a phosphorylation-responsive regulator of microtubule dynamics. *Embo J* **15**, 5290-5298 (1996).

109 Riederer, B. M., Pellier, V., Antonsson, B., Di Paolo, G., Stimpson, S. A., Lutjens, R., Catsicas, S. & Grenningloh, G. Regulation of microtubule dynamics by the neuronal growth-associated protein SCG10. *Proc Natl Acad Sci U S A* **94**, 741-745, doi:10.1073/pnas.94.2.741 (1997).

110 Poulain, F. E. & Sobel, A. The microtubule network and neuronal morphogenesis: Dynamic and coordinated orchestration through multiple players. *Mol Cell Neurosci* **43**, 15-32, doi:10.1016/j.mcn.2009.07.012 (2010).

111 Charbaut, E., Curmi, P. A., Ozon, S., Lachkar, S., Redeker, V. & Sobel, A. Stathmin family proteins display specific molecular and tubulin binding properties. *J Biol Chem* **276**, 16146-16154, doi:10.1074/jbc.M010637200 (2001).

112 Himi, T., Okazaki, T., Wang, H., McNeill, T. H. & Mori, N. Differential localization of SCG10 and p19/stathmin messenger RNAs in adult rat brain indicates distinct roles for these growth-associated proteins. *Neuroscience* **60**, 907-926, doi:10.1016/0306-4522(94)90271-2 (1994).

113 Stein, R., Mori, N., Matthews, K., Lo, L. C. & Anderson, D. J. The NGF-inducible SCG10 mRNA encodes a novel membrane-bound protein present in growth cones and abundant in developing neurons. *Neuron* **1**, 463-476, doi:10.1016/0896-6273(88)90177-8 (1988).

114 Schubart, U. K., Yu, J., Amat, J. A., Wang, Z., Hoffmann, M. K. & Edelmann, W. Normal development of mice lacking metablastin (P19), a phosphoprotein implicated in cell cycle regulation. *J Biol Chem* **271**, 14062-14066, doi:10.1074/jbc.271.24.14062 (1996).

115 Liedtke, W., Leman, E. E., Fyffe, R. E., Raine, C. S. & Schubart, U. K. Stathmin-deficient mice develop an age-dependent axonopathy of the central and peripheral nervous systems. *Am J Pathol* **160**, 469-480, doi:10.1016/S0002-9440(10)64866-3 (2002).

116 Shin, J. E., Miller, B. R., Babetto, E., Cho, Y., Sasaki, Y., Qayum, S., Russler, E. V., Cavalli, V., Milbrandt, J. & DiAntonio, A. SCG10 is a JNK target in the axonal degeneration pathway. *Proc Natl Acad Sci U S A* **109**, E3696-3705, doi:10.1073/pnas.1216204109 (2012).

117 Shin, J. E., Geisler, S. & DiAntonio, A. Dynamic regulation of SCG10 in regenerating axons after injury. *Exp Neurol* **252**, 1-11, doi:10.1016/j.expneurol.2013.11.007 (2014).

118 Greka, A., Navarro, B., Oancea, E., Duggan, A. & Clapham, D. E. TRPC5 is a regulator of hippocampal neurite length and growth cone morphology. *Nat Neurosci* **6**, 837-845, doi:10.1038/nn1092 (2003).

119 Morii, H., Shiraishi-Yamaguchi, Y. & Mori, N. SCG10, a microtubule destabilizing factor, stimulates the neurite outgrowth by modulating microtubule dynamics in rat hippocampal primary cultured neurons. *J Neurobiol* **66**, 1101-1114, doi:10.1002/neu.20295 (2006).

120 Summers, D. W., Milbrandt, J. & DiAntonio, A. Palmitoylation enables MAPK-dependent proteostasis of axon survival factors. *Proc Natl Acad Sci U S A* **115**, E8746-E8754, doi:10.1073/pnas.1806933115 (2018).

121 Selvaraj, B. T., Frank, N., Bender, F. L., Asan, E. & Sendtner, M. Local axonal function of STAT3 rescues axon degeneration in the pmn model of motoneuron disease. *J Cell Biol* **199**, 437-451, doi:10.1083/jcb.201203109 (2012).

122 Graf, E. R., Heerssen, H. M., Wright, C. M., Davis, G. W. & DiAntonio, A. Stathmin is required for stability of the Drosophila neuromuscular junction. *J Neurosci* **31**, 15026-15034, doi:10.1523/JNEUROSCI.2024-11.2011 (2011).

123 Yusuf, M., Leung, K., Morris, K. J. & Volpi, E. V. Comprehensive cytogenomic profile of the in vitro neuronal model SH-SY5Y. *Neurogenetics* **14**, 63-70, doi:10.1007/s10048-012-0350-9 (2013).

124 Dharmadasa, T. & Kiernan, M. C. Riluzole, disease stage and survival in ALS. *The Lancet Neurology* **17**, 385-386, doi:10.1016/s1474-4422(18)30091-7 (2018).

125 Writing, G. & Edaravone, A. L. S. S. G. Safety and efficacy of edaravone in well defined patients with amyotrophic lateral sclerosis: a randomised, double-blind, placebo-controlled trial. *Lancet Neurol* **16**, 505-512, doi:10.1016/S1474-4422(17)30115-1 (2017).

126 Turnbull, J. Reappraisal of an ALS trial: unaccounted procedural risk. *Lancet Neurol* **19**, 717-718, doi:10.1016/S1474-4422(20)30265-9 (2020).

127 Meade, B. R. & Dowdy, S. F. The road to therapeutic RNA interference (RNAi): Tackling the 800 pound siRNA delivery gorilla. *Discov Med* **8**, 253-256 (2009).

128 Kordasiewicz, H. B., Stanek, L. M., Wancewicz, E. V., Mazur, C., McAlonis, M. M., Pytel, K. A., Artates, J. W., Weiss, A., Cheng, S. H., Shihabuddin, L. S., Hung, G., Bennett, C. F. & Cleveland, D. W. Sustained therapeutic reversal of Huntington's disease by transient repression of huntingtin synthesis. *Neuron* **74**, 1031-1044, doi:10.1016/j.neuron.2012.05.009 (2012).

129 Jafar-Nejad, P., Powers, B., Soriano, A., Zhao, H., Norris, D. A., Matson, J., Debrosse-Serra, B., Watson, J., Narayanan, P., Seung, Mazur, C., Kordasiewicz, H., Swayze, E. E. & Rigo, F. The atlas of RNase H antisense oligonucleotide distribution and activity in the CNS of rodents and non-human primates following central administration. *Nucleic Acids Res* **49**, 657-673, doi:10.1093/nar/gkaa1235 (2021).

130 Finkel, R. S., Chiriboga, C. A., Vajsar, J., Day, J. W., Montes, J., De Vivo, D. C., Yamashita, M., Rigo, F., Hung, G., Schneider, E., Norris, D. A., Xia, S., Bennett, C. F. & Bishop, K. M. Treatment of infantile-onset spinal muscular atrophy with nusinersen: a phase 2, open-label, dose-escalation study. *Lancet* **388**, 3017-3026, doi:10.1016/S0140-6736(16)31408-8 (2016).

131 Rigo, F., Chun, S. J., Norris, D. A., Hung, G., Lee, S., Matson, J., Fey, R. A., Gaus, H., Hua, Y., Grundy, J. S., Krainer, A. R., Henry, S. P. & Bennett, C. F. Pharmacology of a central nervous system delivered 2'-O-methoxyethyl-modified survival of motor neuron splicing oligonucleotide in mice and nonhuman primates. *The Journal of pharmacology and experimental therapeutics* **350**, 46-55, doi:10.1124/jpet.113.212407 (2014).

132 Hua, Y., Sahashi, K., Hung, G., Rigo, F., Passini, M. A., Bennett, C. F. & Krainer, A. R. Antisense correction of SMN2 splicing in the CNS rescues necrosis in a type III SMA mouse model. *Genes Dev* **24**, 1634-1644, doi:gad.1941310 [pii]
10.1101/gad.1941310 (2010).

133 Hua, Y., Sahashi, K., Rigo, F., Hung, G., Horev, G., Bennett, C. F. & Krainer, A. R. Peripheral SMN restoration is essential for long-term rescue of a severe spinal muscular atrophy mouse model. *Nature* **478**, 123-126, doi:10.1038/nature10485 (2011).

134 Southwell, A. L., Skotte, N. H., Bennett, C. F. & Hayden, M. R. Antisense oligonucleotide therapeutics for inherited neurodegenerative diseases. *Trends in molecular medicine* **18**, 634-643, doi:10.1016/j.molmed.2012.09.001 (2012).

135 Smith, R. A., Miller, T. M., Yamanaka, K., Monia, B. P., Condon, T. P., Hung, G., Lobsiger, C. S., Ward, C. M., McAlonis-Downes, M., Wei, H., Wancewicz, E. V., Bennett, C. F. & Cleveland, D. W. Antisense oligonucleotide therapy for neurodegenerative disease. *J Clin Invest* **116**, 2290-2296, doi:10.1172/JCI25424 (2006).

136 Miller, T. M., Pestronk, A., David, W., Rothstein, J., Simpson, E., Appel, S. H., Andres, P. L., Mahoney, K., Allred, P., Alexander, K., Ostrow, L. W., Schoenfeld, D., Macklin, E. A., Norris, D. A., Manousakis, G., Crisp, M., Smith, R., Bennett, C. F., Bishop, K. M. & Cudkowicz, M. E. An antisense oligonucleotide against SOD1 delivered intrathecally for patients with SOD1 familial amyotrophic lateral sclerosis: a phase 1, randomised, first-in-man study. *The Lancet Neurology* **12**, 435-442, doi:10.1016/s1474-4422(13)70061-9 (2013).

137 Maimon, R., Chillon-Marinas, C., Snethlage, C. E., Singhal, S. M., McAlonis-Downes, M., Ling, K., Rigo, F., Bennett, C. F., Da Cruz, S., Hnasko, T. S., Muotri, A. R. & Cleveland, D. W. Therapeutically viable generation of neurons with antisense oligonucleotide suppression of PTB. *Nat Neurosci*, doi:10.1038/s41593-021-00864-y (2021).

138 Miller, T., Cudkowicz, M., Shaw, P. J., Andersen, P. M., Atassi, N., Bucelli, R. C., Genge, A., Glass, J., Ladha, S., Ludolph, A. L., Maragakis, N. J., McDermott, C. J., Pestronk, A., Ravits, J., Salachas, F., Trudell, R., Van Damme, P., Zinman, L., Bennett, C. F., Lane, R., Sandrock, A., Runz, H., Graham, D., Houshyar, H., McCampbell, A., Nestorov, I., Chang, I., McNeill, M., Fanning, L., Fradette, S. & Ferguson, T. A. Phase 1-2 Trial of Antisense Oligonucleotide Tofersen for SOD1 ALS. *N Engl J Med* **383**, 109-119, doi:10.1056/NEJMoa2003715 (2020).

139 Rigo, F., Hua, Y., Krainer, A. R. & Bennett, C. F. Antisense-based therapy for the treatment of spinal muscular atrophy. *J Cell Biol* **199**, 21-25, doi:10.1083/jcb.201207087 (2012).

140 Wheeler, T. M., Leger, A. J., Pandey, S. K., MacLeod, A. R., Nakamori, M., Cheng, S. H., Wentworth, B. M., Bennett, C. F. & Thornton, C. A. Targeting nuclear RNA for in vivo correction of myotonic dystrophy. *Nature* **488**, 111-115, doi:10.1038/nature11362 (2012).

141 Lopez-Erauskin, J., Tadokoro, T., Baughn, M. W., Myers, B., McAlonis-Downes, M., Chillon-Marinas, C., Asiaban, J. N., Artates, J., Bui, A. T., Vetto, A. P., Lee, S. K., Le, A. V., Sun, Y., Jambeau, M., Boubaker, J., Swing, D., Qiu, J., Hicks, G. G., Ouyang, Z., Fu, X. D., Tessarollo, L., Ling, S. C., Parone, P. A., Shaw, C. E., Marsala, M., Lagier-Tourenne, C., Cleveland, D. W. & Da Cruz, S. ALS/FTD-Linked Mutation in FUS Suppresses Intra-axonal Protein Synthesis and Drives Disease Without Nuclear Loss-of-Function of FUS. *Neuron* **100**, 816-830 e817, doi:10.1016/j.neuron.2018.09.044 (2018).

142 Koller, E., Vincent, T. M., Chappell, A., De, S., Manoharan, M. & Bennett, C. F. Mechanisms of single-stranded phosphorothioate modified antisense oligonucleotide

accumulation in hepatocytes. *Nucleic Acids Res* **39**, 4795-4807, doi:10.1093/nar/gkr089 (2011).

143 Dowdy, S. F. Overcoming cellular barriers for RNA therapeutics. *Nat Biotechnol* **35**, 222-229, doi:10.1038/nbt.3802 (2017).

144 Stein, C. A., Hansen, J. B., Lai, J., Wu, S., Voskresenskiy, A., Hog, A., Worm, J., Hedtjarn, M., Souleimanian, N., Miller, P., Soifer, H. S., Castanotto, D., Benimetskaya, L., Orum, H. & Koch, T. Efficient gene silencing by delivery of locked nucleic acid antisense oligonucleotides, unassisted by transfection reagents. *Nucleic Acids Res* **38**, e3, doi:10.1093/nar/gkp841 (2010).

145 Akhtar, S., Basu, S., Wickstrom, E. & Juliano, R. L. Interactions of antisense DNA oligonucleotide analogs with phospholipid membranes (liposomes). *Nucleic Acids Res* **19**, 5551-5559, doi:10.1093/nar/19.20.5551 (1991).

146 Iversen, P. L., Zhu, S., Meyer, A. & Zon, G. Cellular uptake and subcellular distribution of phosphorothioate oligonucleotides into cultured cells. *Antisense Res Dev* **2**, 211-222, doi:10.1089/ard.1992.2.211 (1992).

147 Shen, W., De Hoyos, C. L., Migawa, M. T., Vickers, T. A., Sun, H., Low, A., Bell, T. A., Rahdar, M., Mukhopadhyay, S., Hart, C. E., Bell, M., Riney, S., Murray, S. F., Greenlee, S., Crooke, R. M., Liang, X.-H., Seth, P. P. & Crooke, S. T. Chemical modification of PS-ASO therapeutics reduces cellular protein-binding and improves the therapeutic index. *Nature Biotechnology* **37**, 640-650, doi:10.1038/s41587-019-0106-2 (2019).

148 Bennett, C. F., Krainer, A. R. & Cleveland, D. W. Antisense Oligonucleotide Therapies for Neurodegenerative Diseases. *Annu Rev Neurosci* **42**, 385-406, doi:10.1146/annurev-neuro-070918-050501 (2019).

149 Lorson, C. L., Hahnen, E., Androphy, E. J. & Wirth, B. A single nucleotide in the SMN gene regulates splicing and is responsible for spinal muscular atrophy. *Proc.Nat.Acad.Sci.Usa* **96**, 6307-6311 (1999).

150 Bravo-Hernandez, M., Tadokoro, T. & Marsala, M. Subpial AAV Delivery for Spinal Parenchymal Gene Regulation in Adult Mammals. *Methods Mol Biol* **1950**, 209-233, doi:10.1007/978-1-4939-9139-6_12 (2019).

151 Bravo-Hernandez, M., Tadokoro, T., Navarro, M. R., Platoshyn, O., Kobayashi, Y., Marsala, S., Miyanohara, A., Juhas, S., Juhasova, J., Skalnikova, H., Tomori, Z., Vanicky, I., Studenovska, H., Proks, V., Chen, P., Govea-Perez, N., Ditsworth, D., Ciacci, J. D.,

Gao, S., Zhu, W., Ahrens, E. T., Driscoll, S. P., Glenn, T. D., McAlonis-Downes, M., Da Cruz, S., Pfaff, S. L., Kaspar, B. K., Cleveland, D. W. & Marsala, M. Spinal subpial delivery of AAV9 enables widespread gene silencing and blocks motoneuron degeneration in ALS. *Nature Medicine* **26**, 118-130, doi:10.1038/s41591-019-0674-1 (2020).

152 Buie, L. K., Rasmussen, C. A., Porterfield, E. C., Ramgolam, V. S., Choi, V. W., Markovic-Plese, S., Samulski, R. J., Kaufman, P. L. & Borras, T. Self-complementary AAV virus (scAAV) safe and long-term gene transfer in the trabecular meshwork of living rats and monkeys. *Invest Ophthalmol Vis Sci* **51**, 236-248, doi:10.1167/iovs.09-3847 (2010).

153 McCarty, D. M., Monahan, P. E. & Samulski, R. J. Self-complementary recombinant adeno-associated virus (scAAV) vectors promote efficient transduction independently of DNA synthesis. *Gene Ther* **8**, 1248-1254, doi:10.1038/sj.gt.3301514 (2001).

154 Meyer, K., Ferraiuolo, L., Schmelzer, L., Braun, L., McGovern, V., Likhite, S., Michels, O., Govoni, A., Fitzgerald, J., Morales, P., Foust, K. D., Mendell, J. R., Burghes, A. H. & Kaspar, B. K. Improving single injection CSF delivery of AAV9-mediated gene therapy for SMA: a dose-response study in mice and nonhuman primates. *Mol Ther* **23**, 477-487, doi:10.1038/mt.2014.210 (2015).

155 Mendell, J. R., Al-Zaidy, S., Shell, R., Arnold, W. D., Rodino-Klapac, L. R., Prior, T. W., Lowes, L., Alfano, L., Berry, K., Church, K., Kissel, J. T., Nagendran, S., L'Italien, J., Sproule, D. M., Wells, C., Cardenas, J. A., Heitzer, M. D., Kaspar, A., Corcoran, S., Braun, L., Likhite, S., Miranda, C., Meyer, K., Foust, K. D., Burghes, A. H. M. & Kaspar, B. K. Single-Dose Gene-Replacement Therapy for Spinal Muscular Atrophy. *N Engl J Med* **377**, 1713-1722, doi:10.1056/NEJMoa1706198 (2017).

156 Ravindra Kumar, S., Miles, T. F., Chen, X., Brown, D., Dobreva, T., Huang, Q., Ding, X., Luo, Y., Einarsson, P. H., Greenbaum, A., Jang, M. J., Deverman, B. E. & Gradinaru, V. Multiplexed Cre-dependent selection yields systemic AAVs for targeting distinct brain cell types. *Nat Methods* **17**, 541-550, doi:10.1038/s41592-020-0799-7 (2020).

157 Chan, K. Y., Jang, M. J., Yoo, B. B., Greenbaum, A., Ravi, N., Wu, W.-L., Sánchez-Guardado, L., Lois, C., Mazmanian, S. K., Deverman, B. E. & Gradinaru, V. Engineered AAVs for efficient noninvasive gene delivery to the central and peripheral nervous systems. *Nature Neuroscience* **20**, 1172-1179, doi:10.1038/nn.4593 (2017).

158 Van Alstyne, M., Tattoli, I., Delestree, N., Recinos, Y., Workman, E., Shihabuddin, L. S., Zhang, C., Mentis, G. Z. & Pellizzoni, L. Gain of toxic function by long-term AAV9-mediated SMN overexpression in the sensorimotor circuit. *Nat Neurosci* **24**, 930-940, doi:10.1038/s41593-021-00827-3 (2021).

159 Miller, T. M., Kaspar, B. K., Kops, G. J., Yamanaka, K., Christian, L. J., Gage, F. H. & Cleveland, D. W. Virus-delivered small RNA silencing sustains strength in amyotrophic lateral sclerosis. *Ann Neurol* **57**, 773-776, doi:10.1002/ana.20453 (2005).

160 Mueller, C., Berry, J. D., McKenna-Yasek, D. M., Gernoux, G., Owegi, M. A., Pothier, L. M., Douthwright, C. L., Gelevski, D., Luppino, S. D., Blackwood, M., Wightman, N. S., Oakley, D. H., Frosch, M. P., Flotte, T. R., Cudkowicz, M. E. & Brown, R. H. SOD1 Suppression with Adeno-Associated Virus and MicroRNA in Familial ALS. *New England Journal of Medicine* **383**, 151-158, doi:10.1056/nejmoa2005056 (2020).

161 Kingwell, K. Double setback for ASO trials in Huntington disease. *Nat Rev Drug Discov* **20**, 412-413, doi:10.1038/d41573-021-00088-6 (2021).

162 Saberi, S., Stauffer, J. E., Schulte, D. J. & Ravits, J. Neuropathology of Amyotrophic Lateral Sclerosis and Its Variants. *Neurol Clin* **33**, 855-876, doi:10.1016/j.ncl.2015.07.012 (2015).

163 Mackenzie, I. R., Bigio, E. H., Ince, P. G., Geser, F., Neumann, M., Cairns, N. J., Kwong, L. K., Forman, M. S., Ravits, J., Stewart, H., Eisen, A., McClusky, L., Kretzschmar, H. A., Monoranu, C. M., Highley, J. R., Kirby, J., Siddique, T., Shaw, P. J., Lee, V. M. & Trojanowski, J. Q. Pathological TDP-43 distinguishes sporadic amyotrophic lateral sclerosis from amyotrophic lateral sclerosis with SOD1 mutations. *Ann Neurol* **61**, 427-434, doi:10.1002/ana.21147 (2007).

164 Wheaton, M. W., Salamone, A. R., Mosnik, D. M., McDonald, R. O., Appel, S. H., Schmolck, H. I., Ringholz, G. M. & Schulz, P. E. Cognitive impairment in familial ALS. *Neurology* **69**, 1411-1417, doi:10.1212/01.wnl.0000277422.11236.2c (2007).

165 Prudencio, M., Humphrey, J., Pickles, S., Brown, A. L., Hill, S. E., Kachergus, J. M., Shi, J., Heckman, M. G., Spiegel, M. R., Cook, C., Song, Y., Yue, M., Daughrity, L. M., Carlomagno, Y., Jansen-West, K., de Castro, C. F., DeTure, M., Koga, S., Wang, Y. C., Sivakumar, P., Bodo, C., Candalija, A., Talbot, K., Selvaraj, B. T., Burr, K., Chandran, S., Newcombe, J., Lashley, T., Hubbard, I., Catalano, D., Kim, D., Propp, N., Fennessey, S., Consortium, N. A., Fagegaltier, D., Phatnani, H., Secrier, M., Fisher, E. M., Oskarsson, B., van Blitterswijk, M., Rademakers, R., Graff-Radford, N. R., Boeve, B. F., Knopman, D. S., Petersen, R. C., Josephs, K. A., Thompson, E. A., Raj, T., Ward, M., Dickson, D. W., Gendron, T. F., Fratta, P. & Petrucelli, L. Truncated stathmin-2 is a marker of TDP-43 pathology in frontotemporal dementia. *J Clin Invest* **130**, 6080-6092, doi:10.1172/JCI139741 (2020).

166 Klim, J. R., Williams, L. A., Limone, F., Guerra San Juan, I., Davis-Dusenbery, B. N., Mordes, D. A., Burberry, A., Steinbaugh, M. J., Gamage, K. K., Kirchner, R., Moccia, R., Cassel, S. H., Chen, K., Wainger, B. J., Woolf, C. J. & Eggan, K. ALS-implicated protein

TDP-43 sustains levels of STMN2, a mediator of motor neuron growth and repair. *Nat Neurosci* **22**, 167-179, doi:10.1038/s41593-018-0300-4 (2019).

167 Lim, F., Spingola, M. & Peabody, D. S. Altering the RNA binding specificity of a translational repressor. *J Biol Chem* **269**, 9006-9010 (1994).

168 Konermann, S., Lotfy, P., Brideau, N. J., Oki, J., Shokhirev, M. N. & Hsu, P. D. Transcriptome Engineering with RNA-Targeting Type VI-D CRISPR Effectors. *Cell* **173**, 665-676 e614, doi:10.1016/j.cell.2018.02.033 (2018).

169 Jinek, M., Chylinski, K., Fonfara, I., Hauer, M., Doudna, J. A. & Charpentier, E. A programmable dual-RNA-guided DNA endonuclease in adaptive bacterial immunity. *Science* **337**, 816-821, doi:10.1126/science.1225829 (2012).

170 Cong, L., Ran, F. A., Cox, D., Lin, S., Barretto, R., Habib, N., Hsu, P. D., Wu, X., Jiang, W., Marraffini, L. A. & Zhang, F. Multiplex genome engineering using CRISPR/Cas systems. *Science* **339**, 819-823, doi:10.1126/science.1231143 (2013).

171 Ran, F. A., Cong, L., Yan, W. X., Scott, D. A., Gootenberg, J. S., Kriz, A. J., Zetsche, B., Shalem, O., Wu, X., Makarova, K. S., Koonin, E. V., Sharp, P. A. & Zhang, F. In vivo genome editing using Staphylococcus aureus Cas9. *Nature* **520**, 186-191, doi:10.1038/nature14299 (2015).

172 Haapaniemi, E., Botla, S., Persson, J., Schmierer, B. & Taipale, J. CRISPR-Cas9 genome editing induces a p53-mediated DNA damage response. *Nat Med* **24**, 927-930, doi:10.1038/s41591-018-0049-z (2018).

173 Schaefer, K. A., Wu, W. H., Colgan, D. F., Tsang, S. H., Bassuk, A. G. & Mahajan, V. B. Unexpected mutations after CRISPR-Cas9 editing in vivo. *Nat Methods* **14**, 547-548, doi:10.1038/nmeth.4293 (2017).

174 Zhang, C., Konermann, S., Brideau, N. J., Lotfy, P., Wu, X., Novick, S. J., Strutzenberg, T., Griffin, P. R., Hsu, P. D. & Lyumkis, D. Structural Basis for the RNA-Guided Ribonuclease Activity of CRISPR-Cas13d. *Cell* **175**, 212-223 e217, doi:10.1016/j.cell.2018.09.001 (2018).

175 Abudayyeh, O. O., Gootenberg, J. S., Konermann, S., Joung, J., Slaymaker, I. M., Cox, D. B., Shmakov, S., Makarova, K. S., Semenova, E., Minakhin, L., Severinov, K., Regev, A., Lander, E. S., Koonin, E. V. & Zhang, F. C2c2 is a single-component programmable RNA-guided RNA-targeting CRISPR effector. *Science* **353**, aaf5573, doi:10.1126/science.aaf5573 (2016).

176 Rigo, F. & Martinson, H. G. Functional coupling of last-intron splicing and 3'-end processing to transcription in vitro: the poly(A) signal couples to splicing before committing to cleavage. *Mol Cell Biol* **28**, 849-862, doi:10.1128/MCB.01410-07 (2008).

177 Kyburz, A., Friedlein, A., Langen, H. & Keller, W. Direct interactions between subunits of CPSF and the U2 snRNP contribute to the coupling of pre-mRNA 3' end processing and splicing. *Mol Cell* **23**, 195-205, doi:10.1016/j.molcel.2006.05.037 (2006).

178 Hua, Y., Vickers, T. A., Okunola, H. L., Bennett, C. F. & Krainer, A. R. Antisense masking of an hnRNP A1/A2 intronic splicing silencer corrects SMN2 splicing in transgenic mice. *Am J Hum Genet* **82**, 834-848, doi:10.1016/j.ajhg.2008.01.014 (2008).

179 Fischer, L. R., Culver, D. G., Tennant, P., Davis, A. A., Wang, M., Castellano-Sanchez, A., Khan, J., Polak, M. A. & Glass, J. D. Amyotrophic lateral sclerosis is a distal axonopathy: evidence in mice and man. *Exp Neurol* **185**, 232-240, doi:S0014488603004795 [pii] (2004).

180 Killian, J. M., Wilfong, A. A., Burnett, L., Appel, S. H. & Boland, D. Decremental motor responses to repetitive nerve stimulation in ALS. *Muscle Nerve* **17**, 747-754 (1994).

181 Dengler, R., Konstanzer, A., Kuther, G., Hesse, S., Wolf, W. & Struppler, A. Amyotrophic lateral sclerosis: macro-EMG and twitch forces of single motor units. *Muscle Nerve* **13**, 545-550, doi:10.1002/mus.880130612 (1990).

182 Martineau, E., Di Polo, A., Vande Velde, C. & Robitaille, R. Dynamic neuromuscular remodeling precedes motor-unit loss in a mouse model of ALS. *Elife* **7**, doi:10.7554/eLife.41973 (2018).

183 Brill, M. S., Kleele, T., Ruschkies, L., Wang, M., Marahori, N. A., Reuter, M. S., Hausrat, T. J., Weigand, E., Fisher, M., Ahles, A., Engelhardt, S., Bishop, D. L., Kneussel, M. & Misgeld, T. Branch-Specific Microtubule Destabilization Mediates Axon Branch Loss during Neuromuscular Synapse Elimination. *Neuron* **92**, 845-856, doi:10.1016/j.neuron.2016.09.049 (2016).

184 Belmont, L. D. & Mitchison, T. J. Identification of a protein that interacts with tubulin dimers and increases the catastrophe rate of microtubules. *Cell* **84**, 623-631, doi:10.1016/s0092-8674(00)81037-5 (1996).

185 Stegmeier, F., Hu, G., Rickles, R. J., Hannon, G. J. & Elledge, S. J. A lentiviral microRNA-based system for single-copy polymerase II-regulated RNA interference in mammalian cells. *Proc Natl Acad Sci U S A* **102**, 13212-13217, doi:10.1073/pnas.0506306102 (2005).

186 Rodriguez, A., Griffiths-Jones, S., Ashurst, J. L. & Bradley, A. Identification of mammalian microRNA host genes and transcription units. *Genome Res* **14**, 1902-1910, doi:10.1101/gr.2722704 (2004).

187 Miyanohara, A., Kamizato, K., Juhas, S., Juhasova, J., Navarro, M., Marsala, S., Lukacova, N., Hruska-Plochan, M., Curtis, E., Gabel, B., Ciacci, J., Ahrens, E. T., Kaspar, B. K., Cleveland, D. & Marsala, M. Potent spinal parenchymal AAV9-mediated gene delivery by subpial injection in adult rats and pigs. *Mol Ther Methods Clin Dev* **3**, 16046, doi:10.1038/mtm.2016.46 (2016).

188 Guyenet, S. J., Furrer, S. A., Damian, V. M., Baughan, T. D., La Spada, A. R. & Garden, G. A. A simple composite phenotype scoring system for evaluating mouse models of cerebellar ataxia. *J Vis Exp*, doi:10.3791/1787 (2010).

189 Komatsu, M., Waguri, S., Chiba, T., Murata, S., Iwata, J., Tanida, I., Ueno, T., Koike, M., Uchiyama, Y., Kominami, E. & Tanaka, K. Loss of autophagy in the central nervous system causes neurodegeneration in mice. *Nature* **441**, 880-884, doi:nature04723 [pii]
10.1038/nature04723 (2006).

190 Mathiesen, S. N., Lock, J. L., Schoderboeck, L., Abraham, W. C. & Hughes, S. M. CNS Transduction Benefits of AAV-PHP.eB over AAV9 Are Dependent on Administration Route and Mouse Strain. *Mol Ther Methods Clin Dev* **19**, 447-458, doi:10.1016/j.omtm.2020.10.011 (2020).

191 Chiang, P. M., Ling, J., Jeong, Y. H., Price, D. L., Aja, S. M. & Wong, P. C. Deletion of TDP-43 down-regulates Tbc1d1, a gene linked to obesity, and alters body fat metabolism. *Proceedings of the National Academy of Sciences* **107**, 16320-16324, doi:10.1073/pnas.1002176107 (2010).

192 Boillee, S., Vande Velde, C. & Cleveland, D. W. ALS: a disease of motor neurons and their nonneuronal neighbors. *Neuron* **52**, 39-59, doi:S0896-6273(06)00725-2 [pii]
10.1016/j.neuron.2006.09.018 (2006).

193 Boillee, S., Yamanaka, K., Lobsiger, C. S., Copeland, N. G., Jenkins, N. A., Kassiotis, G., Kollias, G. & Cleveland, D. W. Onset and progression in inherited ALS determined by motor neurons and microglia. *Science* **312**, 1389-1392, doi:312/5778/1389 [pii]
10.1126/science.1123511 (2006).

194 Da Cruz, S. & Cleveland, D. W. Understanding the role of TDP-43 and FUS/TLS in ALS and beyond. *Curr Opin Neurobiol* **21**, 904-919, doi:10.1016/j.conb.2011.05.029 (2011).

195 Di Giorgio, F. P., Carrasco, M. A., Siao, M. C., Maniatis, T. & Eggan, K. Non-cell autonomous effect of glia on motor neurons in an embryonic stem cell-based ALS model. *Nat Neurosci* **10**, 608-614 (2007).

196 Ditsworth, D., Maldonado, M., McAlonis-Downes, M., Sun, S., Seelman, A., Drenner, K., Arnold, E., Ling, S. C., Pizzo, D., Ravits, J., Cleveland, D. W. & Da Cruz, S. Mutant TDP-43 within motor neurons drives disease onset but not progression in amyotrophic lateral sclerosis. *Acta Neuropathol* **133**, 907-922, doi:10.1007/s00401-017-1698-6 (2017).

197 Lobsiger, C. S., Boillee, S., McAlonis-Downes, M., Khan, A. M., Feltri, M. L., Yamanaka, K. & Cleveland, D. W. Schwann cells expressing dismutase active mutant SOD1 unexpectedly slow disease progression in ALS mice. *Proc Natl Acad Sci U S A* **106**, 4465-4470, doi:0813339106 [pii]
10.1073/pnas.0813339106 (2009).

198 Lobsiger, C. S. & Cleveland, D. W. Glial cells as intrinsic components of non-cell-autonomous neurodegenerative disease. *Nat Neurosci* **10**, 1355-1360, doi:10.1038/nn1988 (2007).

199 Marchetto, M. C., Muotri, A. R., Mu, Y., Smith, A. M., Cezar, G. G. & Gage, F. H. Non-cell-autonomous effect of human SOD1 G37R astrocytes on motor neurons derived from human embryonic stem cells. *Cell Stem Cell* **3**, 649-657 (2008).

200 Miller, T. M., Kim, S. H., Yamanaka, K., Hester, M., Umapathi, P., Arnson, H., Rizo, L., Mendell, J. R., Gage, F. H., Cleveland, D. W. & Kaspar, B. K. Gene transfer demonstrates that muscle is not a primary target for non-cell-autonomous toxicity in familial amyotrophic lateral sclerosis. *Proc Natl Acad Sci U S A* **103**, 19546-19551, doi:0609411103 [pii]
10.1073/pnas.0609411103 (2006).

201 Nagai, M., Re, D. B., Nagata, T., Chalazonitis, A., Jessell, T. M., Wichterle, H. & Przedborski, S. Astrocytes expressing ALS-linked mutated SOD1 release factors selectively toxic to motor neurons. *Nat Neurosci* **10**, 615-622 (2007).

202 Yamanaka, K., Boillee, S., Roberts, E. A., Garcia, M. L., McAlonis-Downes, M., Mikse, O. R., Cleveland, D. W. & Goldstein, L. S. Mutant SOD1 in cell types other than motor neurons and oligodendrocytes accelerates onset of disease in ALS mice. *Proc Natl Acad Sci U S A* **105**, 7594-7599, doi:0802556105 [pii] 10.1073/pnas.0802556105 (2008).

203 Yamanaka, K., Chun, S. J., Boillee, S., Fujimori-Tonou, N., Yamashita, H., Gutmann, D. H., Takahashi, R., Misawa, H. & Cleveland, D. W. Astrocytes as determinants of disease progression in inherited amyotrophic lateral sclerosis. *Nat Neurosci* **11**, 251-253, doi:nn2047 [pii] 10.1038/nn2047 (2008).

204 Crosson, S. M., Dib, P., Smith, J. K. & Zolotukhin, S. Helper-free Production of Laboratory Grade AAV and Purification by Iodixanol Density Gradient Centrifugation. *Molecular Therapy - Methods & Clinical Development* **10**, 1-7, doi:10.1016/j.omtm.2018.05.001 (2018).

205 Chen, J., Brunner, A. D., Cogan, J. Z., Nunez, J. K., Fields, A. P., Adamson, B., Itzhak, D. N., Li, J. Y., Mann, M., Leonetti, M. D. & Weissman, J. S. Pervasive functional translation of noncanonical human open reading frames. *Science* **367**, 1140-1146, doi:10.1126/science.aay0262 (2020).

206 Kondo, T., Hashimoto, Y., Kato, K., Inagaki, S., Hayashi, S. & Kageyama, Y. Small peptide regulators of actin-based cell morphogenesis encoded by a polycistronic mRNA. *Nat Cell Biol* **9**, 660-665, doi:10.1038/ncb1595 (2007).

207 Galindo, M. I., Pueyo, J. I., Fouix, S., Bishop, S. A. & Couso, J. P. Peptides Encoded by Short ORFs Control Development and Define a New Eukaryotic Gene Family. *PLOS Biology* **5**, e106, doi:10.1371/journal.pbio.0050106 (2007).

208 Arnoult, N., Correia, A., Ma, J., Merlo, A., Garcia-Gomez, S., Maric, M., Tognetti, M., Benner, C. W., Boulton, S. J., Saghatelian, A. & Karlseder, J. Regulation of DNA repair pathway choice in S and G2 phases by the NHEJ inhibitor CYREN. *Nature* **549**, 548-552, doi:10.1038/nature24023 (2017).

209 Anderson, D. M., Anderson, K. M., Chang, C. L., Makarewich, C. A., Nelson, B. R., McAnally, J. R., Kasaragod, P., Shelton, J. M., Liou, J., Bassel-Duby, R. & Olson, E. N. A micropeptide encoded by a putative long noncoding RNA regulates muscle performance. *Cell* **160**, 595-606, doi:10.1016/j.cell.2015.01.009 (2015).

210 Ingolia, N. T., Brar, G. A., Stern-Ginossar, N., Harris, M. S., Talhouarne, G. J., Jackson, S. E., Wills, M. R. & Weissman, J. S. Ribosome profiling reveals pervasive translation outside of annotated protein-coding genes. *Cell Rep* **8**, 1365-1379, doi:10.1016/j.celrep.2014.07.045 (2014).

211 Heiman, M., Kulicke, R., Fenster, R. J., Greengard, P. & Heintz, N. Cell type-specific mRNA purification by translating ribosome affinity purification (TRAP). *Nat Protoc* **9**, 1282-1291, doi:10.1038/nprot.2014.085 (2014).

212 Heiman, M., Schaefer, A., Gong, S., Peterson, J. D., Day, M., Ramsey, K. E., Suarez-Farinas, M., Schwarz, C., Stephan, D. A., Surmeier, D. J., Greengard, P. & Heintz, N. A translational profiling approach for the molecular characterization of CNS cell types. *Cell* **135**, 738-748, doi:10.1016/j.cell.2008.10.028 (2008).

213 Ekstrand, M. I., Nectow, A. R., Knight, Z. A., Latcha, K. N., Pomeranz, L. E. & Friedman, J. M. Molecular profiling of neurons based on connectivity. *Cell* **157**, 1230-1242, doi:10.1016/j.cell.2014.03.059 (2014).

214 Chen, J., Brunner, A. D., Cogan, J. Z., Nuñez, J. K., Fields, A. P., Adamson, B., Itzhak, D. N., Li, J. Y., Mann, M., Leonetti, M. D. & Weissman, J. S. Pervasive functional translation of noncanonical human open reading frames. *Science* **367**, 1140-1146, doi:10.1126/science.aay0262 (2020).

215 Shaner, N. C., Lambert, G. G., Chammas, A., Ni, Y., Cranfill, P. J., Baird, M. A., Sell, B. R., Allen, J. R., Day, R. N., Israelsson, M., Davidson, M. W. & Wang, J. A bright monomeric green fluorescent protein derived from Branchiostoma lanceolatum. *Nat Methods* **10**, 407-409, doi:10.1038/nmeth.2413 (2013).

216 Sanson, K. R., Hanna, R. E., Hegde, M., Donovan, K. F., Strand, C., Sullender, M. E., Vaimberg, E. W., Goodale, A., Root, D. E., Piccioni, F. & Doench, J. G. Optimized libraries for CRISPR-Cas9 genetic screens with multiple modalities. *Nat Commun* **9**, 5416, doi:10.1038/s41467-018-07901-8 (2018).

217 Shalem, O., Sanjana, N. E., Hartenian, E., Shi, X., Scott, D. A., Mikkelson, T., Heckl, D., Ebert, B. L., Root, D. E., Doench, J. G. & Zhang, F. Genome-scale CRISPR-Cas9 knockout screening in human cells. *Science* **343**, 84-87, doi:10.1126/science.1247005 (2014).

218 Gilbert, L. A., Horlbeck, M. A., Adamson, B., Villalta, J. E., Chen, Y., Whitehead, E. H., Guimaraes, C., Panning, B., Ploegh, H. L., Bassik, M. C., Qi, L. S., Kampmann, M. & Weissman, J. S. Genome-Scale CRISPR-Mediated Control of Gene Repression and Activation. *Cell* **159**, 647-661, doi:10.1016/j.cell.2014.09.029 (2014).

219 Konermann, S., Brigham, M. D., Trevino, A. E., Joung, J., Abudayyeh, O. O., Barcena, C., Hsu, P. D., Habib, N., Gootenberg, J. S., Nishimasu, H., Nureki, O. & Zhang, F. Genome-scale transcriptional activation by an engineered CRISPR-Cas9 complex. *Nature* **517**, 583-588, doi:10.1038/nature14136 (2015).

220 Ratni, H., Ebeling, M., Baird, J., Bendels, S., Bylund, J., Chen, K. S., Denk, N., Feng, Z., Green, L., Guerard, M., Jablonski, P., Jacobsen, B., Khwaja, O., Kletzl, H., Ko, C.-P., Kustermann, S., Marquet, A., Metzger, F., Mueller, B., Naryshkin, N. A., Paushkin, S. V., Pinard, E., Poirier, A., Reutlinger, M., Weetall, M., Zeller, A., Zhao, X. & Mueller, L. Discovery of Risdiplam, a Selective Survival of Motor Neuron-2 (SMN2) Gene Splicing Modifier for the Treatment of Spinal Muscular Atrophy (SMA). *Journal of Medicinal Chemistry* **61**, 6501-6517, doi:10.1021/acs.jmedchem.8b00741 (2018).

221 Tanenbaum, M. E., Gilbert, L. A., Qi, L. S., Weissman, J. S. & Vale, R. D. A protein-tagging system for signal amplification in gene expression and fluorescence imaging. *Cell* **159**, 635-646, doi:10.1016/j.cell.2014.09.039 (2014).

222 Schwinn, M. K., Machleidt, T., Zimmerman, K., Eggers, C. T., Dixon, A. S., Hurst, R., Hall, M. P., Encell, L. P., Binkowski, B. F. & Wood, K. V. CRISPR-Mediated Tagging of Endogenous Proteins with a Luminescent Peptide. *ACS Chemical Biology* **13**, 467-474, doi:10.1021/acschembio.7b00549 (2018).

223 Oh-hashi, K., Furuta, E., Fujimura, K. & Hirata, Y. Application of a novel HiBiT peptide tag for monitoring ATF4 protein expression in Neuro2a cells. *Biochemistry and Biophysics Reports* **12**, 40-45, doi:https://doi.org/10.1016/j.bbrep.2017.08.002 (2017).

224 Dixon, A. S., Schwinn, M. K., Hall, M. P., Zimmerman, K., Otto, P., Lubben, T. H., Butler, B. L., Binkowski, B. F., Machleidt, T., Kirkland, T. A., Wood, M. G., Eggers, C. T., Encell, L. P. & Wood, K. V. NanoLuc Complementation Reporter Optimized for Accurate Measurement of Protein Interactions in Cells. *ACS Chemical Biology* **11**, 400-408, doi:10.1021/acschembio.5b00753 (2016).

225 Leonetti, M. D., Sekine, S., Kamiyama, D., Weissman, J. S. & Huang, B. A scalable strategy for high-throughput GFP tagging of endogenous human proteins. *Proc Natl Acad Sci U S A* **113**, E3501-3508, doi:10.1073/pnas.1606731113 (2016).

226 Lim, F. & Peabody, D. S. RNA recognition site of PP7 coat protein. *Nucleic Acids Res* **30**, 4138-4144, doi:10.1093/nar/gkf552 (2002).

227 Liu, J. L., Zabetakis, D., Goldman, E. R. & Anderson, G. P. Selection and evaluation of single domain antibodies toward MS2 phage and coat protein. *Mol Immunol* **53**, 118-125, doi:10.1016/j.molimm.2012.07.010 (2013).

228 Nilaratanakul, V., Hauer, D. A. & Griffin, D. E. Development of encoded Broccoli RNA aptamers for live cell imaging of alphavirus genomic and subgenomic RNAs. *Scientific Reports* **10**, 5233, doi:10.1038/s41598-020-61573-3 (2020).

229 Alhindi, A., Boehm, I. & Chaytow, H. Small junction, big problems: Neuromuscular junction pathology in mouse models of amyotrophic lateral sclerosis (ALS). *Journal of Anatomy*, doi:10.1111/joa.13463 (2021).

230 Sternberg, N. & Hamilton, D. Bacteriophage P1 site-specific recombination. I. Recombination between loxP sites. *J Mol Biol* **150**, 467-486, doi:10.1016/0022-2836(81)90375-2 (1981).

231 Schnütgen, F., Doerflinger, N., Calléja, C., Wendling, O., Chambon, P. & Ghyselinck, N. B. A directional strategy for monitoring Cre-mediated recombination at the cellular level in the mouse. *Nature Biotechnology* **21**, 562-565, doi:10.1038/nbt811 (2003).

232 Philips, T. & Rothstein, J. D. Rodent Models of Amyotrophic Lateral Sclerosis. *Curr Protoc Pharmacol* **69**, 5 67 61-65 67 21, doi:10.1002/0471141755.ph0567s69 (2015).

233 Picher-Martel, V., Valdmanis, P. N., Gould, P. V., Julien, J. P. & Dupre, N. From animal models to human disease: a genetic approach for personalized medicine in ALS. *Acta Neuropathol Commun* **4**, 70, doi:10.1186/s40478-016-0340-5 (2016).

234 Dawson, T. M., Golde, T. E. & Lagier-Tourenne, C. Animal models of neurodegenerative diseases. *Nat Neurosci* **21**, 1370-1379, doi:10.1038/s41593-018-0236-8 (2018).

235 Lutz, C. Mouse models of ALS: Past, present and future. *Brain Res* **1693**, 1-10, doi:10.1016/j.brainres.2018.03.024 (2018).

236 Swarup, V., Phaneuf, D., Bareil, C., Robertson, J., Rouleau, G. A., Kriz, J. & Julien, J. P. Pathological hallmarks of amyotrophic lateral sclerosis/frontotemporal lobar degeneration in transgenic mice produced with TDP-43 genomic fragments. *Brain* **134**, 2610-2626, doi:10.1093/brain/awr159 (2011).

237 Arnold, E. S., Ling, S. C., Huelga, S. C., Lagier-Tourenne, C., Polymenidou, M., Ditsworth, D., Kordasiewicz, H. B., McAlonis-Downes, M., Platoshyn, O., Parone, P. A., Da Cruz, S., Clutario, K. M., Swing, D., Tessarollo, L., Marsala, M., Shaw, C. E., Yeo, G. W. & Cleveland, D. W. ALS-linked TDP-43 mutations produce aberrant RNA splicing and adult-onset motor neuron disease without aggregation or loss of nuclear TDP-43. *Proc Natl Acad Sci U S A* **110**, E736-745, doi:10.1073/pnas.1222809110 (2013).

238 Mitchell, J. C., Constable, R., So, E., Vance, C., Scotter, E., Glover, L., Hortobagyi, T., Arnold, E. S., Ling, S. C., McAlonis, M., Da Cruz, S., Polymenidou, M., Tessarolo, L., Cleveland, D. W. & Shaw, C. E. Wild type human TDP-43 potentiates ALS-linked mutant TDP-43 driven progressive motor and cortical neuron degeneration with pathological features of ALS. *Acta Neuropathol Commun* **3**, 36, doi:10.1186/s40478-015-0212-4 (2015).

239 Chew, J., Gendron, T. F., Prudencio, M., Sasaguri, H., Zhang, Y. J., Castanedes-Casey, M., Lee, C. W., Jansen-West, K., Kurti, A., Murray, M. E., Bieniek, K. F., Bauer, P. O., Whitelaw, E. C., Rousseau, L., Stankowski, J. N., Stetler, C., Daughrity, L. M., Perkerson, E. A., Desaro, P., Johnston, A., Overstreet, K., Edbauer, D., Rademakers, R., Boylan, K. B., Dickson, D. W., Fryer, J. D. & Petrucelli, L. Neurodegeneration. C9ORF72 repeat

expansions in mice cause TDP-43 pathology, neuronal loss, and behavioral deficits. *Science* **348**, 1151-1154, doi:10.1126/science.aaa9344 (2015).

240 Chew, J., Cook, C., Gendron, T. F., Jansen-West, K., Del Rosso, G., Daughrity, L. M., Castanedes-Casey, M., Kurti, A., Stankowski, J. N., Disney, M. D., Rothstein, J. D., Dickson, D. W., Fryer, J. D., Zhang, Y. J. & Petrucelli, L. Aberrant deposition of stress granule-resident proteins linked to C9orf72-associated TDP-43 proteinopathy. *Mol Neurodegener* **14**, 9, doi:10.1186/s13024-019-0310-z (2019).

241 Maathuis, E. M., Drenthen, J., van Doorn, P. A., Visser, G. H. & Blok, J. H. The CMAP scan as a tool to monitor disease progression in ALS and PMA. *Amyotroph Lateral Scler Frontotemporal Degener* **14**, 217-223, doi:10.3109/21678421.2012.732079 (2013).

242 McCampbell, A., Cole, T., Wegener, A. J., Tomassy, G. S., Setnicka, A., Farley, B. J., Schoch, K. M., Hoye, M. L., Shabsovich, M., Sun, L., Luo, Y., Zhang, M., Comfort, N., Wang, B., Amacker, J., Thankamony, S., Salzman, D. W., Cudkowicz, M., Graham, D. L., Bennett, C. F., Kordasiewicz, H. B., Swayze, E. E. & Miller, T. M. Antisense oligonucleotides extend survival and reverse decrement in muscle response in ALS models. *J Clin Invest* **128**, 3558-3567, doi:10.1172/JCI99081 (2018).